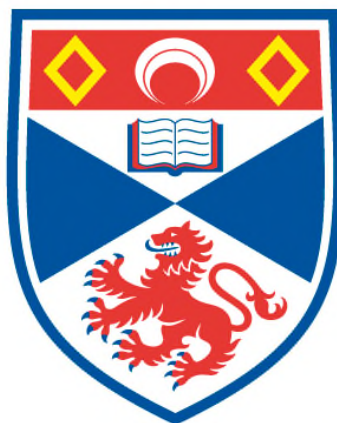


CHEMICAL BONDING PROPERTIES IN SUBSTITUTED DISILYNES

Lukasz Michal Serafin

**A Thesis Submitted for the Degree of PhD
at the
University of St Andrews**



2012

**Full metadata for this item is available in
St Andrews Research Repository
at:**

<http://research-repository.st-andrews.ac.uk/>

Please use this identifier to cite or link to this item:

<http://hdl.handle.net/10023/3638>

This item is protected by original copyright

Chemical Bonding Properties in Substituted Disilynes.

Lukasz Michal Serafin



**University of
St Andrews**

This thesis is submitted in partial fulfilment for the degree of PhD
at the
University of St Andrews

September 2012

Abstract

The molecular structures of the Si_2HX , Si_2Li_2 , SiGeHLi and C_2H_2 species (where $\text{X} = \text{H}$, Li , F and Cl) were studied. All of these species have more than one isomeric form. The critical points on the potential energy surfaces of the Si_2HX , Si_2Li_2 and C_2H_2 species and the minima on the SiGeHLi surface were located. The full six-dimensional potential energy surface (PES) of the Si_2Li_2 molecule was calculated (for the first time) using the CCSD(T)-F12a/cc-pVTZ-F12 level of theory.

The core-valence, zero-point energy and relativistic corrections for the Si_2HLi and Si_2Li_2 species were calculated. Additionally, the electron affinity and Li^+/H^+ binding energies for the Si_2HLi and Si_2Li_2 structures were investigated. Furthermore, the anharmonic vibrational-rotational properties for the Si_2HLi and Si_2Li_2 structures were calculated using second-order perturbation theory.

The recently developed CCSD(T)-F12a method with the cc-pVTZ-F12 basis set was employed to obtain geometries and relative energies (for the Si_2HLi , Si_2HF , Si_2HCl and Si_2Li_2 structures) and vibrational frequencies (for the Si_2H_2 and Si_2Li_2 structures). The CCSD(T) method with the cc-pVXZ, aug-cc-pVXZ and aug-cc-pV(X+d)Z basis sets, CCSD(T)-F12a/cc-pVXZ (where $\text{X}=2-4$) and the B3LYP/6-311+G(d) levels of theory were also used. Comparison was made of the geometric properties and vibrational frequencies calculated at the different levels of theory.

The calculated geometric properties for all the studied species and vibrational frequencies (for the Si_2H_2 structures) show good agreement with the experimental and theoretical literature.

The PES of Si_2Li_2 was used to perform large scale variational vibrational calculations using the WAVR4 program. The first 2400 totally symmetric energy levels were calculated. The low-lying energy levels were qualitatively correct. Conclusive assignments of the vibrational modes of the Si_2Li_2 structures were made for the eleven lowest lying energy levels.

I dedicate this dissertation to my parents Ireneusz and Malgorzata Serafin, who inspired my enthusiasm in science and also gave me the strength to move forward on the way to pursuing my dreams.

I dedicate this work and give special thanks to my beloved partner Iza Cebula for support and patience throughout the entire doctorate program.

I would like to also give a special dedication to the late Dr. Richard Feynman for the inspiration, encouraging scientific curiosity and guidance on how to be a great scientist.

Acknowledgements

First and foremost, I would like to give the most sincere thanks to both of my supervisors Dr. Tanja van Mourik and Dr. Mark M. Law for their direction, assistance, inspirational instructions and patient guidance during the last three and half years.

I want to express my deep appreciation to Dr. van Mourik and Dr. Law for giving me the opportunity to fulfil my dream to study for a PhD degree and allowing me to continue my journey through science.

I am grateful to the University of St. Andrews for financial support for this project and the University of Aberdeen for hospitality during my one-year stay in Aberdeen.

I acknowledge the Eastham Research Computing Facility for providing the essential tools, which allowed me to do all the calculations, and I also thank Dr. Herbert Früchtl for his advice and help with software problems during my doctorate program.

I would like to thank all my friends and colleagues in St. Andrews, Aberdeen and Edinburgh; especially I am grateful to Przemysław Krężolek, Bartosz Kubera, Wiktor Nalepa and Łukasz Bacalski for support and belief in me for the last five years.

I deeply appreciate the possibility to stay in Scotland, the opportunity to make new friendships and unforgettable memories.

I thank my parents, for their unlimited love and support during all these years.

List of Contents

Abstract.....	2
Acknowledgements	4
List of Contents	5
Introduction	7
Theory and methods	13
1 <i>Ab initio</i> and DFT methods.....	14
1.1 Born-Oppenheimer approximation.....	14
1.2 Hartree–Fock method.....	16
1.3 MP2 method.....	20
1.4 Coupled Cluster method.....	22
1.5 Explicitly correlated method-CCSD(T)-F12a/b.....	24
1.6 Density functional theory – DFT.....	30
1.7 Other theoretical methods and concepts employed here.....	34
2 Molecular vibrations	37
2.1 Theoretical introduction.....	37
2.2 Variational method	42
Applications.....	44
3 Acetylene/vinylidene.....	45
3.1 The C ₂ H ₂ isomers.....	45
4 The Si ₂ HX and Si ₂ Li ₂ critical points (where X=H, Li, F and Cl).....	56
4.1 The Si ₂ H ₂ isomers.....	56
4.2 The Si ₂ HF isomers.....	75
4.3 The Si ₂ HCl isomers.....	87

4.4	The Si_2HLi isomers.....	98
4.5	The Si_2Li_2 isomers.	124
4.6	Discussions and conclusions for the Si_2HX and Si_2Li_2 systems (where X= H, Li, F and Cl) and comparison with the C_2H_2 species.	139
5	Electron affinity and Li^+ and H^+ binding energy.	146
5.1	Electron affinity.	146
5.2	Li^+ binding energy.	152
5.3	H^+ binding energy.	155
5.4	Comparison of calculated values with literature and conclusions.....	156
6	SiGeHLi	158
6.1	The SiGeHLi isomers.	158
7	Si_2Li_2 beyond the critical points – constructing and fitting the potential energy surface.....	164
7.1	Theoretical introduction.....	164
7.2	Potential energy surface of the Si_2Li_2 molecule.	171
8	Vibrational properties of the Si_2Li_2 isomers.	182
8.1	Vibrational calculations.	182
9	Conclusions	197
10	Publication and presentations resulting from this thesis	198
10.1	Publication.....	198
10.2	Presentations and posters	198
11	Bibliography	199
12	Appendix	206
12.1	The Neural Network MATLAB script.....	206
12.2	Fortran programs.....	210

Introduction

The aim of the following work is extended investigations of the physical-chemical properties of substituted disilynes, which include: bonding properties, vibrational frequencies, electron affinities, proton binding energies and isomerisation properties. Also a full six-dimensional potential energy surface (PES) with additional variational-vibrational energies will be calculated for the most interesting substituted disilyne species.

Silicon is the second most abundant element in the earth's crust, and thus silicon chemistry can be very interesting to study and investigate. Silicon in various forms such as silicon dioxide (silica) or silicates has been an inherent companion during the long history of human civilization and technology, starting as a main part of brick, cement or porcelain and is currently used as the principal component for semiconductors, batteries and diagnostic industry domains [1]. Applications of silicon have large impact on the modern world economy, so any new knowledge or more accurate physical-chemical properties would be very beneficial.

Silicon is also an essential element in biology, such as a trace element in plants, but mostly employed by various sea species [2]. For instance sea sponges need silicon in order to have structure and other biological forms use silicon to build the striking array of protective shells [3].

Silicon compounds also occur as candidates for interstellar molecules [4-6]. For instance the *ab initio* calculation of IR bands done by Osamura and Kaiser on the Si_2H_x (where $x=1-6$) species was used to search for these molecules in the circumstellar envelope of carbon star IRC+10216 [4, 6]. The silicon abundance in the atmosphere of the He-weak star HD 21699 was investigated recently by Pavlenko et al. [7].

One of the reasons for the many occurrences of silicon compounds in various aspects of the surrounding world is the unusual physical-chemical properties of silicon.

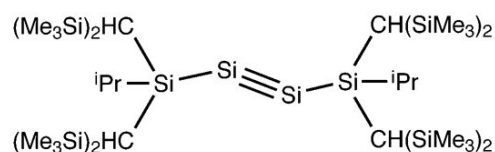
There is interest in the unusual chemical bonding properties of silicon, specially the formation of multiple bonds, which in compounds of elements heavier than carbon (Si, Ge, Sn and Pb) was for a long time doubted because of the considerable Pauli repulsion between the electrons of the inner shells [8-10]. Silicon compounds belong to the carbon group in the periodic table (group 14), so they may have similar physical and chemical properties as carbon compounds and can create similar compounds. However, it was noticed in the early 1980's that heavier elements than carbon can exhibit unusual geometries [11-13], such as dibridged and monobridged structures. Also, the absence of a linear structure as a minimum on the potential energy surface of Si_2H_2 was a big surprise. Explanations of these properties have been reported before [14-17]. Lein et al. investigated the interactions between the EH moieties in E_2H_2 molecules (where E = C, Si, Ge, Sn and Pb). They showed that the bonding between the EH moieties for the E=Si-Pb species (which differ from C) is more favorable in the ($X^2\Pi$) ground state than in the ($e^4\Sigma^-$) excited state as the excitation energy of EH (where E = Si-Pb) is higher than for CH [14]. Furthermore bridged structures of E_2H_2 can be created, because both the doubly- and singly-bridged structures possess three bonding orbital contributions: one σ bond and two E-H donor-acceptor bonds in the dibridged structure, and one π bond, one E-H donor-acceptor bond and one lone-pair donor-acceptor bond in the monobridged isomers [14]. In addition, MRCI-SD/aug-cc-pVQZ calculations of Si_2H_2 structures showed that the triplet species have higher energy than the singlet structures [14].

A comparison of silicon hydrides with carbon analogues can lead to a better understanding of silicon's bonding properties. A full-dimensional quantum study of acetylene/vinylidene isomerisation was done by Zou and Bowman [18]. The global minimum structure is the triply-bonded acetylene form (linear form) followed by a transition state (TS) and doubly-bonded vinylidene (as a second minimum). The heat of isomerisation between acetylene and vinylidene has been studied by Lineberger and co-workers using ultraviolet photoelectron spectroscopy showing a value of 46.4 ± 5.5 kcal/mol [19]. An ab initio investigation of the isomerisation reported the energy of reaction to be 43.91 ± 0.5 kcal/mol (CBS-QCI/APNO model of Petersson [20]) or 45.18 kcal/mol (CCSD(TQ)/CBS by Chang, Shen and Yu [21]). One of the most interesting

classes of silicon species is silicon hydrides in terms of bonding, energetic and structural properties. Comparing the Si_2H_2 isomers to their carbon analogues led to remarkable observations and conclusions. For many years, many theoreticians tried to find the best structure and energetic properties of the Si_2H_2 species. For instance, the earliest calculations by Wirsam [22] showed the acetylene-type form as the minimum, however, a later study disproved this (having two imaginary frequencies [23]) in favour of the vinylidene form. A few years later the global minimum structure corresponding to the dibridged form was found by Lischka and Köhler [12].

Coupled-cluster theory investigations of the Si_2H_2 isomers were performed by Grev and Schaefer [24] and the isomers obtained are as follows with relative energies in parentheses: dibridged (0 kcal/mol), monobridged (8.7 kcal/mol), vinylidene (11.6 kcal/mol) and trans (16.3 kcal/mol). The $\text{Si}(\text{H})_2\text{Si}$ (dibridged C_{2v}) and $\text{HSi}(\text{H})\text{Si}$ (monobridged C_s) isomers were observed experimentally (by microwave and IR spectroscopy [25, 26]). A schematic plot of the Si_2H_2 isomers is shown in Figure 4.1-1 (page 57). The experiments verified the earlier theoretical predictions of Lischka and Köhler [12] and Grev and Schaefer [24].

An effort to find experimentally linear triple bonded Si–Si species has remained a challenge. However, Sekiguchi and co-workers synthesised 1,1,4,4-tetrakis[bis(trimethylsilyl)methyl]-1,4-diisopropyl-2-tetrasilene, a stable compound with a Si–Si triple bond [27], the picture of the compound can be seen below:



X-ray crystallographic analysis confirmed the triple bond as trans-bent with a bond angle of 137.44° , bond length of 2.062 \AA and with the four Si atoms coplanar [27]. The structure is very similar to $(^t\text{Bu}_3\text{Si})_2\text{MeSiSi}\equiv\text{SiSiMe}(\text{Si}^t\text{Bu}_3)_2$, where ^tBu is *tert*-butyl, calculated using DFT methods [28]. The natural bond order (NBO) analysis done by Sekiguchi shows electron occupation of the two π orbitals (1.934 and 1.897 electrons)

[27]. The bond order (Wiberg bond index) of $\text{Si}\equiv\text{Si}$ is 2.618, indicating a genuine Si triple bond, but the value is still less than 3 (the value calculated for acetylene) [27].

Compounds containing mixtures of Si and C elements were investigated as well in addition to Si_2H_2 and C_2H_2 . The Si_2H_2 and SiCH_2 molecules were studied theoretically by Frenking et al. [29] using the MP2 and CCSD(T) levels of theory. They showed that the SiCH_2 species differ from the Si_2H_2 structures. The global minimum of the SiCH_2 structures is the vinylidene form (hydrogens connected to the carbon atom) followed by trans (34 kcal/mol above) and another vinylidene form (hydrogens connected to the silicon atom) which is 84 kcal/mol less stable than the global minimum. A bridged structure was not found. What is really interesting is that the linear form of SiCH_2 is a higher-order saddle point on the PES. Thus, the substitution of a silicon by a carbon atom in C_2H_2 changed the properties of the PES. The geometries represent different stationary points on the PESs. The question should be asked then, what if we substituted one or two hydrogens in Si_2H_2 by other elements such as F, Cl or Li? What properties are we able to find and how do they change our understanding of the small cluster species of the group 14 elements?

We are aware of theoretical work on the Si_2HY and Si_2Y_2 structures (where $\text{Y}=\text{F}, \text{Cl}, \text{Br}$ and Li) done by Bei and Feng [30]. It appears that the Si_2HY and Si_2Y_2 structures were optimized using the RHF/6-31G** level of theory. Thus, the results calculated here will not be compared with such a low-level (uncorrelated) calculation.

Plasmas of silicon are used for chemical vapor deposition (CVD) in the microelectronics industry. Also in the etching of metal surfaces halogenated silanes (SiF_4 and SiCl_4) were found on surfaces such as copper [31, 32]. Moreover many of the reactive silanes produced in such processes were studied experimentally [33], however, other silicon compounds can occur in this type of plasma but because of their transient nature and short lifetime, it is only possible to study them theoretically [34].

Fluorides and chlorides of silicon were investigated both experimentally and theoretically. Experimental thermodynamic studies were done by Walsh [35]. Ignacio and Schlegel investigated theoretically numerous fluorine and chlorine silicon

compounds [36, 37]. An extensive coupled cluster study was performed on a set of mixed silicon hydrides and halides ($\text{SiH}_n\text{X}_{m-n}$ where $\text{X}=\text{F}, \text{Cl}$; $m=1-4$; and $n=0-m$) by Wilson et al. [34]. The work presented theoretical and experimental results such as the geometric properties, atomization energies and enthalpies of formation.

Alkali-silicon species are used as power resource materials or emitters and can also serve as promoters in catalysts [38, 39]. We are aware of the growing importance of lithium and its connection with the silicon atom in modern industry, for example silicon lithium-ion batteries. Thus, any investigation of electronic and bonding properties (vibrations, rotations, anharmonic constants) for small molecules containing Si and Li atoms can enhance the known knowledge of such structures.

The classical and inverted structures of SiH_3Li and SiH_3Na were studied before, both experimentally and theoretically [40, 41]. Small clusters of the Si_nLi_x type (where $n=2-10$ and $x=0-2$) were investigated theoretically [42-45]. The theoretical studies of mixed silicon-lithium clusters $\text{Si}_n\text{Li}_p^{(+)}$ (where $n=1-6$ and $p=1-2$) and Si_nM_p clusters (where $\text{M}=\text{Li}, \text{Na}$ and K , $n \leq 6$ and $p \leq 6$) performed by Aubert-Frecon et al. are significant, as a part of the investigation concerned the Si_2Li_2 and $\text{Si}_2\text{Li}_2^{(+)}$ species. They found that the global minimum is a dibridged structure followed (in the $\text{Si}_2\text{Li}_2^{(+)}$ case) by trans (0.266 eV) and dibridged-planar (1.273 eV) structures. The trans structure in neutral Si_2Li_2 clusters is not a minimum, however, and the dibridged structure is still the global minimum, followed by dibridged-planar (1.420 eV) and monobridged (1.673 eV). Note, that the investigation by Aubert-Frecon et al. did not contain identification of minima and transition states of Si_2Li_2 which will be provided here. Both the SiLi and Si_2Li_2 species were studied experimentally in the gas phase by mass spectrometry by Ihle et al. [46]. Unfortunately, the work was published in a conference proceeding in a limited edition in the 1970's and it is not accessible to us.

PES calculations are very helpful to model chemical reactions including isomerisation processes. Furthermore, ro-vibrational calculations can be performed if a full-dimensional PES is known, which makes spectroscopic astrophysical or molecular identifications easier. However, full-dimensional PES calculations require the

calculation of energies of at least several thousand different configurations of the molecular system. Also the requirement of multidimensional fitting functions during hypersurface construction only increases the complexity of such studies.

The calculation of the critical points on the PES of the Si_2H_2 species was done using DFT and *ab initio* calculations by Jursic [47, 48]. Furthermore, extensive potential energy hypersurface calculations of the SiH_2 system were carried out by Gordon et al. [49] and the potential energy and dipole moment surface of the SiHCl_3 species was investigated by He et al. [50]. Moreover the PES of hydrogen abstraction on the $\text{Si}(100)$ surface was done by Nakmura [51]. An extended PES calculation of the Si_2H_2 structures was performed by Law et al. [52]. Nevertheless full six-dimensional potential energy surfaces of 4-atom species containing silicon atoms are quite rare in the literature.

Thus, any new potential energy surface investigations of small silicon clusters will enhance our understanding and knowledge of molecular dynamics and ro-vibration properties of such systems.

Various energy units were used to simplify comparison of the calculated results with the literature; thus the energy conversion table below was prepared to help the reader. The table is taken from Ref. [53].

Energy Conversion Table					
	Hartree	eV	cm^{-1}	kcal/mol	kJ/mol
Hartree	1	27.2107	219474.63	627.509	2625.5
eV	0.0367502	1	8065.73	23.069	96.4869
cm^{-1}	4.55633×10^{-6}	1.23981×10^{-4}	1	0.0028591	0.011963
kcal/mol	0.00159362	0.0433634	349.757	1	4.184

Theory and methods

In this thesis I used quantum chemical methods to study the geometric and bonding properties of substituted disilynes. The methods used in the present work will be briefly explained below.

1 *Ab initio* and DFT methods.

1.1 Born-Oppenheimer approximation.

The time-independent Schrödinger equation ($\hat{H}\Psi = E\Psi$, where \hat{H} is the Hamiltonian operator, Ψ is the wave function and E is the total energy of the given wavefunction) can be solved exactly only for the H_2^+ molecule and very similar one electron systems. One year after the great achievement of Schrödinger, Born and his PhD student Oppenheimer proposed a “way” to make it possible to compute the wavefunction in practical approximations. The Born-Oppenheimer (BO) approximation is the assumption that the wavefunction ψ of a molecule can be separated into its electronic and nuclear (vibrational, rotational) components [54]:

$$\Psi_{\text{total}} = \Psi_{\text{electronic}} \times \Psi_{\text{nuclear}}. \quad 1.1-1$$

This considers the nuclei as stationary, which is a reasonable approximation, as the nuclei are very heavy in comparison to the electrons. The Hamiltonian operator can be written as:

$$\hat{H} = \hat{T}_N + \hat{T}_e + \hat{V}_{ee}(r) + \hat{V}_{NN}(R) + \hat{V}_{eN}(r, R), \quad 1.1-2$$

where, \hat{T}_N , \hat{T}_e , \hat{V}_{ee} , \hat{V}_{NN} and \hat{V}_{eN} represent the nuclear and electron kinetic energy operators and electron-electron nuclear-nuclear and electron-nuclear interaction potential operators, respectively. The quantity “ r ” stands for all electronic coordinates and “ R ” for all nuclear coordinates.

According to the assumption that nuclear kinetic energy can be neglected, the operator \hat{T}_N (consisting of the kinetic energy operators for each nucleus in the system) can be removed from the total Hamiltonian. Thus, the electronic Schrödinger equation can be expressed as:

$$\hat{H}_e(R)\Psi_i(r, R) = E_i(R)\Psi_i(r, R); \quad i=1, 2, \dots, \infty. \quad 1.1-3$$

In the remaining electronic Hamiltonian ($\hat{H}_e = \hat{T}_e + \hat{V}_{ee}(r) + \hat{V}_{eN}(r, R)$), the nuclear positions are frozen, and the eigenfunctions, $\Psi(r, R)$ and eigenvalue $E_e(R)$ depend parametrically on the nuclear positions. Moreover, for each solution of equation 1.1-3 the nuclear eigenvalue equation is:

$$[\hat{T}_N + \hat{V}_{NN}(R) + \varepsilon_n(R)]\chi(R) = E\chi(R). \quad 1.1-4$$

The $\varepsilon_n(R)$ (electronic energy eigenvalue) allows us to construct the static (time-invariant) electronic potential energy if the nuclear positions remain fixed. Furthermore, repeated calculations at different nuclear positions generate a potential energy surface (PES). The addition of the $\hat{V}_{NN}(R)$ to the $\varepsilon_n(R)$ represents the full internuclear potential energy surface and $\chi(R)$ is the nuclear wave function. The $E\chi(R)$ eigenvalue is the total energy of the molecule.

The Born-Oppenheimer approximation is usually a reasonable approximation, but breaks down when two solutions to the electronic Schrödinger equation come close together energetically. The LiF molecule is a good example [55].

1.2 Hartree-Fock method.

We can consider several methods to solve the Schrödinger equation that include the Born-Oppenheimer approximation.

Hartree with contributions from Slater and Fock formulated the Hartree-Fock method in the 1930's. Slater introduced exponential functions (Slater Type Orbitals), which describe atomic orbitals and express the antisymmetric wave function of fermions in the form of determinants. Fock derived the Fock state and Fock space, which are used to describe the quantum state with a variable or unknown number of particles.

The wavefunction Ψ is expressed as a combination of molecular orbitals ϕ_i . As a consequence of the Pauli principle the wavefunction must be antisymmetric with respect to interchange of any two electron positions [55]. Therefore, to achieve the antisymmetry requirement the Slater determinant (SD) is used. Furthermore the wavefunction is described by a single Slater determinant of N spin-orbitals. Single-electron wave functions (orbitals) are represented in columns while the rows represent the coordinates of space and spin. A two-particle system (x_1 and x_2) the SD can be written as:

$$\Psi(x_1, x_2) = \frac{1}{\sqrt{2}} \begin{vmatrix} \chi_1(x_1) & \chi_2(x_1) \\ \chi_1(x_2) & \chi_2(x_2) \end{vmatrix}. \quad 1.2-1$$

Each unknown Hartree-Fock orbital ϕ_i can be expressed as a linear expansion of a set of known (normalized) basis functions χ , (conventionally called atomic orbitals):

$$\phi_i = \sum_{\alpha}^{M_{\text{basis}}} c_{\alpha i} \chi_{\alpha}, \quad 1.2-2$$

where M_{basis} is the number of basis functions and $c_{\alpha i}$ is the molecular orbital expansion coefficient. To solve for the set of molecular orbital expansion coefficients $c_{\alpha i}$ the variational principle is used, which allows to find the set of coefficients that minimize the energy of the resultant wavefunction [56]. The variation principle states that the energy of an approximate wavefunction is above or the same as the exact energy. The eigenvalue equations for each spinorbital can be then written then as:

$$\hat{F}_i \phi_i = \epsilon_i \phi_i, \quad 1.2-3$$

where ϕ_i are a set of molecular orbitals, called Hartree-Fock molecular orbitals and \hat{F} is

the Fock operator [55]. It describes the kinetic energy of the electron, its attraction to the nuclei and its repulsion from a mean field of the other electrons in the atomic or molecular system.

The matrix form of equation 1.2-2 is non-linear and must be solved iteratively: this procedure is usually called the "self-consistent field method."

Basis sets

There are two types of normalized basis functions χ (shown in equation 1.2-2), which are used in electronic structure calculations: Slater Type Orbitals (STO) and Gaussian Type Orbitals (GTO). Slater Type Orbitals can be expressed as:

$$\chi_{\zeta, l_x, l_y, l_z}(x, y, z) = N x^{l_x} y^{l_y} z^{l_z} e^{-\zeta r} \quad 1.2-4$$

While Gaussian Type Orbitals can be written as:

$$\chi_{\zeta, l_x, l_y, l_z}(x, y, z) = N x^{l_x} y^{l_y} z^{l_z} e^{-\zeta r^2} \quad 1.2-5$$

N is a normalization constant and the sum of l_x , l_y and l_z determines the type of orbitals (for example: $l_x+l_y+l_z=1$ represents a p-orbital) [55] and ζ (zeta) controls the width of the orbital (large ζ gives a tight function, small ζ gives a diffuse function). STO's are more accurate than GTO's, however the GTO's are much easier in computations because of the Gaussian product theorem which states that the product of two arbitrary Gaussian functions on different centers A and B is a single Gaussian located between the two original Gaussians.

All basis sets (no matter what type) vary mostly by the number of functions used. The smallest number of basis functions needed for an atom is called a minimal basis set. For example: for H: 1s and for C: 1s, 2s, 2p_x, 2p_y, 2p_z. Minimal basis sets use fixed-size atomic-type orbitals. However, the minimal basis set is not accurate enough to correctly describe molecular properties, for example bonding. Thus, to improve the basis set the number of basis functions per atom can be increased [56]. If the number of basis functions are doubled (or tripled etc.), this produces a Double Zeta (Triple Zeta etc.) type basis. Now in Double Zeta for H: 1s, 1s' and for C: 1s, 1s', 2s, 2s', 2p_x, 2p_y, 2p_z, 2p_x', 2p_y', 2p_z'. The primed and unprimed orbitals differ in size and allow for different

bonding in different directions [55]. The above improvement allows orbitals to change size but not to change shape. Thus, polarized basis sets are introduced to remove this limitation [56]. Polarized basis sets are constructed by addition of orbitals with higher angular momentum. For example, polarized basis sets add p or higher functions to hydrogen atoms and d or higher functions to carbon atoms. This approach improves the description of molecular bonds [55]. To describe properly anionic molecules or systems with lone-pairs, diffuse functions are needed. Diffuse functions are larger-sized versions of s- and p- type functions [56] and have small ζ exponents (electrons are found far away from the nucleus).

There are many different types of basis sets like Pople style basis sets or correlation consistent basis sets.

The Pople style basis sets were developed by Pople (Nobel Laureate) [57]. STO-3G is a minimal basis set, in which Slater type orbitals are approximated by three Gaussians (3G). Pople's split-valence basis sets are called 3-21G, 6-31G or 6-311G. For example in 6-31G the core orbital is a contracted-GTO, which is a fixed linear combination of six Gaussians, and the valence shell is represented by two orbitals: one contracted-GTO made of three Gaussians and one single Gaussian. Diffuse functions (denoted by +) and polarization functions (denoted by s, p or d labels) can be added to each of the Pople style basis sets.

Correlation consistent basis sets were developed by Dunning [58]. These basis sets are designed to recover the correlation energy of the valence electrons [55] and are mostly used in post-Hartree-Fock methods (discussed below). Correlation consistent split-valence basis sets are known by the acronym cc-pVXZ, which means correlation consistent polarized Valence X-zeta basis (where X=2-10). The correlation consistent basis sets can be augmented by diffuse functions (denoted by prefix "aug-") or additional tight functions. There are also basis sets specially developed to recovery the core-core and core-valence electron correlation (cc-pCVXZ), calculate relativistic corrections (cc-pVXZ-DK) or even designed for specific methods such as the F12 method (cc-pVXZ-F12).

Different sizes of basis sets or different types of basis sets can calculate the molecular energy, geometric properties or vibrational frequencies with a different accuracy and so the performance of different types of basis sets will be studied here.

1.3 MP2 method.

The motion of the electrons is correlated, a phenomenon that is not described by the Hartree-Fock method. On average, electrons are further apart than described by the Hartree-Fock method. The energy difference between the Hartree-Fock energy and exact energy (for a given basis set) is called the electron correlation energy. The neglect of electron correlation in the Hartree-Fock method can lead to unphysical results in comparison to experiment. A number of approaches to this weakness, usually called post-Hartree-Fock methods, have been formulated. These methods include electron correlation in the multi-electron wave function. One of these approaches, Møller–Plesset (MP) perturbation theory, treats correlation as a perturbation of the Fock operator [59].

Møller–Plesset perturbation theory can be expressed mathematically by employing Rayleigh–Schrödinger perturbation theory (RS-PT), which treats the exact Hamiltonian as a sum of the unperturbed Hamiltonian H_0 and a small (external) perturbation H' [59]:

$$\hat{H} = \hat{H}_0 + \lambda \hat{H}', \quad 1.3-1$$

where the λ is a parameter determining the strength of the perturbation [55]. The energy and wavefunction can then be written as a Taylor expansion:

$$\Psi = \lambda^0 \Psi_0 + \lambda^1 \Psi_1 + \lambda^2 \Psi_2 + \lambda^3 \Psi_3 + \dots, \quad 1.3-2$$

$$E = \lambda^0 E_0 + \lambda^1 E_1 + \lambda^2 E_2 + \lambda^3 E_3 + \dots, \quad 1.3-3$$

where Ψ_n is the n -th order correction of the wave function. The n -th order energy or wavefunction is a sum of all terms up to order n if the λ parameter is equal to 1 [55].

Thus we can collect all terms with the same power of λ and get:

$$\begin{aligned} \lambda^0: \hat{H}_0 \Psi_0 &= E_0 \Psi_0 \\ \lambda^1: \hat{H}_0 \Psi_1 + \hat{H}' \Psi_0 &= E_0 \Psi_1 + E_1 \Psi_0 \\ \lambda^2: \hat{H}_0 \Psi_2 + \hat{H}' \Psi_1 &= E_0 \Psi_2 + E_1 \Psi_1 + E_2 \Psi_0 \\ \lambda^n: \hat{H}_0 \Psi_n + \hat{H}' \Psi_{n-1} &= \sum_{i=0}^n E_i \Psi_{n-i}. \end{aligned} \quad 1.3-4$$

The zero-order wavefunction is the Hartree-Fock determinant, and the zero-order energy is just a sum of MO energies [55], thus:

$$E_1 = \langle \phi_0 | \hat{H}' | \phi_0 \rangle. \quad 1.3-5$$

$$MP0 = E(MP0) = \sum_{i=1}^N \epsilon_i, \quad 1.3-6$$

$$MP1 = MP0 + E(MP1) = E(HF). \quad 1.3-7$$

It is seen that the first-order energy is exactly the HF energy.

Note that the electron correlation energy starts at second order [55].

In order to obtain the MP2 formula for a closed-shell molecule, the second-order RS-PT formula involves a sum over doubly-excited determinants. (Singly-excited Slater determinants do not contribute because of the Brillouin theorem [55]). This is obtained by promoting two electrons from occupied orbitals i and j to virtual orbitals a and b .

The difference in the total energy of two Slater determinants is a difference in MO energies, and the second-order Møller–Plesset correction can be written explicitly as:

$$E(MP2) = \sum_{i < j}^{\text{occ}} \sum_{a < b}^{\text{vir}} \frac{[\langle \phi_i \phi_j | \phi_a \phi_b \rangle - \langle \phi_i \phi_j | \phi_b \phi_a \rangle]^2}{\epsilon_i + \epsilon_j - \epsilon_a - \epsilon_b}. \quad 1.3-8$$

Note that eq. 1.3-5 is presented in the Dirac notation, which is also used in the other theoretical chapters. The Dirac "bracket (or bracket)" notation defines the "ket" as the vector denoted by $|\psi\rangle$, and the "bra" as the vector denoted by $\langle\phi|$. The "bra" is the conjugated transpose of the "ket" and the "bracket" is then defined by $\langle\phi|\psi\rangle$ which can be mathematically expressed as:

$$\langle\phi|\psi\rangle \equiv \int \phi^*(x) \psi(x) dx. \quad 1.3-9$$

More details can be found in Ref. [60].

1.4 Coupled Cluster method.

The theoretical background of Coupled Cluster (CC) theory was formed in the 60's by Čížek [61]. Generally it starts from the Hartree-Fock method and adds all types of corrections, single, double, triple etc (S, D, T etc), to the reference wave function [55]. The coupled-cluster wavefunction can be written as an exponential Ansatz [62]:

$$\Psi_{cc} = e^{\hat{T}} \phi_0, \quad 1.4-1$$

where ϕ_0 is a reference HF wavefunction and the cluster operator is written as

$$\hat{T} = \hat{T}_1 + \hat{T}_2 + \hat{T}_3 + \dots \quad 1.4-2$$

\hat{T}_1 is the operator of all single excitations; \hat{T}_2 is the operator of all double excitations and so forth. These excitation operators are expressed as:

$$\hat{T}_1 \phi_0 = \sum_i^{\text{occ}} \sum_a^{\text{vir}} t_i^a \phi_i^a, \quad 1.4-3$$

$$\hat{T}_2 \phi_0 = \sum_{i<j}^{\text{occ}} \sum_{a<b}^{\text{vir}} t_{ij}^{ab} \phi_{ij}^{ab}. \quad 1.4-4$$

The unknown coefficients t_i^a and t_{ij}^{ab} need to be found to obtain the approximate solution Ψ . In equation 1.4-3 and 1.4-4 i, j stand for occupied and a, b for unoccupied orbitals. The ϕ_i^a and ϕ_{ij}^{ab} terms represent single and double excitations from occupied orbitals (a, b) to unoccupied orbitals (i, j), respectively. Taking into consideration the structure of \hat{T} , the exponential operator $e^{\hat{T}}$ can be expanded into a Taylor series:

$$e^{\hat{T}} = 1 + \hat{T}_1 + \left(\hat{T}_2 + \frac{1}{2} \hat{T}_1^2 \right) + \left(\hat{T}_3 + \hat{T}_2 \hat{T}_1 + \frac{1}{6} \hat{T}_1^3 \right) + \dots \quad 1.4-5$$

The \hat{T}_1 operator generates all singly-excited states. The first term in brackets generates all doubly-excited states: the connected \hat{T}_2 excitations (which correspond to two electrons interacting simultaneously) or disconnected \hat{T}_1^2 excitations (which correspond to one non-interacting pair of interacting electrons) [55]. The second term in brackets groups all triply-excited states ("true" \hat{T}_3 or "product" triples $\hat{T}_2 \hat{T}_1$ and \hat{T}_1^3) [55].

The CC and MP methods are closely connected. At fourth order (singles, doubles, triples, and quadruples) in Møller–Plesset perturbation theory (indicated as MP4) the quadruples correspond to the disconnected \hat{T}_2^2 term in CC language and the triples corresponds to \hat{T}_3 . The perturbation theory suggests that the most important term is \hat{T}_3 followed by \hat{T}_2 . If we assume that the perturbation series is well converged at fourth

order, the CCD energy is equivalent to MP4(DQ) and CCSD corresponds to MP4(SDQ). We can therefore obtain MP2, MP3 and MP4(SDQ) in the first iterations of CCSD. The CCSDT method includes also connected triples but is a very expensive method. A hybrid method has been constructed where the triples term arises from fifth-order perturbation theory. This method is labelled CCSD(T) [55]. CCSD(T) is often called "the gold standard of quantum chemistry" for its excellent compromise between accuracy and computational cost [62].

The \mathcal{T}_1 diagnostic can be used to determine the quality of the coupled cluster method. The \mathcal{T}_1 diagnostic is the norm of the vector of the T1 amplitudes scaled by the number of correlated electrons N : $\mathcal{T}_1 = \frac{|\mathbf{T}_1|}{\sqrt{N}}$. Lee et al. [63] suggested that if \mathcal{T}_1 is greater than 0.02 then the wavefunction of the system might have significant multiconfigurational character. Nevertheless, Martin et al. and Cai et al. [64, 65], showed that CCSD(T) gives reasonable results for \mathcal{T}_1 diagnostic values as high as 0.08. Thus, this value will be taken as the upper limit in the coupled cluster calculations performed here.

1.5 Explicitly correlated method-CCSD(T)-F12a/b.

The excellent accuracy of the CCSD(T) method is generally known but the CCSD(T) method suffers from two major problems: $O(N^7)$ scaling of computational cost with increasing molecular size and slow convergence of the correlation energy with increasing basis set size [66]. To obtain very good and fast convergence it is necessary to use large basis sets. Electron correlation is important for the potential energy surface [67]. The explanation of slow convergence of the correlation energy is that the shape of the wavefunction cusp (where two electrons approach each other) for small to intermediate values of interelectronic distances r_{12} is not well described by expansion in products of one-electron functions (orbitals) [68].

Hylleraas in his work in 1929 on the He atom [69] noticed that the wavefunction is linear in the cusp region so he introduced the new idea where the wavefunction Ansatz is augmented with one extra two-electron function r_{12} [68]. The new approach was called the explicitly correlated method R12. The R12 method was implemented by Kutzelnigg and Klopper for MP2 [70] and also extended to coupled cluster [71, 72] and MRCI [73]. The early explicitly correlated methods had problems due to the occurrence of many-electron integrals in the R12 formalism. The three-electron and four-electron integrals are extremely difficult to calculate.

To improve efficiency and other problems many different approximations and new ideas were proposed:

- The resolution of the identity (RI) approximation proposed by Kutzelnigg [74]. The many-electron integrals are expressed in terms of sums of products of simpler two-electron integrals [66, 68].

Mathematically $I = \sum |i\rangle\langle i|$ (where "I" is the identity operator and " $|i\rangle$ " is a orthonormal basis) [75]. In the case of the R12/F12 methods the RI is used to approximate the integrals in the projector \hat{Q}_{12} : $\hat{Q}_{12}|\alpha\beta\rangle\langle\alpha\beta| = \hat{Q}_{12}$ [76]. More detailed explanations can be found in Ref. [74, 75].

- Fixed-amplitude Ansätze and an alternative Ansatz for MP2-R12 [68]. The alternative Ansatz has been used to avoid numerical problems in the optimized

wavefunction in large molecules, and fixed amplitude Ansätze have been used to avoid geminal basis set superposition errors. The advantages and disadvantages of these approaches have been discussed in references [68, 76].

- Dealing with the four-electron integrals by using the weak orthogonality functional of Szalewicz (the weak orthogonality functional is a name for the variational functional introduced by Szalewicz and co-workers [77]).
- The density fitting (DF) approximation was introduced by Ten-no and Manby [78] and is used to rearrange the three-electron integrals before using the resolution of the identity to decompose them into expressions involving only two-electron integrals [78].
- Complementary auxiliary basis sets (CABSs). The resolution of identity uses auxiliary basis sets (ABS) to deal with the many-electron integrals but this approach gives large RI errors so Valeev proposed an approximation that involves expansion in the orthogonal complement of the orbital basis set (OBS) [79]. The new formulation is labelled the complementary auxiliary basis set (CABS) approach [79]. The CABS approach is found to be more numerically robust than the ABS counterpart.

It turned out, however, that even using the above approximations and concepts the accuracy of the correlation energies was still unsatisfactory when small or medium-size basis sets were used [80]. This was solved using a non-linear short-range correlation factor, such as a Slater-type function $F_{12} = \exp(-\gamma r_{12})$. This was proposed by Ten-no [81] and implemented in MP2-F12 by May and Manby [82]. F12 methods use a non-linear short-range correlation factor F_{12} rather than the linear correlation factor r_{12} in the R12 methods [80].

Later many extensions to coupled-cluster theory (CCSD-F12) were introduced [71, 72, 83, 84].

In this work I focus only on the CCSD(T)F12a/b methods developed by Werner and co-workers and implemented in the MOLPRO quantum calculation package [85]. In these

methods the only additional effort as compared to standard CCSD(T) is an initial MP2-F12 calculation [80]. I will introduce this method in more detail below.

In the following i, j, k, l, m, n will denote occupied orbitals; a, b, c, d will denote virtual orbitals; r, s, t, u will denote any orbitals representable in the AO basis; α, β will denote the orbitals of a formally complete virtual space and x, y will denote CABS.

The CCSD-F12 wavefunction has the form:

$$\Psi_{\text{CCSD-F12}} = e^{\hat{T}_1 + \hat{T}_2} \Psi_{\text{HF}}, \quad 1.5-1$$

where Ψ_{HF} is the Hartree-Fock reference function.

$$\hat{T}_1 = t_a^i \hat{E}_i^a, \quad 1.5-2$$

$$\hat{T}_2 = \frac{1}{2} T_{ab}^{ij} \hat{E}_{ij}^{ab} + \frac{1}{2} \mathcal{T}_{\alpha\beta}^{ij} \hat{E}_{ij}^{\alpha\beta}, \quad 1.5-3$$

where \hat{E}_i^a and $\hat{E}_{ij}^{\alpha\beta}$ are the usual spin-free one- and two-electron excitation operators and t_a^i are expansion coefficients.

The \hat{T}_1 and \hat{T}_2 are single and double excitation cluster operators. \hat{T}_1 and the first part of \hat{T}_2 (including the \hat{E}_i^a and \hat{E}_{ij}^{ab} operators for excitations into the standard virtual orbitals a and b) are the same as in standard CCSD, while the new additional term $\mathcal{T}_{\alpha\beta}^{ij}$ adds the explicitly correlated contributions:

$$\mathcal{T}_{\alpha\beta}^{ij} = \langle \alpha\beta | \hat{Q}_{12} F_{12} | mn \rangle T_{mn}^{ij}. \quad 1.5-4$$

The F_{12} operator is a short-range correlation factor. The projector \hat{Q}_{12} is needed to make the F_{12} configurations ($|\Phi_{ij}^{mn}\rangle = \mathcal{F}_{\alpha\beta}^{mn} \hat{E}_{ij}^{\alpha\beta} |\Phi\rangle$) orthogonal.

If we want to describe the wavefunction cusp for $r_{12} \rightarrow 0$ over the whole range of interelectronic distances correctly we need to use different Slater-type functions. Ten-no showed [81] that the Slater-type function $F_{12} = \exp(-\gamma r_{12})$ has better basis set convergence and numerical stability than the linear factor r_{12} . At the same time May and Manby [82] developed the MP2-F12 method where F_{12} is approximated by the frozen linear combination of Gaussians:

$$F_{12} = \sum_i c_i \exp(-\alpha_i r_{12}^2). \quad 1.5-5$$

We can get a simple explicitly correlated form of the CCSD equations by inserting the wavefunction of eq. 1.5-1 into the time-independent Schrodinger equation to get:

$$\langle \tilde{\Phi}_i^a | \Psi_{\text{CCSD-F12}} \rangle = t_a^i, \quad 1.5-6$$

$$\langle \tilde{\Phi}_{ij}^{ab} | \Psi_{\text{CCSD-F12}} \rangle = T_{ab}^{ij} + t_a^i t_b^j. \quad 1.5-7$$

The energy and the singles and doubles residuals (residual is mathematical terminology to deal with integrals or differentials where we look for the approximation with small residual (error) [86, 87]) are:

$$E = \langle \Phi | \hat{H} | \Psi_{\text{CCSD-F12}} \rangle \quad 1.5-8$$

$$R_a^i = \langle \tilde{\Phi}_i^a | \hat{H} - E | \Psi_{\text{CCSD-F12}} \rangle \quad 1.5-9$$

$$R_{ab}^{ij} = \langle \tilde{\Phi}_{ij}^{ab} | \hat{H} - E | \Psi_{\text{CCSD-F12}} \rangle. \quad 1.5-10$$

Werner and co-workers noticed that the dependence on the energy in the residual equations (1.5-9 and 1.5-10) cancels out automatically [68]. The equations (1.5-9 and 1.5-10) contain additionally the explicitly correlated terms but the number of equations is the same as in conventional CCSD.

We can write the CCSD-F12 doubles residual (eq.1.5-10) in matrix form:

$$R_{\text{CCSD-F12}}^{ij} = R_{\text{MP2-F12}}^{ij} + K(\mathcal{D}^{ij}) + K(\mathcal{T}^{ij}) + \alpha_{ij,kl} D^{kl} + G^{ij} + G^{ij\dagger}. \quad 1.5-11$$

The general form of this expression and the explanation of each term is given in [88], except that the Fock-operator terms in the MP2 residual are included in the matrices G^{ij} [68].

The first term is the MP2-F12 residual:

$$R_{\text{MP2-F12}}^{ij} = K^{ij} + fT^{ij} + T^{ij}f - f_{ik}T^{kj} - T^{ik}f_{kj} + C^{mn}T_{mn}^{ij}. \quad 1.5-12$$

Only the last term $C^{mn}T_{mn}^{ij}$ is different from conventional MP2 residuals. The coupling matrices C^{ij} are defined as (using approximation 3C and CABS) [68]:

$$C_{ab}^{ij} = \langle ab | (\hat{f}_1 + \hat{f}_2) \hat{Q}_{12} F_{12} | ij \rangle \approx f_{ax} F_{xb}^{ij} + F_{ax}^{ij} f_{xb}. \quad 1.5-13$$

The integrals that are needed in MP2-F12 are evaluated using the DF (density fitting) approximation (density fitting is a way to approximate the usual two-electron integrals) [78].

The next two important terms in $R_{\text{CCSD-F12}}^{\text{ij}}$ are $K(\mathcal{D}^{\text{ij}})$ and $K(\mathcal{T}^{\text{ij}})$. $K(\mathcal{D}^{\text{ij}})$ is an external exchange operator and includes all contractions of the doubles amplitudes with integrals involving three or four virtual orbitals and has the form [68]:

$$[K(\mathcal{D}^{\text{ij}})]_{\text{ab}} = \langle \text{ab} | r_{12}^{-1} | \text{rs} \rangle \mathcal{D}_{\text{rs}}^{\text{ij}}. \quad 1.5-14$$

The $K(\mathcal{T}^{\text{ij}})$ term describes corrections of the external exchange operators due to the explicitly correlated terms:

$$[K(\mathcal{T}^{\text{ij}})]_{\text{ab}} = V_{\text{ab}}^{\text{mn}} T_{\text{mn}}^{\text{ij}}. \quad 1.5-15$$

$T_{\text{mn}}^{\text{ij}}$ is nonlinear and so leads to multiple RI expansions and also we need to deal with additional integrals over three or four external orbitals [68]. To evaluate the G^{ij} matrices in eq. 1.5-11 a projector is used which is very difficult to approximate accurately in this case and a large basis set is needed to do so.

Werner et al. [66, 68] proposed the new CCSD-F12a approximation to deal with the above problems. They neglected all contributions of the explicitly correlated configurations to the doubles residual $R_{\text{CCSD-F12a}}^{\text{ij}}$ but left $K(\mathcal{T}^{\text{ij}})$ and $C_{\text{ab}}^{\text{ij}}$ in MP2-F12. The new residual can be written as:

$$\Delta R_{\text{CCSD-F12a}}^{\text{ij}} = [V^{\text{mn}} + C^{\text{mn}}] T_{\text{mn}}^{\text{ij}}, \quad 1.5-16$$

where projector in V^{mn} is approximated as $1 - |rs\rangle\langle rs|$ then $V_{\text{rs}}^{\text{mn}} = W_{\text{rs}}^{\text{mn}} - K(F^{\text{mn}})_{\text{rs}}$ and:

$$W_{\text{rs}}^{\text{mn}} = \langle \text{rs} | r_{12}^{-1} F_{12} | \text{mn} \rangle, \quad 1.5-17$$

$$K(F^{\text{mn}})_{\text{rs}} = \langle \text{rs} | r_{12}^{-1} | \text{tu} \rangle F_{\text{tu}}^{\text{mn}}, \quad 1.5-18$$

and C^{mn} has the same form as in eq. 1.5-13.

We note that $K(F^{\text{mn}})$ and $K(\mathcal{D}^{\text{ij}})$ have the same form so the total residual (in matrix form) can be written as:

$$R_{\text{CCSD-F12a}}^{\text{ij}} = R_{\text{MP2}}^{\text{ij}} + \bar{C}^{\text{ij}} + \bar{W}^{\text{ij}} + \hat{K}(\mathcal{D}^{\text{ij}} - \bar{F}^{\text{ij}}) + \alpha_{\text{ij,kl}} D^{\text{kl}} + G^{\text{ij}} + G^{\text{ij}\dagger}, \quad 1.5-19$$

where $\bar{F}_{rs}^{ij} = F_{rs}^{mn} T_{mn}^{ij}$ and $\bar{W}_{rs}^{ij}, \bar{C}^{ij}$ are defined in the same way. We need to remember that the fixed amplitude Ansatz (needed in the 3C approximation) is defined as:

$$\bar{F}_{rs}^{ij} = \frac{3}{8} F_{rs}^{ij} + \frac{1}{8} F_{sr}^{ij}.$$

The operator $\hat{K}(\mathcal{D}^{ij} - \bar{F}^{ij})$ can be computed from integrals in the AO basis and W^{mn} , F^{mn} and C^{mn} are needed in the MP2-F12 part so the computational effort (when the amplitude Ansatz is fixed) scales only as $O(N^5)$ [68, 80].

The energy expression of the approximations CCSD-F12a and CCSD-F12b can be written in more detail as:

$$\varepsilon_{\text{CCSD-F12a}} = D_{ab}^{ij} K_{ab}^{ij} + [W_{rs}^{mn} - K(F^{mn})_{rs} + R_{rs}^{ij}] T_{mn}^{ij}, \quad 1.5-20$$

$$\varepsilon_{\text{CCSD-F12b}} = \varepsilon_{\text{CCSD-F12a}} + D_{ab}^{ij} [W_{rs}^{mn} - K(F^{mn})_{rs}], \quad 1.5-21$$

where R_{rs}^{ij} is the residual of MP2 defined in eq. 1.5-12.

There is no direct F12 correction to the triples, and therefore the basis set error of the triples is not affected by the F12 method [89]. We can get the triples energy by scaling the triples energy contribution:

$$\Delta E_{(T^*)} = \Delta E_{(T)} \frac{E_{\text{corr}}^{\text{MP2-F12}}}{E_{\text{corr}}^{\text{MP2}}}. \quad 1.5-22$$

The study done by Werner and co-workers of the CCSD(T)-F12 method [66, 68] found that the CCSD(T)-F12a level is the better choice if we use basis sets up to triple zeta, because the CCSD(T)-F12a level with larger basis sets can underestimate the basis set limit and lead to worse convergence. The CCSD(T)-F12b level is better for basis sets above triple zeta [66, 68].

1.6 Density functional theory – DFT.

The *ab initio* methods described in the previous sub-chapters have limitations, in particular in the case when we would like to perform accurate calculations on molecules with many atoms and electrons. Density functional theory (DFT) can be an alternative to *ab initio* calculations. The main concept of DFT is that the energy of an electronic system can be expressed in terms of the electron probability density, ρ [90]. The energy functional of the electron density ($E[\rho]$) represents the electronic energy E of the system.

As discussed in the Born-Oppenheimer approximation section (1.1), nuclei have much bigger masses than electrons, therefore nuclei move much slower than electrons. Thus, electrons can be considered as moving in the field of fixed nuclei. Following this, the energy functional ($E[\rho]$) can be divided into three parts: the kinetic energy of the electrons $T[\rho]$, attraction between the nuclei and electrons $E_{ne}[\rho]$, and electron-electron repulsion $E_{ee}[\rho]$. The $E_{ee}[\rho]$ term can be divided into a Coulomb and an Exchange part, $J[\rho]$ and $K[\rho]$, respectively [55]. The $E_{ne}[\rho]$ and $J[\rho]$ are given by:

$$E_{ne}[\rho] = \sum_a \int \frac{Z_a \rho(r)}{|R_a - r|} dr, \quad 1.6-1$$

$$J[\rho] = \frac{1}{2} \iint \frac{\rho(r)\rho(r')}{|r - r'|} dr dr'. \quad 1.6-2$$

Note that nuclear coordinates are represented by “R” and subscript “n” and electron coordinates by “r” and subscript “e”. “Z” denotes the effective nuclear charge.

If a non-interacting uniform electron gas is considered, then $T[\rho]$ and $K[\rho]$ can be written as:

$$T_{TF}[\rho] = C_F \int \rho^{5/3}(r) dr, \quad 1.6-3$$

$$K_D[\rho] = -C_x \int \rho^{4/3}(r) dr, \quad 1.6-4$$

where,

$$C_F = \frac{3}{10} (3\pi^2)^{2/3}, \quad 1.6-5$$

$$C_x = \frac{3}{4} \left(\frac{3}{\pi} \right)^{1/3}. \quad 1.6-6$$

The energy functional can then be expressed as $E_{\text{TF}}[\rho] = T_{\text{TF}}[\rho] + E_{\text{ne}}[\rho] + J[\rho]$ and is known as Thomas-Fermi (TF) theory [91]. When the $K_{\text{D}}[\rho]$ exchange part is included, it is known as Thomas-Fermi-Dirac (TFD) [55, 92].

The Thomas-Fermi-Dirac model represents the kinetic energy very poorly and TFD (or TF) does not predict bonding and therefore molecules do not exist [55].

To fix those issues Kohn and Sham [93] introduced orbitals and they split the kinetic energy functional into two parts: a small correction term and a term which can be calculated exactly [55]. Using this approach a Hamiltonian operator with $0 \leq \lambda \leq 1$ can be written as:

$$\hat{H}_{\lambda} = \hat{T} + \hat{V}_{\text{ext}}(\lambda) + \lambda \hat{V}_{\text{ee}}, \quad 1.6-7$$

where \hat{V}_{ext} is the external potential operator and is equal to \hat{V}_{ne} for $\lambda = 1$. [55]

However, for $\lambda=0$, the exact solution of the Schrödinger equation is approximated by as a Slater determinant which consists of molecular orbitals ϕ_i , and therefore the kinetic energy functional is given as:

$$T_{\text{S}}[\rho] = \sum_{i=1}^N \left\langle \phi_i \left| -\frac{1}{2} \nabla^2 \right| \phi_i \right\rangle. \quad 1.6-8$$

∇ is nabla symbol and represents the differential vector operator. Equation 1.6-8 is the kinetic energy calculated from the Slater determinant and is only an approximation to the real kinetic energy (improved upon TF and TFD).

Moreover the density is approximately expressed in terms of auxiliary one-electron functions (a set of orbitals):

$$\rho(r) = \sum_{i=1}^N |\phi_i(r)|^2. \quad 1.6-9$$

Where $\rho(r)$ denotes the total electron density at a particular point r in space. It can be noticed that a significant component of the electron-electron interaction will be the classical Coulomb interaction as presented in eq.1.6-2. The energy functional can be rewritten as:

$$E_{\text{DFT}}[\rho] = T_{\text{S}}[\rho] + E_{\text{ne}}[\rho] + J[\rho] + E_{\text{xc}}[\rho], \quad 1.6-10$$

Where the exchange-correlation functional E_{xc} is given by:

$$E_{\text{xc}}[\rho] = (T[\rho] - T_{\text{S}}[\rho]) + (E_{\text{ee}}[\rho] - J[\rho]). \quad 1.6-11$$

The first term in parentheses in eq. 1.6-11 is the kinetic correlation energy, while the second one contains both exchange and potential correlation energy.

The exchange and correlation energies in DFT are only short range (in terms of the distance between two electrons) and depend on the density at a given point [55].

The strength of DFT is that only the total density needs to be considered in order to calculate the kinetic energy with good accuracy. The Kohn-Sham [93] (KS) approach was a major breakthrough in this area. They constructed non-interacting electrons with the same density as the physical system. The major advantage of the KS equation over the Thomas-Fermi theory is that the kinetic energy is treated exactly.

The Kohn-Sham equation is given by:

$$\left\{ -\frac{1}{2} \nabla^2 + V_{\text{eff}} \right\} \phi_i = \epsilon_i \phi_i , \quad 1.6-12$$

where the effective potential V_{eff} can be written as:

$$V_{\text{eff}}(\mathbf{r}) = V_{\text{ne}}(\mathbf{r}) + \int \frac{\rho(\mathbf{r}')}{|\mathbf{r}-\mathbf{r}'|} d\mathbf{r}' + V_{\text{xc}}(\mathbf{r}). \quad 1.6-13$$

However, the major problem in DFT is to find suitable and efficient formulas for the exchange-correlation term and this is the main difference between DFT methods: expression of the functional form of the exchange-correlation energy.

The first approach is named the Local Density Approximation (LDA). In the LDA, the density is treated locally as a uniform electron gas, and the exchange correlation energy depends only on the value of the electronic density at each point in space. When we use the Dirac formula (eq. 1.6-5 to 1.6-6) the exchange energy and exchange functional of a uniform electron gas can be written:

$$E_{\text{x}}^{\text{LDA}}[\rho] = -C_{\text{x}} \int \rho^{4/3}(\mathbf{r}) d\mathbf{r} , \quad 1.6-14$$

$$\epsilon_{\text{x}}^{\text{LDA}}[\rho] = -C_{\text{x}} \rho^{1/3} . \quad 1.6-15$$

The correlation functional $\epsilon_{\text{c}}^{\text{LDA}}[\rho]$ is unknown and needs to be fitted to the ground-state energy of a homogeneous electron gas calculated using for example quantum Monte Carlo simulations [94]. An example of a functional that uses the LDA is the functional constructed by Vosko, Wilk and Nusair (VWN) [95].

Improvement on the LDA can be made when the gradient of the electron density is considered. This approach is called Generalized Gradient Approximation (GGA) and can be written:

$$E_{xc} = E_{xc}[\rho(r), \nabla\rho(r)]. \quad 1.6-16$$

This can lead to a significant improvement over the LDA results with accuracy approaching that of correlated wavefunction methods such as MP2 and in some cases surpassing these [96]. A commonly-used GGA functional is the PW91 functional, due to Perdew and Wang [97].

Becke in 1993 [98] introduced an approximation where a functional is a hybrid of exact (Hartree-Fock) exchange with local and gradient-corrected exchange and correlation terms. This approach is often called a hybrid method. A hybrid exchange-correlation functional can be represented as a linear combination of the Hartree-Fock exact exchange functional E_X^{HF} and any combination of exchange and correlation density functionals. The most popular hybrid method is B3LYP [99] and the B3LYP exchange-correlation functional can be written as:

$$E_{xc}^{B3LYP} = (1 - a)E_x^{LSDA} + aE_x^{HF} + b\Delta E_x^{B88} + (1 - c)E_c^{LSDA} + cE_c^{LYP}. \quad 1.6-17$$

The parameters a , b and c are determined by fitting the functional's predictions to experimental or accurately calculated thermochemical data. Typical values are $a = 0.20$, $b = 0.72$ and $c = 0.81$ [100].

1.7 Other theoretical methods and concepts employed here.

NBO-Natural Bond Orbital method

In this work the Natural Bond Orbital (NBO) method was employed to determine the Lewis structures and understand the bonding properties of the molecules studied. NBO analysis is a technique for studying hybridization and covalency in polyatomic wave functions. The natural “orbitals” were introduced by Löwdin [101] and described as the unique set of orthonormal one-electron functions. Mathematically the one-electron functions are represented as eigenorbitals of the first-order reduced density operator [102]. Thus, according to Weinhold et al. [102] "... natural bond orbitals (NBOs) provide the most accurate possible 'natural Lewis structure' picture of the wavefunction ψ , because all orbital details (polarization coefficients, atomic hybrid compositions, etc.) are mathematically chosen to include the highest possible percentage of the electron density".

A bonding NBO σ_{AB} between atoms A and B is constructed from directed orthonormal hybrids h_A , h_B (Natural Hybrid Orbitals or NHO's) with corresponding polarization coefficients c_A , c_B [102, 103]:

$$\sigma_{AB} = c_A h_A + c_B h_B, \quad 1.7-1$$

where σ_{AB} is a filled NBO. These NBOs are able to describe covalency effects in molecules. The hybrids h_A and h_B are formed from a set of effective valence-shell atomic orbitals (Natural Atomic Orbitals or NAOs) optimized for the wave function used [103]. NBO transformed wavefunctions give good agreement with concepts such as Lewis structures and covalency in molecules. However, the general transformation to NBOs also yields unoccupied orbitals, which can be employed to describe non-covalent effects [103]. The most important ones are the antibonding σ_{AB}^* which are given by:

$$\sigma_{AB}^* = c_B h_A - c_A h_B. \quad 1.7-2$$

The natural hybrids, h_A and h_B are the same valence-shell hybrids that formed the bond function σ_{AB} . The energy associated with antibonding orbitals can be obtained by

deleting these orbitals from the basis set and recalculating the total energy [103]. The total energy E can then be written as:

$$E = E_{\sigma\sigma} + E_{\sigma\sigma^*}, \quad 1.7-3$$

where $E_{\sigma\sigma} = E_{\text{Lewis}}$ and $E_{\sigma\sigma^*} = E_{\text{non-Lewis}}$ are the covalent and non-covalent contributions, respectively. $E_{\text{non-Lewis}}$ is typically much less than 1% of E_{Lewis} [102].

The interaction between a filled orbital σ and an unfilled orbital σ^* gives rise to a stabilisation energy which can be approximated by second order perturbation theory:

$$\Delta E_{\sigma\sigma^*}^{(2)} = -2 \frac{\langle \sigma | \hat{F} | \sigma^* \rangle^2}{\epsilon_{\sigma^*} - \epsilon_{\sigma}}, \quad 1.7-4$$

where \hat{F} is the Fock operator and $\epsilon_{\sigma^*}, \epsilon_{\sigma}$ are NBO orbital energies. These interactions between filled orbitals σ and unfilled orbitals σ^* can be described as “donor-acceptor interactions” or “charge transfer” [103].

Relativistic corrections

Relativistic effects are important for calculations that require high accuracy results even for light atoms like hydrogen. The relativistic effect can be determined as the difference between electronic properties obtained from calculations that take into account the true velocity of light and electronic properties that assume that the velocity of light is infinite, as done in traditional treatments of quantum chemistry [104].

The Schrödinger equation does not contain relativistic information and the unification of quantum mechanics with special relativity was accomplished by Dirac in 1928 [105].

The Dirac free particle equation is:

$$(\vec{\alpha}\hat{p} + \vec{\beta}mc^2)\Psi = E\Psi, \quad 1.7-5$$

where m is the rest mass of the electron, \hat{p} is the momentum operator, c is the speed of light, and α and β are vector operators. The Dirac equation is computationally more difficult to solve than the Schrödinger equation and because the negative part of the spectrum (the positronic part with the energy eigenvalues less than or equal to $-mc^2$) cannot be treated variationally. Moreover the Dirac equation can be solved only for one-electron systems, thus a generalization of the Dirac equation is necessary to construct the N -particle Hamiltonian. This Hamiltonian is called the Dirac-Coulomb-Breit Hamiltonian which is applied using a four-component spinor formalism [104] and

represents the full-relativistic approach. This approach was used to develop the Dirac-Hartree-Fock (DHF) theory. Unfortunately, a DHF calculation is 64 times more expensive than a corresponding non-relativistic Hartree-Fock calculation. Thus, additional approximations are necessary to calculate relativistic effects for heavy atoms and systems containing a large number of electrons. The expensive four-component spinor part can be transformed into a two-component form [104, 106], and the resulting equations are usually used in first-order perturbation theory [104] which gives the Pauli Hamiltonian:

$$\hat{H}_p = \hat{H}_0 + \hat{H}_{MV} + \hat{H}_{D1+2} + \hat{H}_{SO}, \quad 1.7-6$$

where \hat{H}_0 is the non-relativistic Coulomb Hamiltonian, \hat{H}_{MV} is the mass-velocity operator, \hat{H}_{D1+2} is the one- and two-electron Darwin operator and \hat{H}_{SO} is the spin-orbit operator. For light atoms, the spin-orbit interactions and the two-electron Darwin term are not so important and can be neglected [106]. Cowan and Griffin showed that the resulting one-electron mass-velocity-Darwin (MVD) Hamiltonian can be used to calculate the relativistic corrections in a good agreement with the DHF method [107]. The mass velocity (MV) term, which describes the energy correction E^{MV} to the kinetic energy of the electrons is always negative [106]. In contrast, the energy corrections of one-electron term E^{D1} are always positive. The D1 term describes the correction to the distance between the electrons and the nuclei [106]. The Cowan-Griffin approach [107] will be used here as the method to calculate the relativistic corrections.

2 Molecular vibrations

2.1 Theoretical introduction.

Classical approach

In the limit of infinitely small amplitudes the vibration of a molecule can be represented mathematically by classical expressions for the kinetic and potential energies of the molecule. Initially a molecule is treated as N coupled masses and analyzed in terms of vibration, rotation and translation motion. The simple form of the kinetic energy (as seen in eq. 2.1-1) employs the Cartesian coordinates x_i , y_i and z_i , which are displacements from the equilibrium position of the point mass i ,

$$T = \frac{1}{2} \sum_{i=1}^n m_i (\dot{x}_i^2 + \dot{y}_i^2 + \dot{z}_i^2), \quad 2.1-1$$

and where m_i is the atomic mass. A dot over a symbol means the time derivative. The equation can be rewritten in a compact form where for simplicity the coordinates x_i , y_i and z_i are replaced by a new set of coordinates g_i , where $g_1 = \sqrt{m_1}x_1$, $g_2 = \sqrt{m_1}y_1$, $g_3 = \sqrt{m_1}z_1$, $g_4 = \sqrt{m_2}x_2$ etc. (mass-weighted Cartesian displacement coordinates) [108]. Then the equation is:

$$T = \frac{1}{2} \sum_{i=1}^{3n} \dot{g}_i^2. \quad 2.1-2$$

For small amplitudes of vibration the equation of the potential energy is:

$$V = \frac{1}{2} \sum_{i,j=1}^{3n} f_{ij} g_i g_j. \quad 2.1-3$$

The terms f_{ij} in eq. 2.1-3 are the “force constants”.

It is now possible to write Newton's equations of motion, since we have obtained T and V. V is a function of the displacements and T is a function of the velocities only, so the equation of motion is [108]:

$$\ddot{g}_i + \sum_j^{3n} f_{ij} g_j = 0, \quad i = 1, 2, \dots, 3N \quad 2.1-4$$

The solution of this set of 3n simultaneous second-order differential equations, are the well known harmonic oscillator equations [109]:

$$g_i = A_i \cos(2\pi c \omega_i t + \phi_i), \quad 2.1-5$$

where ω_i is the vibrational “frequency” (in cm^{-1}), ϕ is a phase factor and A_i is the amplitude of the motion of the atom. If we substitute equations 2.1-5 into the differential equations, then we can obtain the expression:

$$\sum_j^{3n} (f_{ij} - \lambda \delta_{ij}) A_j = 0 \quad 2.1-6$$

where $\lambda = 4\pi^2 \omega^2 c^2$ and δ_{ij} is the Kronecker delta.

Equation 2.1-5 shows that each atom is oscillating near its equilibrium position with a simple harmonic motion [108]. In a polyatomic nonlinear molecule with N atoms $3N-6$ normal modes can be found which are commonly known as the normal modes of vibration or fundamental frequencies of the molecule. A normal mode is a motion of all atoms in the molecule: the motion of each atom is described by three Cartesian displacements (along the x , y and z direction) [110]. We can find translational and rotational modes in a molecule. The translational modes refer to the modes where all the atoms are moving in the same direction. The rotational modes refer to the change of the orientation of the molecule (rotations). Three harmonic frequencies corresponding to translational modes and three harmonic frequencies corresponding to rotational modes (of the molecule as a whole) are zero in a nonlinear molecule. In a linear molecule three harmonic frequencies corresponding to translational modes and two harmonic frequencies corresponding to rotational modes (of the molecule as a whole) are zero, as rotation around its molecular axis does not exist. Thus, a nonlinear molecule with N atoms has $3N - 6$ while a linear molecule has $3N - 5$ normal modes of vibration.

Normal coordinates

In order to solve the Schrödinger equation for the harmonic oscillator, the kinetic and potential energies need to be present as a sum of separate terms. Thus, the Cartesian coordinates need to be replaced by a new coordinate system. The conventional “normal coordinates” Q will be used [108]. The “normal coordinates” are the displacement of atoms from their equilibrium positions, and correspond to a normal mode vibration. The “normal coordinates” (Q_k) can be defined in terms of the mass-weighted Cartesian coordinates g_i :

$$Q_k = \sum_{i=1}^{3n} l'_{ki} g_i, \text{ where } k=1, 2, \dots, 3n. \quad 2.1-7$$

In terms of the new coordinates, we can express the kinetic and potential energies in diagonal form as:

$$T = \frac{1}{2} \sum_{k=1}^{3N} \dot{Q}_k^2 \text{ and } V = \frac{1}{2} \sum_{k=1}^{3N} \lambda_k \dot{Q}_k^2. \quad 2.1-8$$

where $\lambda_k = 4\pi^2 \omega_k^2 c^2$.

Quantum mechanical approach

To a reasonable approximation the rotational and vibrational parts of the Hamiltonian can be treated separately in the wave mechanics approach [108]. Thus the vibrational wavefunction ψ_v and rotational wavefunction ψ_r combine as a product to give the total wavefunction ψ , and can be written as:

$$\psi \cong \psi_v \psi_r. \quad 2.1-9$$

ψ_r is a function of the rotational coordinates and ψ_v is a function of the vibrational coordinates.

The vibrational Hamiltonian in terms of the normal coordinates Q_k can be obtained from the classical approach as a vibrational wave equation:

$$\frac{-h^2}{8\pi^2} \sum_{k=1}^{3N-6} \frac{\partial^2 \psi_v}{\partial Q_k^2} + \frac{1}{2} \sum_{i=k}^{3N-6} \lambda_k Q_k^2 \psi_v = E_v \psi_v, \quad 2.1-10$$

Where h is Planck's constant and E_v is the vibrational energy.

Equation 2.1-10 can be written as $3N-6$ independent equations one for each Q_k since

$$\psi_v = \psi(Q_1) \psi(Q_2) \dots \psi(Q_{3N-6}), \quad 2.1-11$$

and the vibrational energy E_v can be expressed as the sum of $3N-6$ terms

$$E_v = E_1 + E_2 + E_3 + \dots + E_{3N-6} \quad 2.1-12$$

Thus, it is possible to express the equations 2.1-10 and 2.1-11 as $3N-6$ independent equations each in one variable for $k=1$ to $3N-6$,

$$\frac{-h^2}{8\pi^2} \frac{d^2 \psi(Q_k)}{dQ_k^2} + \frac{1}{2} \lambda_k Q_k^2 \psi(Q_k) = E(k) \psi(Q_k). \quad 2.1-13$$

Eq. 2.1-13 is the well-known harmonic oscillator, in terms of the normal coordinates Q_k . Thus, the solution ψ_v of the vibrational problem can be expressed as a product of

harmonic oscillator functions $\psi(Q_k)$ [108] and the total vibrational energy E_v can be expressed as the sum of the energies of 3N–6 harmonic oscillators.

The energy levels for a harmonic oscillator are

$$E_{v_i} = hc\omega_i \left(v_i + \frac{1}{2} \right), \quad 2.1-14$$

where “ v_i ” is the vibrational quantum number $v_i = 0, 1, 2, \dots$. Thus a molecule vibrates even at 0 K and occupies the lowest energy level of the potential energy surface.

Anharmonicity

The harmonic vibrations discussed above are very useful for describing small displacements from equilibrium at the bottom of the potential energy well. However, in reality the molecular vibrations are more complex. When higher vibrational excitations of a molecule need to be considered anharmonic vibrations are important for a proper description of the potential energy curve. Higher terms such as cubic and quartic terms of the potential function need to be taken into account [109].

Nielsen [109, 111] used the perturbation method to obtain a general form of the anharmonic oscillator. Thus, when normal coordinates “ q_i ” ($q_i = \lambda_i^{1/2} Q_i \hbar$) are used to express the harmonic and anharmonic terms in the same units (cm^{-1}), the potential energy equation is written

$$V = \frac{1}{2} hc \sum_i \omega_i q_i^2 + hc \sum_i \sum_j \sum_k k_{ijk} q_i q_j q_k + hc \sum_i \sum_j \sum_k \sum_l k_{ijkl} q_i q_j q_k q_l + \dots \quad 2.1-15$$

Unfortunately an exact solution for the Schrödinger equation cannot be obtained if the above equation is introduced. Nevertheless, it was noticed that the quadratic part of the potential energy is much larger than the cubic part for small but finite displacements of the nuclei. Thus perturbation theory can be used to calculate corrections to the vibrational energy for higher-order parts of the vibrational Hamiltonian [109]. The first and second-order corrections to the energy for a non-degenerate system can be evaluated quite easily, so the potential and the total energies can be written in the form:

$$V = V^{(0)} + \lambda V^{(1)} + \lambda^2 V^{(2)} \quad 2.1-16$$

$$E = \sum_i hc\omega_i \left(v_i + \frac{1}{2} \right) + \lambda E^{(1)} + \lambda^2 E^{(2)} , \quad 2.1-17$$

where

$$V^{(0)} = \frac{1}{2} hc \sum_i \omega_i q_i^2 \quad 2.1-18$$

$$V^{(1)} = hc \sum_{ijk} k_{ijk} q_i q_j q_k \quad 2.1-19$$

$$V^{(2)} = hc \sum_{ijkl} k_{ijkl} q_i q_j q_k q_l , \quad 2.1-20$$

and $E^{(1)}, E^{(2)}$ are the first and second-order corrections [109]. Thus, the energy equation can be rewritten in the form

$$E = \sum_i hc\omega_i \left(v_i + \frac{1}{2} \right) + hc \sum_{ij} \chi_{ij} \left(v_i + \frac{1}{2} \right) \left(v_j + \frac{1}{2} \right) + \dots \quad 2.1-21$$

where χ_{ij} and χ_{ii} are the anharmonic constants and the mathematical forms of these can be found in [109].

2.2 Variational method

The variational method is the other main approach used to compute vibrational quantum state energies and wave functions and can be used instead of perturbation theory. In fact a variational approach is essential when large amplitude motions are involved: perturbation theory breaks down when the assumption of small amplitude vibrations is not justified. The idea of the variational method is to choose a "trial" wavefunction for the problem, which must have adjustable parameters. These parameters are varied until the energy of the wavefunction is minimized. The resulting wavefunction and its corresponding energy are the variational approximations to the exact wavefunction and energy. The variational approach has been generalised to give upper bounds to each of the lowest n energy levels of a system [112].

To perform a variational calculation we need to have [112]:

- a potential energy surface for the molecular system;
- a coordinate system to describe all relevant molecular geometries;
- basis functions which will be combined to give the trial wavefunction.

Basis functions for each coordinate ($r_1, r_2, \theta_1, \theta_2$ etc.) for a many-atomic problem can be represented as: $Q_m(r_1), R_n(r_2), P_i(\theta_1), P_j(\theta_2)$ etc, where the angular functions (of θ) could be Legendre polynomials and the stretching functions could be Morse or harmonic oscillator functions for example [112]. An alternative to this finite basis representation (FBR) is the discrete variable representation (DVR) which considers the wavefunction at fixed values of the vibrational coordinates [113].

The computational approach then includes the following steps:

- The chosen basis set is used to compute the elements of the Hamiltonian matrix.
- The Hamiltonian matrix is constructed from the matrix elements prepared above. The Hamiltonian matrix can be written as: $H_{ss'} = \langle P_i P_j Q_m \dots | \hat{H} | P_i' P_j' Q_m' \dots \rangle$, where s is a compound index running over the basis functions, \hat{H} is the Hamiltonian operator, Q_m, R_n, P_i, P_j are the functions dependent on the vibrational coordinates ($r_1, r_2, \theta_1, \theta_2$) and the integration runs over all of these

coordinates [112]. The large number of basis functions allows one to obtain vibrational energies close to the true ones. To be sure that the calculated energy is reliable, the convergence needs to be demonstrated, and this can be checked by systematically increasing the basis set size.

- The last step is diagonalization of the Hamiltonian matrix. This step is often the longest in the whole calculation. To speed up the diagonalization an iterative procedure [112], or a diagonalization-truncation method [114] can be employed instead of direct-diagonalization [115].

In the following studies I will use the WAVR4 program [116] which combines DVR and FBR basis sets and use a diagonalization-truncation method. The FBR is used for the angular coordinates while the DVR is used for radial coordinates and is obtained as a transformation from a corresponding FBR [112, 117]. A more detailed explanation can be found in Ref. [116, 117].

Applications

“The most exciting phrase to hear in science, the one that heralds the most discoveries, is not "Eureka!" but "That's funny..."

Isaac Asimov

3 Acetylene/vinylidene


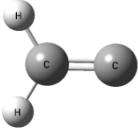
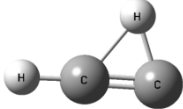
3.1 The C₂H₂ isomers.

Silicon belongs to the carbon group (group 14) in the periodic table; therefore it may have similar physical and chemical properties as carbon and can form similar compounds. A comparison of the acetylene/vinylidene isomers with substituted silicon structures is an interesting topic in the context of bonding properties.

Computational methods

The acetylene/vinylidene isomers have been studied by Zou and Bowman [118]. They performed full-dimensional quantum-chemical calculations of acetylene/vinylidene isomerisation. First, we attempted to reproduce the results achieved by Zou and Bowman. Coupled-cluster level of theory including the single and double excitations with perturbative treatment of triple contributions – CCSD(T) [61] and Dunning's correlation consistent basis set of triple- ζ quality with diffuse functions (aug-cc-pVTZ) were applied [58, 119]. The same level of theory was used by Zou and Bowman. All computations were performed with MOLPRO version 2006.1 [120]. The MP2 [121] and HF [122] levels of theory (with the same basis set) were used to compare with the CCSD(T) method. The results obtained are listed in Table 3.1-1.

Table 3.1-1. Geometric properties of the acetylene/vinylidene isomers with the corresponding picture of the structure. Bond distances are listed in ångström and angles in degrees. The aug-cc-pVTZ basis set was used.

		Acetylene HCCH			
		CCSD(T)	MP2	HF	Literature ^b
	H1C1	1.0639	1.0617	1.0625	1.0640
	C-C	1.2102	1.2121	1.1921	1.2102
		Vinylidene HHCC			
		CCSD(T)	MP2	HF	Literature ^b
	H1C2 ^b	1.0872	1.0845	1.0836	1.0872
	C-C	1.3069	1.2993	1.2979	1.3068
	α CCH1	120.12	119.66	119.70	120.10
energy [cm ⁻¹] ^a		15407	18158	12340	15407
^a energy relative to the HCCH minimum.					
^b C2-refer to the carbon atom connected to terminal hydrogens					
		TS1 HCHC			
		CCSD(T)	MP2	HF	Literature ^b
	H1C1 ^c	1.0732	1.0706	1.0693	1.0733
	H2C1 ^c	1.3910	1.2378	1.3276	1.3910
	C-C	1.2604	1.2669	1.2549	1.2604
	α CCH1	178.55	179.21	178.14	178.50
	α CCH2	53.70	58.31	56.05	53.70
	energy [cm ⁻¹] ^a	16408	17131	20085	16408
^a energy relative to the HCCH minimum					
^b values calculated at CCSD(T) were taken from reference [118]					
^c C1-refer to the carbon atom connected to terminal hydrogen (H1)					

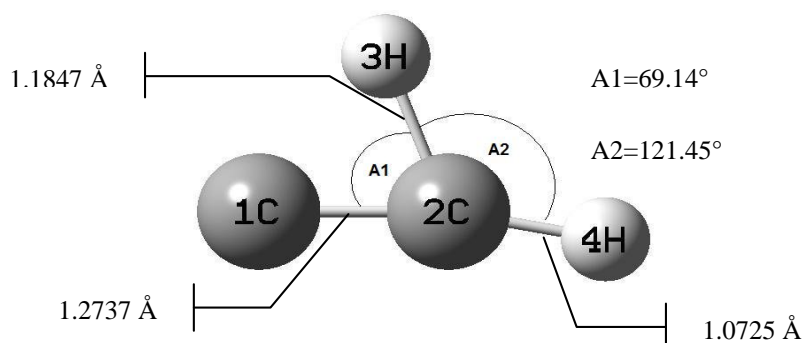
Vinylidene lies 15406.9 cm⁻¹ above acetylene, whereas the transition state linking these minima (TS1) lies 16407.8 cm⁻¹ above acetylene (at the CCSD(T) level of theory). The calculated bond distances, angles and energies agree with those obtained by Zou and Bowman as shown in Table 3.1-1.

The geometric properties obtained with the MP2 and HF methods are similar to those calculated by CCSD(T) except for the TS1 structure (at the MP2 level). The MP2 method *underestimates* the H2C2 bond distance by about 0.1532 Å (in comparison to

the CCSD(T) level) and *overestimates* the CCH2 angle by about 4.6°. The MP2 TS1 energy (17131.0 cm⁻¹) is smaller than the corresponding vinylidene energy (18158.1 cm⁻¹), which is unexpected as a transition state should have larger energy than both minima connected by the transition state. It could mean that TS1 calculated at the MP2 level of theory is not the real TS1 structure but a new critical point. Thus, additional minimization and frequency calculations at the CCSD(T)/aug-cc-pVTZ level were employed to investigate this issue.

During the above studies a third minimum was found (no imaginary frequencies) with an energy 15969.9 cm⁻¹ larger than that of acetylene (at the CCSD(T)/aug-cc-pVTZ level). The third minimum represents a monobridged structure reported previously by Chesnut and others [123-125]. Figure 3.1-1 shows the structure of this monobridged minimum.

Figure 3.1-1. Monobridged isomer obtained at the CCSD(T)/aug-cc-pVTZ level (the structure is planar).



A comparison of the geometries of the monobridged and TS1 isomers shows that the A1 angle in the monobridged isomer (CCH2 in Table 3.1-1) is about 15° larger than in TS1; however, the A2 angle (CCH1 in Table 3.1-1) is about 6° smaller. The C–C distance in the monobridged minimum is 0.0133 Å longer than in TS1, however, the H2C2 distance (3H2C in Figure 3.1-1) is 0.2063 Å shorter.

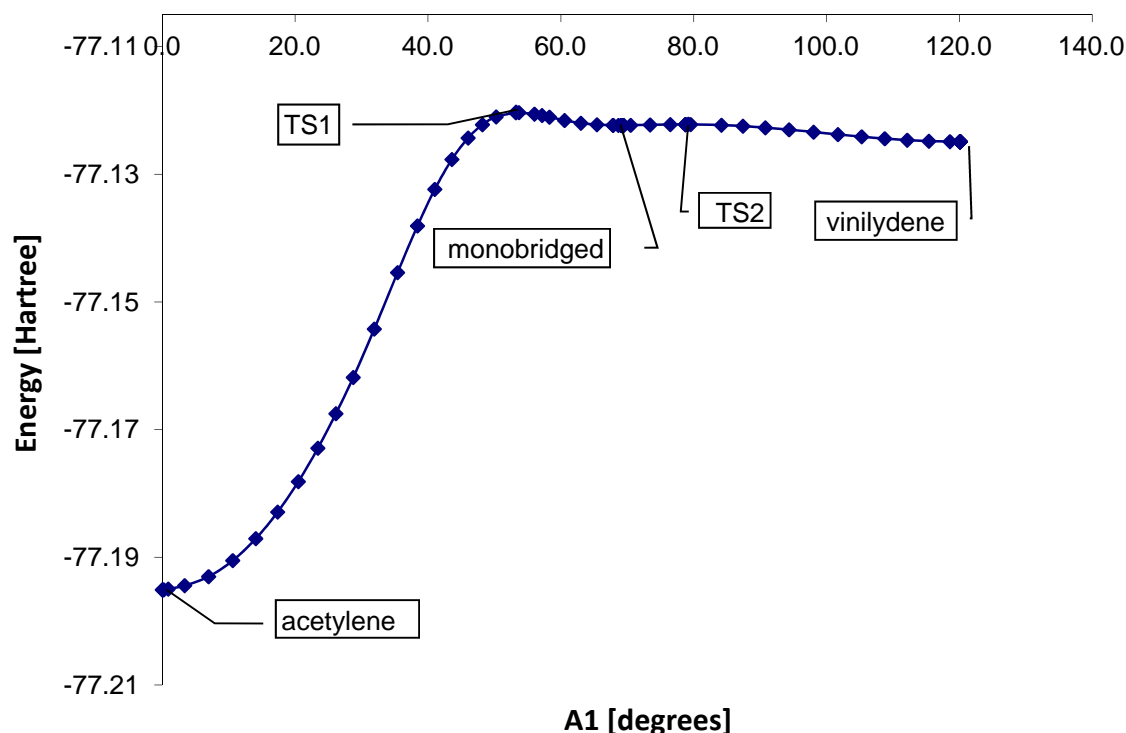
We used the Quadratic Steepest Descent (QSD) reaction path method implemented in MOLPRO to obtain the whole reaction path from acetylene through TS1, monobridged, and TS2 (a new transition state between the monobridged and vinylidene isomers, see below) to vinylidene. The QSD algorithm was formulated by Sun and Ruedenberg [126]. The reaction path is obtained from serial exact steepest-descent lines of local quadratic approximations to the potential energy surface [126].

This achieves a good accuracy and more efficiently evaluates the energy-gradient-Hessian set (where the Hessian is calculated exactly) and no additional corrective optimizations off the steepest-descent line are required [126]. All the QSD reaction path method calculations were done with CCSD(T)/aug-cc-pVTZ.

The energy is plotted as a function of the A1 angle (see Figure 3.1-1) for several points obtained by the QSD reaction path method. The whole reaction path is presented in Figure 3.1-2. The QSD reaction path calculation reveals a second transition state, TS2, which connects the monobridged and vinylidene minima.

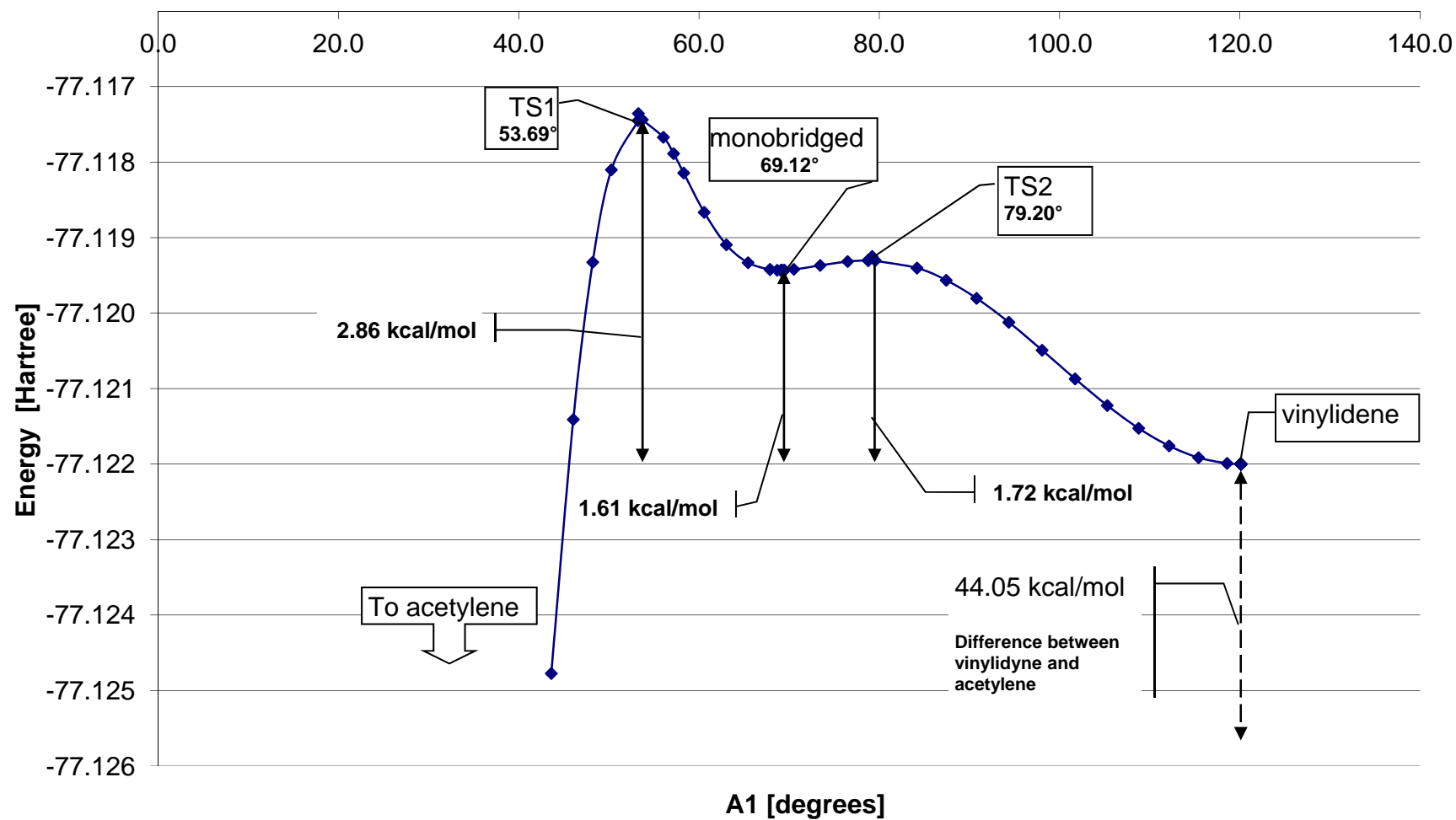
Figure 3.1-2 does not show clearly all information such as the exact position of the new transition state (TS2), which lies between the monobridged and the vinylidene isomers. An expanded view of the part between the TS1 and vinylidene is therefore presented in Figure 3.1-3. It can be clearly seen that the TS2 structure occurs at 79.2°. The energy difference between the monobridged and the TS2 structures is very small (0.11 kcal/mol) and the energy difference between vinylidene and TS2 is 1.72 kcal/mol. The energy difference between TS1 and vinylidene is 2.86 kcal/mol and between monobridged and vinylidene 1.61 kcal/mol.

Figure 3.1-2. Variation of energy along the reaction path between the acetylene and vinylidene isomers. The calculations were done at the CCSD(T)/aug-cc-pVTZ level.



The C_2H_2 isomers were re-optimized with CCSD(T) in conjunction with the family of Dunning's correlation-consistent basis set augmented with diffuse functions aug-cc-pVXZ (with cardinal numbers $X=2-5$) [58, 119]. The aug-cc-pVXZ basis set will be abbreviated as AVXZ (where $X=2-5$), respectively. The minimization method (Quadratic Steepest Descent) implemented in MOLPRO was used in all calculations. The convergence comparisons of all minimum structures obtained with increasing basis set size are shown below in Figure 3.1-4 to Figure 3.1-5.

Figure 3.1-3. Extended view of the energy along the reaction path between the acetylene and vinylidene isomers. The calculations were done at the CCSD(T)/aug-cc-pVTZ level.



Note that the monobridged structure was not found with the aug-cc-pVDZ basis set. CCSD(T)/aug-cc-pVDZ optimization starting from the monobridged structure led to the vinylidene form. However, all three isomers were found with the aug-cc-pVXZ (X=3–5) basis sets.

The experimental (obtained using microwave spectroscopy) acetylene C–C bond length is 1.202 Å (r_e equilibrium internuclear distance) [127] and 1.208 Å (r_0 effective internuclear distance) [127]. The C–C bond lengths obtained with the aug-cc-pV5Z (1.2059 Å), aug-cc-pVQZ (1.2069 Å) and aug-cc-pVTZ (1.2103 Å) basis sets agree very well with the experimental data but the aug-cc-pVDZ basis set appears to *overestimate* the bond length (CCSD(T)/aug-cc-pVDZ value: 1.2301 Å).

It can be seen that the bond lengths differences have a similar pattern for C–C and H–C distances: a larger difference is found between the results obtained with the aug-cc-pVDZ/aug-cc-pVTZ than with the aug-cc-pVTZ/aug-cc-pVQZ basis sets and aug-cc-pVQZ/aug-cc-pV5Z basis sets. Only small changes can be seen with increasing basis set size beyond aug-cc-pVTZ.

We also considered the energy difference between the global minimum (acetylene) and the local minima (monobridged and vinylidene), which is shown in Figure 3.1-6. The known experimental energy difference between acetylene and vinylidene is 46.4 ± 5.5 kcal/mol [19]. The aug-cc-pVXZ (X=3-5) basis sets give energy results close to the experimental data, whereas aug-cc-pVDZ underestimates the experimental value.

Figure 3.1-4. Variation of the C–C distance with increasing basis set at the CCSD(T) level of theory.

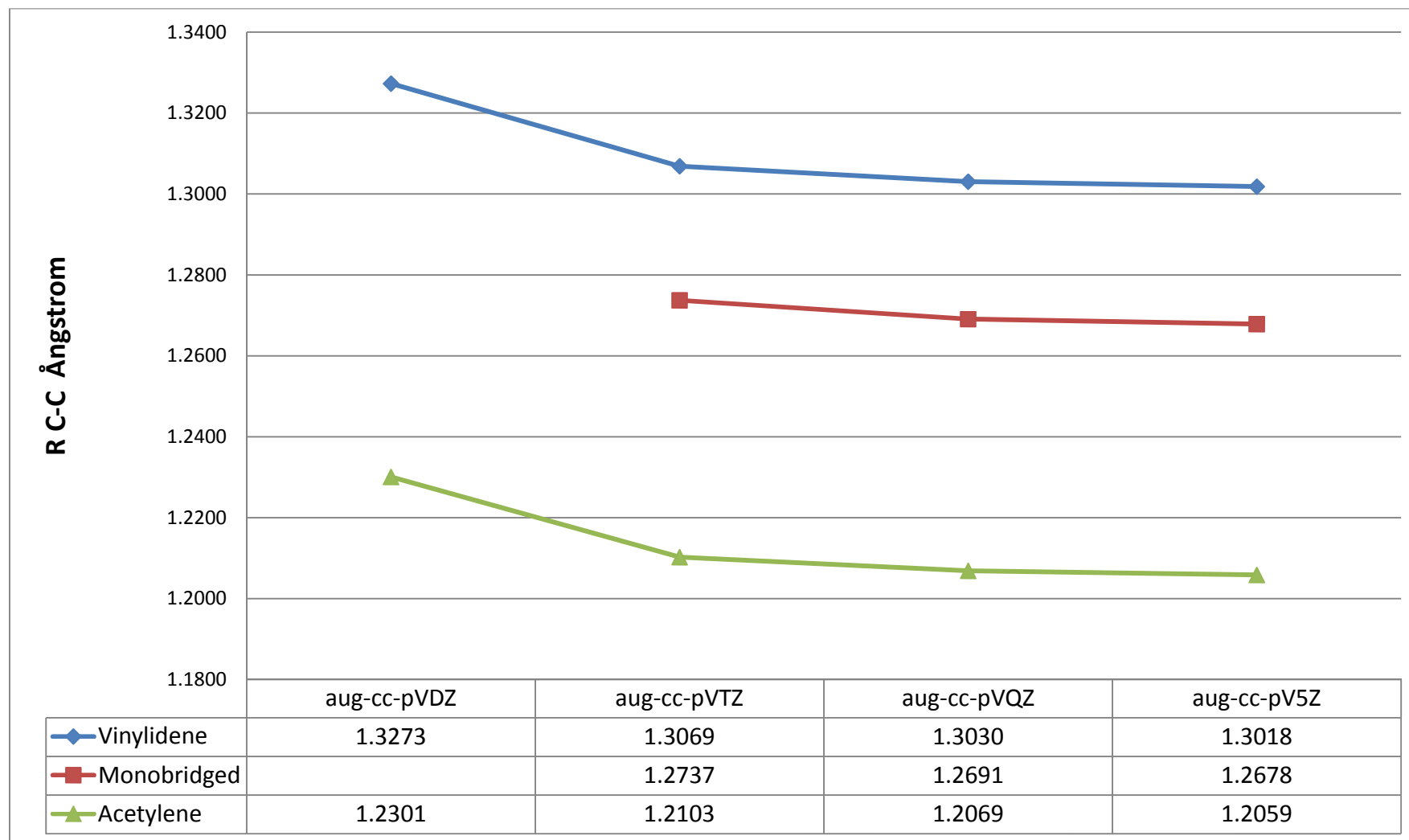


Figure 3.1-5. Variation of the H1–C1 distance with increasing basis set at the CCSD(T) level of theory.

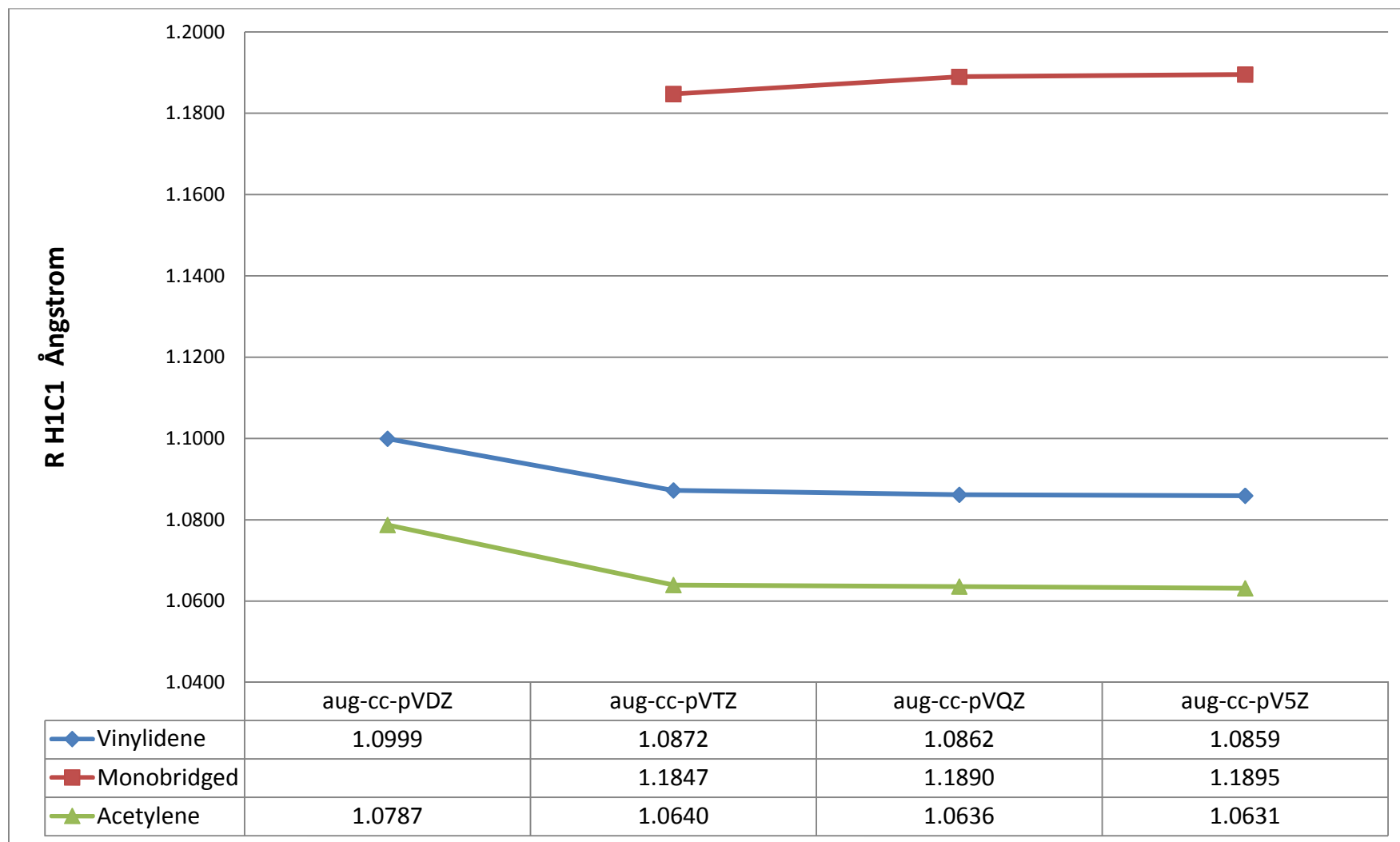


Figure 3.1-6. Energy difference between the acetylene, vinylidene and monobridged isomers at the CCSD(T) level.

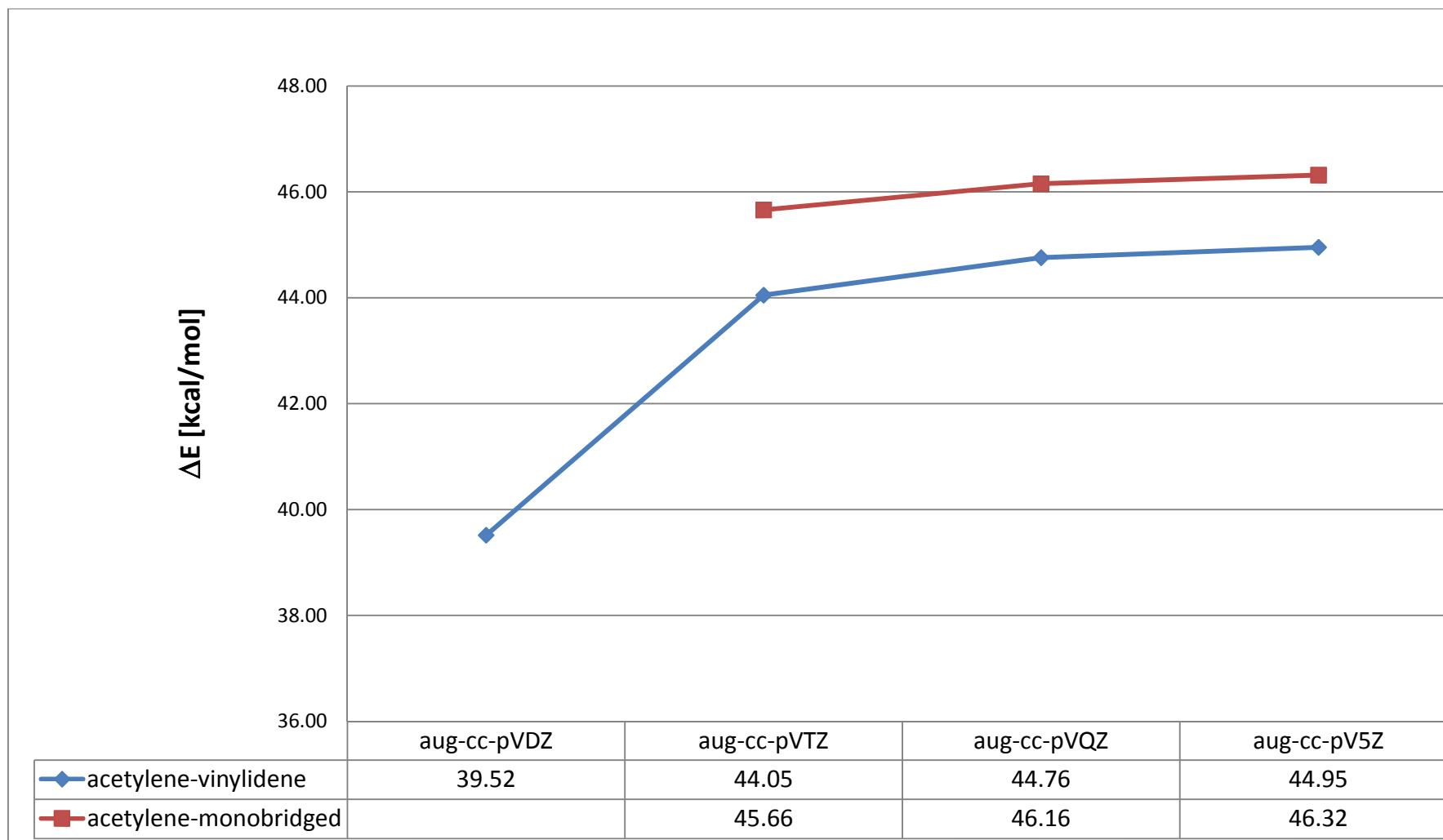


Figure 3.1-2 shows that there is only a small energy difference between TS2 and the monobridged isomer. Table 3.1-2 shows the energy difference as a function of basis set size and with zero-point-energy (ZPE) correction included.

Table 3.1-2. Relative energy of the monobridged and TS2 structures, calculated with CCSD(T)/aug-cc-pVXZ (X=3-5). The calculations include ZPE corrections.

monobridged-TS2	aug-cc-pVTZ	aug-cc-pVQZ	aug-cc-pV5Z
ΔE [kcal/mol]	0.1657	0.1512	0.1625

It can be seen that the energy difference remains, even when using the large aug-cc-pV5Z basis set (0.1625 kcal/mol).

Conclusions

Our calculated geometries are in good agreement with those of Zou and Bowman [118] and the experimental values [127]. Zou and Bowman [118], however, did not present the monobridged structure that exists on the C_2H_2 PES. The monobridged isomer has however been reported in the literature before by Bittner and Köppel, Palaudoux and Hochlaf and others [124, 125, 128, 129]. In the most of these publications the titles and abstracts did not refer to the monobridged structure with the result that the existence of the monobridged structure on the C_2H_2 PES is not commonly known. The CCSD(T)/aug-cc-pV5Z level used here to calculate the geometric and isomerisation properties for the monobridged and TS2 structures is higher than that used by Bittner and Köppel (CCSD(T)/aug-cc-pVTZ), Palaudoux and Hochlaf (CCSD(T)/cc-pVQZ) but lower than used by Joseph and Varandas (CCSD(T)-F12a/aug-cc-pVQZ) and Boyé-Péronne, Gauyacq, and Liévin (MRCI/aug-cc-pVQZ).

A comparison of the bonding properties of the C_2H_2 , Si_2H_2 , Si_2HLi and Si_2Li_2 structures will be done at the end of Chapter 4.

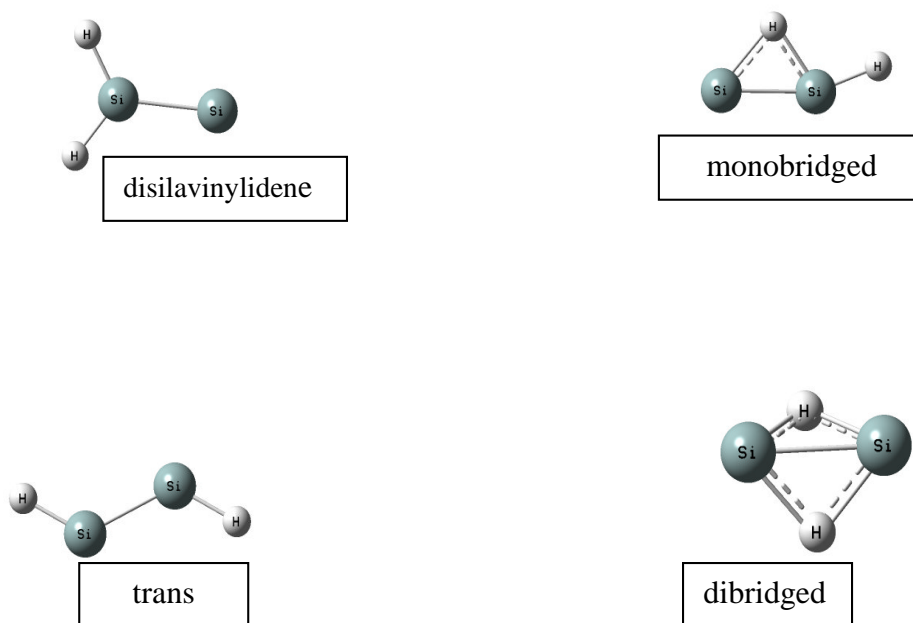
4 The Si₂HX and Si₂Li₂ critical points (where X=H, Li, F and Cl).

The Si₂HX and Si₂Li₂ systems (where X= H, Li, F and Cl) exhibit unusual structural isomerism, and this aspect in particular has attracted the interest of both experimentalists and theoreticians. Our computational studies of the Si₂HX and Si₂Li₂ structures can provide extensive knowledge of their physicochemical properties. The Si₂H₂ structures were studied theoretically and experimentally before [24, 43, 52]. The Si₂HX and Si₂Li₂ structures (where X= Li, F and Cl) were studied in Ref. [24, 43] and using a low level of theory in Ref. [30]. However, these structures will be studied for the first time here using the recently developed CCSD(T)-F12a method [66, 68]. Additionally the transition states and reaction paths between the minima for the Si₂HX and Si₂Li₂ systems (where X= Li, F and Cl) will be also studied for the first time here.

4.1 The Si₂H₂ isomers.

Silicon-containing species are of vital importance in many high technology industries, and the Si₂H₂ system is particularly fascinating. It is an interesting molecule to compare with its carbon analogue, acetylene. Electronic structure calculations have shown that the ground-state electronic structure of Si₂H₂ is different from C₂H₂. The most influential work on Si₂H₂ was done by Grev and Schaefer [24]. They performed coupled-cluster theory investigations and the isomers obtained are as follows: dibridged (C_{2v}), monobridged (C_s), disilavinylidene (C_{2v}) and trans (C_{2h}). The dibridged and monobridged isomers have been observed experimentally by microwave and IR spectroscopy [25, 26].

Figure 4.1-1. The structures optimized by Grev and Schaefer [24] which were used as starting points for the optimizations performed here.



Computational methods

Initially all the Si_2H_2 isomers were optimized with the CCSD(T)/AVXZ, CCSD(T)-F12a/VXZ-F12 (see later for details), B3LYP/6-311+G(d) and MP2/6-31G(d) level of theories (where $X=2-4$). The Si_2H_2 structures optimized by Grev and Schaefer [24] were taken as the starting geometries (Figure 4.1-1).

Harmonic vibrational frequency computations were performed for the optimized structures to characterise these as minima or transition states (TS). The frequency calculations were also done at the CCSD(T)-F12a/VXZ-F12 and B3LYP/6-311+G(d) level of theory. The frequency values calculated at the CCSD(T)/aug-cc-pVTZ level were taken from Ref. [52]. Note, that the B3LYP/6-311G(d) level does not contains polarization functions for the H atom which might introduce some inaccuracies for the bridged structures.

The HSiSiH, HSiHSi, HHSiSi and SiHHSi formulae refer, respectively, to the trans, monobridged, vinylidene and dibridged isomers. The DM_TS, MV_TS and MT_TS formulae represent the transition states on the paths between the dibridged and monobridged structures, monobridged and vinylidene and between the monobridged and trans structures, respectively. The optimized structures of the isomers and transition states of Si₂H₂ are depicted in Figure 4.1-2. The energies relative to the dibridged isomer (the global minimum) are listed at the bottom of Figure 4.1-2. The reaction paths between the critical points are represented schematically by lines. The pictures in Figure 4.1-2 show (multiple) bond properties obtained from Natural Bond Orbital (NBO) [102, 103] calculations. The NBO calculations were performed at the CCSD/cc-pV(T+d)Z level of theory using the Gaussian 98 [130] software package. We use the \$CHOOSE keylist in the NBO program to specify alternative bonding patterns for the Si₂H₂ species. This procedure allows us to verify that the NBO program has not inadvertently missed the "true" multiply-bonded structure. More details about this procedure can be found in Ref. [115, 130]. The results of these calculations correspond well with those by Chesnut and Jursic [47, 123], who suggested that the Si₂H₂ isomers contain the same multi or single bonds as our analysis. The same procedure of obtaining the multiple bonded properties will be employed in the following sub-chapters.

The calculated geometric parameters for the minima and saddle points are given in Table 4.1-1 and Table 4.1-2, respectively. Note that in the monobridged structure values of bond distance and angle of a bridged atom will be present as Si2H1 and Si1Si2H1, respectively, where Si2 represents the silicon connected to the terminal hydrogen atom. Similar approach will be employed in the next sub-chapters.

It can be seen that the shortest Si–Si bond length occurs in the triply-bonded trans structure (2.1231 Å) followed by the doubly-bonded monobridged (2.1352 Å) and the doubly-bonded vinylidene (2.2201 Å) isomers. The singly-bonded dibridged isomer contains the longest Si-Si bond length (2.2281 Å).

Figure 4.1-2. The optimized structures of the Si_2H_2 isomers and transition states with energies relative to the global minimum (the dibridged isomer). The calculations were done at the CCSD(T)/aug-cc-pVTZ level of theory.

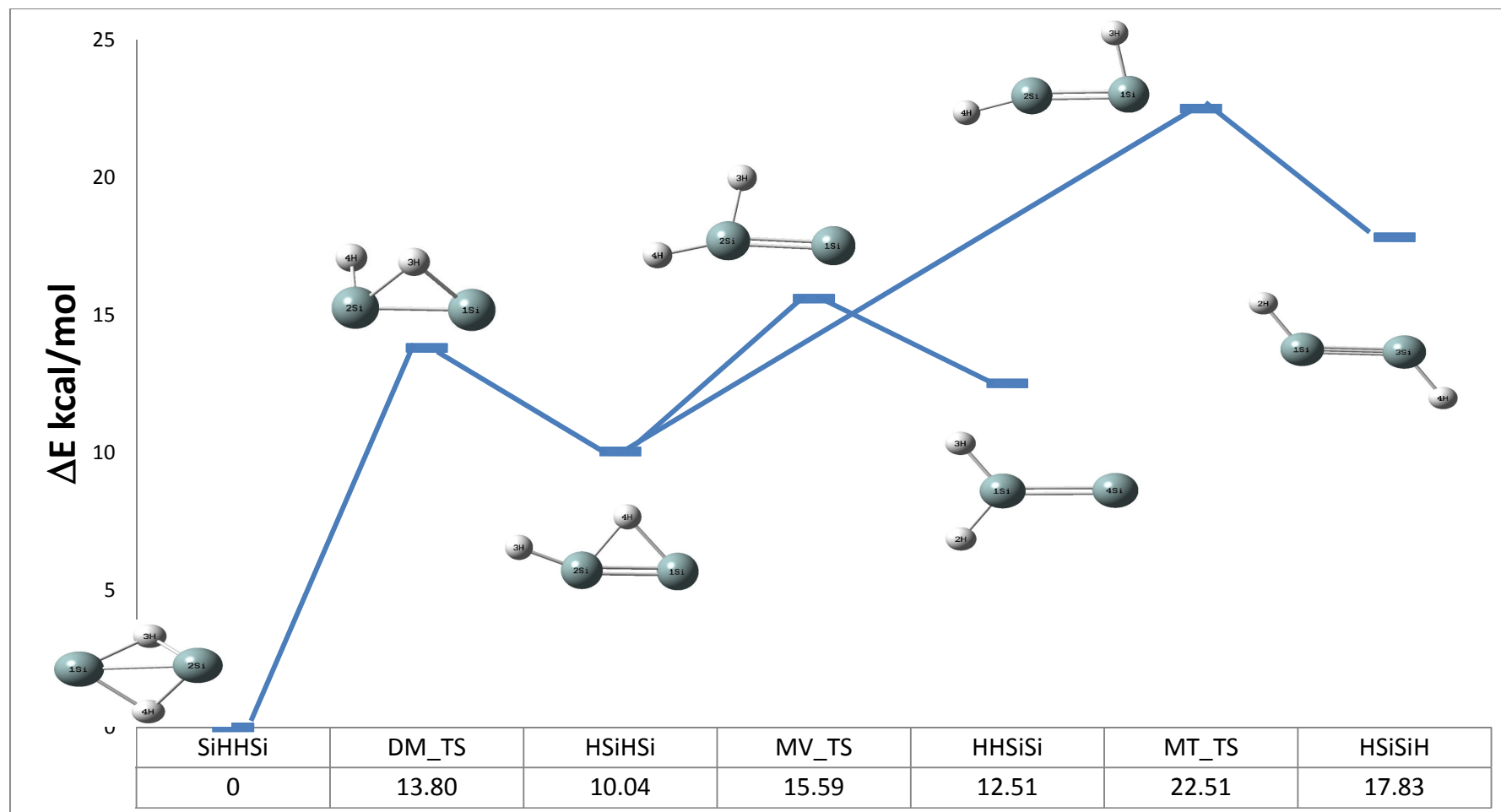


Table 4.1-1. Geometric properties of the Si₂H₂ minima calculated at the CCSD(T)/ aug-cc-pVTZ level.

	HHSiSi, C _{2v}	HSiSiH, C _{2h}	SiHHSi, C _{2v}	HSiHSi, C _s
Si2H1 ^a				1.6416
SiSi ^a	2.2201	2.1231	2.2281	2.1352
H2Si2 ^a	1.4865	1.4922	1.6762	1.4910
β HSiSiH ^b	180.00	180.00	104.59	0.00
α Si1Si2H1 ^b				52.29
α Si1Si2H2 ^b	123.81	124.90	48.35	159.22
^a ångström				
^b degrees				

Table 4.1-2. Geometric properties of the Si₂H₂ transition states calculated at the CCSD(T)/ aug-cc-pVTZ level.

	DM-TS, C ₁	MV-TS, C _s	MT-TS, C _s
Si2H1 ^a	1.7071	1.5244	1.5386
SiSi ^a	2.2250	2.1625	1.1412
H2Si1 ^a	1.5169	1.4817	1.4979
β HSiSiH ^b	82.54	180.00	180.00
α Si1Si2H1 ^b	48.18	82.03	80.18
α Si1Si2H2 ^b	95.91	164.18	165.4
^a ångström			
^b degrees			

The dibridged form has the lowest energy followed by the monobridged form with ΔE= 10.04 kcal/mol, then vinylidene with ΔE=12.51 kcal/mol and the trans isomer with ΔE= 17.83 kcal/mol. Coupled-cluster theory investigations of the Si₂H₂ isomers performed by Grev and Schaefer [24] showed the energies relative to the dibridged isomer as follows: monobridged (8.7 kcal/mol), vinylidene (11.6 kcal/mol) and trans (16.3 kcal/mol). The relative energies calculated here are about 1.3 kcal/mol higher than those obtained by Grev and Schaefer. However, note that the basis sets employed are different. Grev and Schaefer used TZ2P/TZ2df, whereas we employed aug-cc-pVTZ. A more detailed comparison of the relative energies will be done later in this sub-chapter.

CCSD(T)- F12 calculations

The performance of the recently developed CCSD(T)-F12 method [66, 68] (referred to as F12 in this thesis), as implemented in MOLPRO version 2010.1 [85], was studied for the Si_2H_2 system. According to the literature [66, 68, 132], the F12 method has faster convergence properties and gives more accurate results than CCSD(T) calculations with similar basis set size. They even suggested that CCSD(T)/aug-cc-pV5Z quality results can be achieved with CCSD(T)-F12 using the aug-cc-pVTZ basis. A detailed explanation of the CCSD(T)-F12a method can be found in Chapter 1.5. We were interested in the accuracy of the geometric properties, relative energies and harmonic vibration frequencies when the F12 method was employed. Comparison of the calculated results with the experimental values can be helpful to estimate the most effective level of theory. The chosen level of theory will be used to compute the energies required for constructing the Si_2Li_2 potential energy surface (PES) (Chapter 7.2).

In the first step the geometric properties were investigated with increasing basis set size. The CCSD(T)-F12a method in conjunction with the specially developed basis sets denoted as cc-pVXZ-F12 ($X=2-4$) [133] was employed. In the following, these basis sets will be further abbreviated as VXZ-F12. The VXZ-F12 orbital basis set was combined with the OptRI auxiliary basis set [134], which is necessary for the CABS resolution of the identity step [79]. The cc-pVXZ/JKFIT ($X=2-4$) [135] basis set of Weigend was used for density fitting of the Fock and exchange matrices, while the density fitting of the remaining integral quantities employed the aug-cc-pVXZ/MP2FIT ($X=2-4$) basis sets of Weigend et al. [136]. The approximation 3C(FIX) [66, 68, 81], which is the default in MOLPRO 2010.1, was employed in the preliminary density-fitting MP2-F12 computations. The Geminal Slater Exponent value of $\gamma=1$ for the cc-VXZ-F12 ($X=2-4$) basis sets was employed here. The triples energy was automatically scaled, see equation 1.5-22, as suggested in the MOLPRO manual in all calculations performed here. The F12 approach described above will be also used in the other (F12) calculations done here.

The geometric properties for the Si₂H₂ minima calculated at different levels of theory are shown in Table 4.1-3.

Table 4.1-3. Geometric properties of the Si₂H₂ isomers at the CCSD(T)-F12a/cc-pVXZ-F12 (X=2-4) level of theory.

	HSiHSi				SiHHSi		
	VDZ-F12	VTZ-F12	VQZ-F12		VDZ-F12	VTZ-F12	VQZ-F12
Si ₂ H ₁ ^a	1.6315	1.6334	1.6332				
SiSi ^a	2.1217	2.1182	2.1170	SiSi ^a	2.2104	2.2073	2.2061
H ₂ Si ₂ ^a	1.4876	1.4976	1.4872	HSi ^a	1.6650	1.6675	1.6679
β HSiSiH ^b	0.00	0.00	0.00	β HSiSiH ^b	104.35	104.15	104.06
α Si1Si2H1 ^b	52.11	52.31	52.38				
α Si1Si2H2 ^b	158.53	159.26	159.45	α SiSiH ^b	48.41	48.56	48.60
^a ångström							
^b degrees							

	HHSiSi				HSiSiH		
	VDZ-F12	VTZ-F12	VQZ-F12		VDZ-F12	VTZ-F12	VQZ-F12
SiSi ^a	2.2094	2.2056	2.2047	SiSi ^a	2.1116	2.1073	2.1064
HSi ^a	1.4816	1.4822	1.4818	HSi ^a	1.4868	1.4872	1.4870
β HSiSiH ^b	180.00	180.00	180.00	β HSiSiH ^b	180.00	180.00	180.00
α SiSiH ^b	123.55	123.58	123.57	α SiSiH ^b	124.44	124.79	124.82
^a ångström							
^b degrees							

Upon basis set extension in the VXZ-F12 (X=2–4) series, all Si–Si bond lengths are reduced, but the amount of the reduction depends on the type of structure considered. The difference (from X=2 to 4) is 0.0047 Å for the monobridged and vinylidene, 0.0043 Å for the dibridged and 0.0052 Å for the trans structure. There is no similar pattern in the Si–H bond length and angles. The Si–H bond lengths increased or decreased (upon basis set extension); the same situation can be seen with the angles.

To investigate the convergence properties of the CCSD(T)/aug-cc-pVXZ and CCSD(T)-F12a/cc-pVXZ-F12 methods (where X=2–4), a comparison of the energies relative to

the global minimum was made. The CCSD(T)/aug-cc-pVXZ and CCSD(T)-F12a/cc-pVXZ-F12 levels of theory will be abbreviated as AVXZ and VXZ-F12, respectively. The results can be seen in Figure 4.1-3 to Figure 4.1-5.

Figure 4.1-3. Energy of the HSiHSi isomer (relative to the dibridged isomer) as function of VXZ-F12 and AVXZ basis set size.

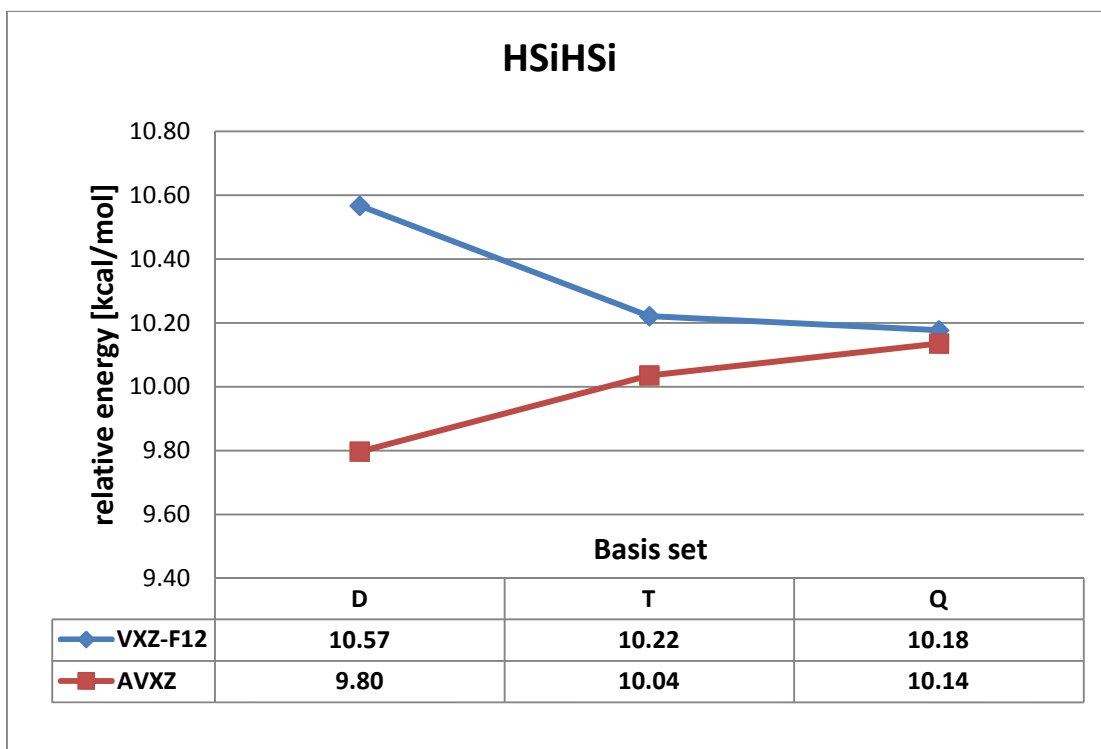


Figure 4.1-4. Energy of the HHSiSi isomer (relative to the dibridged isomer) as function of VXZ-F12 and AVXZ basis set size.

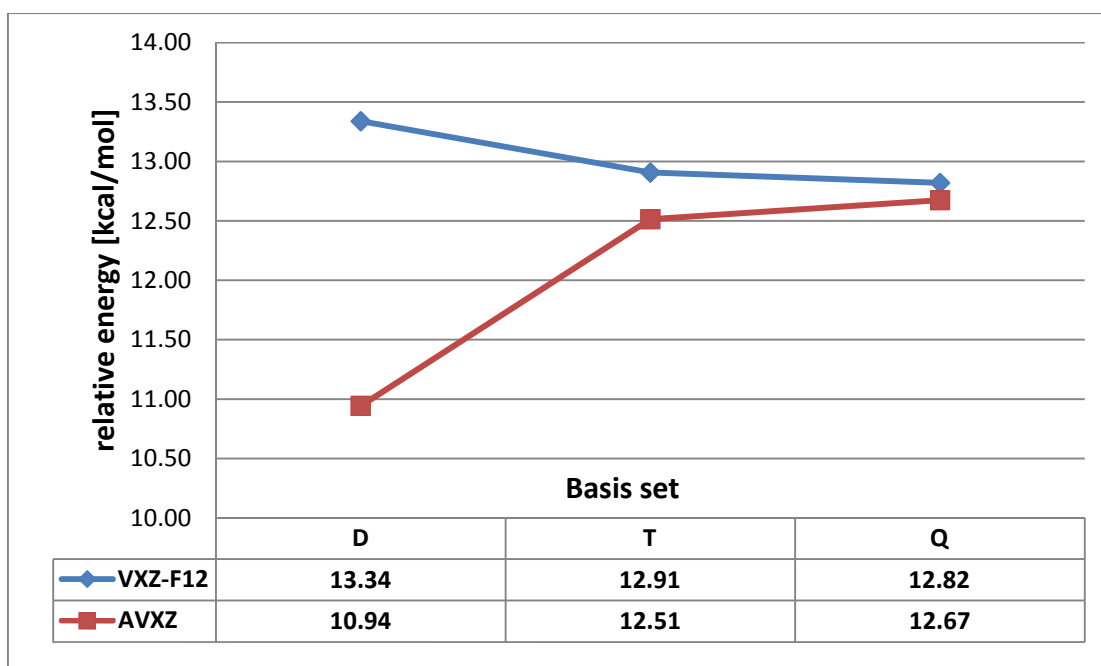
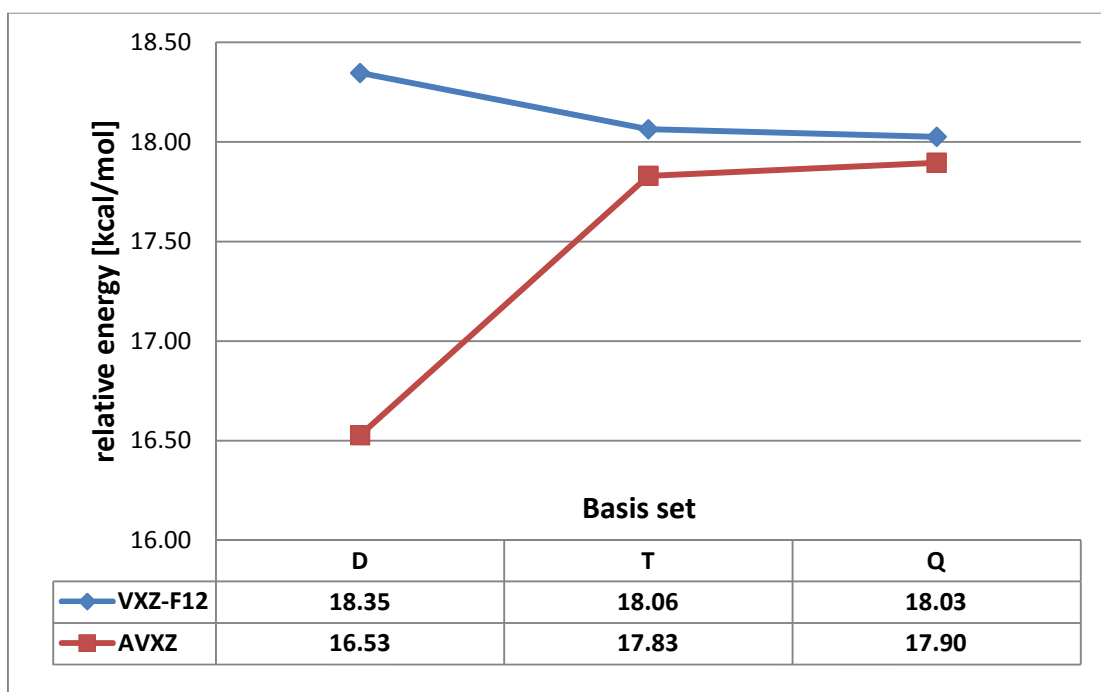


Figure 4.1-5. Energy of the HSiSiH isomer (relative to the dibridged isomer) as function of VXZ-F12 and AVXZ basis set size.



The differences in the isomerisation energy with respect to increasing basis set size are larger at the standard CCSD(T)/AVXZ level than at the CCSD(T)-F12a/VXZ-F12 level

of theory. The largest difference for the AVXZ level is 1.57 kcal/mol (between double and triple- ζ); this is reduced with further basis set extension by 0.16 kcal/mol (both differences for the vinyl isomer). In the VXZ-F12 calculations the largest difference between double and triple- ζ is 0.43 kcal/mol then a further 0.09 kcal/mol from VTZ-F12 to VQZ-F12 (both differences for the vinyl isomer). Thus, a larger change can be seen upon basis set extension from the VDZ to VTZ level, than from the VTZ to VQZ level. This pattern exists in all of the studied Si₂H₂ isomers, and shows that the isomerisation energies are converging with increasing basis set size.

Comparisons of the Si–Si bond distances of the calculated isomers with respect to increasing basis set size were made. The CCSD(T)/AVXZ and CCSD(T)-F12a/VXZ-F12 (where X=2–4) levels of theory were employed. Note, that the Si–Si distance values calculated at the AVQZ level were taken from reference [52]; the rest of the calculations were performed here. The results are shown in Figure 4.1-6 to Figure 4.1-9. The CCSD(T)-F12 method gives shorter Si–Si distances than conventional CCSD(T), and the distances vary less with basis set size. The AVQZ result is achieved already by the VDZ-F12 level in all of the isomers. This confirms the statement by Werner et al. [66], who suggested that CCSD(T)-F12 calculations are usually more accurate and convergence is reached faster, as compared to CCSD(T) calculations with the same basis set limit (the standard Dunning’s types of basis sets). The largest difference between distances calculated with basis sets of double and triple- ζ quality is 0.0043 Å (in the trans isomer) for the VXZ-F12 level and 0.0362 Å (in the dibridged isomer) for the AVXZ level. Moreover, the largest difference when the basis set is increased from triple to quadruple- ζ quality is 0.0012 Å (in the dibridged isomer) for the VXZ-F12 level and 0.0135 Å (in the dibridged isomer) for the AVXZ level. It is likely that the complete basis set (CBS) limit has been nearly achieved at the VQZ-F12 level.

The geometric properties were calculated using different *ab initio* and DFT methods with various levels of basis set. The equilibrium semi-experimental values of the dibridged geometric properties were taken from reference [52]. The semi-experimental results presented here were produced by applying anharmonic corrections to the experimental rotational constants [137] of the dibridged and monobridged species. The

anharmonic corrections were calculated using second order perturbation theory from the CCSD(T)/cc-pV(Q+d)Z potential energy surface of Law et al. [52]. More details can be found in Ref [52]. Thus, the geometric properties and harmonic vibration frequencies used as references here are semi-experimental. Below CCSD(T)/V(6+d)Z is used as an abbreviation for the CCSD(T)/cc-pV(6+d)Z calculations performed by the authors of Ref. [52]. In the following discussion the B3LYP/6-311+G(d), MP2/6-31G(d), CCSD(T)/AVTZ and CCSD(T)-F12a/VTZ-F12 methods will be abbreviated as B3LYP, MP2, CCSD(T) and F12, respectively. The results are shown in Table 4.1-4.

The calculated Si–Si distance agrees well with the semi-experimental value for all theoretical methods used here. The largest difference can be seen for CCSD(T)/AVTZ (0.0291 Å) and the smallest for the MP2/6-31G(d) level (0.0065 Å). The CCSD(T)/V(6+d)Z level and the MP2/6-31G(d) method reproduced the semi-experimental Si–H value to 0.0037 Å and 0.0059 Å, respectively. The AVTZ and B3LYP methods give larger errors for the Si–H distance. The HSiSiH dihedral angle values computed with the CCSD(T) and CCSD(T)/V(6+d)Z levels agree well with the semi-experimental HSiSiH dihedral angle value; the error is only 0.53° and 0.07°, respectively. However, it can be seen that the MP2 method *overestimates* the dihedral angle by 6.33° while the B3LYP method *underestimates* by 1.45°. Both the F12 methods employed here (VDZ-F12 and VTZ-F12) reproduce well the semi-experimental values (distances and angles). Whereas, VTZ-F12 gives a more accurate angle. Note, that by using the VTZ-F12 level we are able to reproduce with good accuracy the results calculated at the CCSD(T)/V(6+d)Z level.

Figure 4.1-6. Si–Si bond length variation with increasing basis set size for the SiHHSi isomer.

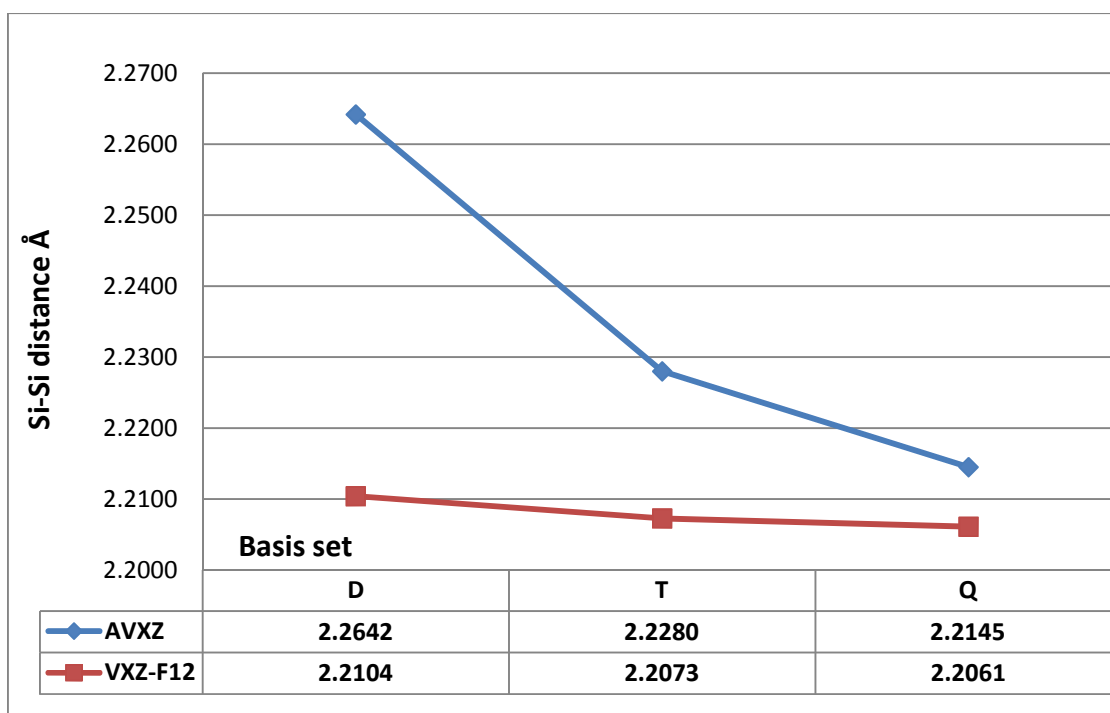


Figure 4.1-7. Si–Si bond length variation with increasing basis set size for the HSiHSi isomer.

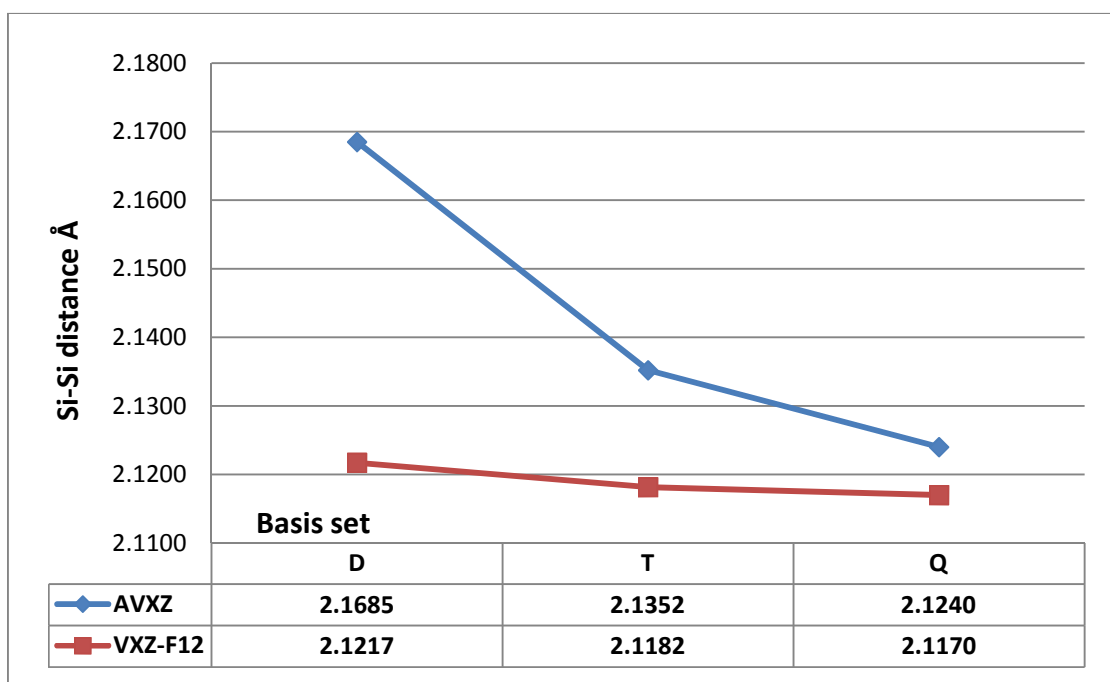


Figure 4.1-8. Si–Si bond length variation with increasing basis set size for the HHSiSi isomer.

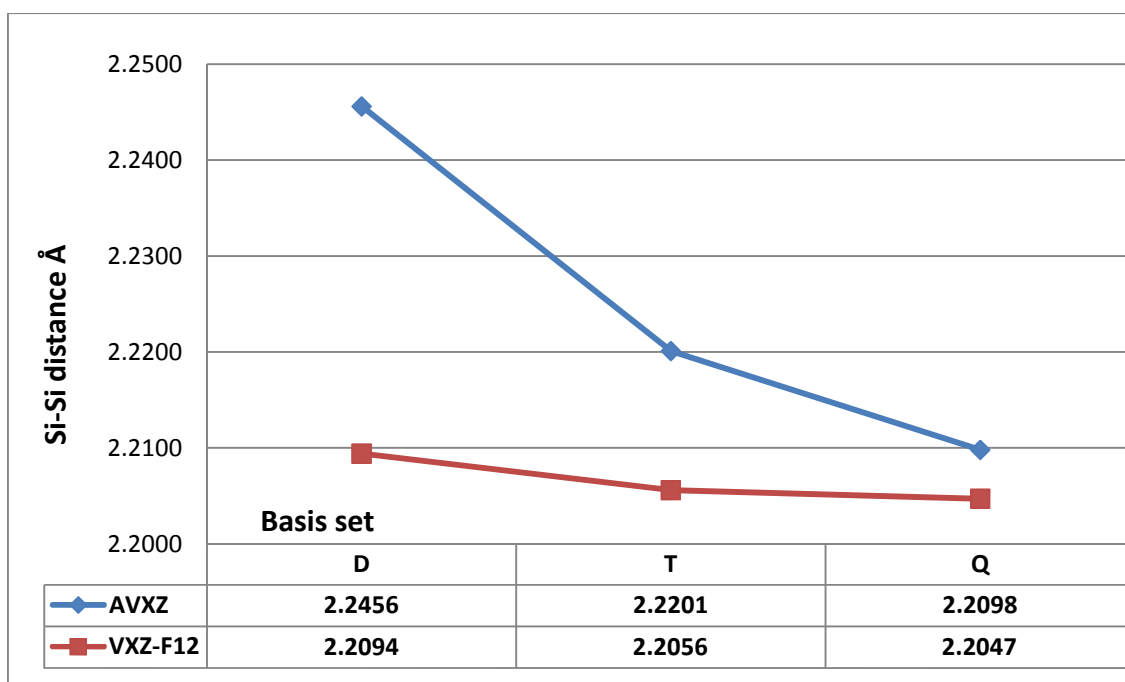


Figure 4.1-9. Si–Si bond length variation with increasing basis set size for the HSiSiH isomer.

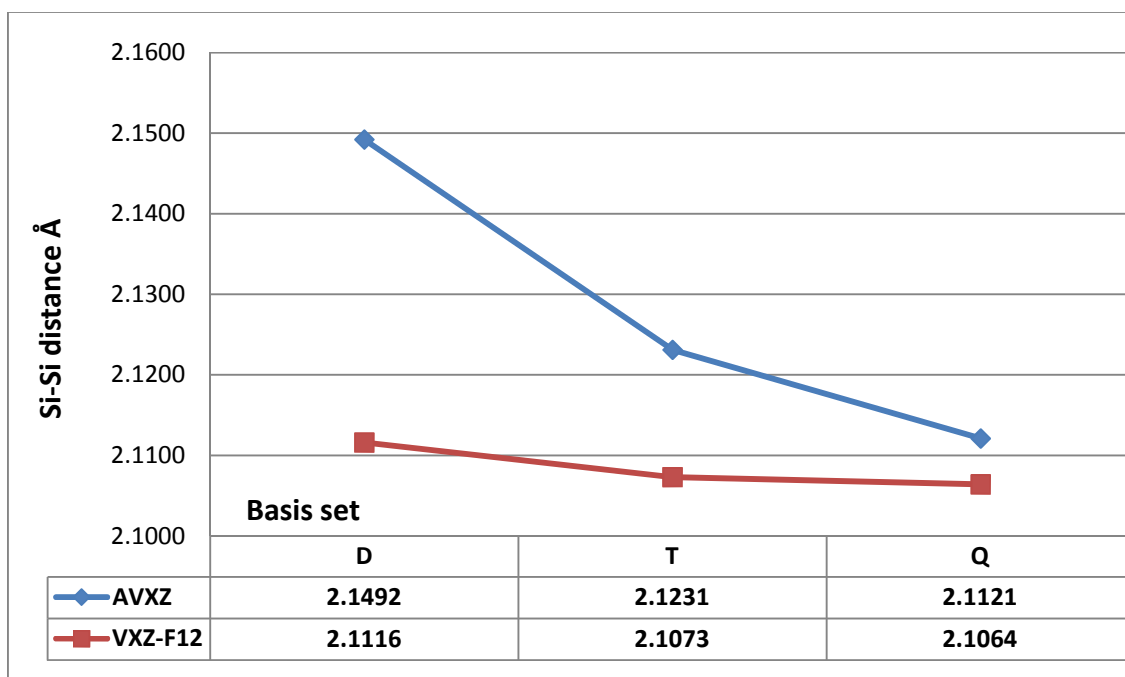


Table 4.1-4. Comparison of the calculated geometric properties of the dibridged isomer with the semi-experimental values.

	SiSi ^a	HSi ^a	β HSiSiH ^b
B3LYP/6-311+G(d)	2.1896	1.6877	102.61
MP2/6-31G(d)	2.2055	1.6696	110.39
CCSD(T)/AVTZ	2.2281	1.6762	104.59
CCSD(T)/V(6+d)Z *	2.2067	1.6674	104.13
CCSD(T)-F12a/VDZ-F12	2.2104	1.6650	104.35
CCSD(T)-F12a/VTZ-F12	2.2073	1.6675	104.15
Semi-Expt. *	2.1990	1.6637	104.06

^a ångström
^b degrees
* taken from reference [52]

The ground-state values (r_0) of the geometric properties of the monobridged isomer were taken from Ref. [25, 26]. A comparison of the CCSD(T)-F12a/VXZ-F12 results with available literature values is shown in Table 4.1-5.

Table 4.1-5. Comparison of the calculated geometric properties of the monobridged isomer with literature values.

	monobridged		
	CCSD(T)-F12a/ VDZ-F12	CCSD(T)-F12a/ VTZ-F12	Semi- Experimental *
SiSi ^a	2.1217	2.1182	2.119
Si2H1 ^a	1.6315	1.6334	1.629
2HSi2 ^a	1.4876	1.4976	1.474
α Si1Si2H1 ^b	52.11	52.31	52.50
α Si1Si2H2 ^b	158.53	159.26	157.50

^a ångström
^b degrees
* taken from reference [26]. Note that the experimental geometry was obtained by fixing the Si1Si2H1 angle to its CISD/TZ2P value of 52.5 degrees. These are “ r_0 ” values.

Both F12 levels (VDZ-F12 and VTZ-F12) reproduce well the semi-experimental values (distances and angle). However, the VTZ-F12 level gives slightly better results (for both

distances and angles) for the bridged hydrogen atom and for the Si–Si bond length, whereas VDZ-F12 gives better values for the terminal hydrogen atom (both distances and angles). Note, that the semi-empirical values are ground-state values (r_0), while the values calculated here are equilibrium ones. Thus, the calculated and semi-empirical values are not exactly comparable.

A comparison of the relative energies for the Si_2H_2 minima using the popular DFT B3LYP/6-311+G(d), standard CCSD(T)/AVTZ and the F12 (CCSD(T)-F12a/VTZ-F12) methods is shown in Table 4.1-6.

Table 4.1-6. Relative energy (kcal/mol) of the Si_2H_2 isomers computed at different levels of theory.

	dibridged	monobridged	disilavinylidene	trans
CCSD(T)/AVTZ	0.00	10.57	13.34	18.35
CCSD(T)-F12a/VTZ-F12	0.00	10.22	12.91	18.06
B3LYP/6-311+G(d)	0.00	9.54	8.34	16.68

The work of Grev and Schaefer [24] shows that the relative energy (at the CCSD(T)/TZ2df/TZ2p level of theory) of the monobridged isomer relative to the dibridged global minimum is 10.0 kcal/mol. The vinyl isomer lies 12.2 kcal/mol above the dibridged isomer and the trans isomer lies 17.3 kcal/mol above the global minimum. Both *ab initio* methods used here agree well with the results of Grev and Schaefer. However, the DFT method *underestimates* all values computed by Grev and Schaefer (with an average absolute difference is 1.7 kcal/mol). Moreover, according to the DFT method the vinyl isomer is more stable than the monobridged structure. Thus, the DFT method does not reproduce the order of stability of the Si_2H_2 isomers properly in comparison with the CCSD(T) results by Grev and Schaefer and the *ab initio* calculations done here.

Frequencies

Harmonic frequencies were computed for the optimized structures using various DFT and *ab initio* methods. We used the same methods as employed for calculating the relative energies (Table 4.1-6). In the following discussion the B3LYP/6-311+G(d), CCSD(T)/AVTZ and CCSD(T)-F12a/VTZ-F12 methods will be abbreviated as B3LYP, CCSD(T) and F12 respectively. The calculated harmonic frequencies are listed in Table 4.1-7.

The frequencies will be discussed separately for each isomer.

In the dibridged structure both the *ab initio* (CCSD(T) and F12) sets of vibrational frequency values are similar: the largest difference between the results calculated with the two different methods is 19 cm^{-1} (for the highest frequency vibration mode). A comparison of the frequencies calculated with the B3LYP level with the *ab initio* results shows large *underestimations* using B3LYP for the vibrational frequencies, especially for the higher frequency modes: for the first to fourth modes the average difference is 89 cm^{-1} . However, the fifth vibration is *overestimated* (average difference between B3LYP and *ab initio*) by about 69 cm^{-1} . All these methods calculated similar values for the lowest frequency (sixth) vibrational mode. The average absolute difference between the frequencies calculated with B3LYP and the *ab initio* (CCSD(T) and F12) methods is 72 cm^{-1} .

Table 4.1-7. Harmonic frequencies for the Si₂H₂ isomers calculated at different levels of theory; the results are listed in descending order of wavenumber (cm⁻¹) units.

Si ₂ H ₂				
	CCSD(T)/ AVTZ ^a	CCSD(T)-F12a/ VTZ-F12	B3LYP/ 6-311+G(d)	
<u>dibridged</u>				
	1631	1650	1592	SiH sym. str.
	1544	1562	1500	SiH antisym. str.
	1221	1236	1119	SiH antisym. str.
	1152	1167	1013	SiH antisym. str.
	909	921	985	Butterfly
	515	529	522	SiSi str.
<u>monobridged</u>				
	2186	2195	2172	SiH _t str.
	1644	1664	1620	Si ₂ H _b sym. str.
	1136	1163	997	Si ₂ H _b antisym. str.
	602	611	610	SiSi str.
	454	460	446	H _b SiH _t scissors
	159	153	41	out of plane
<u>vinyl</u>				
	2235	2247	2220	SiH antisym. str.
	2207	2221	2193	SiH sym str.
	887	895	895	SiH ₂ scissors
	517	523	520	SiSi str.
	334	337	334	SiH ₂ wag
	263	270	268	SiH ₂ rock
<u>trans</u>				
	2192	2210	2171	SiH antisym. str.
	2187	2201	2165	SiH sym. str.
	609	603	626	SiH sym. bend
	561	568	561	SiSi str.
	287	265	225	SiH antisym. bend
	242	211	204	HSiSiH torsion
^a taken from reference [51]				

For the monobridged isomer, the CCSD(T) and F12 levels of theory give similar frequency values; the average difference is 12 cm⁻¹. The largest difference (26 cm⁻¹) is found for the third mode. The B3LYP frequencies show better agreement with the

corresponding *ab initio* results than for the dibridged isomer, except the third and last vibrations which are hugely *underestimated* (more than 100 cm^{-1}); however, the average difference (55 cm^{-1}) is lower than that of the dibridged isomer.

All methods give similar frequency results for the vinyl structure. The average difference is between 8.5 cm^{-1} (from CCSD(T) to F12) and 10 cm^{-1} (from B3LYP to F12).

Five of the calculated vibration frequencies for the trans isomer (the first four and the last mode) have similar values, for all three methods. The average difference is between 15 cm^{-1} (from CCSD(T) to F12) and 26 cm^{-1} (from B3LYP to F12). However, significant differences in the fifth vibration can be seen. The B3LYP method *overestimates* the fifth vibration frequency by 62 cm^{-1} compared to the CCSD(T) level.

We compared our results with the values presented in two papers from the literature: the very recent paper by Law et al. [52] and the paper by Grev and Schaefer [24]. We chose the CCSD(T)/cc-pCV(T+d)Z method (Law et al.) and CCSD(T)/TZ2df/TZ2p (Grev and Schaefer) as references. CCSD(T)/cc-pCV(T+d)Z will be abbreviated as CVTZd and CCSD(T)/TZ2df/TZ2p as TZ2df.

The CCSD(T) results obtained here agree perfectly with the CCSD(T)/AVTZ results from Law et al. [52] (as they of course should). The average absolute difference for the frequencies of all isomers calculated with F12 and CVTZd is 9 cm^{-1} and the average absolute difference between the F12 and TZ2df results is 23 cm^{-1} . A similar difference with comparison to the CVTZd calculation (10 cm^{-1}) can be seen for the CCSD(T) level. From all methods considered here, DFT showed the largest differences: 44 cm^{-1} (between B3LYP and CVTZd) and 28 cm^{-1} (between B3LYP and TZ2df).

The semi-experimental values of the dibridged harmonic frequencies were taken from [52]. Calculations of harmonic frequencies using different *ab initio* and DFT methods with various sizes of basis sets were performed. The CCSD(T)/cc-pV(Q+d)Z method will be abbreviated by VQZd. The B3LYP/6-311+G(d), CCSD(T)/aug-cc-pVTZ and

CCSD(T)-F12a/cc-pVTZ-F12 abbreviations remain the same as in the previous paragraphs. A comparison of the calculated harmonic frequencies with the semi-experimental values can be seen in Table 4.1-8.

Table 4.1-8. Comparison of calculated harmonic frequencies with literature values.

Dibridged				
B3LYP/ 6-311+G(d)	CCSD(T)/ AVTZ	CCSD(T)-F12a/ VTZ-F12	CCSD(T)/ V(Q+d)Z *	Semi-Expt. *
522	529	514	528	
985	921	909	918	922
1013	1167	1152	1170	
1119	1236	1221	1239	1226
1500	1562	1543	1560	1552
1592	1650	1631	1649	
* values taken from reference [52]				

The B3LYP method gives the largest error (average absolute difference of 74 cm^{-1}) especially for the fourth vibration mode. All the *ab initio* methods reproduced the semi-experimental values with similar accuracy. The average absolute error for AVTZ is 7 cm^{-1} , for F12 9 cm^{-1} and for VQZd 8 cm^{-1} . Moreover, for the highest vibration modes the F12 level reproduced the semi-experimental values with the best accuracy (with an average error of 7 cm^{-1}), whereas for the AVTZ and VQZd levels the average error is 10 cm^{-1} . Thus, we can conclude that the *ab initio* methods employed here reproduced the literature frequency values well and it is hard to determine the most accurate method.

4.2 The Si₂HF isomers.

The next studied structures are compounds similar to the Si₂H₂ species; however, a hydrogen atom will be substituted by a fluorine atom. The Si₂H₂ isomers of Grev and Schaefer [24] will be taken as starting geometries. Two different monobridged structures (one with a hydrogen as a bridged atom, the second one with a bridged fluorine) were considered. Average literature (theoretical) values of the Si–F bond distances were used in the fluorine substituted starting geometries.

Computational methods

The structures were optimized again with the CCSD(T)/aug-cc-pVXZ, CCSD(T)-F12a/cc-pVTZ-F12 and B3LYP/6-311+G(d) levels of theory (where X=2-4). All *ab initio* calculations were performed using MOLPRO versions 2006.1-2010.1 [85, 120] software packages whereas the DFT calculations were done using Gaussian 03 [138].

Harmonic vibrational frequency computations were done at the optimized structures to characterise these as minima or transition states (TS). The frequency calculations were done at the CCSD(T)/aug-cc-pVTZ and B3LYP/6-311+G(d) levels of theory.

The HSiSiF, FSiHSi, HFSiSi and SiHFSi formulae refer to, respectively, the trans, monobridged, vinylidene and dibridged isomers, respectively. The VD_TS, MV_TS and MT_TS symbols represent the transition states on the paths between the vinyl and dibridged structures (surprisingly), between the monobridged and vinylidene structures and between the monobridged and trans structures, respectively. Note, that in the following discussion all the correlation consistent basis sets employed here (such as aug-cc-pVXZ (where X=2–4)) will be abbreviated as AVXZ, and the methods such as: CCSD(T)/aug-cc-pVTZ, CCSD(T)-F12a/cc-pVTZ-F12 and B3LYP/6-311+G(d) will be abbreviated as CCSD(T), F12 and B3LYP, respectively. We used the NBO [102, 103] method to establish the (multiple) bonded properties (only for the minima) as presented in the previous Si₂H₂ sub-chapter (4.1). The CCSD/cc-pV(T+d)Z level of theory

utilizing the Gaussian 03 software package was employed. The isomers and transition states obtained are listed in Table 4.2-1 and Table 4.2-2.

All the calculated isomers of Si₂HF and transition states are depicted in Figure 4.2-1. The energies relative to the monobridged structure (global minimum) are listed at the bottom of Figure 4.2-1. The reaction paths between the critical points are represented schematically by lines.

Table 4.2-1. Geometric properties of the calculated Si₂HF minima.

	CCSD(T)/AVTZ			
	HFSiSi, C _s	HSiSiF, C _s	SiHFSi, C _s	FSiHSi, C _s
SiF ^a	1.6163	1.6049	1.9003	1.6069
SiSi ^a	2.2348	2.1546	2.2696	2.1395
HSi ^a	1.4855	1.5100	1.7108	1.7002 ^c
β HSiSiF ^b	180.00	180.00	106.60	0.00
α SiSiF ^b	126.16	142.46	53.34	160.83
α SiSiH ^b	126.03	95.95	48.45	50.27 ^c

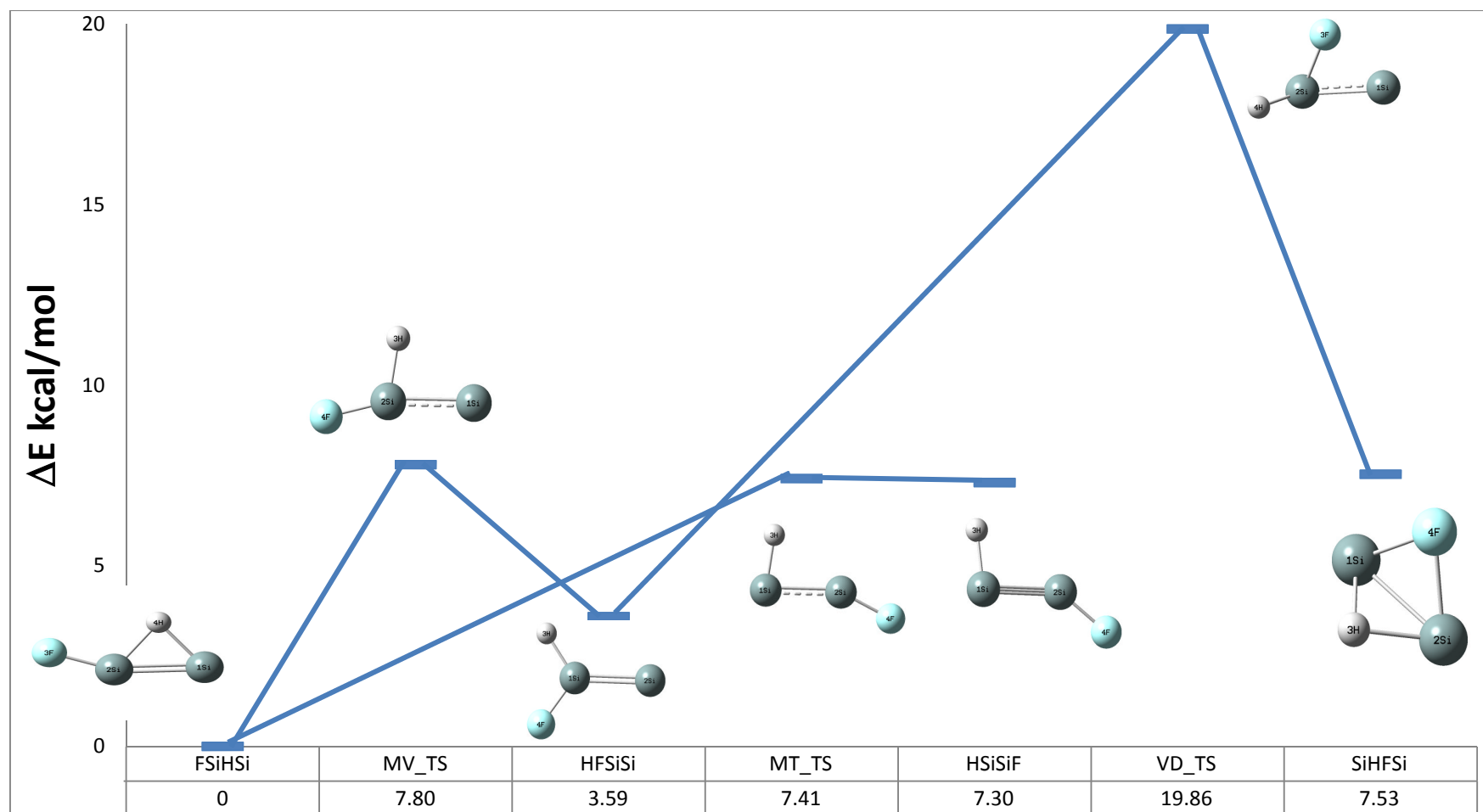
^a ångström
^b degrees
^c The Si2H and Si1Si2H values between the silicon (connected to the terminal fluorine atom) and the bridged hydrogen atom.

Table 4.2-2. Geometric properties of the calculated Si₂HF transition states.

	CCSD(T)/AVTZ		
	VD_TS, C ₁	MV_TS, C _s	MT_TS, C _s
SiF ^a	1.8033	1.6056	1.6039
SiSi ^a	2.2314	2.1584	2.1519
HSi ^a	1.4931	1.5286	1.5274
β HSiSiF ^b	84.10	180.00	180.00
α SiSiF ^b	60.94	165.73	154.55
α SiSiH ^b	126.9	81.91	82.80

^a ångström
^b degrees

Figure 4.2-1. The optimized structures of the Si₂HF isomers and transition states with energies relative to the global minimum (monobridged). The calculations were done at the CCSD(T)/aug-cc-pVTZ level of theory.



Note that the F-bridged starting structure (HSiFSi) converged to the vinylidene form, so apparently there is no fluorine-bridged structure as a minimum.

The shortest Si-Si bond length occurs in the doubly-bonded monobridged structure (2.1395 Å) followed by the triply-bonded trans structure (2.1546 Å), the doubly-bonded vinylidene structure (2.2348 Å) and then the singly-bonded dibridged structure (2.2696 Å). Note, that it is unusual that a doubly-bonded structure has a shorter Si-Si bond length than a triply-bonded structure. It is not clear why this issue occurs here. Additional studies are necessary to explain this issue. The calculation shows that the Si-F distances have a length of around 1.6 Å, except that of the dibridged structure, which is 1.90 Å (the bridged atoms usually have longer bond lengths). The Si-H distances in the vinylidene and the trans isomers have a length around 1.5 Å whereas the bridged structures (monobridged and dibridged) show Si-H distances of around 1.71 Å. All the isomers except the dibridged structure are planar.

The monobridged form has the lowest energy followed by the vinylidene form with $\Delta E = 3.59$ kcal/mol, then the trans form with $\Delta E = 7.30$ kcal/mol and the dibridged form with $\Delta E = 7.53$ kcal/mol. On the reaction paths between the minima three transition states were found: MV_TS is the transition state between the monobridged and vinylidene structures (7.80 kcal/mol above the global minimum), MT_TS is the transition state between the monobridged and trans structures (7.41 kcal/mol above the global minimum) and VD_TS is the transition state between the vinyl and dibridged structures (19.86 kcal/mol above the global minimum).

A comparison of the geometric properties calculated with increasing basis set level was performed. The calculated geometric properties at the CCSD(T)/AVXZ (where X=2-4) levels of theory are listed in Table 4.2-3. The "Si2" in the table represents the silicon connected to the terminal fluorine atom.

Table 4.2-3. Geometric properties of the Si₂HF isomers calculated at the CCSD(T)/AVXZ (X=2–4) level of theory.

HFSiSi				FSiHSi			
	AVDZ	AVTZ	AVQZ		AVDZ	AVTZ	AVQZ
SiF ^a	1.6618	1.6163	1.6055	Si2F ^a	1.6533	1.6069	1.5967
SiSi ^a	2.2613	2.2348	2.2244	SiSi ^a	2.1783	2.1395	2.1281
HSi ^a	1.4956	1.4855	1.4826	HSi2 ^a	1.7173	1.7002	1.6920
β HSiSiF ^b	180.00	180.00	180.00	β HSiSiF ^b	0.00	0.00	0.00
α SiSiF ^b	124.24	126.16	125.62	α Si1Si2F ^b	158.64	160.83	160.59
α SiSiH ^b	128.20	126.03	126.28	α Si1Si2H ^b	49.73	50.27	50.32
^a ångström							
^b degrees							

HSiSiF				SiHFSi			
	AVDZ	AVTZ	AVQZ		AVDZ	AVTZ	AVQZ
SiF ^a	1.6510	1.6049	1.5946	SiF ^a	1.9338	1.9003	1.8857
SiSi ^a	2.1856	2.1546	2.1437	SiSi ^a	2.3111	2.2696	2.2549
HSi ^a	1.5187	1.5100	1.5043	HSi ^a	1.7255	1.7108	1.7051
β HSiSiF ^b	180.00	180.00	180.00	β HSiSiF ^b	106.30	106.60	106.80
α SiSiF ^b	138.57	142.46	140.49	α SiSiF ^b	53.45	53.33	53.28
α SiSiH ^b	99.45	95.95	97.69	α SiSiH ^b	48.02	48.44	48.61
^a ångström							
^b degrees							

The change in the bond lengths (Si–Si, Si–H and Si–F) is larger from AVDZ to AVTZ than from AVTZ to AVQZ. This indicates that the bond lengths are converging with increasing basis set size. The Si–Si distance and the relative energy are shown in Figure 4.2-2 and Figure 4.2-3.

Figure 4.2-2. Si–Si bond length variation with increasing basis set size for the Si₂HF isomers.

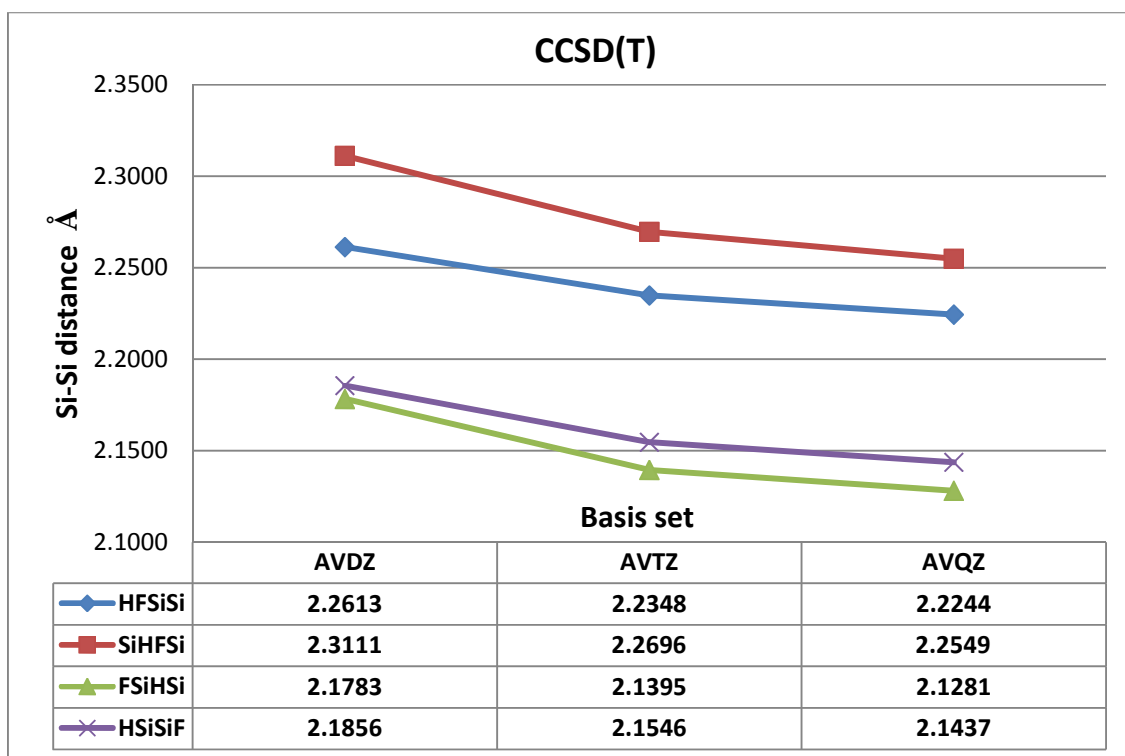
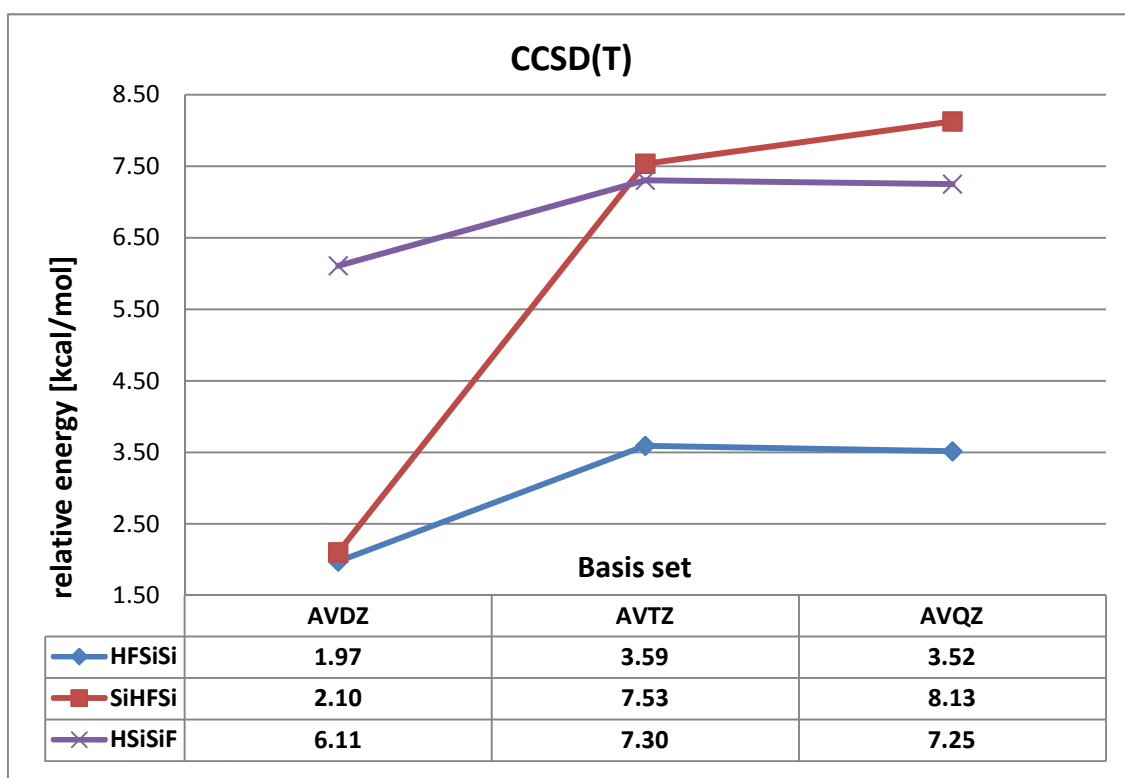


Figure 4.2-3. Relative energy of the Si₂HF isomers (relative to the monobridged isomer) as a function of AVXZ basis set size.



The Si–Si distance appears to converge with increasing basis set size for all four isomers which is clearly illustrated in Figure 4.2-2. Figure 4.2-3 shows a picture of the dependence of the isomerisation energy on basis set size; a significantly large improvement for the AVDZ to AVTZ basis set extension can be seen for the dibridged structure (5.43 kcal/mol) with a smaller increase (0.60 kcal/mol), when extension from the AVTZ to AVQZ level was performed. The vinyl and trans structures also show significant improvement for the AVDZ to AVTZ basis set extension; however, the change is not as large as for the dibridged isomer (1.62 kcal/mol and 1.19 kcal/mol, respectively). The very small change (actually a decrease) of the isomerisation energies from the AVTZ to AVQZ basis set shows that the vinyl and trans isomers have nearly reached convergence. Whereas, the AVDZ basis set gives the wrong isomerization energies and different minima ordering. It can be concluded then that AVDZ basis set is too small to properly calculate isomerization energies of the Si₂HF species.

CCSD(T)- F12 calculations

In addition to CCSD(T)-F12a/cc-pVTZ-F12, the CCSD(T)/cc-pVTZ and B3LYP/6-311+G(d) levels of theory were also employed for comparison. We used MOLPRO 2010.1 [85] and Gaussian 09 [138, 139]. Note, that in the following discussion the CCSD(T)/cc-pVTZ level will be abbreviated as CCSD(T), the CCSD(T)-F12a/cc-pVTZ-F12 level as F12 and the B3LYP/6-311+G(d) level of theory as B3LYP. The “Si2” in table represents the silicon connected to the terminal fluorine atom.

Table 4.2-4. Geometric properties computed at various levels of theory.

	Si ₂ HF		
	CCSD(T)/ AVTZ	CCSD(T)-F12a/ VTZ-F12	B3LYP/ 6-311+G(d)
dibridged			
SiF ^a	1.9003	1.8812	1.9292
SiSi ^a	2.2696	2.2477	2.2763
HSi ^a	1.7108	1.7026	1.7212
β HSiSiF ^b	106.60	106.74	105.42
α SiSiF ^b	53.33	53.31	53.85
α SiSiH ^b	48.44	48.70	48.61
monobridged			
Si ₂ F ^a	1.6069	1.5911	1.6249
SiSi ^a	2.1395	2.1213	2.1228
HSi ₂ ^a	1.7002	1.6892	1.7173
β HSiSiF ^b	0.00	0.00	0.00
α Si1Si2F ^b	160.83	160.91	160.95
α Si1Si2H ^b	50.27	50.41	50.91
vinyl			
SiF ^a	1.6163	1.5997	1.6356
SiSi ^a	2.2348	2.2195	2.2299
HSi ^a	1.4855	1.4816	1.4868
β HSiSiF ^b	180.00	180.00	180.00
α SiSiF ^b	126.16	125.34	125.33
α SiSiH ^b	126.03	126.40	126.83
trans			
SiF ^a	1.6049	1.5892	1.6222
SiSi ^a	2.1546	2.1379	2.1435
HSi ^a	1.5100	1.5030	1.5145
β HSiSiF ^b	180.00	180.00	180.00
α SiSiF ^b	142.46	140.61	146.07
α SiSiH ^b	95.95	97.42	92.67
^a ångström			
^b degrees			

The good general agreement in the bond lengths for all the methods used here can be seen in Table 4.2-4. However, it was shown in the Si₂H₂ Chapter 4.1 that the F12

method gives the most accurate result with comparison to the experimental values, and thus, this method will be taken as a reference. The largest average absolute difference is 0.033 Å (for the dibridged structure between the B3LYP and F12 methods) and the smallest is 0.008 Å (for the vinyl structure between the AVTZ and F12 methods). For the first three isomers the angle values obtained by the F12 method are reproduced (by the B3LYP and CCSD(T) methods) with an average accuracy of 0.41° however, in the trans structure a different picture can be seen. The B3LYP method shows a difference as large as 5.5° for the SiSiF angle and the CCSD(T) as small as 1.5° for the SiSiH angle. Nevertheless the average absolute difference is 3.4° (when the differences between the F12 and the B3LYP and CCSD(T) methods are considered).

A comparison of the relative energies for the Si₂HF minima calculated using the DFT (B3LYP/6-311+G(d)) method, the CCSD(T)/AVTZ and F12 (CCSD(T)-F12a/VTZ-F12) methods was made and is shown in Table 4.2-5.

Table 4.2-5. Relative energies (kcal/mol) of the Si₂HF isomers calculated by various methods.

	dibridged	monobridged	vinyl	trans
CCSD(T)/AVTZ	7.53	0.00	3.59	7.30
CCSD(T)-F12a/VTZ-F12	8.71	0.00	3.72	7.37
B3LYP/6-311+G(d)	2.29	0.34	0.00	5.64

Both *ab initio* methods show similar values of the relative energy except for the dibridged structure. The CCSD(T) level *underestimates* the relative energy (with comparison to the F12 method) by around 1.2 kcal/mol (dibridged). The DFT method *underestimates* all of the relative energies. Moreover, the DFT method shows that the global minimum is the vinyl structure followed by the monobridged, dibridged and trans structures. Thus, the DFT method does not reproduce the isomerisation energies properly with comparison to the *ab initio* calculations.

Frequencies

Harmonic vibrational frequencies were calculated at the B3LYP/6-311+G(d) level in addition to the CCSD(T)/AVTZ level of theory. The calculated results are listed in Table 4.2-6.

Table 4.2-6. Harmonic frequencies for the Si₂HF isomers calculated at different levels of theory; the results are listed in descending order of wavenumber (cm⁻¹) units.

Si ₂ HF			
	CCSD(T)/ AVTZ	B3LYP/ 6-311+G(d)	
<u>dibridged</u>			
	1473.6	1432.4	SiH sym. str.
	969.8	877.3	SiH antisym. str.
	839.9	854.0	butterfly
	570.3	548.0	SiSi/SiF in-phase str.
	448.5	444.1	SiSi/SiF out-of-phase str.
	166.6	144.3	HF antisym. twist
<u>monobridged</u>			
	1628.2	1602.1	SiH sym. str.
	1053.0	940.3	SiH antisym. str.
	920.2	888.5	SiSi/SiF out-of-phase str.
	481.7	477.4	SiSi/SiF in-phase str.
	193.6	191.8	SiSiF in-plane bend
	118.7	35.5	out-of-plane
<u>vinyl</u>			
	2222.3	2202.8	SiH str.
	880.1	850.5	SiF str.
	778.7	773.4	SiSiH bend
	472.4	466.1	SiSi str.
	302.3	293.3	out-of-plane
	136.7	137.2	SiHF rock
<u>trans</u>			
	2108.8	2072.3	SiH str.
	908.1	877.9	SiF str.
	503.6	518.2	SiSi str./H in-plane-bend
	423.6	431.6	H in-plane-bend
	124.8	65.4	out-of-plane
	93.4	58.7	SiSiF/SiSiH out-of-phase bend

In the dibridged isomer the B3LYP method reproduced the CCSD(T) results quite well only for the fifth vibration mode: with a difference of 4.3 cm^{-1} . However, the rest of the vibration frequencies calculated by the B3LYP method have larger differences: for example the first vibration is *underestimated* by 41.2 cm^{-1} and the second vibration by 92.5 cm^{-1} . Nevertheless, the average absolute difference is only 32.8 cm^{-1} when all vibration modes are considered.

The monobridged isomer is a bizarre example of reproduction of harmonic frequencies by the B3LYP method. Firstly we have the fourth and fifth vibrations reproduced with an average difference of only 3.0 cm^{-1} and secondly, the second and last vibration modes have large differences of 112.7 cm^{-1} and 83.2 cm^{-1} , respectively. The average absolute difference for all vibrations is 43.3 cm^{-1} , which is the largest difference of all the Si_2HF isomers.

The B3LYP method gives the smallest difference for the vinyl isomer; the average difference for all vibrations is only 11.7 cm^{-1} . The best accuracy occurs for the last vibration mode (0.6 cm^{-1}) and the worst for the second vibration (29.6 cm^{-1}).

The third and fourth vibration modes in the trans isomer are reproduced with an average accuracy of about 11 cm^{-1} . Nevertheless a large difference (59.4 cm^{-1}) can be seen for the fifth vibration and the average absolute difference (when all the vibrations modes are considered) is 30.6 cm^{-1} .

Comparison of calculated geometries with the literature

As was mentioned in the Introduction chapter the Si_2HF structures calculated by Bei and Feng [30] were obtained with too low-level of theory to do reliable comparison with the results calculated here. To the author's knowledge no other literature results (spectroscopic or theoretical) exist for the Si_2HF species. Experimental studies of similar compounds such as SiH_2F_2 [140] or SiF_3 [141] can be found in the literature since the late 50's; however, the recent paper by Wilson et al. [34] on the SiH_xCl_y and SiH_xF_y (where $x=0-3$ and $y=1-3$) compounds is the most useful for our purpose as their

studies contain both experimental and theoretical values. The SiF_2 , SiHF and SiH_3F species from this publication were chosen for comparison. The calculated Si–F distances in the above species (computed at the CCSD(T)/aug-cc-pV(Q+d)Z level of theory) are: 1.598 Å, 1.611 Å and 1.599 Å respectively and the experimental (equilibrium) Si–F bond lengths are 1.591 Å, 1.603 Å and 1.5945 Å respectively. Our calculated Si–F values are in the range 1.5892 Å (in the trans isomer for F12) to 1.6356 Å (in the vinyl isomers for the B3LYP method). The calculated Si–H distances in the above (SiHF and SiH_3F) species (computed at the CCSD(T)/aug-cc-pV(Q+d)Z level of theory) are: 1.528 Å and 1.475 Å respectively and the experimental (equilibrium) Si–H bond lengths are: 1.529 Å and 1.4761 Å respectively. Our calculated Si–H values are in the range: 1.4816 Å (in the vinyl isomer for AVTZ) to 1.5145 Å (in the trans isomers for the F12 method). Note, that we consider here only the values of terminal atoms as the bond distances for bridged atoms are generally longer. It can be seen that our calculated results are in good agreement with the literature.

4.3 The Si₂HCl isomers.

The procedure of calculations of the Si₂HCl structures is the same as for Si₂HF. Initially the Si₂H₂ structures optimized by Grev and Schaefer [24] were used but with one hydrogen atom substituted by a chlorine atom. Two different monobridged structures (one with a hydrogen as a bridged atom, the second one with a bridged chlorine) were considered. Average literature (theoretical) values of the Si–Cl bond distances were used in substituted-chlorine starting geometries.

Computational methods

Initially we were interested in the isomerisation properties of structures and relative energies calculated with the CCSD(T)/aug-cc-pVXZ, CCSD(T)-F12a/cc-pVTZ-F12 and B3LYP/6-311+G(d) levels of theory (where X=2–4). All the *ab initio* calculations were performed using MOLPRO versions 2006.1-2010.1 [85, 120] whereas the DFT calculations were performed with Gaussian 03 and 09 [138, 139]. The minimization and transition state (TS) searching was performed by using the quadratic steepest descend algorithm implemented in the MOLPRO computational programs. Harmonic frequencies were done at the optimized structures at the CCSD(T)/aug-cc-pVTZ, and B3LYP/6-311+G(d) levels of theory, and the structures were verified as minima or transition states by the absence or presence of imaginary vibrational frequencies. As in the previous chapter, the correlation consistent basis sets used (aug-cc-pVXZ (where X=2–4)) will be abbreviated as AVXZ, and the methods such as: CCSD(T)-F12a/cc-pVTZ-F12 will be abbreviated as F12, CCSD(T)/AVTZ as CCSD(T) and B3LYP/6-311+G(d) as B3LYP. The NBO [102, 103] calculations were performed at the CCSD/cc-pV(T+d)Z level of theory using the Gaussian 03 software package. The NBO calculations of the optimized minima were done to establish (multiple) bonded properties as presented in the earlier Si₂H₂ sub-chapter (4.1). The calculated geometric properties using the CCSD(T)/AVTZ method are listed in Table 4.3-1 and Table 4.3-2.

Table 4.3-1. Geometric properties of calculated Si₂HCl minima.

	CCSD(T)/AVTZ			
	SiHClSi, C _s	ClSiHSi, C _s	HClSiSi, C _s	HSiSiCl, C _s
SiCl ^a	2.3392	2.0613	2.0750	2.0567
SiSi ^a	2.2880	2.1398	2.2306	2.1512
HSi ^a	1.7120	1.6857 ^c	1.4844	1.5040
β HSiSiCl ^b	101.62	0.00	180.00	180.00
α SiSiCl ^b	60.72	160.65	122.28	137.66
α SiSiH ^b	48.07	50.61 ^c	128.47	104.56

^a ångström
^b degrees
^c The Si2H and Si1Si2H values between the silicon (connected to the terminal chlorine atom) and the bridged hydrogen atom.

Table 4.3-2. Geometric properties of calculated Si₂HCl transition states.

	DM_TS, C ₁	DV_TS, C _s	MT_TS, C _s
SiCl ^a	2.2299	2.0556	2.0543
SiSi ^a	2.1798	2.1626	2.1515
HSi ^a	1.4848	1.5257	1.5322
β HSiSiCl ^b	54.90	180.00	180.00
α SiSiCl ^b	70.84	164.49	158.76
α SiSiH ^b	173.02	82.66	81.46

^a ångström
^b degrees

The HSiSiCl, ClSiHSi, HClSiSi and SiHClSi formulae refer to: the trans, monobridged, vinylidene and dibridged isomers, respectively. The DM_TS, DV_TS and MT_TS formulae represent the transition states on the paths between: the dibridged and monobridged structures, dibridged and vinyl and between the monobridged and trans structures, respectively.

The same structure types as found in the Si₂H₂ system were obtained. The calculation were done at the CCSD(T)/AVTZ level of theory. The Si₂HCl system possesses four minima. The global minimum is the Si–Si singly-bonded dibridged structure and 4.38 kcal/mol above lies the Si–Si doubly-bonded monobridged structure. The energy relative to the global minimum of the Si–Si doubly-bonded vinyl structure is 8.01

kcal/mol and the relative energy of the Si–Si triply-bonded trans structure is 11.79 kcal/mol. Three transition states were found, the first one lies on the reaction path between the dibridged and monobridged isomers. Two further transition states connect the dibridged isomer with the vinyl and monobridged with trans isomers, respectively. The reaction path showing relative energies and pictures of the calculated structures can be seen in Figure 4.3-1.

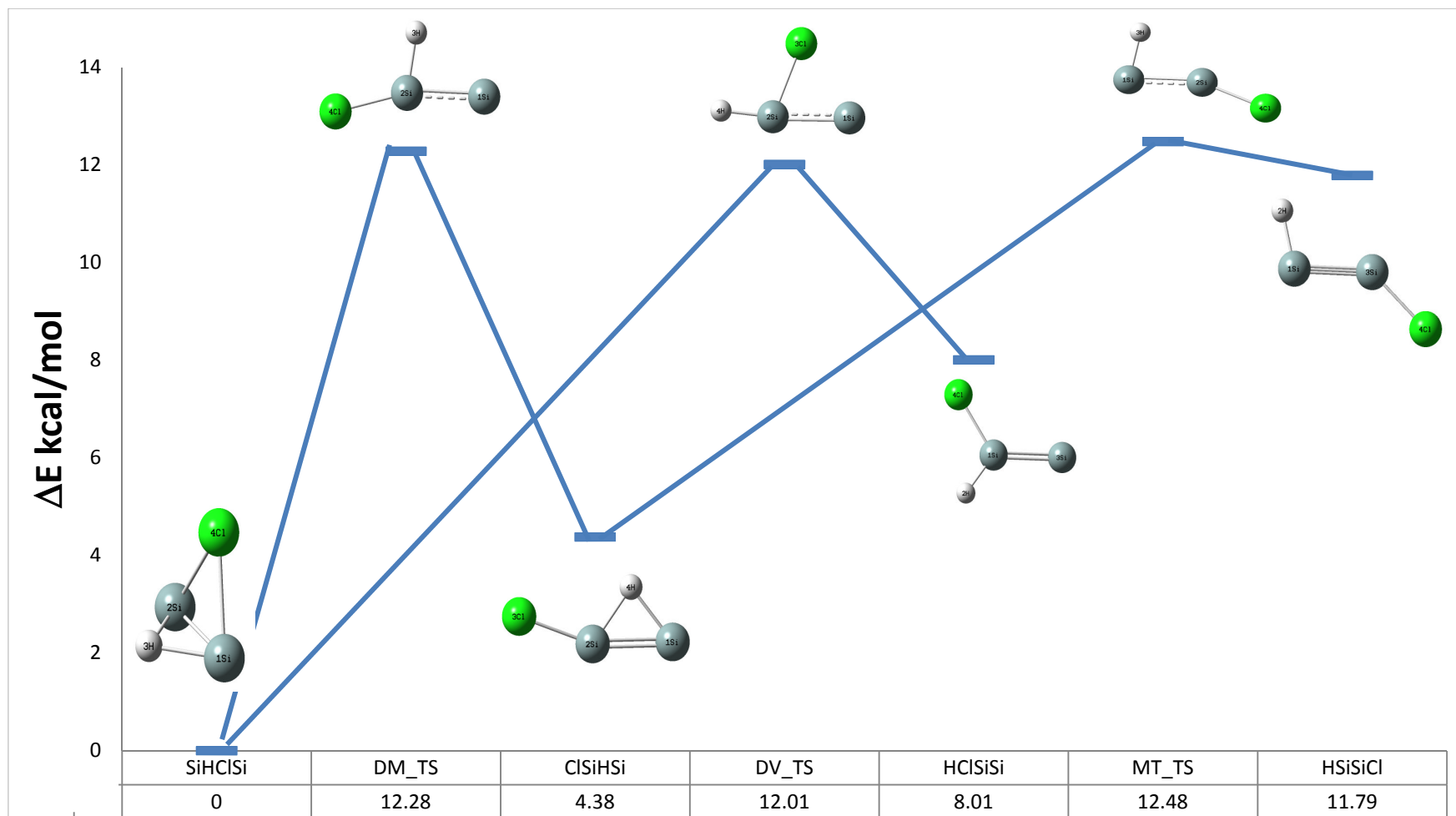
A comparison of the geometric properties of the four isomers calculated with CCSD(T) and increasing basis set level (AVXZ where X=2–4) is shown in Table 4.3-3. The “Si2” in table represents the silicon connected to the terminal chlorine atom.

Table 4.3-3. Geometric properties of the Si₂HCl isomers calculated with CCSD(T)/AVXZ (where X=2–4) level of theory.

	SiHClSi				ClSiHSi		
	AVDZ	AVTZ	AVQZ		AVDZ	AVTZ	AVQZ
SiCl ^a	2.3979	2.3392	2.3239	Si2Cl ^a	2.1000	2.0613	2.0496
SiSi ^a	2.3279	2.2880	2.2746	SiSi ^a	2.1740	2.1398	2.1278
HSi ^a	1.7267	1.7120	1.7057	HSi2 ^a	1.7004	1.6857	1.6790
β HSiSiCl ^b	101.18	101.62	101.65	β HSiSiCl ^b	0.00	0.00	0.00
α SiSiCl ^b	60.96	60.72	60.70	α Si1Si2Cl ^b	159.76	160.65	160.66
α SiSiH ^b	47.62	48.07	48.18	α Si1Si2H ^b	50.30	50.61	50.63
^a ångström							
^b degrees							

	HClSiSi				HSiSiCl		
	AVDZ	AVTZ	AVQZ		AVDZ	AVTZ	AVQZ
SiCl ^a	2.1135	2.0750	2.0620	SiCl ^a	2.0944	2.0567	2.0447
SiSi ^a	2.2558	2.2306	2.2201	SiSi ^a	2.1779	2.1512	2.1399
HSi ^a	1.4939	1.4844	1.4811	HSi ^a	1.5143	1.5040	1.4992
β HSiSiCl ^b	180.00	180.00	180.00	β HSiSiCl ^b	180.00	180.00	180.00
α SiSiCl ^b	120.78	122.28	122.37	α SiSiCl ^b	136.17	137.66	136.95
α SiSiH ^b	130.21	128.47	128.06	α SiSiH ^b	105.45	104.56	105.18
^a ångström							
^b degrees							

Figure 4.3-1. The optimized structures of the Si_2HCl isomers and transitions states with energies relative to the global minimum (dibridged). The calculations were done at the CCSD(T)/aug-cc-pVTZ level of theory.



The variations of the relative energies and Si–Si bond distance with increasing basis set size are shown in Figure 4.3-2 and Figure 4.3-3, respectively.

Both figures show the same convergence pattern. The largest change occurs from AVDZ to AVTZ, whereas only a small change happens upon further basis set improvement. This shows that the results are converging.

Figure 4.3-2. Si–Si bond length variation with increasing basis sets size for the Si₂HCl isomers.

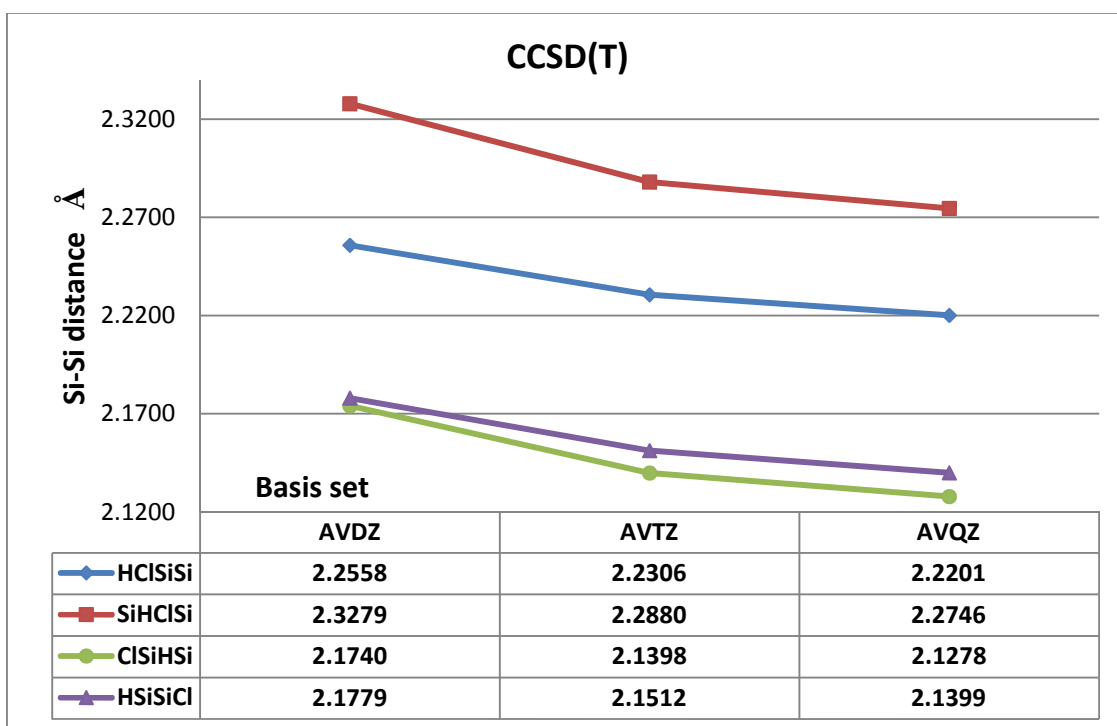
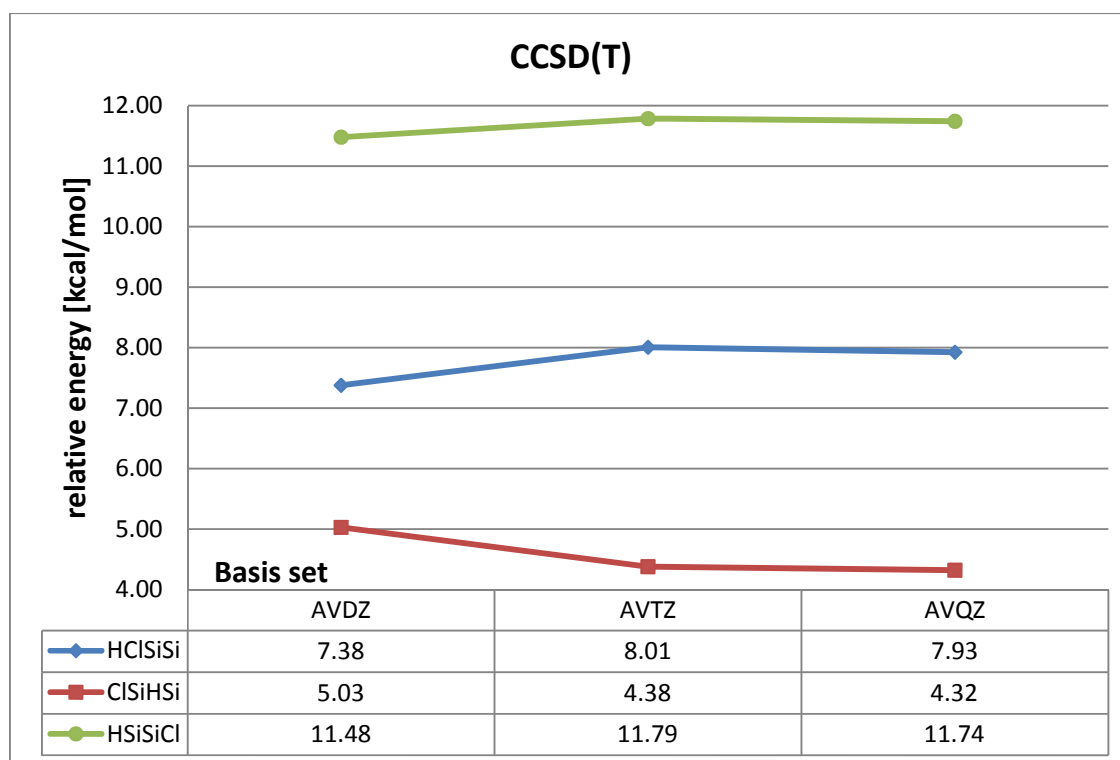


Figure 4.3-3. Relative energy of the Si₂HCl isomers (relative to the dibridged isomer) as a function of AVXZ basis set size.



CCSD(T)- F12 calculations

A comparison of the results obtained with the CCSD(T)/AVTZ method, the recently developed CCSD(T)-F12a/VTZ-F12 method and the B3LYP/6-311+G(d)) method is shown in Table 4.3-4. The “Si2” in table represents the silicon connected to the terminal chlorine atom.

The F12 method will be taken as the reference. Table 4.3-4 shows that all the methods give similar Si–Cl bond distances with differences ranging from 0.0623 Å (difference between the F12 and B3LYP results in the dibridged isomer) to 0.0191 Å (difference between the F12 and CCSD(T) results in the monobridged isomer). The F12 Si–Si distance is reproduced by the CCSD(T) and B3LYP methods with good accuracy. The largest difference (0.0207 Å between the F12 and CCSD(T) results) occurs for the dibridged isomer while the smallest (0.0028 Å between the F12 and B3LYP results) occurs for the monobridged isomer. The average absolute difference for the Si–Si

distances (when differences between the F12 and the CCSD(T) and B3LYP methods are considered) is 0.0115 Å and the average absolute difference for the calculated Si–H distance is 0.0084 Å.

Table 4.3-4. Geometric properties computed at various levels of theory.

	Si ₂ HCl		
	CCSD(T)/ AVTZ	CCSD(T)-F12a/ VTZ-F12	B3LYP/ 6-311+G(d)
dibridged			
SiCl ^a	2.3392	2.3124	2.3747
SiSi ^a	2.2880	2.2673	2.2876
HSi ^a	1.7120	1.7035	1.7187
β HSiSiCl ^b	101.62	101.74	101.38
α SiSiCl ^b	60.72	60.64	61.21
α SiSiH ^b	48.07	48.28	48.29
monobridged			
Si ₂ Cl ^a	2.0613	2.0422	2.0720
SiSi ^a	2.1398	2.1220	2.1248
HSi ₂ ^a	1.6857	1.6751	1.6941
β HSiSiCl ^b	0.00	0.00	0.00
α Si ₁ Si ₂ Cl ^b	160.65	160.79	161.33
α Si ₁ Si ₂ H ^b	50.61	50.73	51.28
vinyl			
SiCl ^a	2.0750	2.0544	2.0846
SiSi ^a	2.2306	2.2159	2.2234
HSi ^a	1.4844	1.4800	1.4852
β HSiSiCl ^b	180.00	180.00	180.00
α SiSiCl ^b	122.28	122.57	122.98
α SiSiH ^b	128.47	127.67	127.86
trans			
SiCl ^a	2.0567	2.0372	2.0648
SiSi ^a	2.1512	2.1350	2.1430
HSi ^a	1.5040	1.4979	1.5091
β HSiSiCl ^b	180.00	180.00	180.00
α SiSiCl ^b	137.66	137.14	141.57
α SiSiH ^b	104.56	104.94	99.94
^a ångström			
^b degrees			

The CCSD(T) and B3LYP methods reproduced the angles obtained by the F12 method (in the dibridged, monobridged and vinyl isomers) well. The average absolute difference is 0.40° , however, in the trans isomer the B3LYP method fails. The angles computed at this level are *underestimated* (SiSiH) by about 5.0° or *overestimated* (SiSiCl) by about 4.4° , whereas the CCSD(T) method reproduced the angles with average absolute error around 0.45° . A similar situation was seen for the Si₂HF species where the B3LYP method reproduced the angle values with an average absolute error around 4° . Thus, we can conclude that the B3LYP method employed here is not accurate enough in calculation of the trans species.

A comparison of the relative energies for the Si₂HCl minima using the B3LYP/6-311+G(d) method, the CCSD(T)/AVTZ method and the F12 (CCSD(T)-F12a/VTZ-F12) method was made and is shown in Table 4.3-5.

Table 4.3-5. Relative energies (kcal/mol) of the Si₂HCl isomers calculated by various methods.

	dibridged	monobridged	vinyl	trans
CCSD(T)/AVTZ	0.00	4.38	8.01	11.79
CCSD(T)-F12a/VTZ-F12	0.00	4.31	8.12	11.79
B3LYP/6-311+G(d)	0.00	5.46	5.32	10.99

Both *ab initio* methods show similar values of the relative energy. However, the DFT method *underestimates* the relative energy. Moreover, the DFT method shows that the vinyl structure is the second minimum above the global minimum (dibridged) instead of the monobridged structure. Thus, the DFT method does not reproduce the isomerisation energies properly in comparison to the *ab initio* calculations.

Frequencies

The harmonic frequencies were calculated using the CCSD(T)/AVTZ and B3LYP/6-311+G(d) methods. The results are listed in Table 4.3-6.

Table 4.3-6. Calculated harmonic frequencies for the Si₂HCl isomers computed at different levels of theory; the results are listed in descending order in wavenumber (cm⁻¹) units.

Si ₂ HCl			
	CCSD(T)/ AVTZ	B3LYP/ 6-311+G(d)	
<u>dibridged</u>			
	1440.7	1421.8	SiH sym. str.
	951.3	876.6	SiH antisym. str.
	828.3	844.6	Butterfly
	501.9	491.5	SiSi str.
	353.0	333.3	SiCl sym. str.
	217.7	192.5	HCl antisym. twist
<u>monobridged</u>			
	1624.0	1604.1	SiH sym. str.
	1067.2	935.7	SiH antisym. str.
	686.0	671.5	SiSi/SiCl in-phase str.
	389.3	379.0	SiSi/SiCl out-of-phase str.
	153.8	155.4	ClSiH bend
	97.0	44.3	out-of-plane
<u>vinyl</u>			
	2224.1	2203.4	SiH str.
	730.8	741.9	SiSiH bend
	583.9	565.8	SiSi/SiCl in-phase str.
	441.6	432.0	SiSi/SiCl out-of-phase str.
	278.2	270.0	out-of-plane
	88.8	92.9	SiSiCl rock
<u>Trans</u>			
	2132.0	2098.2	SiH str.
	647.5	631.2	SiSi/SiCl out-of-phase str.
	472.9	491.7	H in-plane bend
	396.0	383.0	SiSi/SiCl in-phase str.
	90.5	74.8	SiSiH/SiSiCl out-of-phase bend
	49.4	73.3	out-of-plane

In the dibridged isomer the B3LYP method reproduced the CCSD(T) frequencies for the first, and third to fifth vibrations quite well, with an average absolute difference of 16 cm⁻¹. However, the second vibrational frequency calculated by the B3LYP method has an error of 75 cm⁻¹ and the last vibration frequency has an error of 25 cm⁻¹

(compared to the CCSD(T) value). Nevertheless, the average absolute difference is only 27 cm^{-1} when all vibration modes are considered.

The monobridged isomer is another bizarre example of reproduction of harmonic frequencies by the B3LYP method. Firstly we have the fifth vibration with an error of only 1.5 cm^{-1} and secondly, the second vibration mode with a difference of 131.5 cm^{-1} and the last vibration frequency with a difference of 53 cm^{-1} . The worst agreement (for all the Si_2HCl isomers) can be seen for the monobridged structure, for which the average absolute difference is 38 cm^{-1} .

The vinyl isomer shows an entirely different picture. The B3LYP method gives the smallest differences compared with CCSD(T); the average absolute difference is 12 cm^{-1} . The best accuracy occurs for the last vibration mode (4.1 cm^{-1}) and the worst for first vibration (21 cm^{-1}).

From the second to the fifth vibration mode in the trans isomer, the B3LYP method reproduced the CCSD(T) results with an agreement of 16 cm^{-1} . Nevertheless, the largest error (34 cm^{-1}) can be seen for the first vibration and the average absolute difference (when all the vibrational modes are considered) is 20 cm^{-1} .

It was noticed that the B3LYP method reproduced poorly the frequencies assigned as the SiH antisymmetric stretch and out-of-plane vibration in the H-bridged and dibridged structures. This pattern was also seen in the Si_2H_2 and Si_2HF species and will be seen in the subsequent Si_2HLi and Si_2Li_2 sub-chapters. Furthermore, a similar situation where the B3LYP method reproduced poorly the frequencies assigned as out-of-plane can be seen in the trans structures in the Si_2HF and Si_2HCl species.

Comparison of calculated values with literature

As was mentioned in the Introduction chapter the Si_2HCl structures calculated by Bei and Feng [30] were obtained with too low a level of theory to do a reliable comparison with the results calculated here. Nevertheless, although no structural and frequency

information is available for Si_2HCl from either experiment or theory (except the above one), we will compare with similar structures such as SiH_3Cl , SiHCl_3 or SiCl_3 . Experimental work on the SiH_3Cl and SiCl_3 molecules has been done since 1956 [35, 142, 143]. The theoretical work of Wilson et al. [34] is the most useful. They showed theoretical results and experimental results (done by [35]) of the $\text{SiH}_m\text{Cl}_{m-n}$ (where $m=1-4$ and $n=0-m$) molecules such as the SiCl , SiCl_4 , SiHCl_3 , SiH_3Cl or SiH_2Cl_2 species. The calculated (CCSD(T)/aug-cc-pV(Q+d)Z level of theory) Si–Cl bond distances range from 2.069 Å (SiCl) to 2.021 Å (SiCl_4). For the experimental results, the distances range from 2.020 Å (SiH_3Cl) to 2.057 Å (SiCl). The next most important work was done by Ding and Zhu [50]. They calculated a potential energy surface (PES) which they used to study Si–H stretching-bending overtones in SiHCl_3 . The calculated Si–Cl equilibrium distance is 2.0306 Å. The Si–Cl distances calculated here range from 2.1135 Å (the vinyl isomers calculated with the CCSD(T)/AVDZ level) to 2.0372 Å (the trans isomer at the CCSD(T)-F12a/VTZ-F12 level). Comparison of the Si-H distances calculated here with the theoretical work of Wilson et al. [34] follows. The calculated Si–H distances in the SiHCl_3 , SiH_3Cl and SiH_2Cl_2 species (computed at the CCSD(T)/aug-cc-pV(Q+d)Z level of theory) are: 1.462 Å, 1.474 Å and 1.468 Å respectively and the experimental (equilibrium) Si–H bond lengths are: 1.464 Å, 1.4749 Å and 1.4671 Å respectively. Our calculated Si–H values are in the range 1.4800 Å (in the vinyl isomer for AVTZ) to 1.5091 Å (in the trans isomers for the F12 method). Note, that we did not consider the dibridged structure in this comparison as the bridged atoms generally have longer bond distances. It can be seen that our calculated results are in good agreement with the experimental and theoretical literature for similar molecules.

4.4 The Si₂HLi isomers.

Substituted silicon hydride isomers are very interesting from a technological point of view, especially when the substituted atom is lithium. This is because of the growing importance of lithium and its connection with the silicon atom in modern industry, such as the development of silicon lithium-ion batteries. However, a lithium-ion battery has limitations: it is less reversible than carbon-lithium batteries at room temperature [144-146] and fading of capacity was observed [147]. An investigation of electronic and bonding properties for small molecules consisting of Li and Si atoms can be very valuable and helpful to solve the overwhelming problems occurring now and in the future in research involving compounds containing Si and Li atoms.

Computational methods

The calculations were carried out with MOLPRO versions 2006.1-2010.1 and Gaussian versions 98-03 [120, 130, 138]. The Si₂H₂ structures optimized by Grev and Schaefer [24] were taken as the starting geometries, where one of the H atoms was replaced by the Li atom. We explored two different monobridged structures: with Li as the bridging atom and with H as the bridging atom. Average literature (theoretical) values of the Si–Li bond distances were used in the substituted-lithium starting geometries. All geometry optimization calculations were performed at the CCSD(T)-F12a/cc-pVTZ-F12 [133, 134, 148] and B3LYP/6-311+G(d) levels of theory and with CCSD(T) with the aug-cc-pVXZ, cc-pVXZ and aug-cc-pV(X+d)Z basis sets (where X=2–4) [58, 149, 150]. The vibrational frequency calculations were performed at the CCSD(T)/aug-cc-pVXZ and B3LYP/6-311+G(d) levels of theory. The frequencies were used for the identification of transition states (TS) and minima. The correlation consistent basis sets used here, aug-cc-pVXZ cc-pVXZ and aug-cc-pV(X+d)Z will be abbreviated as AVXZ, VXZ and AV(X+d)Z (where X=2–4). The methods such as: CCSD(T)-F12a/cc-pVTZ-F12 will be abbreviated as F12, CCSD(T)/AVTZ as CCSD(T) and B3LYP/6-311+G(d) as B3LYP respectively. Natural Bond Order (NBO) calculations were done at the CCSD/aug-cc-pV(T+d)Z level of theory using Gaussian 98 with NBO 3.1 implemented.

The LiSiHSi, HSiLiSi and SiHLiSi formulae refer to the H-bridged, Li-bridged and dibridged isomers, respectively. The D-LiM_TS, LiM-HM_TS formulae refer to the transition states on the paths between the dibridged and Li-bridged structures, and the Li-bridged and H-bridged structures, respectively.

The optimized structures of the Si₂HLi isomers and transition states are depicted in Figure 4.4-1. The pictures show the multiple-bonding properties of the optimized isomers obtained from the NBO calculations. The energies relative to the dibridged structure (global minimum) are listed at the bottom of Figure 4.4-1. The reaction paths between critical points are represented schematically by lines.

Figure 4.4-1 shows the optimized isomers with the bonding properties taken from NBO calculations. All the isomers are bridged structures. The global minimum is a dibridged (SiHLiSi) form and Li-bridged (HSiLiSi) and H-bridged (LiSiHSi) local minima were found. The energy differences between the global minimum and the local minima are 4.12 kcal/mol and 8.91 kcal/mol for the Li-bridged and H-bridged structures, respectively. The Li- and H-bridged isomers contain a double Si=Si bond, whereas the dibridged isomer is a single-bonded structure. In all the isomers lone pairs can be found on one or two silicon atoms. We also investigated cis and linear forms but they were found to be higher-order transition states.

Table 4.4-1. Geometric properties of the calculated Si₂HLi minima.

	CCSD(T)/AVTZ		
	SiHLiSi, C _s	HSiLiSi, C _s	LiSiHSi, C _s
SiLi _a	2.6291	2.5306 ^c	2.4349
SiSi _a	2.1994	2.1188	2.1582
HSi _a	1.6800	1.4954	1.6383 ^d
β HSiSiLi _b	86.73	180.00	0.00
α SiSiLi _b	65.28	68.48 ^c	156.49
α SiSiH _b	49.11	168.75	51.47 ^d

^a ångström

^b degrees

^c The Si1Li and Si2Si1Li values between the silicon and the bridged lithium atom.

^d The Si2H and Si1Si2H values between the silicon (connected to the terminal lithium atom) and the bridged hydrogen atom.

Table 4.4-2. Geometric properties of the calculated Si₂HLi transition states

	CCSD(T)/AVTZ	
	D–LiM_TS, C ₁	LiM–HM_TS, C _s
SiLi _a	2.5851	2.4245
SiSi _a	2.2055	2.1987
HSi _a	1.5354	1.5167
β HSiSiLi _b	84.75	0.00
α SiSiLi _b	67.75	137.40
α SiSiH _b	91.80	97.50

^a ångström

^b degrees

Figure 4.4-1. The optimized structures of the Si_2HLi isomers and transition states with energies relative to the global minimum (dibridged). The calculations were done at the CCSD(T)/aug-cc-pVTZ level of theory.

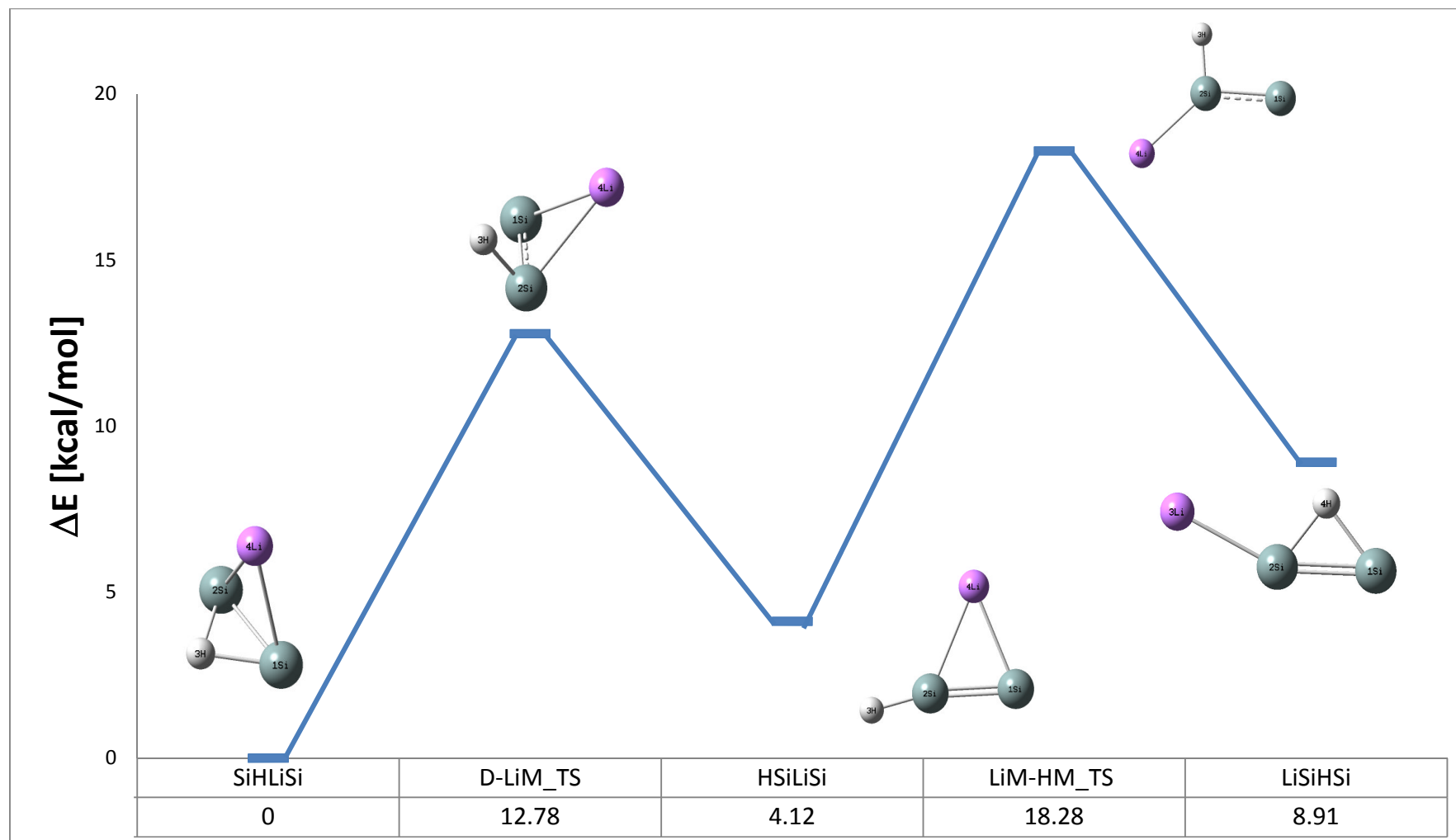


Table 4.4-1 presents the geometric properties of the structures optimised at the CCSD(T)/aug-cc-pVTZ level of theory. The “Si2” or “Si1” in table represents the silicon connected or not connected to the terminal atom.

We see that the shortest Si–Si bond occurs in the Li-bridged structure (2.1188 Å), followed by the H-bridged (2.1582 Å) and the di-bridged (2.1994 Å) structures. In the previous sub-chapters it was found that the bridged atom has longer bond lengths. This is also found here: the calculated Si–Li and Si–H bonds in the bridged isomers have lengths of 2.6291 Å (SiHLiSi), 2.5306 Å (HSiLiSi), 1.6800 Å (SiHLiSi) and 1.6383 Å (LiSiHSi). The Si–Li and Si–H bond lengths of the terminal atoms are shorter: 2.4349 Å and 1.4954 Å for LiSiHSi and HSiLiSi, respectively. All isomers except the dibridged structure are planar.

We also performed a more extended investigation of disilynes substituted by Li atoms in comparison to the Si₂HF and Si₂HCl structures, as these are particularly interesting for the high-tech industry as shown in the Introduction chapter.

We performed calculations with several series of basis sets to choose the most effective basis set. The performance of the AVXZ and VXZ basis sets was first assessed, followed by a comparison of the results obtained with the AVXZ and AV(X+d)Z basis sets (where X=2–4). The CCSD(T) method was employed in all of the calculations. The CBS limit has also been evaluated using the model proposed by Halkier et al [151]. Details of this model will be discussed later.

The comparison of the results obtained with the AVXZ and VXZ basis sets aims to investigate the importance of the inclusion of diffuse functions in the basis sets. The geometric properties calculated with the VXZ basis sets can be found in Table 4.4-3 to Table 4.4-5. The relative energies calculated with these basis sets are presented in the form of graphs (Figure 4.4-2 and Figure 4.4-3). The “Si2” or “Si1” in table represents the silicon connected or not connected to the terminal atom.

Table 4.4-3. Geometric properties of the SiHLiSi isomer at the CCSD(T)/AVXZ and CCSD(T)/VXZ (where X=2–4) levels of theory.

SiHLiSi						
	AVDZ	AVTZ	AVQZ	VDZ	VTZ	VQZ
SiLi ^a	2.6633	2.6291	2.6235	2.6505	2.6257	2.6228
SiSi ^a	2.2306	2.1994	2.1866	2.2272	2.1989	2.1858
HSi ^a	1.6957	1.6800	1.6738	1.6965	1.6802	1.6729
β HSiSiLi ^b	88.40	86.73	87.30	84.73	85.80	86.79
α SiSiLi ^b	65.24	65.28	65.37	65.16	65.23	65.37
α SiSiH ^b	48.87	49.11	49.22	48.97	49.13	49.21
^a ångström						
^b degrees						

Table 4.4-4. Geometric properties of the LiSiHSi isomer at the CCSD(T)/AVXZ and CCSD(T)/VXZ (where X=2–4) levels of theory.

LiSiHSi						
	AVDZ	AVTZ	AVQZ	VDZ	VTZ	VQZ
Si2Li ^a	2.4563	2.4349	2.4350	2.4518	2.4320	2.4337
SiSi ^a	2.1873	2.1582	2.1471	2.1820	2.1571	2.1466
HSi2 ^a	1.6612	1.6383	1.6421	1.6588	1.6470	1.6415
β HSiSiLi ^b	0.00	0.00	0.00	0.00	0.00	0.00
α Si1Si2Li ^b	155.01	156.49	155.56	155.25	156.27	155.97
α Si1Si2H ^b	51.36	51.47	51.45	51.42	51.43	51.45
^a ångström						
^b degrees						

Table 4.4-5. Geometric properties of the HSiLiSi isomer at the CCSD(T)/AVXZ and CCSD(T)/VXZ (where X=2–4) levels of theory.

	HSiLiSi					
	AVDZ	AVTZ	AVQZ	VDZ	VTZ	VQZ
Si1Li ^a	2.5702	2.5306	2.5245	2.5620	2.5281	2.5234
SiSi ^a	2.1483	2.1188	2.1079	2.1460	2.1187	2.1075
HSi2 ^a	1.5070	1.4954	1.4930	1.5053	1.4952	1.4928
β HSiSiLi ^b	180.00	180.00	180.00	180.00	180.00	180.00
α Si2Si1Li ^b	68.17	68.48	68.62	68.15	68.45	68.63
α Si1Si2H ^b	167.84	168.75	168.08	168.14	168.39	167.86

^a ångström
^b degrees

Figure 4.4-2. Energy of the HSiLiSi isomer (relative to the dibridged isomer) as a function of VXZ and AVXZ basis set size.

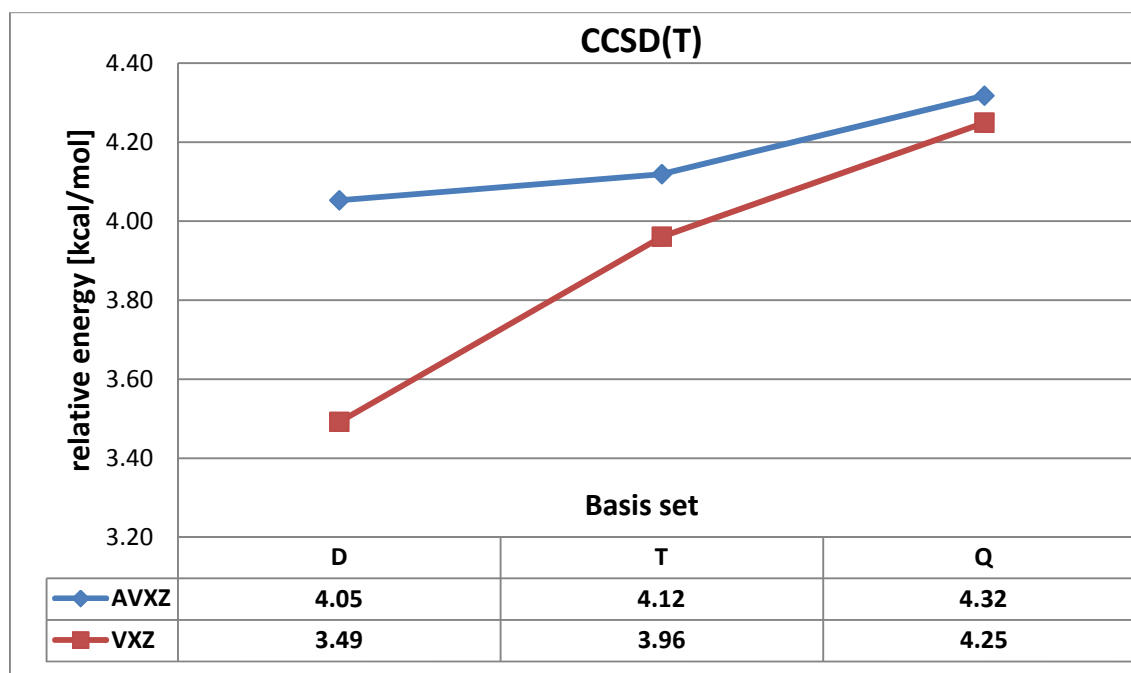
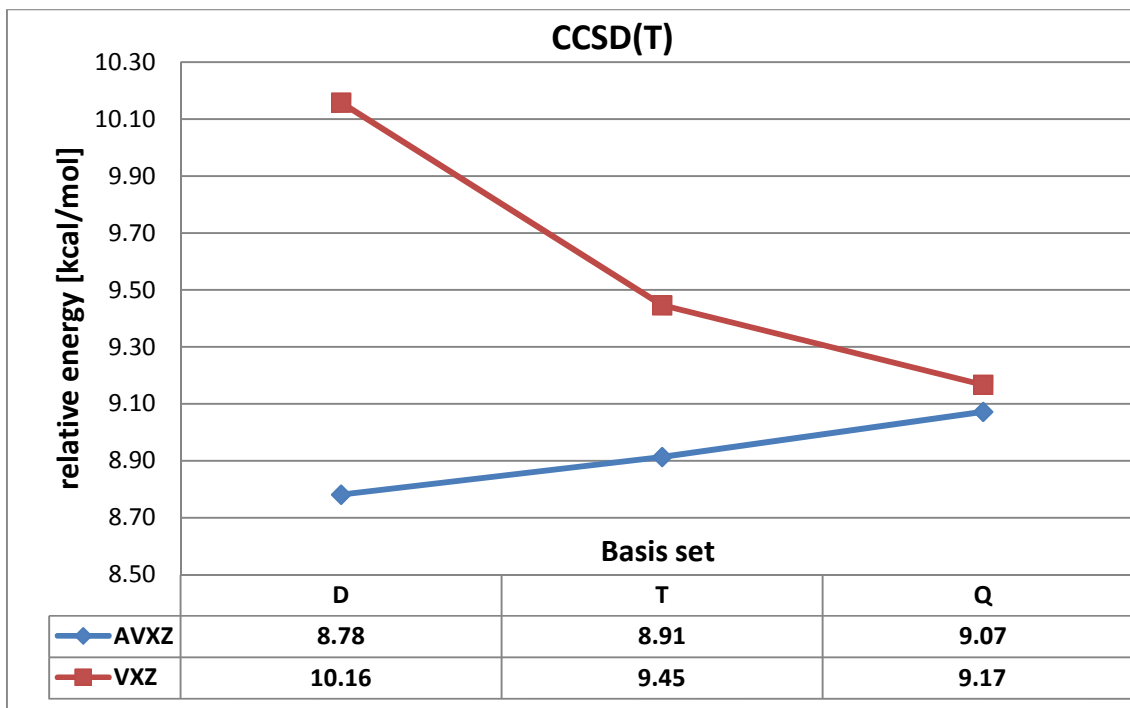


Figure 4.4-3. Energy of the LiSiHSi isomer (relative to the dibridged isomer) as a function of VXZ and AVXZ basis set size.



A large difference between the relative energies calculated with the VDZ and AVDZ basis sets can be seen for both isomers: the energy difference is 0.56 kcal/mol (HSiLiSi) and 1.38 kcal/mol (LiSiHSi). The energy difference decreases (VXZ) or increase (AVXZ) with increasing basis set size. At the quadruple- ζ quality level, the differences are only 0.07 kcal/mol (HSiLiSi) and 0.10 kcal/mol (LiSiHSi). The VXZ basis set significantly *under-* or *over-*estimates the relative energies at the double and triple- ζ quality level of theory. However, at the quadruple- ζ quality level the differences are so small that we can conclude that at this level and above diffuse functions are not necessary for calculating good-quality isomerisation energies in “SiHLi” systems. A similar pattern can be seen for the Si–Si bond distances: at the quadruple- ζ quality level the differences are as small as 0.0004 Å (HSiLiSi) and not larger than 0.0008 Å (SiHLiSi).

A comparison of the results obtained with the AVXZ and AV(X+d)Z basis sets aims to assess the importance of inclusion of tight d functions on the heavy atoms (silicon in our case) in the basis sets for calculation of geometric and energetic properties. All

calculations were performed using the CCSD(T) method. The calculated geometric properties of the Si₂HLi isomers are listed in Table 4.4-6 to Table 4.4-8. The “Si2” or “Si1” in table represents the silicon connected or not connected to the terminal atom.

Table 4.4-6. Geometric properties of the SiHLiSi isomer at the CCSD(T)/AVXZ and CCSD(T)/AV(X+d)Z (where X=2–4) levels of theory.

	SiHLiSi					
	AVDZ	AVTZ	AVQZ	AV(D+d)Z	AV(T+d)Z	AV(Q+d)Z
SiLi ^a	2.6633	2.6291	2.6235	2.6597	2.6270	2.6232
SiSi ^a	2.2306	2.1994	2.1866	2.2166	2.1933	2.1827
HSi ^a	1.6957	1.6800	1.6738	1.6841	1.6753	1.6711
β HSiSiLi ^b	88.40	86.73	87.30	88.40	86.76	86.92
α SiSiLi ^b	65.24	65.28	65.37	65.37	65.32	65.41
α SiSiH ^b	48.87	49.11	49.22	48.84	49.11	49.22

^a ångström
^b degrees

Table 4.4-7. Geometric properties of the LiSiHSi isomer at the CCSD(T)/AVXZ and CCSD(T)/AV(X+d)Z (where X=2–4) levels of theory.

	LiSiHSi					
	AVDZ	AVTZ	AVQZ	AV(D+d)Z	AV(T+d)Z	AV(Q+d)Z
Si2Li ^a	2.4563	2.4349	2.4350	2.4559	2.4361	2.4333
SiSi ^a	2.1873	2.1582	2.1471	2.1756	2.1530	2.1452
HSi2 ^a	1.6612	1.6383	1.6421	1.6518	1.6439	1.6402
β HSiSiLi ^b	0.00	0.00	0.00	0.00	0.00	0.00
α Si1Si2Li ^b	155.01	156.49	155.56	154.37	156.03	154.76
α Si1Si2H ^b	51.36	51.47	51.45	51.19	51.40	51.41

^a ångström
^b degrees

The results listed in Table 4.4-6 to Table 4.4-8 showed that the bond lengths (Si-Si H-Si and Si-Li) decrease upon increasing basis set size for both the AVXZ and AV(X+d)Z basis set series. In contrast, there is no clear pattern for the angles; the results fluctuate upon increasing basis set size. The variations in the Si–Si bond lengths upon increasing AVXZ and AV(X+d)Z basis set size are shown in Figure 4.1-6 to Figure 4.1-9.

Table 4.4-8. Geometric properties of the HSiLiSi isomer at the CCSD(T)/AVXZ and CCSD(T)/AV(X+d)Z (where X=2–4) levels of theory.

	HSiLiSi					
	AVDZ	AVTZ	AVQZ	AV(D+d)Z	AV(T+d)Z	AV(Q+d)Z
Si1Li ^a	2.5702	2.5306	2.5245	2.5653	2.5287	2.5236
SiSi ^a	2.1483	2.1188	2.1079	2.1382	2.1144	2.1057
HSi2 ^a	1.5070	1.4954	1.4930	1.5021	1.4934	1.4921
β HSiSiLi ^b	180.00	180.00	180.00	180.00	180.00	180.00
α Si2Si1Li ^b	68.17	68.48	68.62	68.27	68.51	68.70
α Si1Si2H ^b	167.84	168.75	168.08	167.40	168.66	167.96

^a ångström
^b degrees

The variations in the isomerisation energies and Si–Si bond lengths upon increasing AVXZ and AV(X+d)Z basis set size are shown in Figure 4.4-4 and Figure 4.4-5.

The change in the HSiLiSi isomerisation energy with increasing basis set size from double to triple- ζ is larger for the AV(X+d)Z than for the AVXZ the basis set (0.34 kcal/mol for AV(X+d)Z and 0.07 kcal/mol for AVXZ). However, when increasing the size of the basis set from triple to quadruple- ζ the conclusions are opposite: the difference is larger for the AVXZ basis set (0.2 kcal/mol) than for the AV(X+d)Z basis set (0.10 kcal/mol).

The AVXZ basis sets show larger changes in the LiSiHSi isomerisation energy than the AV(X+d)Z basis sets over the whole range of basis set sizes. The energy changes by 0.13 kcal/mol from AVDZ to AVTZ and by 0.16 kcal/mol from AVTZ to AVQZ. However, for the AV(X+d)Z basis set series the same changes of the basis set size (from DZ to TZ and TZ to QZ) give energy differences of only 0.01 kcal/mol and 0.10 kcal/mol, respectively.

Figure 4.4-4. Energy of the HSiLiSi isomer (relative to the dibridged isomer) as a function of AVXZ and AV(X+d)Z basis set size.

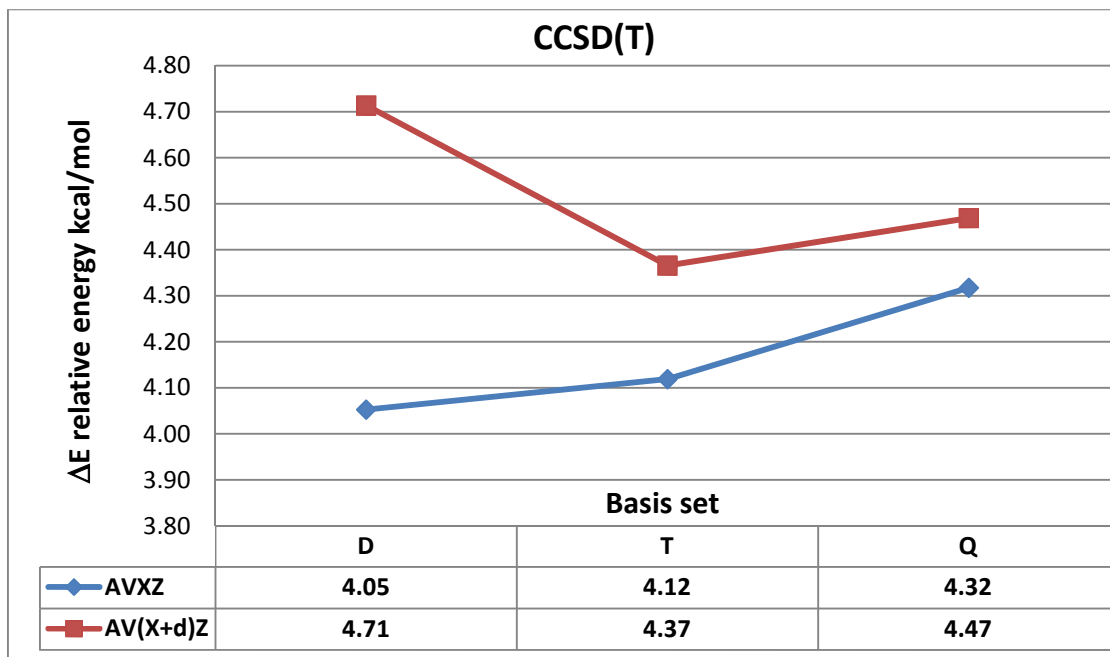


Figure 4.4-5. Energy of the LiSiHSi isomer (relative to the dibridged isomer) as a function of AVXZ and AV(X+d)Z basis set size.

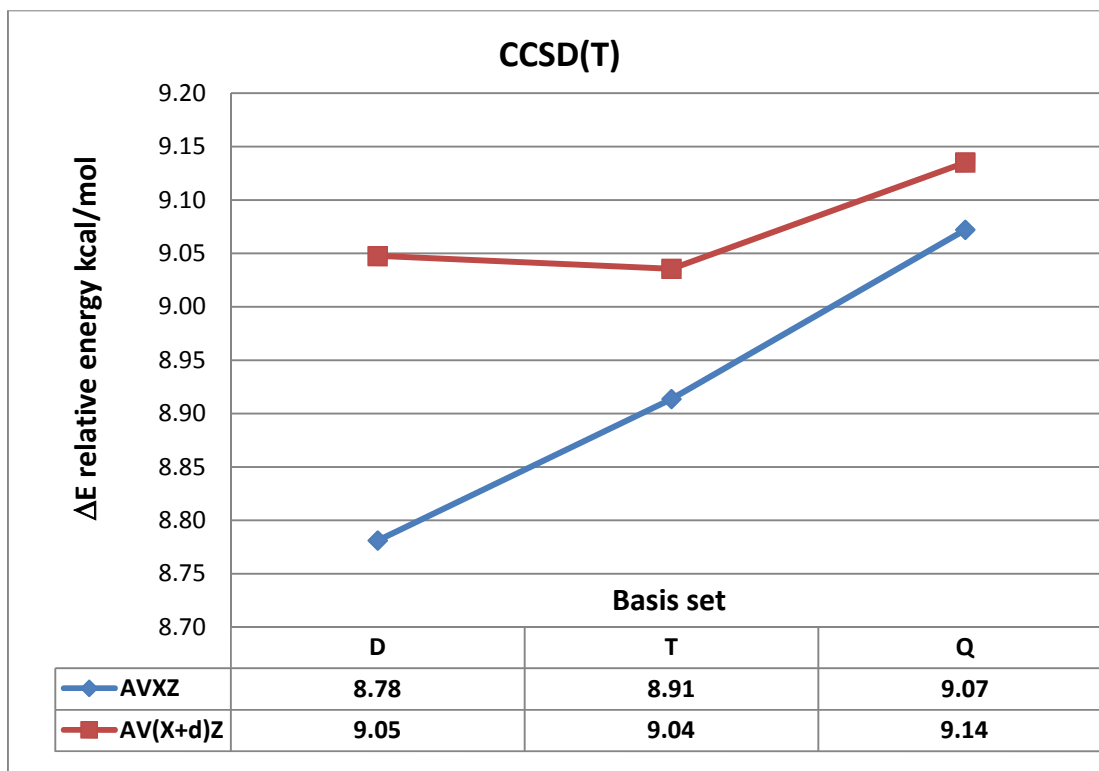


Figure 4.4-6. Si–Si bond length variation with increasing basis set size for the HSiLiSi isomer.

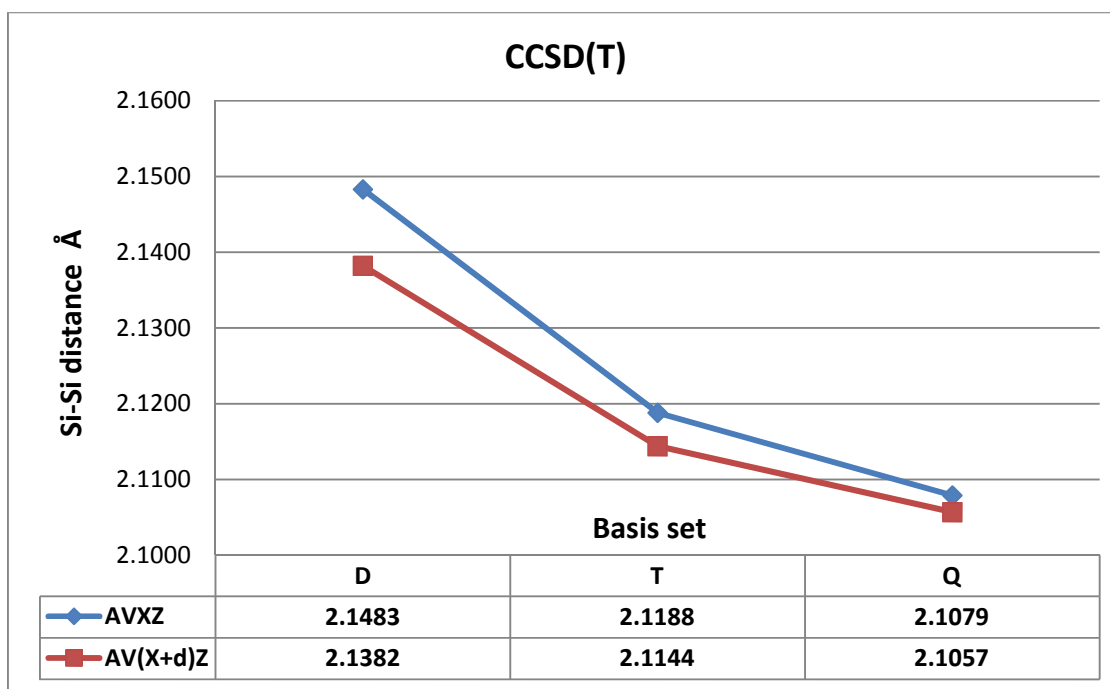


Figure 4.4-6 to Figure 4.4-8 show the variation of Si-Si bond distance with increasing basis set size (employing the AVXZ and AV(X+d)Z basis set families) for the three minimum-energy structures. A smooth convergence pattern is observed for all three isomers and for both basis set series. Note also that the difference between the results obtained with the AVQZ and AV(Q+d)Z basis sets is quite small: from 0.0019 Å (for LiSiHSi) to 0.0039 Å (for SiHLSi). It can be seen that the addition of tight d functions to the heavy atoms does not significantly improve the geometric properties when basis sets as large as quadruple- ζ are employed.

Figure 4.4-7. The Si–Si bond length variation with increasing basis set size for the LiSiHSi isomer.

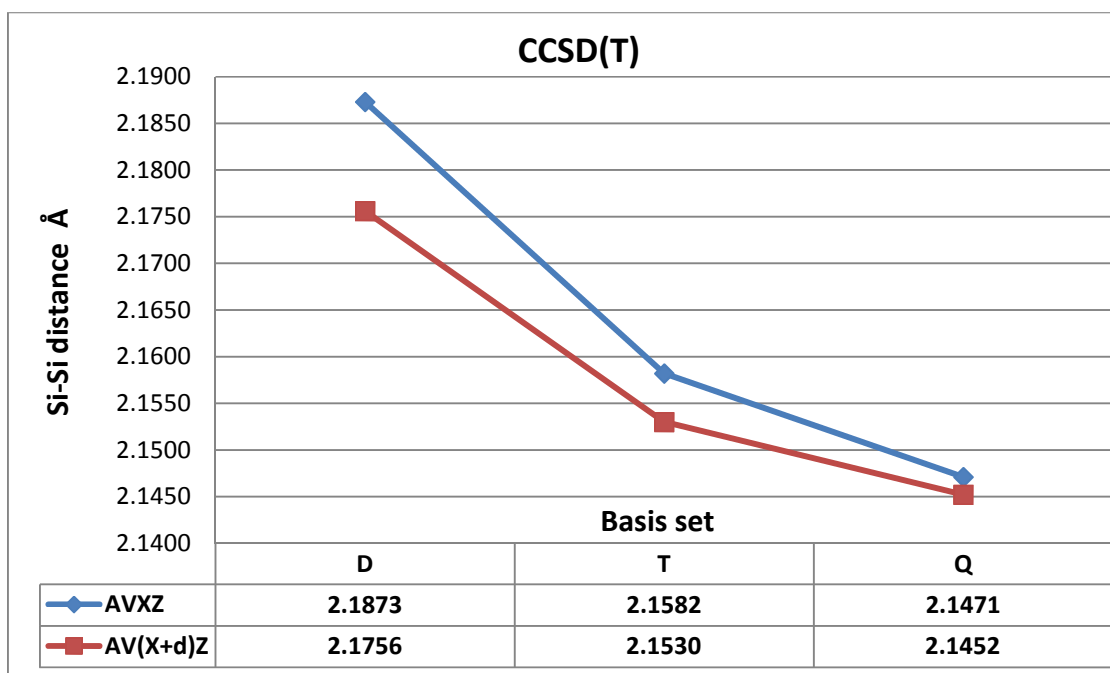
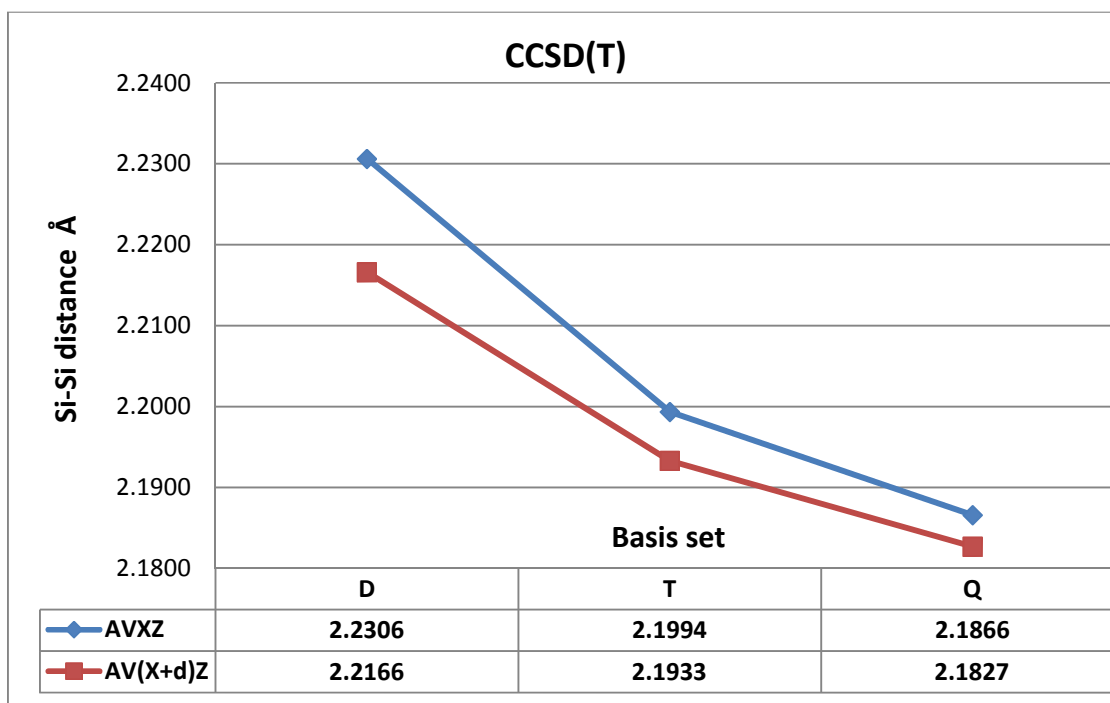


Figure 4.4-8. The Si–Si bond length variation with increasing basis set size for the SiHLiSi isomer.



Complete Basis Set (CBS) limit

Knowledge of the Complete Basis Set (CBS) limit provides insight into the basis set error of a computational method. The CBS limits were estimated by extrapolating the AVTZ–AVQZ and AV(T+d)Z–AV(Q+d)Z correlation energies using the extrapolation model proposed by Halkier et al. [151]. Equation 4.4-1 shows the CBS model by Halkier et al., where E_X represents the correlation energy calculated with the X basis set and E_{X-1} represents the correlation energy calculated with the X–1 basis set. The correlation energies were obtained as a difference between the HF energy and the CCSD(T) (total) energy at the X or X-1 basis set level. The extrapolated E_{CBS} energy was then added to the HF energy at the X basis set level to obtain the CBS limit. More details can be found in Ref. [151]. Figure 4.4-9 and Figure 4.4-10 show the calculated CBS limits (using the highest QZ level employed in this work) compared with the AVXZ and AV(X+d)Z relative energies for the isomers that lie above the global minimum.

$$E_{\text{CBS}} = \frac{X^3}{X^3 - (X-1)^3} E_X - \frac{(X-1)^3}{X^3 - (X-1)^3} E_{X-1} \quad 4.4-1$$

It can be seen that the AVXZ calculations are quite far away from the CBS limit, even for the quadruple- ζ basis set; the error is 0.18 kcal/mol for LiSiHSi and 0.17 kcal/mol for HSiLiSi. This suggests that calculations with larger basis sets, such as AV5Z or AV6Z are required to yield results close to the CBS limit.

Figure 4.4-9 and Figure 4.4-10 show that the AV(X+d)Z results are much closer to the CBS limit than the AVXZ results. The error is 0.05 (HSiLiSi) kcal/mol and 0.10 kcal/mol (LiSiHSi), so it is possible to achieve results close to the CBS limit using the AV(Q+d)Z basis set.

Figure 4.4-9. Energies of LiSiHSi (relative to the dibridged isomer) calculated with the AVXZ and AV(X+d)Z basis sets. The CBS limit obtained by extrapolation of the AVTZ/AVQZ and AV(T+d)Z/AV(Q+d)Z results is shown as well.

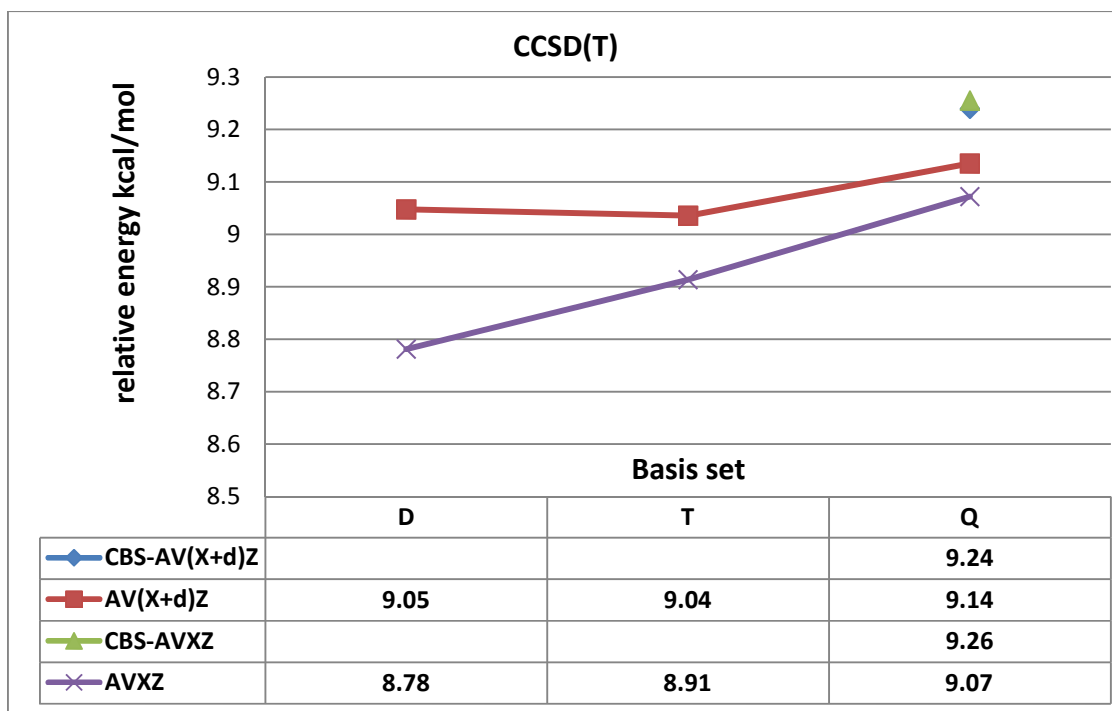
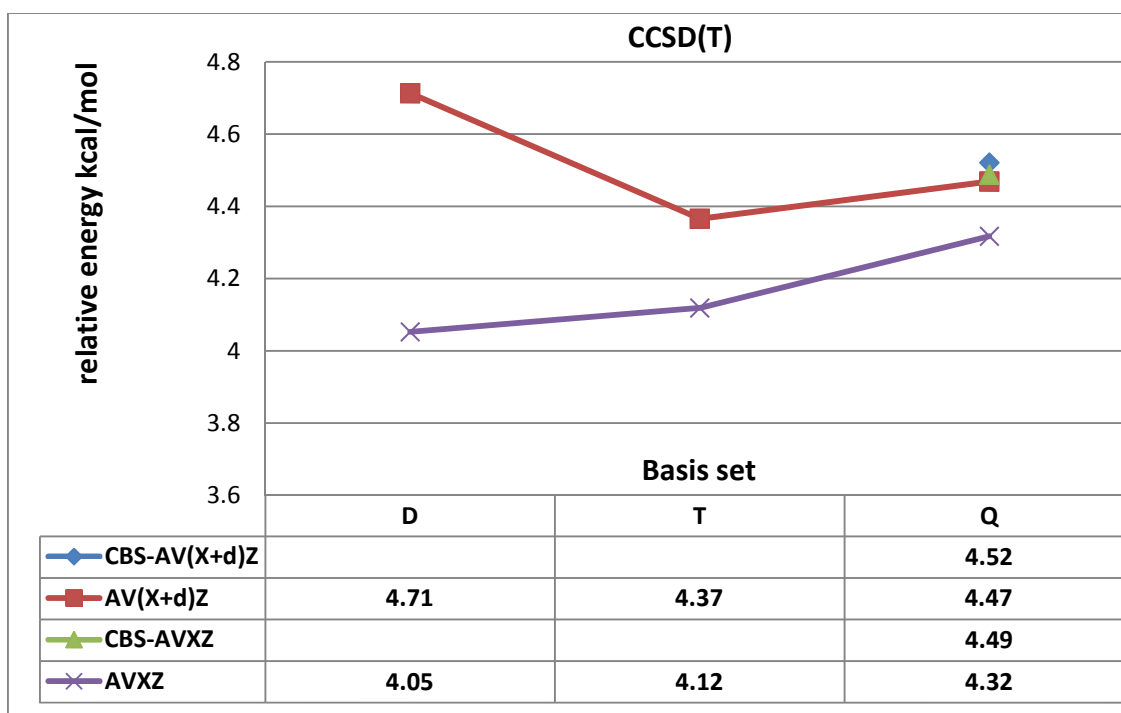


Figure 4.4-10. Energies of HSiLiSi (relative to the dibridged isomer) calculated with the AVXZ and AV(X+d)Z basis sets. The CBS limit obtained by extrapolation of the AVTZ/AVQZ and AV(T+d)Z/AV(Q+d)Z results is shown as well.



CCSD(T)- F12 calculations

We performed calculations using the recently developed CCSD(T)-F12a method.

Note, that in the following discussion the CCSD(T)/cc-pVTZ level will be abbreviated as CCSD(T), the CCSD(T)-F12a/cc-pVTZ-F12 level as F12 and the B3LYP/6-311+G(d) level of theory as B3LYP, respectively. The geometric properties calculated by the above methods can be found in Table 4.4-9. The “Si2” or “Si1” in table represents the silicon connected or not connected to the terminal atom.

Table 4.4-9 shows that all three methods give similar results for the Si–Si, Si–Li and Si–H bond distances. However, the F12 method will be taken as a reference here. The difference between the results obtained with the F12 and CCSD(T) methods ranges from 0.0005 Å (H-bridged structure) to 0.0195 Å (dibridged structure). The results obtained with the F12 and B3LYP methods range from 0.0031 Å (H-bridged structure) to 0.0215 Å (dibridged structure). The average absolute difference is 0.0127 Å when the difference between F12 and CCSD(T)-B3LYP methods and bond distances are considered. For the dibridged and Li–bridged structures The CCSD(T) and B3LYP methods reproduced the angles obtained by the F12 method well; the average absolute difference is no higher than 0.97° (difference between the F12 and B3LYP methods in the dibridged structure), whereas it is only 0.41° in the Li–bridged structure. However, in the H-bridged structure the B3LYP method fails to accurately reproduce the SiSiLi angle obtained by the F12 method. The B3LYP method *overestimates* this angle by 5.56° while the difference between the F12 and CCSD(T) results is only 1.15°. The SiSiH angle predicted by the B3LYP method in the H–bridged structure has an average absolute difference of 2.2°.

Table 4.4-9. Geometric properties computed at various levels of theory.

	Si ₂ HLi		
	CCSD(T)/ AVTZ	CCSD(T)-F12a/ VTZ-F12	B3LYP/ 6-311+G(d)
dibridged			
SiLi ^a	2.6291	2.6214	2.6043
SiSi ^a	2.1994	2.1798	2.1854
HSi ^a	1.6800	1.6704	1.6919
β HSiSiLi ^b	86.73	86.95	84.77
α SiSiLi ^b	65.28	65.43	65.19
α SiSiH ^b	49.11	49.27	49.77
Li-bridged			
Si1Li ^a	2.5306	2.5224	2.5055
SiSi ^a	2.1188	2.1027	2.0961
HSi2 ^a	1.4954	1.4924	1.4958
β HSiSiLi ^b	180.00	180.00	180.00
α Si2Si1Li ^b	68.48	68.70	68.52
α Si1Si2H ^b	168.75	167.99	167.35
H-bridged			
Si2Li ^a	2.4349	2.4344	2.4130
SiSi ^a	2.1582	2.1417	2.1448
HSi2 ^a	1.6383	1.6399	1.6542
β HSiSiLi ^b	0.00	0.00	0.00
α Si1Si2Li ^b	156.49	155.34	160.90
α Si1Si2H ^b	51.47	51.45	52.53
^a ångström			
^b degrees			

A comparison of the relative energies for the Si₂H₂ minima computed using the DFT (B3LYP/6-311+G(d)) method, the CCSD(T)/AVTZ and F12 (CCSD(T)-F12a/VTZ-F12) methods is shown in Table 4.4-10.

Table 4.4-10. Relative energy (kcal/mol) comparison of the Si₂HLi isomers calculate by various methods.

	dibridged	Li-bridged	H-bridged
CCSD(T)/AVTZ	0.00	4.12	8.91
CCSD(T)-F12a/VTZ-F12	0.00	4.40	9.23
B3LYP/6-311+G(d)	0.00	3.22	8.66

The two *ab initio* methods show similar values of the relative energies. On the other hand, the DFT method *underestimates* the relative energies (by about 0.9 kcal/mol average in both of the cases).

Frequencies

Harmonic vibrational frequencies were calculated at the B3LYP/6-311+G(d) level as well as the CCSD(T)/AVTZ level of theory. The calculated results are listed in Table 4.4-11.

The discussion on the frequencies will be presented in the same manner as in the previous sub-chapters.

The B3LYP method reproduced the third, fourth and fifth vibration frequencies in the dibridged structure calculated with CCSD(T) with an average absolute difference of 2.9 cm⁻¹; however, the second and last vibrations are *underestimated* by 114.4 cm⁻¹ and 113.6 cm⁻¹, respectively. Nevertheless, the average absolute difference for the B3LYP method is only 44.5 cm⁻¹ if we consider all calculated vibrational frequencies.

The B3LYP frequency values of the Li-bridged structure show the best agreements with the corresponding CCSD(T) results; the average absolute difference (when all vibrations are considered) is only 9.6 cm⁻¹ and is the lowest of all the Si₂HLi isomers.

Table 4.4-11. Harmonic frequencies for the Si₂HLi isomers calculated at different levels of theory; the results are listed in descending order of wavenumber (cm⁻¹).

	Si ₂ HLi		
	CCSD(T)/AVTZ	B3LYP/6-311+G(d)	
<u>dibridged</u>			
	1496.9	1466.7	SiH sym. str.
	1182.5	1068.1	SiH antisym. str.
	540.3	546.2	SiSi/SiH out-of-phase str.
	392.8	394.9	SiLi/SiH in-phase str.
	319.5	320.2	Butterfly
	170.4	56.8	HLi twist
<u>Li-bridged</u>			
	2156.9	2143.6	SiH str.
	592.8	610.8	SiSi/SiH out-of-phase str.
	415.6	414.2	SiLi/SiH in-phase str.
	362.7	369.9	H in-plane bend
	238.3	222.3	out-of-plane
	223.5	221.5	LiH bend
<u>H-bridged</u>			
	1563.0	1531.8	SiH sym. str.
	1119.9	975.6	SiH antisym. str.
	606.9	614.6	SiSi/SiLi out-of-phase. str.
	415.5	415.3	SiSi/SiLi in-phase str.
	85.6	97.9	LiH bend
	39.5	62.2	out-of-plane

The H-bridged structure shows a similar picture as in the dibridged structure; the third, fourth and fifth frequencies are reproduced by the B3LYP method with an average absolute difference of only 6.7 cm⁻¹, whereas the second vibration is significantly *underestimated* compared to the CCSD(T) value by 144.2 cm⁻¹. The average absolute difference, 36.4 cm⁻¹ (when all vibration frequencies are considered) is however, smaller than in the dibridged structure.

Anharmonicity

Anharmonic properties were calculated using second order perturbation theory. The MP2/aug-cc-pVTZ level of theory was employed (the Gaussian 09 software package). The calculated rotational constants, anharmonic constants and dipole moments are given in Table 4.4-12. The harmonic and fundamental vibration frequencies are listed in Table 4.4-13.

The A_e – C_e rotational constants show that all the Si_2HLi isomers are asymmetric top molecules, however, the LiSiHSi isomer is a nearly-symmetric top molecule as the B_e and C_e rotational constant are almost the same.

The Δ symbol in Table 4.5-10 represents the difference between harmonic and fundamental vibrations ($\Delta_n = \omega_n - \nu_n$). In general, anharmonic effects decrease the frequencies. However, negative values Δ_n can be seen in the HSiLiSi and SiHLiSi isomers. Negative values of Δ are unusual but examples of such vibrational modes are known in the literature [152, 153].

Table 4.4-12. Calculated rotational and anharmonic constants of the Si₂HLi isomers.

	HSiLiSi	LiSiHSi	SiHLiSi
Dipole μ [D]	5.7191	9.0900	6.2548
Rotational Constants (cm^{-1})			
A_e	0.487003	3.151909	0.452632
B_e	0.241140	0.124859	0.244121
C_e	0.161282	0.120102	0.163333
A_0	0.483976	3.020182	0.451167
B_0	0.241048	0.126223	0.243649
C_0	0.160389	0.120481	0.162358
Anharmonic Constants (cm^{-1})			
χ_{11}	-36.11	-24.77	-16.26
χ_{12}	-1.04	-23.12	-40.76
χ_{13}	-1.75	-4.62	-5.58
χ_{14}	-5.02	-1.06	-0.16
χ_{15}	-0.83	-1.02	-7.79
χ_{16}	-3.37	-13.80	5.16
χ_{22}	-2.25	-54.28	-53.03
χ_{23}	-0.13	5.39	3.94
χ_{24}	-0.94	-0.03	0.18
χ_{25}	0.02	-0.93	-11.70
χ_{26}	3.25	6.91	-7.28
χ_{33}	-1.59	-2.53	-2.28
χ_{34}	-3.58	-3.02	-0.99
χ_{35}	-16.39	-2.73	-1.28
χ_{36}	1.50	-0.29	0.86
χ_{44}	-1.62	-1.62	-1.62
χ_{45}	-4.79	1.10	-2.44
χ_{46}	2.14	4.28	18.92
χ_{55}	-1.73	-2.26	0.78
χ_{56}	-0.21	-46.62	-0.41
χ_{66}	2.66	3.52	-1.72

Table 4.4-13. Calculated harmonic and fundamental frequencies at the MP2/ aug-cc-pVTZ level. Δ is the difference between the fundamental and harmonic frequencies.

	HSiLiSi	LiSiHSi	SiHLiSi
Harmonic vibration frequencies (cm^{-1})			
ω_1	2200.71	1629.64	1545.35
ω_2	589.89	1248.63	1312.39
ω_3	424.11	602.69	539.39
ω_4	398.75	409.33	391.13
ω_5	323.48	77.30	324.39
ω_6	224.24	60.50	173.23
Fundamentals vibration frequencies (cm^{-1})			
ν_1	2122.50	1558.29	1488.26
ν_2	585.98	1134.17	1178.52
ν_3	398.71	595.01	533.32
ν_4	389.42	406.72	403.57
ν_5	330.45	42.79	314.14
ν_6	209.67	37.47	178.42
Δ (cm^{-1})			
Δ_1	78.22	71.35	57.09
Δ_2	3.92	114.46	133.86
Δ_3	25.40	7.68	6.08
Δ_4	9.33	2.61	-12.43
Δ_5	-6.97	34.51	10.25
Δ_6	14.57	23.04	-5.19
$(\Delta_n = \omega_n - \nu_n)$			

Corrections

In this section, we investigate how core-valence contributions, zero-point vibrational motion and relativistic corrections affect the Si_2HLi isomerisation energy.

Most calculations focus on correlating only the valence electrons as these dominate the properties of atoms and molecules. However, correlation effects involving the electrons in low-lying core orbitals may be important if the goal of a calculation is to achieve chemically accurate isomerization energies or thermochemical properties (with errors less than 1 kcal/mol). The structures optimized at the CCSD(T)-F12a/VTZ-F12 level of theory were taken as starting structures.

To calculate core-valence interactions the CCSD(T) method was employed with the aug-cc-pCVXZ (where X=2–3) basis sets [154, 155], which were specifically designed to recover core-core and core-valence electron correlation. The CCSD(T)/aug-cc-pCVXZ (where X=2–3) basis sets will be abbreviated as ACVXZ. An appended label “fc” or “cc” indicates frozen-core or correlated-core. The core-valence correlation contribution ($E_{\text{core_ACVXZ}}$) was obtained as the energy difference between frozen-core ACVXZ-fc and correlated-core ACVXZ-cc (Si 2s, 2p and Li 1s orbitals correlated) calculations. The differences were then added to the energies calculated at the CCSD(T)-F12a/VTZ-F12 level. This allowed the evaluation of relative energies of the Si₂HLi isomers that include core-valence correlation contributions. The calculated CCSD(T)/ACVDZ and CCSD(T)/ACVTZ results are compared to CCSD(T)-F12/VTZ-F12 relative energies in Table 4.4-14.

Table 4.4-14. Comparison of the relative energies computed at the VTZ-F12 level and the ACVXZ relative energies (where X=2-3) with core-valence contributions. Energies in kcal/mol.

	HSiLiSi	LiSiHSi	SiHLiSi
ACVDZ	4.521	9.432	0.000
ACVTZ	4.658	9.451	0.000
VTZ-F12	4.400	9.231	0.000

The differences between the ACVTZ and VTZ-F12 relative energies are 0.258 and 0.220 kcal/mol for HSiLiSi and LiSiHSi, respectively, whereas the differences between the ACVDZ and VTZ-F12 relative energies are 0.121 and 0.201 kcal/mol for HSiLiSi and LiSiHSi, respectively.

The neglect of relativistic corrections can lead to an incorrect prediction of the isomerisation energy. Recently even the potential energy surface calculation of light molecules such as H₃⁺ included relativistic corrections; for H₃⁺ an overall 9-figure accuracy was achieved [156]. The work of Tarczay et al. [106] shows the effect of the relativistic contribution to the SiH₃[−] inversion barrier and on the isomerisation barriers of (H, C and N) systems, so we were eager to calculate such corrections in our work.

The relativistic correction was evaluated (at the CCSD(T) level) as the sum of the expectation values for the mass-velocity and the one-electron Darwin terms. This type of relativistic correction is suggested by Tarczay et al. [106] as fast and effective for small molecules. Thiel et al. [157] used this approach as the relativistic correction in their NH₃ 6D-PES calculations (employing the CCSD(T)/AVTZ-fc level of theory). The AVTZ-DK basis set [58, 149, 158], which is specially designed for relativistic corrections and the standard AVTZ basis set were employed. A comparison of the CCSD(T)/AVTZ-DK ($E_{\text{rel_DK}}$), CCSD(T)/AVTZ ($E_{\text{rel_AVTZ}}$) and CCSD(T)-F12/VTZ-F12 results can be found in Table 4.4-15. However, Tarczay et al. suggested that the correlation-consistent basis sets of Dunning may not yield converged results for either the relativistic HF energies or the related correlation contribution for the mass-velocity and Darwin energy corrections [106]. The calculated relativistic contributions were added to the energies calculated at the CCSD(T)-F12a/VTZ-F12 level. This allowed the evaluation of relative energies of the Si₂HLi isomers that include relativistic effects.

Table 4.4-15. Comparison of the relative energies at the VTZ-F12 levels with the corrected energies: $E_{\text{rel_AVTZ}}$ and $E_{\text{rel_DK}}$. Energies in kcal/mol.

	HSiLiSi	LiSiHSi	SiHLiSi
AVTZ-DK	4.661	9.222	0.000
AVTZ	4.629	9.467	0.000
VTZ-F12	4.400	9.231	0.000

For HSiLiSi, the relative energies with the relativistic contributions are larger than the corresponding uncorrected results (0.229 and 0.261 kcal/mol). However, for LiSiHSi, the corrected relative energies are smaller for the AVTZ-DK level (by 0.009 kcal/mol) but larger for the AVTZ level (by 0.236 kcal/mol) compared to the uncorrected results. The relative energies computed with the AVTZ-DK and AVTZ relativistic corrections differ from each other; slightly for the HSiLiSi isomers (0.032 kcal/mol) and significantly for the LiSiHSi isomer (0.245 kcal/mol). We assume that the relativistic effects calculated at the AVTZ-DK level are more accurate, as the AVTZ-DK basis set is designed for use with Douglas-Kroll-Hess Hamiltonians [159].

The zero-point vibrational correction (E_{zpe}) was obtained from calculations performed at the MP2/aug-pVTZ level of theory. The E_{zpe} includes anharmonic corrections.

All the corrections are added to the energies calculated at the VTZ-F12 level (E in Hartree). The final corrected energies are given by $E_{corr_DK}=E+E_{core}+E_{rel_DK}+E_{zpe}$ or $E_{corr_AVTZ}=E+E_{core}+E_{rel_AVTZ}+E_{zpe}$. These results are compared to the isomerisation energies obtained at the CCSD(T)-F12/VTZ-F12 and CCSD(T)/AV(Q+d)Z levels of theory (see Table 4.4-16).

Table 4.4-16. Comparison of the relative energies at the AV(Q+d)Z, and VTZ-F12 levels with the corrected energies: E_{corr_AVTZ} and E_{corr_DK} . Energies in kcal/mol.

	AV(Q+d)Z	VTZ-F12	E_{corr_AVTZ}	E_{corr_DK}
HSiLiSi	4.469	4.400	4.612	4.765
LiSiHSi	9.135	9.231	9.105	9.061

The corrected relative energies of the HSiLiSi species are larger than the corresponding uncorrected results. However, the corrected relative energies of the LiSiHSi species are smaller when compared to the uncorrected results. The isomerization energies computed with the AVTZ-DK and AVTZ relativistic corrections differ significantly from each other. The AVTZ-DK correction gives larger relative energies (by 0.153 kcal/mol) for the HSiLiSi species, whereas lower relative energies (by 0.044 kcal/mol) are obtained for the LiSiHSi species compared to the AVTZ correction. Note, that we did not encounter convergence problems for the AVTZ basis set during the calculations as suggested by Tarczay et al [106]. It is assumed that the AVTZ-DK basis set gives more accurate results. However, to say this conclusively comparison with experimental results is necessary.

Comparison of calculated geometries with the literature

As was mentioned in the Introduction chapter, the Si_2HLi structures calculated by Bei and Feng [30] were obtained at a too low a level of theory to do reliable comparison with the results calculated here. There are no other experimental or theoretical data available for Si_2HLi . On the other hand, experimental data exist for bigger molecules containing Si–Li bonds. Many of these were synthesized by Sekiguchi’s research group

[160-162] but the Si or Li atoms are usually connected to big bulky groups like ^tBu. We took a number of crystallographic data of XSi–Li bond distances (as close to our structures as possible where X=H or Si) as a reference for comparison to our calculations. These works show the range of Si–Li distances (Li in bridged position) from 2.645 Å to 2.657 Å [163] and where Li is in a terminal position of 2.580 Å and 2.531 Å [164, 165]. Thus, our calculations are in good agreement with experimental data.

4.5 The Si₂Li₂ isomers.

Computational methods

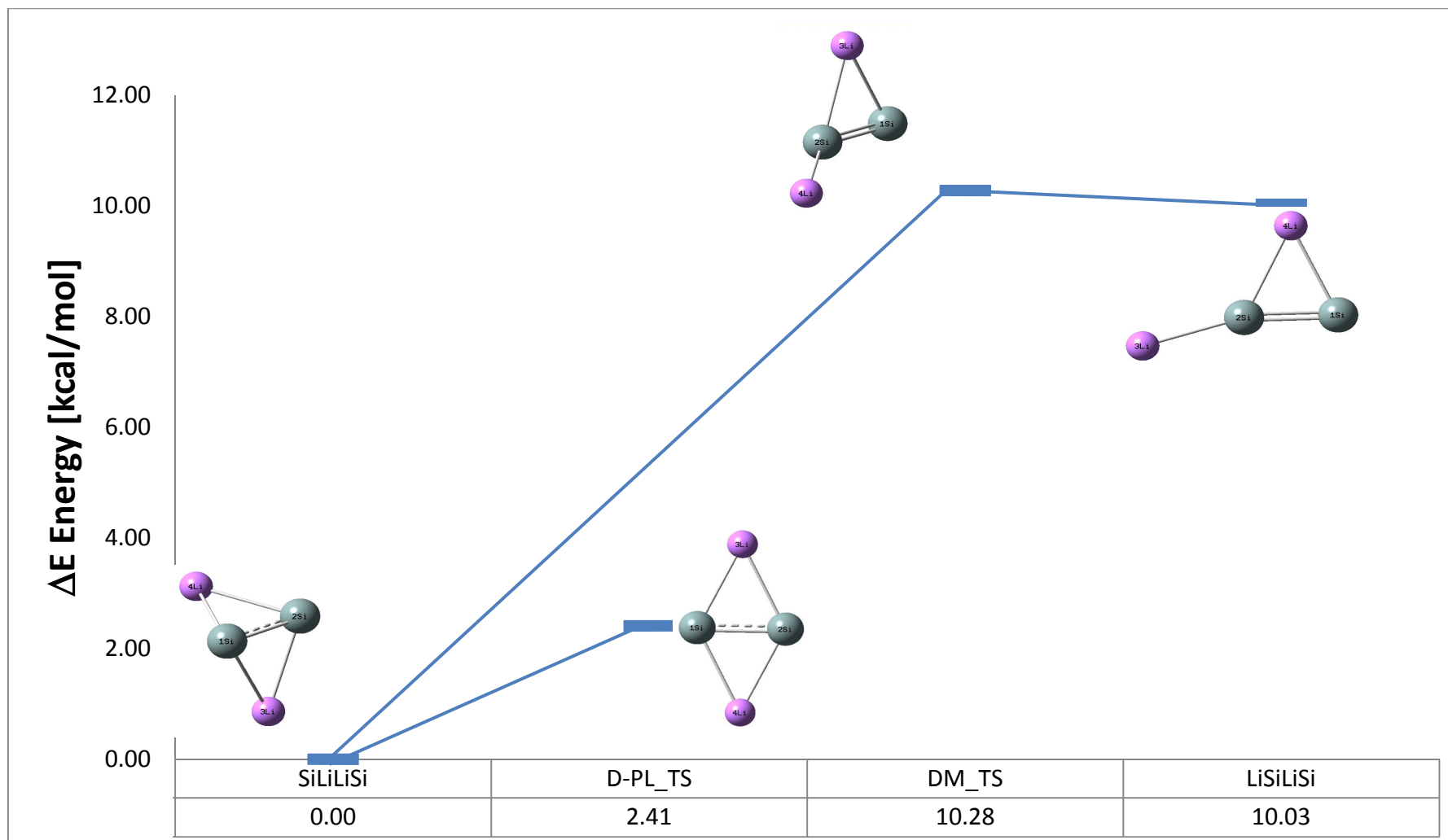
The Si₂H₂ structures optimized by Grev and Schaefer [24] were taken as the starting geometries, where both of the H-atoms were replaced by Li-atoms. Average literature (theoretical) values of the Si–Li bond distances were used in the substituted-lithium starting geometries. These structures were optimized with the CCSD(T)/aug-cc-pVXZ, CCSD(T)-F12a/cc-pVTZ-F12 and B3LYP/6-311+G(d) methods (where X=2–4).

Harmonic vibrational frequency computations were performed for the optimized structures to characterise these as minima or transition states (TS). The frequency calculations were also done at the CCSD(T)/aug-cc-pVTZ, CCSD(T)-F12a/cc-pVTZ-F12 and B3LYP/6-311+G(d) levels of theory.

All the calculated isomers and transition states are depicted in Figure 4.5-1. The LiSiLiSi and SiLiLiSi formulae refer to the monobridged and dibridged isomers, respectively. The D–PL_TS and DM_TS abbreviations represent the transition states on the paths between the dibridged and dibridged-planar structures and between the dibridged and monobridged structures, respectively. The energies relative to the dibridged structure (global minimum) are listed at the bottom of Figure 4.5-1. The reaction paths between critical points are represented schematically by lines. The pictures in Figure 4.5-1 show (multiple) bonded properties (minima and TS) obtained from Natural Bond Orbital (NBO) calculations [102, 103]. The NBO calculations were performed at the CCSD/cc-pV(T+d)Z level of theory using the Gaussian 98 [138] software package.

Note, that in the following discussion all the employed correlation consistence basis sets (such as aug-cc-pVXZ (where X=2–4)) will be abbreviated as AVXZ, and the methods such as: CCSD(T)-F12a/cc-pVTZ-F12 and B3LYP/6-311+G(d) will be abbreviated as F12 and B3LYP, respectively.

Figure 4.5-1. The optimized structures of the Si_2Li_2 isomers and transition states with energies relative to the global minimum (dibridged). The calculations were done at the CCSD(T)/aug-cc-pVTZ level of theory.



Two minima and two transition states (TS) were found on the Si₂Li₂ potential energy surface (PES). The global minimum is the singly-bonded dibridged structure and above with an energy difference of 10.28 kcal/mol lies the Li-bridged structure. Figure 4.5-1 shows two TS; DM_TS connects the dibridged and monobridged structures. D-PL_TS is a transition state on the reaction path where the non-planar structure (dibridged) becomes planar (D-PL_TS) and then turns in to a symmetrically equivalent (dibridged) structure. Similar “*flip over*” motions can be found on the PESs of the Si₂H₂ species or the NH₃ species [24, 157].

The geometric properties of the optimized structures are listed in Table 4.5-1.

Table 4.5-1. Geometric properties of the calculated Si₂Li₂ structures. The calculations were done at the CCSD(T)/aug-cc-pVTZ level of theory.

	SiLiLiSi, C _{2v}	LiSiLiSi, C _s	D_PL_TS, C _{2h}	DM_TS, C ₁
Si ₂ Li ₂ ^a	2.5616	2.5738	2.5286	2.5671
SiSi ^a	2.1848	2.1494	2.1812	2.1541
Li ₂ Si ₂ ^a		2.4105		2.4028
β LiSiSiLi ^b	101.85	180.00	180.00	118.24
α Si ₂ Li ₂ Li ^b		165.90		140.56
α Si ₂ Li ₂ Li ^b	64.76	63.90	64.44	64.36
^a ångström				
^b degrees				

Table 4.5-1 shows that the shortest Si-Si bond length is found in the Li-bridged structure (2.1494) followed by DM_TS (2.1541 Å), D-PL_TS (2.1812 Å) and the dibridged structure (2.1848 Å). The Si-Li bond distances in the dibridged structures (the SiLiLiSi and D_PL_TS structures) are equal as the structures are symmetrical. The bridged Li atoms in both monobridged structures (the Li-bridged and DM_TS structures) have longer bond distances (2.5738–2.5671 Å, respectively) than the terminal Li atoms (2.4105–2.4028 Å, respectively), which was seen before in the previous sub-chapter (4.4).

Table 4.5-2. Geometric properties of the Si_2Li_2 isomers calculated at the CCSD(T)/AVXZ (X=2–4) level of theory.

	SiLiLiSi				LiSiLiSi		
	AVDZ	AVTZ	AVQZ		AVDZ	AVTZ	AVQZ
$\text{Si}_2\text{Li}_2^{\text{a}}$	2.5950	2.5616	2.5553	$\text{Si}_2\text{Li}_2^{\text{a}}$	2.6003	2.5738	2.5718
SiSi^{a}	2.2133	2.1848	2.1713	SiSi^{a}	2.1763	2.1494	2.1383
$\text{LiSiSi}_2^{\text{a}}$				$\text{LiSiSi}_2^{\text{a}}$	2.4315	2.4105	2.4100
$\beta \text{HSiSiLi}^{\text{b}}$	100.27	101.85	102.47	$\beta \text{HSiSiLi}^{\text{b}}$	180.00	180.00	180.00
$\alpha \text{SiSiLiLi}^{\text{b}}$				$\alpha \text{SiSiLiLi}^{\text{b}}$	166.38	165.92	164.59
$\alpha \text{SiSiLi}_2^{\text{b}}$	64.76	64.76	64.86	$\alpha \text{SiSiLi}_2^{\text{b}}$	64.30	63.90	63.87
^a ångström							
^b degrees							

Figure 4.5-2 and Figure 4.5-3 show the variations in the isomerisation energies and Si–Si bond lengths upon increasing AVXZ basis set size.

Figure 4.5-2 shows that the largest change occurs from AVDZ to AVTZ, whereas only a small change happens upon further basis set improvement. In contrast, the Figure 4.5-3 shows the opposite picture the smallest change occurs from AVDZ to AVTZ, whereas a large change happens upon further basis set improvement. Thus, larger basis sets are required to achieve convergence.

Figure 4.5-2. Si–Si bond length variation with increasing basis set size for the Si₂Li₂ isomers.

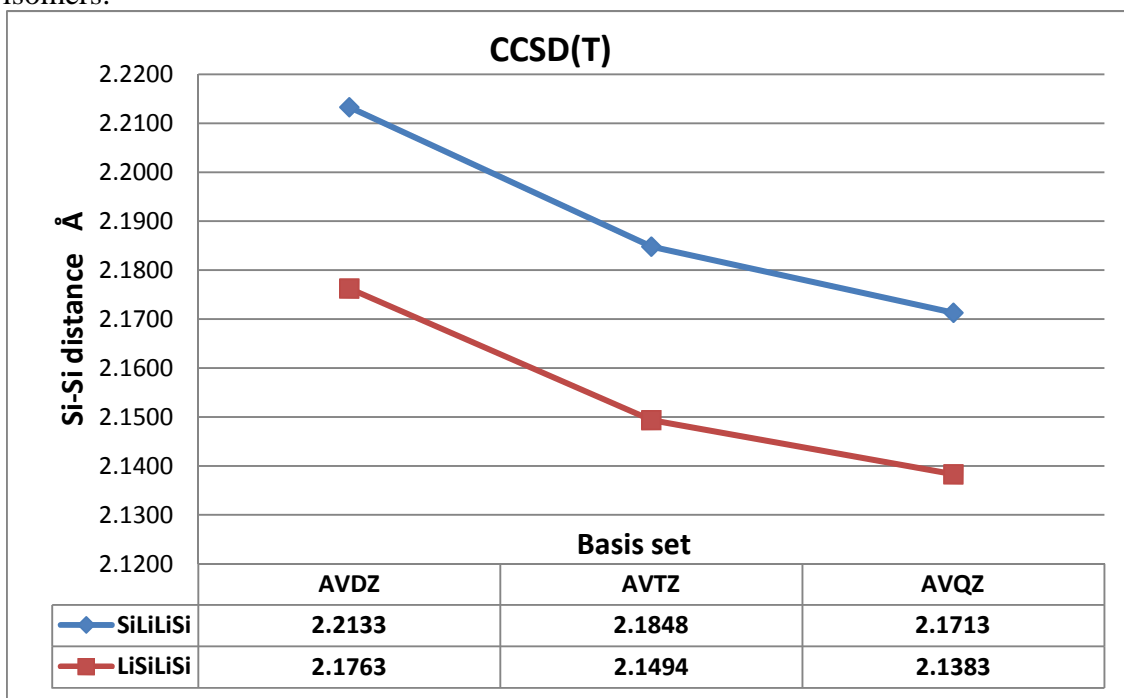
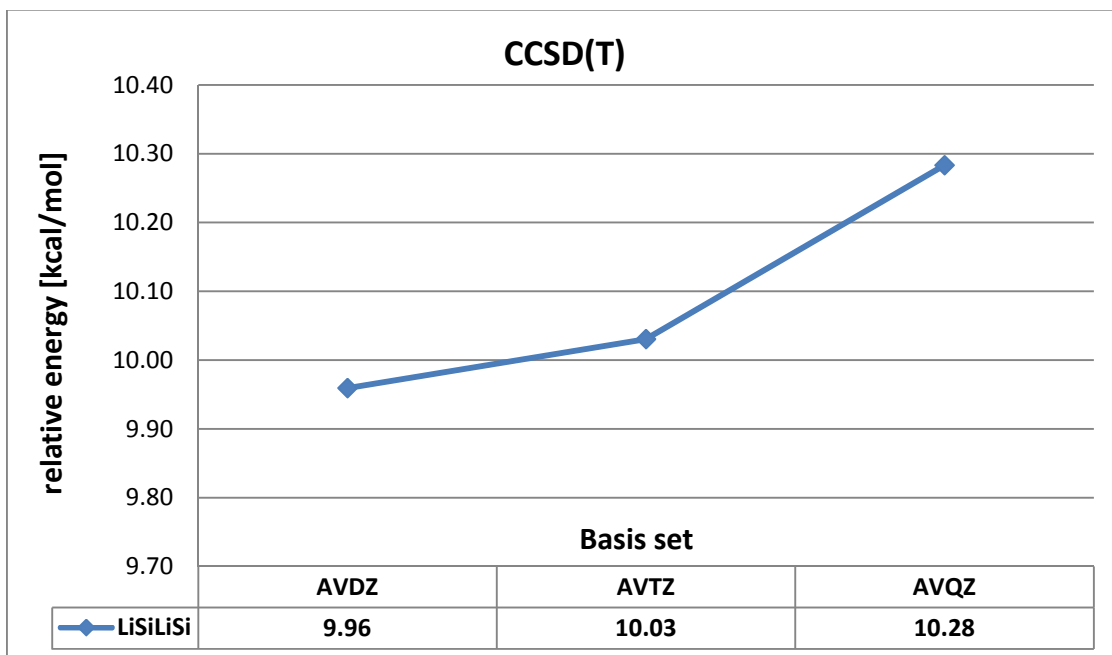


Figure 4.5-3. Energy of the LiSiLiSi isomer (relative to the dibridged isomer) as a function of AVXZ basis set size.



CCSD(T)- F12 calculations

A comparison of the results obtained with the CCSD(T)/AVTZ method, the recently developed CCSD(T)-F12a/VTZ-F12 method and the B3LYP/6-311+G(d) method is shown in Table 4.5-3.

Table 4.5-3. Comparison of geometric properties calculated by various methods.

	Si ₂ Li ₂		
	CCSD(T)/ AVTZ	CCSD(T)-F12a/ VTZ-F12	B3LYP/ 6-311+G(d)
dibridged			
Si ₂ Li ₂ ^a	2.5616	2.5524	2.5363
SiSi ^a	2.1848	2.1660	2.1635
β LiSiSiLi ^b	101.85	102.58	98.76
α SiSiLi ₂ ^b	64.76	64.90	64.75
monobridged			
Si ₂ Li ₂ ^a	2.5738	2.5697	2.5671
SiSi ^a	2.1494	2.1335	2.1291
Li ₁ Si ₂ ^a	2.4105	2.4098	2.3915
β LiSiSiLi ^b	180.00	180.00	180.00
α Si ₁ Si ₂ Li ₁ ^b	165.92	164.22	165.78
α Si ₁ Si ₂ Li ₂ ^b	63.90	63.85	64.36
^a ångström			
^b degrees			

The three methods produce bond distance values in the dibridged structure with good agreement to each other. However, assuming the F12 method presumably gives the most accurate results, these will be taken as a reference. The calculated bond distance differences vary from 0.0025 Å (Si–Si bond length difference between the B3LYP and F12 methods) to 0.0188 Å (Si–Si length difference between the CCSD(T) and F12 methods). The average absolute difference of the calculated bond distances is 0.014 Å (difference between the CCSD(T) and F12 methods) and 0.0093 Å (difference between the B3LYP and F12 methods), respectively. The SiSiLi angles are reproduced with

good agreement as well. The largest difference is 0.15° (difference between the B3LYP and F12 results and between the CCSD(T) and F12 results), and the smallest is found for the F12 and CCSD(T) methods (0.14°). However, it can be seen that the B3LYP method *underestimates* the dihedral angle by 3.82° (compared with F12) while, the CCSD(T) method gives a difference of 0.73° .

The bond distances for the monobridged structure are reproduced by the methods employed with good agreement to each other. Once again the F12 method will be taken as a reference. The smallest calculated difference is 0.0007 \AA (Li1–Si2 lengths between the CCSD(T) and F12 methods) and the largest is 0.0183 \AA (Li1–Si2 lengths between the B3LYP and F12 methods). The average absolute difference of the calculated bond distances is 0.0069 \AA (difference between the CCSD(T) and F12 methods) and 0.0084 \AA (difference between the B3LYP and F12 methods), respectively. Both methods *overestimate* the SiSiLi1 angle by about 1.72° (for the CCSD(T) method) and about 1.58° (for the B3LYP method) with comparison to the F12 method. The SiSiLi2 angle is reproduced by the employed methods with good agreement to each other; the largest difference is 0.05° (between the CCSD(T) and F12 methods) and the smallest is 0.51° (between the B3LYP and F12 methods).

A comparison of the relative energies of the Si_2Li_2 minima calculated using the DFT (B3LYP/6-311+G(d)) method, CCSD(T)/AVTZ and F12 (CCSD(T)-F12a/VTZ-F12) methods is shown in Table 4.5-4.

Table 4.5-4. Relative energy (kcal/mol) comparison of the Si_2Li_2 isomers calculated by various methods.

	dibridged	Li-bridged
CCSD(T)/AVTZ	0.00	10.03
CCSD(T)-F12a/VTZ-F12	0.00	10.45
B3LYP/6-311+G(d)	0.00	9.19

The *ab initio* methods show similar values of the relative energy. On the other hand the DFT method *underestimates* the relative energy by 1.26 kcal/mol.

Frequencies

The same methods as in the previous paragraphs were employed to compare calculated harmonic frequencies. The results can be found in Table 4.5-5. The results are listed in descending order in wavenumber units (cm^{-1}).

Table 4.5-5. Calculated harmonic frequencies for the Si_2Li_2 isomers calculated at different levels of theory; the results are listed in descending order in wavenumber units (cm^{-1}).

	Si_2Li_2			
	CCSD(T)/ AVTZ	CCSD(T)-F12/ VTZ-F12	B3LYP/ 6-311+G(d)	
<u>dibridged</u>				
	543.4	553.9	556.0	SiSi str.
	420.2	423.8	415.8	SiLi antisym. str.
	406.5	408.9	403.0	SiLi sym. str.
	197.1	196.6	184.0	SiLi antisym. str.
	189.4	191.0	178.7	SiLi antisym. str.
	113.2	106.6	116.8	butterfly
<u>monobridged</u>				
	610.6	617.0	623.1	SiSi/SiLi _t in-phase str.
	420.9	425.1	422.6	SiLi/SiLi antisym. str.
	420.4	423.6	416.9	SiLi/SiLi sym. str.
	210.0	212.7	203.5	SiSiLi _b bend
	60.1	60.2	65.8	LiSiLi bend
	38.6	39.8	50.8	out-of-plane

In the dibridged structure both *ab initio* (CCSD(T) and F12) methods give similar vibration wavenumber values: the largest difference is 10 cm^{-1} (the first vibrational mode). The average absolute difference between the CCSD(T) and F12, B3LYP and CCSD(T) and B3LYP and F12 methods is 4.2 cm^{-1} , 7.9 cm^{-1} and 8.5 cm^{-1} , respectively.

For the monobridged isomer the CCSD(T) and F12 levels of theory give similar frequency values, the average absolute difference is only 2.9 cm^{-1} . The largest

difference (6 cm^{-1}) can be seen for the first vibration mode and the smallest difference (0.1 cm^{-1}) for the fifth vibration mode. The B3LYP frequency calculations show slightly better agreement with the two *ab initio* methods than in the dibridged structure except the first and last vibrations (12.5 cm^{-1} and 12.2 cm^{-1}) for the difference between the B3LYP and CCSD(T) methods and the last vibration (11 cm^{-1}) for the difference between the B3LYP and F12 methods. However the average absolute differences (7 cm^{-1} and 8 cm^{-1}) between the B3LYP and *ab initio* results are lower than in the dibridged case.

Anharmonicity

Anharmonic properties were calculated using perturbation theory. The MP2/aug-cc-pVTZ level of theory and the Gaussian 09 software package were used. The calculated rotational constants, anharmonic constants and dipole moments are given in Table 4.5-5. The harmonic and fundamental vibrations are listed in Table 4.5-6.

The A_e – C_e rotational constants show that all the Si_2Li_2 isomers are asymmetric top molecules. Note the presence of large positive values for the anharmonic constants χ_{23} and χ_{26} in Table 4.5-6. This will be discussed in more detail in Chapter 8.

The $\Delta\text{ (cm}^{-1}\text{)}$ symbol in Table 4.5-7 represents the difference between the harmonic and fundamental vibrations ($\Delta_n = \omega_n - \nu_n$). In general, anharmonic effects decrease the frequencies. However, negative values Δ_n can be seen for the SiLiLiSi isomers. Negative values of Δ are unusual but examples of such vibrational modes are known in the literature [152, 153].

Table 4.5-6. Calculated rotational and anharmonic constants of the Si₂Li₂ isomers.

	LiSiLiSi	SiLiLiSi
Dipole μ [D]	8.70	6.29
Rotational Constants (cm^{-1})		
Ae=	0.4910	0.2432
Be=	0.1187	0.1880
Ce=	0.0956	0.1505
A0=	0.4880	0.2421
B0=	0.1193	0.1883
C0=	0.0957	0.1490
Anharmonic Constants (cm^{-1})		
χ_{11}	-2.03	-2.23
χ_{12}	-0.76	-1.25
χ_{13}	-3.40	0.80
χ_{14}	0.81	0.20
χ_{15}	-1.25	-0.78
χ_{16}	-0.33	0.49
χ_{22}	-1.77	-0.83
χ_{23}	-0.41	30.16
χ_{24}	0.55	-0.89
χ_{25}	-0.01	-3.32
χ_{26}	-1.01	20.69
χ_{33}	-1.74	-0.69
χ_{34}	-0.32	-0.73
χ_{35}	0.90	0.28
χ_{36}	1.55	-4.04
χ_{44}	-2.02	-2.63
χ_{45}	-0.19	0.44
χ_{46}	-0.16	-1.24
χ_{55}	-0.75	-1.06
χ_{56}	0.05	0.79
χ_{66}	-2.31	-1.19

Table 4.5-7. Calculated harmonic and fundamental frequencies. Δ is the difference between the fundamental and harmonic frequencies.

	LiSiLiSi	SiLiLiSi
Harmonic vibration frequencies (cm^{-1})		
ω_1	610.03	548.39
ω_2	424.53	422.22
ω_3	416.39	408.37
ω_4	216.03	196.36
ω_5	57.96	193.51
ω_6	40.33	104.06
Fundamental vibration frequencies (cm^{-1})		
ν_1	603.50	543.65
ν_2	400.75	433.85
ν_3	412.06	442.40
ν_4	212.34	208.21
ν_5	56.21	199.47
ν_6	35.75	97.69
Δ (cm^{-1})		
Δ_1	6.52	4.74
Δ_2	23.78	-11.63
Δ_3	4.32	-34.04
Δ_4	3.68	-11.86
Δ_5	1.76	-5.96
Δ_6	4.58	6.37
$(\Delta_n = \omega_n - \nu_n)$		

Corrections

We investigated the same set of corrections as in the Si_2HLi sub-chapter: core-valence interactions, zero-point vibrational corrections and relativistic corrections.

The CCSD(T)-F12a method and the specially designed cc-pCVTZ-F12 basis set [166] was employed to calculate the core-valence interactions. An appended label “fc” or “cc” indicates the frozen-core or correlated-core approximation. The core-valence correlation contribution (E_{core}) was obtained as the energy difference between frozen-core CVTZ-F12-fc and correlated-core CVTZ-F12-cc (Si 2s, 2p and Li 1s orbitals correlated) calculations. The differences were then added to the energies calculated at the

CCSD(T)-F12a/VTZ-F12 level. This allowed the evaluation of relative energies of the Si_2Li_2 isomers that include core-valence correlation contributions. The calculated results are compared to VTZ-F12 relative energies in Table 4.5-8.

Table 4.5-8. Comparison of the relative energies computed at the VTZ-F12 level and the CVTZ-F12 relative energies with core-valence contributions. Energies in kcal/mol.

	<u>LiSiLiSi</u>
CCSD(T)-F12a	
CVTZ-F12	10.9515
VTZ-F12	10.4472

Table 4.5-9 shows a difference of 0.5 kcal/mol between the CVTZ-F12 and VTZ-F12 relative energies. The difference is larger than in the Si_2HLi case by about 0.25 kcal/mol.

The relativistic correction was evaluated at the CCSD(T) level as the sum of the expectation values for the mass-velocity and the one-electron Darwin terms. The specially designed AVTZ-DK basis set and the ordinary Dunning's AVTZ basis set were employed and a comparison of the results obtained with these two basis sets and the effects of these on the isomerisation energies was made. A comparison of the CCSD(T)/AVTZ-DK ($E_{\text{rel_DK}}$), CCSD(T)/AVTZ ($E_{\text{rel_AVTZ}}$) and CCSD(T)-F12/VTZ-F12 results can be found in Table 4.5-9. The calculated relativistic contributions were added to the energies calculated at the CCSD(T)-F12a/VTZ-F12 level. This allowed the evaluation of relative energies of the Si_2Li_2 isomers that include relativistic effects.

Table 4.5-9. Calculated relativistic correction for the Si_2Li_2 isomers at the CCSD(T)/AVTZ-DK and CCSD(T)/AVTZ level. The results are listed in kcal/mol.

	<u>LiSiLiSi</u>
AVTZ-DK	10.403
AVTZ	10.477
VTZ-F12	10.447

For LiSiLiSi, the relative energies with the relativistic contributions are larger by 0.044 kcal/mol (for AVTZ) but smaller by 0.03 kcal/mol (for AVTZ-DK), compared to the

uncorrected results. The relative energies computed with the AVTZ-DK and AVTZ relativistic corrections differ from each other (by 0.074 kcal/mol) for the LiSiLiSi isomer. Again, we assume that the relativistic effects calculated at the AVTZ-DK level are more accurate, as the AVTZ-DK basis set is designed for use with Douglas-Kroll-Hess Hamiltonians.

It can be seen that for both Si₂HLi and Si₂Li₂ the biggest changes in relative energies are when core-valence contributions are added, whereas the relativistic effects corrections only slightly change the relative energies. Thus, it can be concluded that for the Si₂XLi species (where X=H or Li) core-valence contributions are more important than relativistic effects.

The zero-point vibrational corrections (E_{zpe}) were obtained from anharmonic calculations performed at the MP2/aug-pVTZ level of theory. The E_{zpe} includes anharmonic corrections.

All the corrections are added to the energies calculated at the CCSD(T)-F12a/VTZ-F12 level of theory (E in Hartree). The final corrected energy is given by $E_{\text{corr-DK}} = E + E_{\text{core}} + E_{\text{rel-DK}} + E_{\text{zpe}}$ or $E_{\text{corr-AVTZ}} = E + E_{\text{core}} + E_{\text{rel-AVTZ}} + E_{\text{zpe}}$.

A comparison of the uncorrected energies with the corrected energies calculated at the different levels of theory is listed Table 4.5-10.

Table 4.5-10. Comparison of the relative energies of the LiSiLiSi isomer at the CCSD(T)/AVQZ and CCSD(T)-F12/VTZ-F12 level with the corrected energies: $E_{\text{corr-AVTZ}}$ and $E_{\text{corr-DK}}$. Energies listed in kcal/mol.

	AVQZ	VTZ-F12	$E_{\text{corr-AVTZ}}$	$E_{\text{corr-DK}}$
LiSiLiSi	10.283	10.447	10.846	10.920

The corrected energies $E_{\text{corr-AVTZ}}$ and $E_{\text{corr-DK}}$ show an increase in the relative energy, in comparison to AVQZ, of 0.563 kcal/mol and 0.637 kcal/mol, respectively and, in comparison to, of VTZ-F12 0.399 kcal/mol and 0.473 kcal/mol, respectively. The basis sets employed (AVTZ-DK and AVTZ) yield different isomerization energies. The

AVTZ-DK basis set gives a relative energy (for the LiSiLiSi species) that is larger by 0.074 kcal/mol than the results obtained with AVTZ basis set. However, the difference between the two basis sets is smaller than that obtained in the Si_2HLi sub-chapter. Also convergence problems have not been seen during the AVTZ calculations as suggested by Tarczay et al. [106]. In this case the relative energy difference between the AVTZ and AVTZ-DK is less than 0.1 kcal/mol.

Comparison of calculated geometries with literature

Both SiLi and Si_2Li_2 were studied in the gas phase by mass-spectrometry [46, 103, 167]. Unfortunately, we could not access the paper, as it was published in a limited conference edition. There are no other experimental results on Si_2Li_2 structures known to the author. However, (as was shown in the Si_2HLi sub-chapter) experimental results can be found for bigger molecules that contain Si or Li atoms connected to bulky groups like ^tBu . The crystallographic data of Si–Li bond distances of these structures synthesized by several research groups [163, 165] were taken as the experimental reference. These works show the range of the Si–Li distances (Li in bridged position) from 2.645 Å to 2.657 Å [163] and where Li is in a terminal position from 2.531 Å to 2.580 Å [164, 165]. Our calculated Si–Li distances are in the range of 2.3915 Å (the B3LYP method) to 2.4315 Å (CCSD(T)/AVDZ) for terminal Li atoms. The range of the Si–Li distances for the bridged Li atom is from 2.5009 Å (the B3LYP method) to 2.5951 Å (CCSD(T)/AVDZ). Thus, our calculations are in good agreement with the experimental data.

As was mentioned in the Introduction chapter the Si_2Li_2 structures calculated by Bei and Feng [30] were obtained with a too low a level of theory to allow a meaningful comparison with the results calculated here. Nevertheless, theoretical work on the Si_xLi_y structures (where $x=1-6$ and $y=1-2$) done by others can be found [42-45]. The most important is the series of articles by Rabilloud et al. [43]. These studies are mostly focused on electron affinity, charge transfer, dipole moment and Li-binding energies of the Si_xLi_y clusters rather than geometric or vibrational properties. Nevertheless the articles report the dibridged structure (SiLiLiSi) as the global minimum followed by the

dibridged planar structure (11.23 kcal/mol above the global minimum) and Li-bridged structure (29.93 kcal/mol above the global minimum) [43]. Rabilloud et al. reported the dibridged planar structure as an isomer (minimum) but our work shows that this is a transition state. The reported Si-Li bond distance (calculated at the B3LYP/6-31G(d) level of theory) of the dibridged structure is 2.53 Å and angle (LiSiLi) is 46.5° [43]. It can be seen that our calculated Si-Li bond distances agree well with the literature however, the (LiSiLi) angle (obtained by Rabilloud et al.) is around 43° too small with comparison to our calculations.

4.6 Discussions and conclusions for the Si_2HX and Si_2Li_2 systems (where X= H, Li, F and Cl) and comparison with the C_2H_2 species.

The Si–Si bond distances calculated at the CCSD(T)-F12a/VTZ-F12 level of theory will be taken as reference in the comparisons below. The multiply-bonding properties in the Si_2HX and Si_2Li_2 structures studied here (where X= H, Li, F and Cl) were obtained from NBO analyses. The NBO procedure is explained in Chapters 1.7 and 4.1.

Vinyl

There are similar bonding properties in the HHSiSi , HClSiSi and HFSiSi vinylidene-like structures. All structures have nominally doubly-bonded Si–Si bond. The shortest Si–Si bond is found in the HHSiSi structure (2.2056 Å) and the longest one in the HFSiSi structure (2.2195 Å). There is no vinylidene form in the Si_2Li_2 and Si_2HLi cases.

Trans

A triply-bonded trans structure is found in the HSiSiH , ClSiSiH and FSiSiH cases. The shortest Si–Si bond is found in the HSiSiH structure (2.1073 Å) and the longest one in the FSiSiH structure (2.1379 Å). There is no trans form for Si_2Li_2 and Si_2HLi .

The trans structure is nominally triply-bonded between the Si atoms but the bonding interaction is rather weaker than a full triple bond. This will be explained in more detail below.

Dibridged

The dibridged form occurs in all Si_2HX and Si_2Li_2 systems (where X= H, Li, F and Cl). These structures contain nominally a singly-bonded Si–Si bond. The longest Si–Si bond occurs in SiClHSi (2.2673 Å) and the shortest one in SiLiLiSi (2.1660 Å).

The Si–Si bond in the dibridged structure actually has between singly- and doubly-bonding character as the bonding interaction is rather stronger than a full single bond. This will be explained in more detail below.

Li-bridged

Li-bridged structures occur in the Si_2HLi and Si_2Li_2 cases. Both Li-bridged forms are Si–Si doubly-bonded and the shortest Si–Si bond (2.1027 Å) occurs in HSiLiSi followed by LiSiLiSi (2.1335 Å). Additionally the Si–Si bond in the HSiLiSi structure is the shortest from all Si_2HX and Si_2Li_2 molecules (where X= H, Li, F and Cl).

H-bridged

All H-bridged structures have a doubly-bonded Si–Si. The shortest Si–Si bond occurs in the HSiHSi structure (2.1182 Å) and the longest one in the LiSiHSi structure (2.1417 Å). The H-bridged structure is found in all cases except the Si_2Li_2 species.

The Si–Si bond in the H- or Li-bridged structure has between doubly- and triply-bonding character as the bonding interaction is rather stronger than a full double bond. This will be explained in more detail below.

Bonding properties of the Si_2HX and Si_2Li_2 molecules (where X= H, Li, F and Cl)

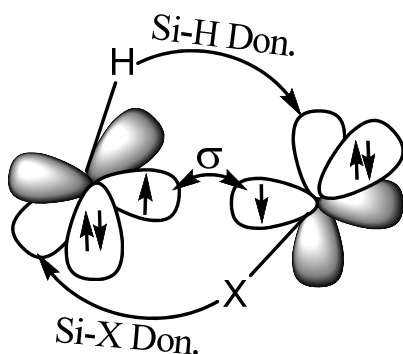
Lein et al. [14] discussed the bonding in Si_2H_2 in terms of bond formation between two SiH moieties. We will use the results of Lein et al. to help us attempt an explanation for the bonding properties of the Si_2HX and Si_2Li_2 molecules (where X= H, Li, F and Cl). The pictures shown here will be presented in a similar manner to those presented in reference [14].

In the vinyl structures we have one σ -type and one π -type Si–Si bond that create a doubly-bonded structure; the terminal Si atom has also one lone-pair. The vinyl structures found here are not significantly different from the other vinylidene-type structures found in the literature [11, 14, 168]. It is not clear why there is no vinyl form for Si_2Li_2 and Si_2HLi .

In the dibridged structures empty $p(\pi)$ orbitals interact with the Si–H/Si–X bond and with the electron lone-pair of the other Si–H/Si–X bond as shown in Figure 4.6-1. The stabilization of the bridged structure comes from the donor-acceptor interactions as

Si-H \rightarrow p(π) is stronger than the electron lone-pair \rightarrow p(π) orbital. The Si-H/Si-X bonds are also better donors than the lone-pairs as the lone-pairs are built from s type orbitals and H, Cl and F have higher electronegativities than Si [14]. Thus, in the dibridged structures the Si-H/Si-X bonds are tilted toward the empty p(π) orbitals of the other SiH/SiX moiety; this leads to the butterfly type of structure. Folding of the Si-H/Si-X bonds along the Si-Si bond is presumably reducing repulsion between the hydrogen and silicon valence s orbitals [11].

Figure 4.6-1. Qualitative model for the orbital interactions between two SiH-SiX moieties in the dibridged orientation. Si-H/Si-X Don. represents the Si-H/Si-X donor to the empty p orbital interaction; overlap of unpaired electrons yields a σ bond.



NBO analyses also showed that in the lithium substituted dibridged structures both Si lone-pairs interact strongly with the SiLiSi bridged parts. This can explain the shorter Si-Si bond distance in the lithium substituted dibridged structures than in the Cl-, F- and H-substituted dibridged structures.

In the monobridged structures a lone-pair on the second of the SiH/SiX (right-side lone-pair on both (a) and (b) in Figure 4.6-2) moieties creates a σ type bond with the empty p orbital of the first SiH/SiX moiety. Additionally we have a Si-Si π bond, as shown in Figure 4.6-2. Besides the above bonding interactions we have also the lone-pair from the first SiH/SiLi moiety (left-side lone-pair on both (a) and (b) in Figure 4.6-2) which can interact partially as a lone-pair donor to the empty p orbital of the second SiH/SiX moiety. This interaction does not create a bond but might be responsible for some bonding properties in the monobridged structures and is presented in Figure 4.6-2 as a dotted arrow. Similar interactions were seen during NBO calculations in the LiSiHSi as

well as HSiLiSi structures. The charge transfer (donor-acceptor) energy between the lone-pair of Si (as shown in Figure 4.6-2-(a)/(b)) and the antibond of SiH/SiLi is 23.7 kcal/mol (HSiLiSi), and 2.9 kcal/mol (LiSiHSi). The energy differences between H-bridged and Li-bridged shown above can be explained by the higher electronegativity of hydrogen (2.20) compared with lithium (0.98). The higher electronegativity makes the interacting Si-H and empty p orbital twist toward each other. The tilting of the empty p orbitals of the acceptor SiX moiety moves the terminal Li, Cl or F atom towards the bridging H atom. In the Li-bridged structures this tilting movement was not found because of the lower electronegativity of lithium. The lack of the twisting of the SiH/SiLi moieties in the Li-bridged structures makes the distances between the lone-pair of the SiLi moiety and the empty p orbital of the SiH/SiLi moiety and between the π bond (connecting both moieties) shorter which gives a higher interaction energy. These stronger interactions, combined with the higher electronegativity of the H moiety compared with the Li moiety (right-part of Figure 4.6-2-(b)), reduce the Si-Si bond distance in HSiLiSi and may explain why this Si-Si bond distance is the shortest from all of the Si₂HX and Si₂Li₂ structures (where X= Li, F and Cl).

In the trans structures the lone-pair (SiH/SiX) \rightarrow π (SiH/SiX) donation is enhanced by outwardly tilting the Si-H/Si-X bond which leads to the trans-bent form [14] as shown in Figure 4.6-3.

The above analyses explain why the bond lengths in the monobridged isomers are shorter or slightly longer (Si₂H₂) than in the triply-bonded trans isomers, as in the trans structures the SiH/SiX moieties are too far away to interact as strongly as in the monobridged structures.

Figure 4.6-2. Qualitative model for the orbital interactions between two SiH-SiX moieties in (a) H-bridged and (b) Li-bridged orientations. Si-H/Si-X Don. represents the Si-H/Si-X donor \rightarrow empty p orbital interaction; overlap of the unpaired electrons yields a π bond and LP Don. represents lone-pair donor to the empty p orbital interaction. Explanation of the dotted arrows can be found in the text above.

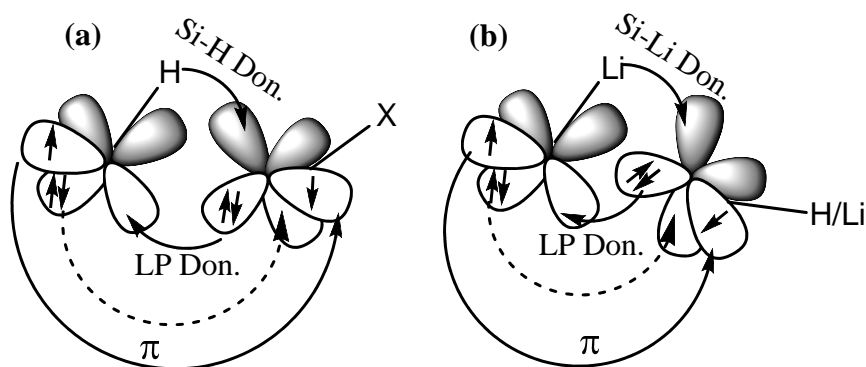
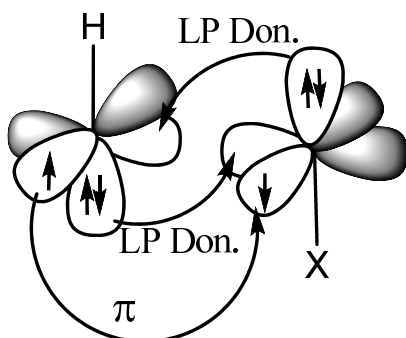


Figure 4.6-3. Qualitative model for the orbital interactions between two SiH-SiX moieties in the trans orientation. LP Don. represents the lone-pair donor to the empty p orbital interaction and the overlap of the unpaired electrons yields a π bond.



Comparison of the C_2H_2 , Si_2H_2 , Si_2HLi and Si_2Li_2 structures

The bonding differences between C_2H_2 and Si_2H_2 have been discussed in the literature before [11, 14, 168] and so we have not attempted to explain this in detail again. The bonding differences between the Si_2HX and Si_2Li_2 (where $X = H, Li, F$ and Cl) structures were discussed above. Comparison of the C_2H_2 , Si_2H_2 , Si_2HLi and Si_2Li_2 structures shows that the disilynes (Si_2H_2 , Si_2HLi and Si_2Li_2) have significantly different isomerisation properties than the C_2H_2 species: the global minimum is

dibridged (in all the disilynes) instead of a linear acetylene structure (which is the global minimum for C_2H_2), followed by the monobridged isomer (in all cases) and vinyl isomer (in the C_2H_2 and Si_2H_2 species). The trans-bent structure exists only in the Si_2H_2 case. Monobridged structures (with hydrogen or lithium as the bridged atom) occur in all cases. However, the monobridged structures in the C_2H_2 and Si_2Li_2 species lie in shallow potential energy wells on the respective potential energy surfaces. The energy differences between the transition state and monobridged structure are 0.16 kcal/mol (C_2H_2 ; CCSD(T)/AV5Z) and 0.06 kcal/mol (Si_2Li_2 ; CCSD(T)-F12a/VTZ-F12). Thus, it is unlikely that these monobridged structures can be observed experimentally.

Differences in the vibrational frequencies of the different species are also observed. In the Si_2H_2 and Si_2HLi structures the Si–H stretches have the highest frequency values (between 1500-2200 cm^{-1}), while in the Si_2Li_2 structures the Si–Si stretches have the highest frequency values (between 500-620 cm^{-1}). Most of the Si–Li vibration motions lie below 500 cm^{-1} , except the Si–Li stretches in $LiSiHSi$ (606 cm^{-1}) and $LiSiLiSi$ (617 cm^{-1}). These can be partially explained by the higher atomic mass of the Li atom than the H atom. It is not clear why the presence of the Li atom in the disilynes (Si_2HLi and Si_2Li_2) decreases the number of isomers found and we have not attempted to explain this issue in detail. Nevertheless, it was noticed during our calculations that the trans and vinyl structures occurred only as higher-order transition states on the Si_2Li_2 and Si_2HLi potential energy surfaces.

The comparisons of the different level of theories used to study the Si_2HX and Si_2Li_2 species (where X= H, Li, F and Cl) calculations tell us that diffuse function are not essential when we used the level CCSD(T)/VQZ and above. Moreover, the results calculated at the CCSD(T)/AV(Q+d)Z level with the additional thigh d functions were shown to be very close to the CBS limit. The CCSD(T)/VDZ and B3LYP/6-311G(d) levels of theory are in some cases not accurate enough to describe the isomerization energies, geometric properties or harmonic vibrations. Note, that the B3LYP/6-311G(d) level does not contains polarization functions for the H atom which might give wrong results for the bridged structures. The CCSD(T)-F12/VTZ-F12 level of theory yielded an accuracy comparable to CCSD(T)/V(6+d)Z for geometric properties and to

CCSD(T)/V(Q+d)Z for harmonic vibration frequencies as shown in chapter 4.1. Thus, I recommend this level of theory as the most accurate in calculations of small silicon clusters. The CCSD(T)-F12/VTZ-F12 level of theory will be used in subsequent full-dimensional potential energy surface calculations.

5 Electron affinity and Li⁺ and H⁺ binding energy.

5.1 Electron affinity.

The electron affinity is a very important physical-chemical property used, for instance, in thermochemical cycles to determine molecular bond energy or electron detachment energy which can be used in the advanced electronics industry. Electron affinity also plays a role in silicon and quantum dot (nanocrystal) semiconductor chemistry [169], molecular clusters [170] and flat panel displays [171].

In general electron affinity can be described as the energy difference between an uncharged atomic or molecular species and its negative ion [172]. A clear definition of electron affinity was provided in review work by Hotop and Lineberger [173, 174]: “The electron affinity, EA, of an atom A is the difference between the total energies (E_{tot}) of the ground state of A and its negative ion A^- ” and is expressed by the equation:

$$EA(A) = E_{\text{tot}}(A) - E_{\text{tot}}(A^-). \quad 5.1-1$$

Thus, for example, when the neutral atom lies energetically above the anion then electron affinity is positive [172]. Anions of atoms with positive electron affinities exist long enough to be studied experimentally, whereas anions of atoms with negative electron affinities exist only for a few picoseconds and so, are of less interest to chemists [172]. The electron affinity usually depends on the nuclear charge, electronic configuration and size of the atom.

Atomic and molecular electron affinities can also be described as the binding energy of an electron to the atom or molecule [172]. Molecular systems (and atoms) can have positive as well as negative electron affinities. For instance, benzene has a negative electron affinity, whereas anthracene and pyrene have positive electron affinities [172]. Interestingly, diamond and diamond-like carbon materials have a negative electron affinity and thus, can be used as electron field emitters [175, 176].

To measure molecular or atomic electron affinities experimentally photo-detachment spectroscopy is used. This technique uses the photoelectric effect and gives electron

affinity results with an accuracy of around 0.25 kcal/mol [172]. However, sometimes it is hard to find the electron affinity using experimental methods, and then computational methods can be very helpful.

Several levels of theory were proposed in the literature for the calculation of electron affinities. The first method used to get electron affinities with good accuracy is the Gaussian-2 (G2) method [177]. G2 theory is a technique which consists of a sequence of well-defined *ab initio* calculations to obtain a total energy of a given molecular species [178]. Geometries are optimized using second-order Møller–Plesset perturbation theory. For the energy, correlation level calculations are done using Møller–Plesset perturbation theory up to fourth-order and with quadratic configuration interaction. The G2 method uses large basis sets, including multiple sets of polarization functions in the correlation calculations.

Other authors suggest that *ab initio* methods such as CI and CC are the best tool for the calculation of electron affinities [172, 179]. However, to obtain good accuracy, one needs to use basis sets that are close to the CBS limit.

Pople and co-workers presented a comparison between electron affinities calculated with the G2 method and several DFT methods [177]. The paper shows that DFT methods are quite good in comparison with the G2 level, which is still the most accurate, but also computationally more expensive. Schaefer considers the DFT methods as efficient for the calculation of electron affinities, as they are fast and still yield good accuracy [172]. Jensen compared four methods for calculation of electron affinities: HF, BHHLYP, B3LYP and BLYP with the aug-pc-2 basis set (though similar results can be obtained using the 6-311+G(d) basis set) [180]. Jensen claims that B3LYP gives an accuracy with comparison to experimental values of ≈ 1 kcal/mol.

To choose the most effective method and basis set, benchmark tests were performed on the Si–Si molecule and the Li atom, and the results were compared with experimental electron affinities. The following three methods were used: MP2/aug-cc-pVTZ, M06-2X/6-311+G(d) and B3LYP/6-311+G(d). Unrestricted reference wavefunctions were used in all calculations done here. We also used the MP2/aug-cc-pVDZ and MP2/aug-cc-pVQZ methods. However, we encountered convergence difficulties during the

optimization calculations, and this issue will be discussed later. All calculations were performed with the Gaussian 09 program [139].

The adiabatic EA is defined as:

$$EA = E(\text{optimized neutral system}) - E(\text{optimized anion system}) \quad 5.1-2$$

In both types of calculations (except those on the Li atom) the zero point energy (ZPE) was included.

Table 5.1-1. Electron affinity of the Si₂ molecule.

	MP2/ AVTZ	B3LYP/ 6-311+G(d)	M06-2X/ 6-311+G(d)	Exp. ^a	Exp. ^b
EA [eV]	2.27	2.16	2.15	2.199(0.012)	2.176(0.002)
^a value taken from reference [181]					
^b value taken from reference [182]					

Table 5.1-2. Electron affinity of the Li atom.

	MP2/ AVTZ	B3LYP/ 6-311+G(d)	M062X/ 6-311+G(d)	Exp. ^a
EA [eV]	0.35	0.56	0.52	0.62
^a value taken from reference [172]				

The B3LYP/6-311+G(d) level of theory gives electron affinities that are closest to the experimental values for the Si₂ and Li species. The difference between the calculated and experimental values is only 0.039 eV or 0.016 eV (for Si₂) and 0.06 eV (for Li). M06-2X/6-311+G(d) gives slightly worse results with the differences between the calculated and experimental results being around 0.049 or 0.026 eV (for Si₂) and 0.10 eV (for Li). The MP2/aug-cc-pVTZ results are worse than the DFT results: the differences between the experimental and computational results are 0.071 or 0.094 eV (for the Si₂ molecule) and 0.27 eV (for the Li atom). The calculated B3LYP/6-311+G(d) Li electron affinity showed a difference of 0.002 eV compared with the result obtained by Jensen at the B3LYP/aug-pc-2 level of theory [180]. However, the MP2/aug-cc-pVTZ and M06-2X/6-311+G(d) levels of theory give differences of 0.21 eV and 0.037 eV, respectively.

Electron affinities of the Si₂HLi isomers

To calculate the electron affinities for the Si₂HLi minima the same methods were used as in the previous section.

Table 5.1-3. Electron affinities of the Si₂HLi isomers.

	MP2/ AVTZ	B3LYP/ 6-311+G(d)	M06-2X/ 6-311+G(d)
HSiLiSi			
EA [eV]	0.59	1.01	0.88
LiSiHSi			
EA [eV]	0.64	1.05	0.90
SiHLiSi			
EA [eV]	0.66	0.74	0.58

If we consider only the DFT methods, we can see that the two monobridged structures, HSiLiSi and LiSiHSi, have electron affinities of ≈ 0.9 -1.0 eV, whereas the SiHLiSi electron affinity is smaller (≈ 0.58 -0.74 eV). It was noticed during the DFT calculations (B3LYP/6-311+G(d) and M06-2X/6-311+G(d)) that electron attachment changed the nature of the global minimum. The global minimum of the Si₂HLi⁻ species is the Li-bridged structure followed by the dibridged (relative energies of 3.07 kcal/mol and 0.55 kcal/mol for B3LYP and M06-2X, respectively) and H-bridged (3.62 kcal/mol and 2.85 kcal/mol, respectively) structures, respectively. The MP2 method shows a different pattern: the HSiLiSi structure has a smaller electron affinity in comparison with LiSiHSi and SiHLiSi. The electron affinities computed with MP2 have very similar magnitudes for all three isomers.

We investigated this issue in more detail. The investigation showed that the MP2/aug-cc-pVXZ calculations (where X=2-4) fail for the anionic HSiLiSi structure. The MP2/aug-cc-pVDZ and MP2/aug-cc-pVTZ calculations optimized to different local minima and the optimization calculation at the MP2/aug-cc-pVQZ level was not successful (calculations crashed several times). The SiSiH angle in the anionic structure optimized at the MP2/AVDZ level is 180° (linear), whereas the MP2/AVTZ level gives a SiSiH angle of 139° (bent). It was seen in chapter 4 that the AVDZ basis set is not

accurate enough for obtaining reliable geometric properties, and thus, only the MP2/AVTZ results are listed in Table 5.1-3. It was also noticed, that calculations at the MP2/AVDZ and MP2/AVQZ levels suffered from convergence problems. Trying to overcome this issue, we calculated the force constants at the start of the geometry optimization, used tight convergence criteria and different optimization algorithms (Newton-Raphson, GDIIS and quadratic convergent SCF). HF/aug-cc-pVXZ (where X= 2 and 4) with the stable=opt keyword was used to ensure that the calculated structure was a minimum. Additionally an initial guess was read using the Guess=Read keyword at the start of the MP2/aug-cc-pVXZ calculation (where X= 2 and 4) in an effort to determine a real minimum. All the endeavours failed.

To avoid further convergence problems we decided to just use the B3LYP method for the electron affinity calculations for Si_2Li_2 , as this method gave results that were closest to the experimental values (for Si_2 and Li).

Electron affinities of the Si_2Li_2 isomers

In sub-chapter (4.5) it was mentioned that the Si_2Li_2 PES contains two minima: a dibridged isomer (SiLiLiSi), which is the global minimum and a monobridged isomer (LiSiLiSi) which lies 0.43 eV (10.037 kcal/mol) above the global minimum.

Table 5.1-4. Electron affinities of the Si_2Li_2 isomers.

	B3LYP/ 6-311+G(d)
LiSiLiSi	
eV	0.98
SiLiLiSi	
eV	0.70

The calculated EA values show a similar pattern as for the Si_2HLi isomers: the electron affinity for the monobridged structure (LiSiLiSi) is much larger than that of the dibridged structure (SiLiLiSi): 0.98 eV and 0.70 eV, respectively. The attachment of an electron does not change the nature of the global minimum for the Si_2Li_2 species.

Discussion – comparison of calculated values with literature and conclusions

There are a number of previous papers on electron affinities, which can be used for comparison. The work of Schaefer et al. [183] on the $\text{Si}_2\text{H}/\text{Si}_2\text{H}^-$ structures used many different computational methods, however, we only take the CCSD(T)/AVTZ results as the most relevant to our studies. The Si_2H electron affinity computed with the CCSD(T)/AVTZ level is 2.30 eV which is very close to the experimental value (2.31 eV) [183]. Note that the calculated electron affinities for the Si_2HLi isomers are about 1 eV smaller. The same issue holds for Si_2Li_2 . Yang and co-workers [45] calculated the electron affinity for Si_nLi molecules (where $n=2-8$) using G3 and MP2(full)/6-31G(d). The calculated electron affinity of the Si_2Li is 1.87 eV and 1.88 eV for G3 and MP2(full)/6-31G(d), respectively. Our calculated electron affinity for Si_2Li_2 is between 0.70 eV and 0.98 eV. It is not clear why the electron affinities calculated here are around 1 eV smaller than those computed for Si_2H and Si_2Li . Clearly, for the Si_2H^- and Si_2Li^- systems the detachment of an electron requires more energy than for the Si_2HLi^- and Si_2Li_2^- systems. We have not attempted to explain this in detail.

We can conclude that the B3LYP/6-311+G(d) method gives the most accurate electron affinity results of all the methods employed here in comparison to experimental and high-quality literature results. It is probably possible to get more accurate electron affinity results than those obtained with B3LYP/6-311+G(d) by using the G2 or G3 methods, however, these methods are more demanding of CPU time.

5.2 Li⁺ binding energy.

The mechanism of lithium storage in silicon type materials has been studied for many years as these materials are important in developing high-density Li rechargeable batteries. Li⁺ can be adsorbed on, or inserted into, different types of layered Si structures or Si surfaces. Our calculations on small Si-containing molecules can provide new insight into the Li⁺ binding. The Li⁺ binding energy can be defined as:

$$E_b = - [E(\text{Si}_2\text{HLi}) - E(\text{Si}_2\text{H}^-) - E(\text{Li}^+)]. \quad 5.2-1$$

The Li⁺ binding energy in the Si₂HLi structures was calculated as shown in eq. 5.2-1. The Si₂HLi and Si₂H⁻ structures were optimized and the ZPEs were included. The geometry optimisation of Si₂H⁻ yielded bent and bridged structures. The calculations were performed at the CCSD(T)/aug-cc-pVTZ and B3LYP/6-311+G(d) levels of theory but counterpoise corrections were not included here. The unrestricted reference wavefunctions were used for the ionic species. The computed Li⁺ binding energies for the Si₂HLi structures are listed in Table 5.2-1.

Table 5.2-1. Li⁺ binding energies of the Si₂HLi isomers.

	CCSD(T)/ AVTZ	B3LYP/ 6-311+G(d)
HSiLiSi		
eV	2.54	2.68
LiSiHSi		
eV	2.03	1.79
SiHLiSi		
eV	2.39	2.15

Table 5.2-1 shows that the Li⁺ binding energy is larger for the HSiLiSi and SiHLiSi isomers (Li-as the bridged atom) than for the LiSiHSi isomer (Li-as the terminal atom). The B3LYP/6-311+G(d) method gives Li⁺ binding energies of 2.68 eV, 2.15 eV and 1.79 eV for HSiLiSi, LiSiHSi and SiHLiSi, respectively, whereas the CCSD(T)/aug-cc-pVTZ level of theory gives binding energies of 2.54 eV, 2.39 eV and 2.03 eV, respectively.

Note that the Li⁺ binding energies were not corrected for BSSE. BSSE tends to be very small in DFT calculations. CCSD(T) is however much more sensitive to BSSE, and whereas we use a relatively large basis set in the CCSD(T) calculations (aug-cc-pVTZ), the BSSE may still be sufficiently large to affect the Li⁺ binding energies. For comparison, CCSD(T)/cc-pVTZ calculations on N₂ yielded a BSSE value of about 0.08 eV [184], of similar magnitude as the differences between the B3LYP and CCSD(T) Li⁺ binding energies. Thus, it may be that the CCSD(T) binding energies are slightly overestimated.

The calculations of the Li⁺ binding energy were done for the Si₂Li₂ structures using the same levels of theory as employed for Si₂HLi. The Si₂Li₂ and Si₂Li⁻ structures were optimized and the ZPEs were included but the counterpoise corrections were not included. Equation 5.2-2 was used to calculate the Li⁺ binding energies of the Si₂Li₂ structures. To avoid optimization of Si₂Li⁻ towards the bridged (SiLiSi⁻) structure, which is unwanted for the bridged Li binding energy of the LiSiLiSi isomer, the terminal Li angle (LiSiSi-bent) was frozen (at 165.0°). The calculated Li⁺ binding energy results are listed in Table 5.2-2.

$$E_b = - [E(\text{Si}_2\text{Li}_2) - E(\text{Si}_2\text{Li}^-) - E(\text{Li}^+)] \quad 5.2-2$$

Table 5.2-2. Li⁺ binding energy of the Si₂Li₂ isomers

	CCSD(T)/ AVTZ	B3LYP/ 6-311+G(d)
LiSiLiSi ^a		
eV	2.31	1.48
LiSiLiSi ^b		
eV	1.62	0.84
SiLiLiSi		
eV	2.05	1.24
^a Li ⁺ - SiLiSi-bridged		
^b Li ⁺ - LiSiSi-bent		

The same pattern can be seen as was observed for Si₂HLi: the B3LYP/6-311+G(d) method yields larger binding energies for the LiSiLiSi and SiLiLiSi isomers (SiLiSi-

bridged) than the LiSiLiSi isomer (LiSiSi-bent), 1.48 eV, 1.24 eV and 0.84 eV, respectively. The CCSD(T)/aug-cc-pVTZ method gives binding energies of 2.31 eV, 2.05 eV and 1.62 eV, respectively. Thus, the B3LYP/6-311+G(d) results are smaller than the CCSD(T)/aug-cc-pVTZ results by about 0.72-0.83 eV. It therefore appears that B3LYP underestimates the Li^+ binding energies.

5.3 H⁺ binding energy.

The H⁺ binding energy was also investigated for the Si₂HLi isomers. The equation to calculate the H⁺ binding energy is similar to that for the Li⁺ binding energy and can be written as shown in equation 5.3-1.

$$E_b = - [E(\text{Si}_2\text{HLi}) - E(\text{Si}_2\text{Li}^-)] \quad 5.3-1$$

Obviously there is no H⁺ in this equation because the electronic energy of H⁺ is 0. The Si₂HLi and Si₂Li⁻ structures were optimized and the ZPEs were included. The geometry optimisation of Si₂Li⁻ yielded a bent and bridged structures similar to the Si₂H⁻ case. The calculated H⁺ binding energy results are listed in Table 5.3-1.

Table 5.3-1. H⁺ binding energy of the Si₂HLi isomers

	CCSD(T)/ AVTZ	B3LYP/ 6-311+G(d)
LiSiHSi		
eV	12.48	15.35
HSiLiSi		
eV	11.60	14.49
SiHLiSi		
eV	11.96	14.86

It can be seen that there is a large difference between the CCSD(T)/aug-cc-pVTZ and B3LYP/6-311+G(d) results (about 3 eV), but once again the pattern is the same as for the Si₂HLi and Si₂Li₂ isomers: the H⁺ binding energy is larger for the LiSiHSi and SiHLiSi isomers (H-as the bridged atom), than for the HSiLiSi isomers (H-as the terminal atom). It therefore appears that B3LYP *overestimates* the proton affinities.

5.4 Comparison of calculated values with literature and conclusions

The smaller binding energy for terminal atoms (in LiSiHSi , LiSiLiSi and HSiLiSi) can be explained by the weaker connection between the Si and X atoms (where $\text{X}=\text{Li}$ or H) as compared to the bridged structures for which the stabilization energy of the SiXSi 3-centre-2-electron bond is larger. Furthermore, two bonds need to be broken to detach a bridged atom instead of one for the terminal atom. Nevertheless, it is not clear why the binding energy of the monobridged structures is larger (by about 0.25–0.50 eV) than that of the dibridged structure. Note, that we tried to calculate the Li^+ and H^+ binding energies using a larger basis set (aug-cc-pVQZ) for the CCSD(T) method but we encountered convergence problems during the Si_2H^- and Si_2Li^- optimization calculations which could not be solved.

The calculated Li^+ binding energy is similar in magnitude to those of typical Li substituted hydrocarbon structures reported in the literature [185, 186]. Unfortunately, there are no experimental or calculated results for the Li^+ binding energy for Si structures but there are some for carbon structures. For example, Yang and co-workers [186] have done experimental and theoretical work on lithium complexes of polycyclic aromatic hydrocarbons. They used ZEKE (zero-electron-kinetic-energy) spectroscopy [186] and the B3LYP/6-311+G(d,p) method. They obtained Li^+ binding energies of 1.7 eV (experimental) and 1.59 eV (computational) for the Li-naphthalene species and 2.16 eV (experimental) and 1.93 eV (calculated) for the Li-perylene species. Decouzon et al. [187] used the B3LYP/6-311+G(3df,2dp) level of theory to calculate the Li^+ binding energy for alkylo-benzene derivatives. The calculated Li^+ binding energies are in the 1.8–1.9 eV range.

Kramer and van Santen [188] showed that the H^+ binding energy for zeolite structures ranges between 14.63–12.49 eV [188]. Iton and co-workers [189] used the G1 and G2 methods to calculate the H^+ binding energy of Si-H for H_3SiO^- and $\text{H}_3\text{SiO}_3\text{H}$, and calculated values of 15.44 eV and 7.7 eV, respectively. Our calculated values (for Si-H) are about 12 eV for CCSD(T)/aug-cc-pVTZ and about 15 eV for B3LYP/6-311+G(d).

We can conclude that calculated H^+ and Li^+ binding energy results obtained by the CCSD(T)/AVTZ level of theory give reasonable values which are in good agreement with those in the literature. The B3LYP/6-311+G(d) method in some cases *underestimates* or *overestimates* the H^+ and Li^+ binding energy. Thus, B3LYP is not reliable for calculating the H^+ and Li^+ binding energy in small silicon clusters.

6 SiGeHLi

6.1 The SiGeHLi isomers.

The next element below silicon in group 14 of the periodic table is germanium. The Ge_2H_2 structures were studied extensively in the 1990's by Schaefer and co-workers [168, 190, 191]. Their work shows that germanium compounds (such as Ge_2H_2) possess similar properties as the corresponding Si_2H_2 structures. We are interested in Si–Ge compounds as the superlattices are quite important in the atomically controlled semiconductor hetero-structures [192]. In particular we consider SiGeHLi.

Computational methods

The Si_2H_2 structures optimized by Grev and Schaefer [24] were used as starting structures for the geometry optimizations. One Si atom was substituted by a Ge atom and one H atom by a Li atom. Average literature (theoretical) values of the Si–Li and Si–Ge bond distances were used in the starting geometries.

Nine starting geometries were prepared: two H-bridged structures (where the Li atom is terminal to the Ge or Si atom), two Li-bridged structures (where the H atom is terminal to the Ge or Si atom), two vinyl structures (where the Li and H atoms are both connected to the Ge or the Si atom and the H atom is connected to the other atom), two trans structures (where the Li atom is connected to the Ge or the Si atom) and one dibridged structure. These structures were optimized at the B3LYP/6-311+G(d) level of theory. Harmonic vibrational frequencies were computed from the optimized structures at the B3LYP/6-311+G(d) level, which were verified as minima or transition states by the absence or presence of imaginary vibrational frequencies. It is known from Chapter 4 that the B3LYP/6-311+G(d) level of theory can give imprecise geometric and energetic properties and vibrational frequencies. However, this method is fast and accurate enough to perform the preliminary calculations. A higher level of theory will be employed in the future if necessary.

We located a dibridged, two Li-bridged and one H-bridged structure (see Figure 6.1-1). The energies relative to the dibridged structure (the global minimum) are listed at the

bottom of Figure 6.1-1. The calculated geometric properties of the SiGeHLi structures are given in Table 6.1-1.

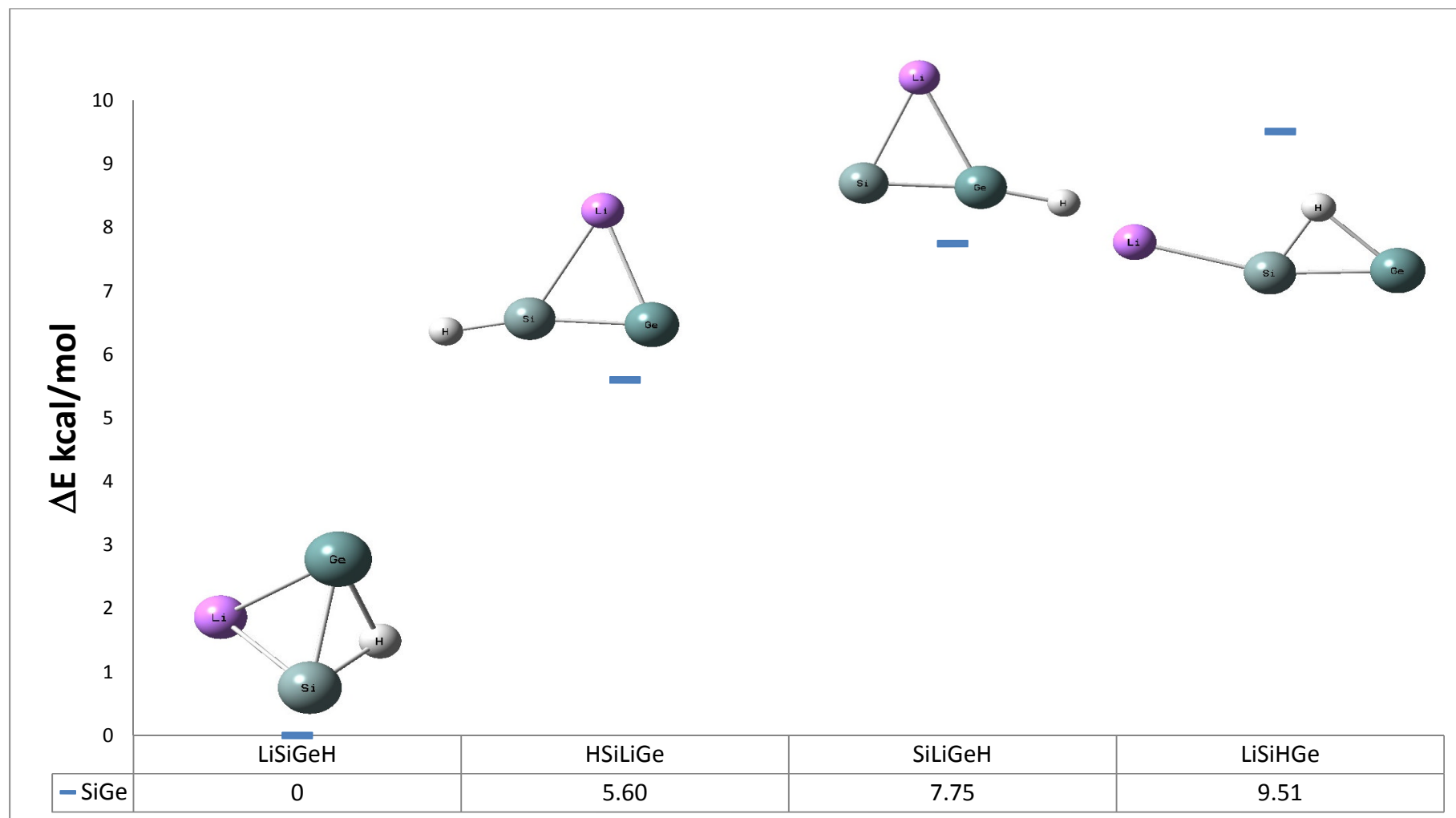
The HSiLiGe, SiLiGeH, LiSiHGe and LiSiGeH formulae refer to, respectively, the Li-bridged_1, Li-bridged_2, H-bridged and dibridged isomers, respectively.

The dibridged form has the lowest energy followed by the Li-bridged_1 form with $\Delta E = 5.60$ kcal/mol, then the Li-bridged_2 form with $\Delta E = 7.75$ kcal/mol and the H-bridged form with $\Delta E = 9.51$ kcal/mol. The geometric properties calculated at the B3LYP/6-311+G(d) level of theory are listed in Table 6.1-1.

Table 6.1-1. Geometric properties of the SiGeHLi isomers at the B3LYP/6-311+G(d) level of theory.

	B3LYP/6-311+G(d)		
	LiSiGeH	HSiLiGe	LiSiHGe
SiLi a	2.58	2.62	2.41
SiGe a	2.24	2.14	2.20
HSi a	1.66	1.49	1.62
b HSiGeLi b	75.9	180.0	0.0
a SiGeLi b	67.0	64.4	163.0
a SiGeH b	47.0	166.3	45.9
SiLiGeH			
SiLi a	2.52		
SiGe a	2.13		
HGe a	1.55		
b HSiGeLi b	180.0		
a SiGeLi b	69.3		
a SiGeH b	169.8		
^a Ångström			
^b degrees			

Figure 6.1-1. The SiGeHLi isomers located by B3LYP/6-311+G(d) with energies relative to the global minimum (dibridged).



It can be seen that the shortest Si–Ge bond length occurs in the SiLiGeH structure (2.13 Å) followed by the HSiLiGe structure (2.14 Å), the LiSiHGe structure (2.20 Å) and the LiSiGeH structure (2.24 Å). The two Li–bridged structures differ in the connection of the H atom. It is interesting, that simple geometric difference significantly affect the isomerization energy significantly. This should be investigated in more detail.

The results show that the Si–Li distances vary from 2.41 Å (LiSiHGe) to 2.62 Å (HSiLiGe). The shortest Ge–H bond distance is found in the SiLiGeH structure (1.55 Å). The smallest Si–H bond distance is found in the HSiLiGe structure (1.49 Å) followed by the LiSiHGe structure (1.62 Å) and the LiSiGeH isomers (1.66 Å). All of the isomers except SiLiHGe are planar.

Harmonic vibrational frequencies were calculated at the B3LYP/6-311+G(d) level. The results are listed in Table 6.1-2 below.

Table 6.1-2. Calculated harmonic frequencies for the SiGeHLi isomers at B3LYP/6-311+G(d) level of theory; the results are listed in descending order in wavenumber (cm^{-1}) units.

	B3LYP/ 6-311+G(d)	
<u>dibridged</u>		
	1492.9	SiH sym. str.
	947.0	SiH antisym. str.
	453.7	GeSi/SiH/SiLi str.
	389.9	SiLi/SiH str.
	196.4	butterfly
	150.2	SiLi/GeLi out of phase str./butterfly
<u>Li bridged_1</u>		
	2142.0	SiH str.
	521.7	GeSi/SiH in-phase str.
	401.4	SiLi str.
	275.9	H in-plane bend
	203.6	SiHLi bend
	105.9	out-of-plane
<u>Li bridged_2</u>		
	2074.8	GeH str.
	515.8	HGeSi bend/GeSi str.
	404.6	SiLi str.
	354.8	H in-plane bend
	229.7	out-of-plane
	205.0	GeHLi bend
<u>H bridged</u>		
	1592.2	SiH sym. str.
	820.7	SiH antisym. str.
	554.8	GeSi/SiLi/SiH str.
	382.7	SiH/SiLi str.
	78.7	SiHLi bend
	58.3	out-of-plane

Comparison of calculated values with literature and conclusion

To the best of our knowledge no literature results (spectroscopic or theoretical) exist for the SiGeHLi species. However, data for similar molecules, such as Ge₂H₂ or SiGeH₆ exist in the literature [190, 191]. The most relevant work done by Leszczynski et al. [190] was taken as reference. The work of Leszczynski et al. contains both theoretical and experimental results (using microwave spectroscopy) of the SiGeH₆ structure. The Si–Ge, Si–H and Ge–H bond distances calculated at the CCSD(T)/TZP level of theory are 2.385 Å, 1.478 Å and 1.531 Å, respectively, whereas the experimental bond distances are 2.358(3) Å, 1.494(6) Å and 1.538(3) Å, respectively. The Si–Ge bond distances calculated in this chapter for SiGeLiH isomers range from 2.13 Å to 2.24 Å. While the Si–H and Ge–H bond distances are; 1.49 Å and 1.55 Å, respectively. We used only the bond distances of terminal H atoms in this comparison, as the bond distances for bridged atoms are generally longer. It can be seen that our calculated results are in good agreement with the literature values.

A comparison of the Si₂HLi and SiGeHLi structures shows significant geometric and energetic similarities: the global minimum is the dibridged structure followed by the Li-bridged and H-bridged structures in the two (Si₂HLi and SiGeHLi) species. A comparison of the B3LYP/6-311+G(d) results for the Si–Li bond distances and the XSiLi and XSiH (where X=Si or Ge) angles in the two (Si₂HLi and SiGeHLi) species shows significant similarities too. The harmonic frequency values for the Si–H stretch in the two species are also similar. However, in the SiGeHLi species the harmonic frequency values are generally lower which may be explained by weaker bonding in the Ge containing compound and because of the higher mass of Ge. The bonding properties of the SiGeHLi structures are similar to the Si₂HLi structures and these are explained in the conclusions section at the end of Chapter 4.

7 Si_2Li_2 beyond the critical points – constructing and fitting the potential energy surface.

7.1 Theoretical introduction.

The potential energy surface (PES) is a concept that uses the Born–Oppenheimer approximation to represent the relationship between the energy of a molecule and its geometry [110]. In the Born–Oppenheimer approximation the solution of the nuclear Schrödinger equation can be presented as movement of the nuclei on the potential energy surface. Also the PES is independent of the nuclear masses [55].

The “ball and spring model” is used in the following discussion. If we start to stretch or compress the spring (bond) of our model then the potential energy will increase and this behaviour can be plotted as a curve as shown in Figure 7.1-1. There is no distortion of the bond length at the q_e point, which is the equilibrium bond length. Real molecules behave similarly to the ball and spring model; however, they constantly vibrate even at 0 K. As a result of this a molecule never stays at the bottom of the curve, but rather occupies one of the vibrational levels [110] as shown in Figure 7.1-1. Near the equilibrium bond length (q_e), the bottom of the curve is described well by a quadratic equation (corresponding to a simple harmonic oscillator). However, when we move away from q_e the potential energy deviates from the quadratic curve due to anharmonicity [110].

Figure 7.1-1. Model of a potential energy surface. The horizontal lines represent the vibrational levels. More detailed explanation of the figure can be found in the text.

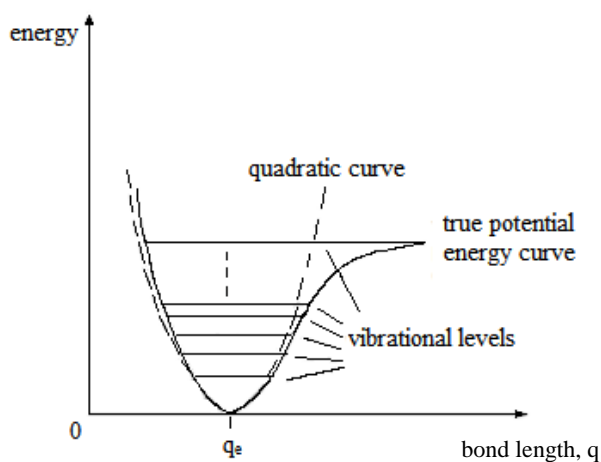


Figure 7.1-1 shows a curved (one-dimensional) representation of a PES suitable for a diatomic molecule. However, if the molecule is constructed from more than two atoms then additional dimensions appear. For example a triatomic molecule has three geometric parameters; two bond lengths (q_1 and q_2) and one angle (q_3). Thus, a triatomic PES is a 3-D “surface” and is called a potential energy hypersurface. An n -dimensional hypersurface can be defined as $E=f(q_1, q_2, \dots, q_i)$, where f is the function that describes how the energy varies with q_i [110].

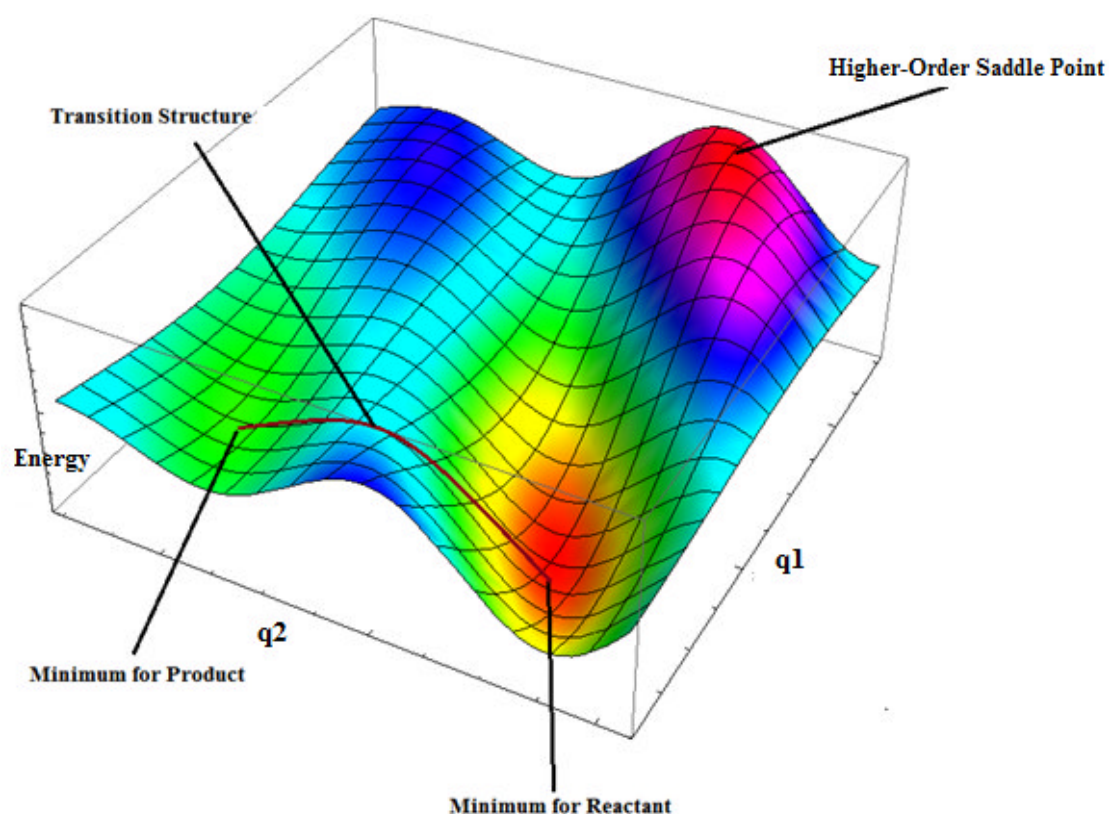
If the first derivatives (gradient) of a point on the potential energy surface is zero then this point is a stationary point. A stationary point can be described as a point where a marble placed on the surface would remain balanced. A stationary point can be described mathematically as shown in eq. 7.1-1.

$$\frac{\partial E}{\partial q_1} = \frac{\partial E}{\partial q_2} = \dots = 0 \quad 7.1-1$$

Consider a 2-D hypersurface (two geometric parameters q_1 and q_2) of a reaction including one reactant and one product as depicted in Figure 7.1-2. This visualisation of the PES can be helpful to describe various types of stationary points. Locally the lowest-energy points of the surface are energy minima and any small changes of one of the geometric parameters (q_1 or q_2) increases the energy. The global minimum (here minimum for reactants) has the lowest energy on the whole PES. The pathway connecting the two lowest energy points through a saddle-shaped surface is called a reaction path. The “centre” of the saddle-shaped region is called a transition state

(Transition Structure in Figure 7.1-2) or saddle point and is also a stationary point [110]. A minimum and transition state can be mathematically distinguished by calculating the second derivatives of the energy. A transition state has one negative second derivative, whereas for a minimum all second derivatives are positive. When more than one of the second derivatives are negative, the stationary point is called a higher-order saddle point. For example, a second-order saddle point corresponds to the maximum along two paths connecting stationary points [110].

Figure 7.1-2. 3D model of a potential energy surface generated using the Mathematica program [193] (function $V=q_1*\sin(q_1)*\cos(q_1+q_2)$).



It can be said that the essence of chemistry is the study of the stationary points on the potential energy surface and the reaction paths between them.

The concept of the chemical potential energy surface was introduced by the dissertation of Marcelin [194] before groundwork of the transition state by Eyring [195]. The first PES of the H_3^+ species was calculated by Eyring and Polanyi in 1931 [196].

Even for a simple three-atom system at least several thousand single-point calculations are needed to construct a reasonable potential energy surface. To accurately approximate the shape of a potential energy surface from the calculated points, commonly these points are fitted numerically to a multidimensional function. This function has the form of a mathematical equation, and evaluation of the equation can be used to establish any stationary points on the potential energy surface.

The easiest way to describe a simple two-body potential is by the following equation: $V = \frac{1}{2}k_2(r - r_e)^2$ where r is the internuclear distance between the two atoms, r_e is the equilibrium bond distance and k is a constant. When anharmonic motions are included the equation can be rewritten as:

$$V = \frac{1}{2}k_2(r - r_e)^2 + \frac{1}{6}k_3(r - r_e)^3 + \dots \quad 7.1-2$$

The above equation is written in the form of a Taylor series. However, to describe a real PES curve the equation needs to contain an large number of terms, thus, from a practical point of view this approach is inefficient and the Morse potential [197] is commonly used instead. Nevertheless, these approaches are true only for two-body systems, thus, other mathematical concepts are necessary to describe a many-body PES. For example: Collins et al. [198] represent the PES as a weighted sum of force fields, which are represented by Taylor series and centred at numerous reference geometries [199]. Meyer et al. [200] used an n-mode representation of the PES in their Multiconfiguration Time Dependent Hartree (MCTDH) quantum calculations [201]. A many-body PES can also be described: using the Morse-spline [202], Shepard interpolation [203], pot-fit [204] or interpolated moving least squares (IMLS) methods [205]. On the other hand, Carrington et al. [206] showed that an artificial Neural Network tool can be used to fit any function. Thus, the Neural Network concept is very useful as a potential energy surface least squares fitting tool and will be used here. A more detailed explanation can be found below.

Neural Network (NN)

The artificial Neural Network concept developed in the 90's [207, 208] has recently become very popular as it gives efficient and effective fits.

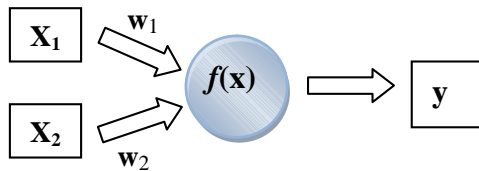
The learning ability of a brain inspired scientists to create artificial Neural Networks (ANNs) which are represented by a mathematical model.

A simple mathematical implementation can be seen in eq. 7.1-3. Figure 7.1-3 is basically a graphical representation of equation 7.1-3.

$$y(x) = f(\sum_{i=0}^n w_i x_i) \quad 7.1-3$$

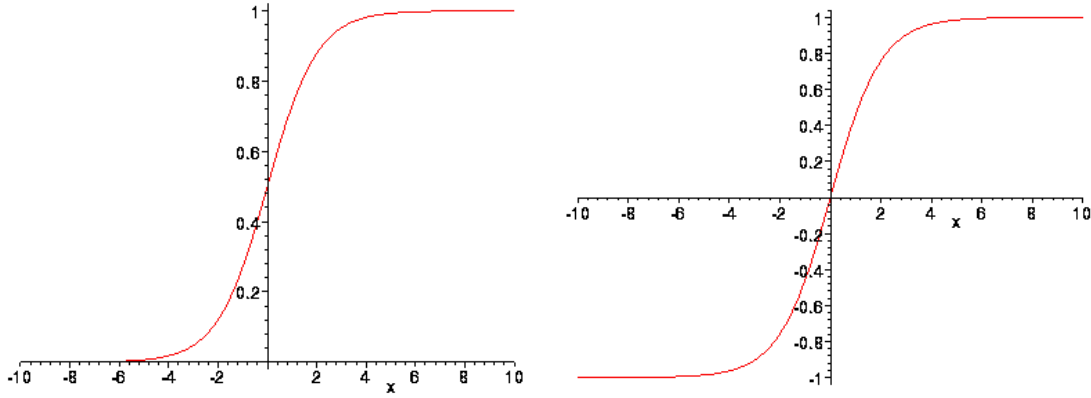
Equation 7.1-3 and Figure 7.1-3 can be explained as follows: x is a neuron with i inputs ($x_0 \dots x_i$) and one output y . The input is weighted ($w_0 \dots w_i$) and f is a transfer function that determines the output [209].

Figure 7.1-3. Simple representation of a Neural Network. The x_i represent inputs, w_i weights, y output and $f(x)$ a transfer function, respectively.



The most effective and popular transfer function is a sigmoid function. There are two types of sigmoid functions employed; *logsig* and *tansig*, which differ in their output range. The *logsig* output is in the range from 0 to 1 and *tansig* is from -1 to +1. The *logsig* function can be described mathematically as: $f(x) = \text{logsig} = \frac{1}{1 + \exp(-x)}$ and the *tansig* is represented as $f(x) = \text{tansig} = \frac{2}{1 + \exp(-2x)} - 1$. A graphical representation of the sigmoid functions can be seen in Figure 7.1-4.

Figure 7.1-4. The figure on the left represents the *logsig* function and the one on the right the *tansig* function. The figure was generated using the Mathematica program [193].



For computational purposes the feed-forward Neural Network (FNN) is commonly used. The FNN is composed of layers of neurons. The artificial neurons in the FNN are organized as layers of nonlinear “nodes”. The signal from the inputs travels only forward to the outputs. There is no feedback so the layers of the “nodes” do not affect each other [209]. For a given node each of the inputs (x_i) is weighted (w_i), then the sum of the weighted inputs and the bias (b) is passed through the transfer function (f), which produces the corresponding scalar output. The final network output is a linear combination of the node scalar outputs.

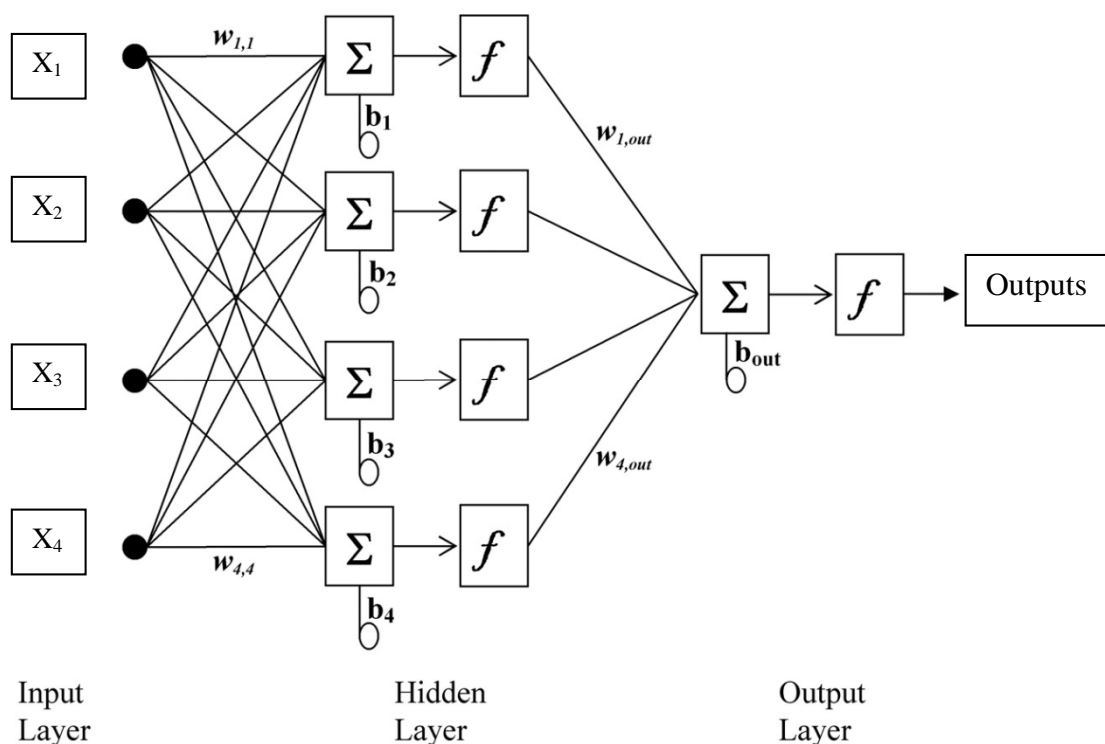
A graphical representation of the FNN can be seen in Figure 7.1-5 and the corresponding mathematical equation is including the *tansig* transfer function:

$$V(\vec{x}) = a + \sum_{p=1}^n C_p \left(\frac{2}{(1 + e^{-2(\vec{w}_p \cdot \vec{x} + b_p)})} - 1 \right). \quad 7.1-4$$

The \vec{x} is a vector representation of coordinates and \vec{w}_p is the corresponding vector of weights.

Equation 7.1-4 and Figure 7.1-5 represent the type of the Neural Network employed here.

Figure 7.1-5. Graphical representation of the feed-forward Neural Network (FNN).



In NN terminology the “ a ”, “ C_p ” and “ w_p ” are all “weights” and the “ b_p ” are biases. The x_i represent the internal coordinates of the system. The neurons are functions of linear combinations of the coordinate (input) values. The output of the FNN is a linear combination of the chosen sigmoid functions [206]. In this work the chosen sigmoid functions are *tansig*.

Carrington et al. [206] presented a series of NN least squares fits of the H_2O , $HOOH$ and H_2CO PESs with comparisons to the literature. They showed that the fits obtained by the Neural Network approach give more accurate results than fits obtained by other potential functions [206]. Eq. 7.1-4 is highly nonlinear in the parameters “ w_p ” and “ b_p ” so, Carrington et al. suggested (after several tests) the Levenberg–Marquardt (LM) algorithm [210] as the most accurate training algorithm. The same Levenberg–Marquardt training algorithm will be used here.

7.2 Potential energy surface of the Si_2Li_2 molecule.

The Si_2Li_2 molecule was chosen for extensive full-dimensional potential energy surface (PES) studies. The PES is very interesting from a dynamical point of view, as it displays shallow potential well between the monobridged minimum and the corresponding transition state. In addition, the dibridged and monobridged isomers are close in energy with a low energetic barrier for interconversion. These features could lead to interesting vibrational dynamics such as wide-amplitude vibrational motions with relatively low energies. Additionally, the molecule was experimentally studied using mass spectrometry in the 1970's [46]. The PES calculations done here could be helpful for further insightful experimental studies like microwave or infrared spectroscopy. A similar approach has been seen in the Si_2H_2 case where the critical point calculations of Grev and Schaefer [24] were used as the starting point for experimental studies of Destombes et al. [25, 26] which ended up with successful detection of two Si_2H_2 isomers.

All the single-point calculations were performed at the CCSD(T)-F12a/cc-pVTZ-F12 level of theory using the MOLPRO version 2010.1 computational package. The CCSD(T)-F12a/cc-pVTZ-F12 method will be abbreviated as F12 below. The ground state (singlet) surface only was considered. Extrapolation to the CBS limit was not attempted here; however, the discussion presented in Chapter 4.1 illustrated that the F12 method allows achieving the same level of accuracy as the CCSD(T)/cc-pV(6+d)Z level used for example in the work of Law et al. [52]. Discussion in the previous chapters for Si_2H_2 , Si_2HLi and Si_2Li_2 showed that the F12 method gives results with good agreement to experimental values and convergence with increasing basis set size is faster than for ordinary CCSD(T) calculations. Relativistic, core-valence and higher-order electron correlation corrections were not included here. The cc-pVTZ-F12 basis set contains 7s7p4d2f basis functions for each Si atom and 6s6p3d2f basis functions for each Li atom. The average time of a single-point calculation for C_1 symmetry on one node of the new EastChem computational cluster (12-core Westmere nodes - 2.93 GHz for each core) at the University of St Andrews was around 400 s.

Energies for 45501 geometries were calculated at the F12 level. 18829 points were used in the final least-squares fit. Of these 720 points were calculated on a local grid, 17387 points were generated by the diffusion Monte Carlo (DMC) method (see below) and 722 points were calculated on a wider grid. The PES includes the two known minima (dibridged and monobridged) and the two transition states (dibridged-planar and dibridged–monobridged). These critical points will be abbreviated as SiLiLiSi, LiSiLiSi, D–PL_TS and DM_TS, respectively.

The procedure for generation of the PES contains the following steps:

Initially 244 geometries were calculated near each critical point. These points were generated as displacements (as shown in Table 7.2-1) from the critical points. The bond length-bond angle coordinate system was used at this stage. 268 points from a total of 988 were excluded in the final fit as (by symmetry) they duplicated geometries. The PES is invariant to permutation of the atoms that lead to equivalent geometries and identical energies.

Table 7.2-1. Displacement steps (middle column), used in first step of sampling.

	Step	unit
SiSi	0.01	Å
SiLi	0.0225	Å
SiLi	0.0225	Å
SiSiLi	1	degrees
SiSiLi	1	degrees
LiSiSiLi	5	degrees

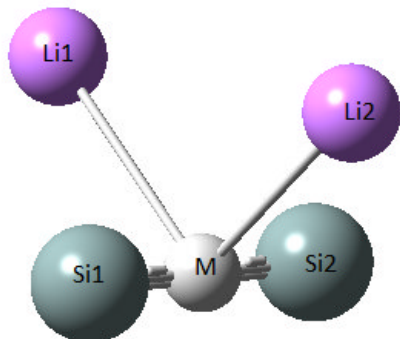
These 720 points were used to fit an initial potential energy surface. The initial PES was used to sample further geometries near each of the critical points by taking the random positions of the walkers in vibrational quantum diffusion Monte Carlo (DMC) calculations. The simple diffusion Monte Carlo method developed by Anderson [211] was employed. A key aspect of the concept is the similarity between the Schrödinger equation and the diffusion equation [211]. The diffusion Monte Carlo method involves the random movement of imaginary particles (*psi*-particles). This random walk method allows the calculation of the ground state energy of a system [211]. The distribution of

psi-particles is connected to the ground state wave-function. When a DMC calculation is repeated for example with artificially low atomic masses then the distribution of *psi*-particles will be much further from the equilibrium geometry. Separate DMC calculations at different atomic masses (4m, 2m, m, and m/4) were performed. The “m” represents the masses of ^{28}Si and ^7Li . This approach helps to sample the geometries over a wider range. Each batch of the calculated points (sampled by the DMC method) was refitted before preparation of a new batch. 17387 points were calculated at this stage. The DMC software was written by Law et al. [212].

The DMC calculations were performed using 1000 iterations with 1000 of the *psi*-particles. Initially a value of 10^{-16} s was used as the time step and then reduced to 10^{-17} s during the calculation.

The procedure of wider sampling of geometries in the final step was as follows. The fit of the 18107 points calculated at the previous sampling steps was used in an initial sampling procedure. Satellite coordinates were used at this stage, as illustrated in Figure 7.2-1. M is the centre of the mass of the two silicon atoms, Si1MLi1 and Si1MLi2 are the vector angles and ϕ is the angle between the SiSiLi1 and SiSiLi2 planes.

Figure 7.2-1. Graphical representation of the satellite coordinates. The Si_i and Li_i symbols represent silicon and lithium atoms. M is the centre of the mass of the two silicons.



Only geometries with energies predicted to be below 50000 cm^{-1} (relative to the dibridged structure) were selected for the *ab initio* calculations in both the DMC and wider grid procedure.

Two sampling grids were used as the first grid sampling approach showed huge inefficiency. The radial coordinate ranges for these sampling grids are given in Table 7.2-2. Only 900 points were useful from the first batch of 6000 points. These 900 points match our criteria: the \mathcal{T}_1 diagnostic was below 0.08 and the energy below 50000 cm^{-1} (relative to the dibridged isomer). The \mathcal{T}_1 threshold value employed (0.08) was suggested by papers of Martin et al. and Cai et al. [64, 65], who suggested that CCSD(T) gives reasonable results for \mathcal{T}_1 diagnostic values as high as 0.08. Note, that most points experienced convergence problems as they sample the surface at extreme geometries. For example the Si–Si bond length was very short or very long (below 1.5 \AA or above 3.5 \AA), the same situation was observed for the Si–Li and Li–Li distances. To overcome these problems the second coordinates range (as seen in Table 7.2-2) was implemented. A total of 27126 points were calculated for both wide grid sampling approaches. 16699 points converged and 9067 of these were below 50000 cm^{-1} . 8575 points (from a total of 27126) had a \mathcal{T}_1 diagnostic above 0.08 and 2597 of them converged. Thus, these 2597 points contain considerable multireference character.

Table 7.2-2. Coordinates sampling ranges.

	first grid	second grid
SiSi ^a	1.2 – 4.2	1.5 – 3.9
MLi1 ^a	1.45 – 3.95	1.75 – 3.5
MLi2 ^a	1.7 – 3.2	1.9 – 2.9
α SiMLi1 ^b	10 – 100	10 – 100
α SiMLi2 ^b	20 – 170	20 – 170
ϕ ^b	0 – 180	0 – 180
^a ångström		
^b degrees		

The ranges of \mathcal{T}_1 diagnostic values obtained during the PES calculations are listed in Table 7.2-3 for geometries around the four critical points considered here.

Table 7.2-3. \mathcal{T}_1 diagnostic of the Si₂Li₂ structures.

	\mathcal{T}_1 diagnostic
	Range from min to max values
SiLiLiSi	0.0163–0.0324
LiSiLiSi	0.0182–0.0412
D_PL_TS	0.0162–0.0292
DM_TS	0.0182–0.0700

The \mathcal{T}_1 diagnostic values around most of the critical points are below 0.042. However, a few points with \mathcal{T}_1 diagnostic above 0.055 were found near the DM_TS structure.

Fitting procedure

The Neural Network method, described above was used in the fitting procedure.

To construct a PES precisely, it must be invariant with respect to all permutations of identical atoms [213]. The concept of polynomial invariants developed by Bowman [213] was used here. The polynomial invariant approach is constructed from basis functions which contain the internuclear distances R_i . These functions are invariant with respect to permutations of like atoms and can be obtained in terms of primary and secondary polynomials [213]. If the atoms of the Si₂Li₂ species are labeled as Si(1),

Si(2), Li(3) and Li(4), respectively, and six internuclear distances represent the distances between these atoms (shown in

Table 7.2-4), then auxiliary variables are given as:

$$e_0 = (R_2 + R_5)/2,$$

$$e_1 = (R_1 + R_4)/2,$$

$$f_0 = (R_2 + R_4)/2,$$

$$f_1 = (R_1 + R_5)/2,$$

The degree-1 invariant polynomial can be written as:

$$P_1 = (R_5 + R_2 + R_1 + R_4)/4,$$

The three degree-2 primary invariant polynomials are given below:

$$P_2 = (e_0^2 + e_1^2)/2,$$

$$P_4 = (f_0^2 + f_1^2)/2,$$

$$P_5 = (R_3^2 + R_2^2 + R_4^2 + R_5^2)/4,$$

and degree-3 invariant polynomials:

$$P_7 = (R_1^3 + R_2^3 + R_4^3 + R_5^3)/4$$

We have also polynomials which are equal to the Si-Si and Li-Li internuclear distances.

$$P_3 = R_3,$$

$$P_6 = R_6,$$

Table 7.2-4. Internuclear distances R_1 – R_6 of the Si_2Li_2 structures.

R_i	Internuclear distances
R_1	Si(2)–Li(3)
R_2	Si(1)–Li(3)
R_3	Si(1)–Si(2)
R_4	Si(2)–Li(4)
R_5	Si(1)–Li(4)
R_6	Li(3)–Li(4)

The potential energy surface was determined using the Neural Network toolbox implemented in MATLAB 2009 [214] provided by the University of Aberdeen. The default feed forward Neural Network code (implemented in MATLAB) was modified for our purpose and can be found in Appendix. Equation 7.1-4 is the functional form

used to fit the *ab initio* points. This functional form is a sum of tan-sigmoid functions. The w_p , C_p etc. parameters were defined earlier. The x represents the vector of internal coordinates. The coordinates were automatically scaled to $(-1, +1)$ by the MATLAB program. The Cartesian coordinates (DMC), the bond length and angle coordinates (local grid) and the satellite coordinates (wider grid) were transformed firstly to the six internuclear distances then to the seven polynomial invariants. This was done by a FORTRAN subroutine program which can be found in Appendix. These polynomial invariants were used in each fitting process.

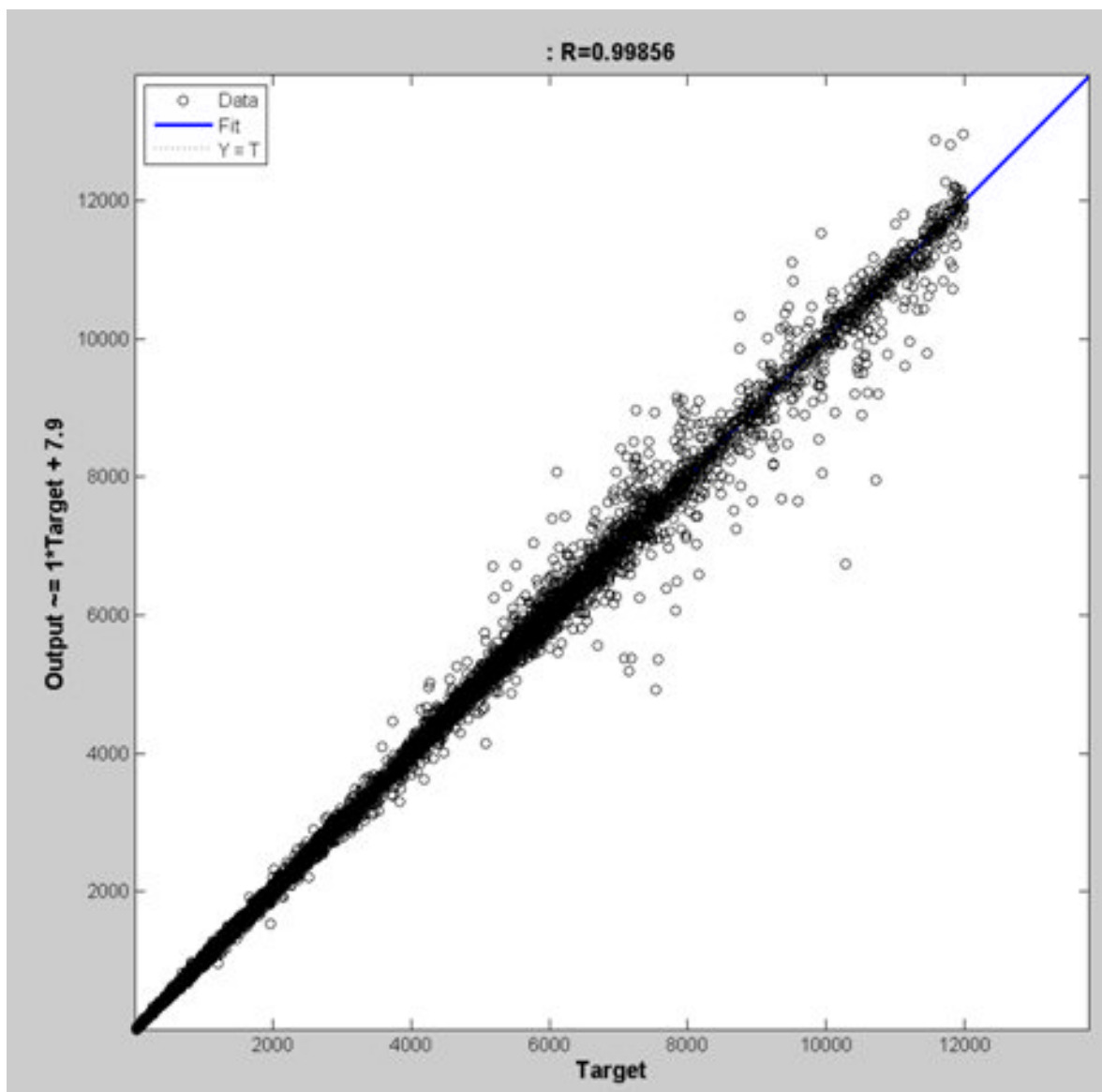
The Neural Network toolbox divided the sampled data into three subsets: a training set, a validation set and a test set. The main subset is the training set. At this stage the gradient of the performance function is computed and used for updating the network weights and biases. The validation set measures network generalization and is used to stop training when generalization is not improving. The test set provides an independent measure of training performance and has no effect on the training procedure. The points used in the fitting procedure (training, validation and test) are randomly divided in the Neural Network tool box according to the percentage of points defined for each subset. To construct the most accurate fit (according to the number of points used in each subset), benchmark tests were performed. The benchmark showed that 80% of the points used in the training, 10% in the validation and 10% in the test set, gives the most accurate and smooth fits. The influence of the number of neurons used during the training process on the accuracy of fits was also studied. It was found that 96 neurons gave the best results. In the Neural Network procedure the geometry of each point was represented by the values of the seven invariant polynomials and the energy was fitted.

Initially three fits were performed: for the points with relative energies below 50000 cm^{-1} , 35000 cm^{-1} and 30000 cm^{-1} , respectively. 27174 points were used in the 50000 cm^{-1} fit, 24530 points in the 35000 cm^{-1} fit and 23668 points in the 30000 cm^{-1} fit. Unfortunately these fits showed bad training performance as the best root mean square error achieved was 408.6 cm^{-1} . It was noticed that our wider grid sampling approach did not properly cover the surface above relative energy of 16000 cm^{-1} . Thus, we did not get enough points (on the surface above 16000 cm^{-1}) to provide a reasonable fit. Note

that 16000 cm^{-1} is the maximum energy achieved by the DMC sampling process. To overcome this issue another four fits were performed, with relative energy cut-offs at 6000 cm^{-1} , 12000 cm^{-1} , 15000 cm^{-1} and 20000 cm^{-1} , respectively. 18277 points were used in the 6000 cm^{-1} fit, 18829 points in the 12000 cm^{-1} fit, 19522 points in the 15000 cm^{-1} fit and 21055 points in the 20000 cm^{-1} fit.

The 6000 cm^{-1} fit showed the best training performance with root mean square error of 11.7 cm^{-1} . However, this fit did not cover the part of the surface which contains the vinyl and trans type geometries and these are crucial for the ro-vibrational calculations. Thus, the fit of 12000 cm^{-1} in the order of the next best performance was chosen. The 12000 cm^{-1} fit has a performance of 33.7 cm^{-1} (root mean square error). This fit covers the whole surface needed for further calculations. The NN outputs on the 12000 cm^{-1} fit are given in Figure 7.2-2. The plot includes all of the training, validation and test data sets. The root mean square error for the validation and test sets (combined) is 53.5 cm^{-1} . As expected this is larger than the corresponding value for the training set but still reasonable. It was noticed that several dozen points are outliers. Moreover, for the points in the range $0\text{--}4000\text{ cm}^{-1}$ the maximum difference (between calculated and fitted energies) is 822 cm^{-1} , for the points between $4000\text{--}8000\text{ cm}^{-1}$ the maximum difference is 2058 cm^{-1} , and for the points in range $8000\text{--}12000\text{ cm}^{-1}$ the maximum difference is 2707 cm^{-1} . However, the average absolute difference between calculated and fitted energies for the points up to 4000 cm^{-1} is 1.29 cm^{-1} and 91.65 cm^{-1} for the points between 4000 cm^{-1} and 8000 cm^{-1} . The average absolute difference for points above 8000 cm^{-1} is 322.25 cm^{-1} . The outlier points were generated by the wider grid sampling procedures, for which the sampling was quite sparse. Thus, the Neural Network toolbox had not enough points in those regions to achieve much better fitting. Nevertheless the 12000 cm^{-1} fit is sufficiently accurate to be used for reasonable vibration-rotation calculations using the WAVR4 program [215] (but see comment below about a “hole”).

Figure 7.2-2. Relationship between the outputs of the network and the targets (input energies). R is the regression value between outputs and targets. The circles represent the data. The numbers on the x and y axes are in cm^{-1} . The plot includes all of the training, validation and test data sets.



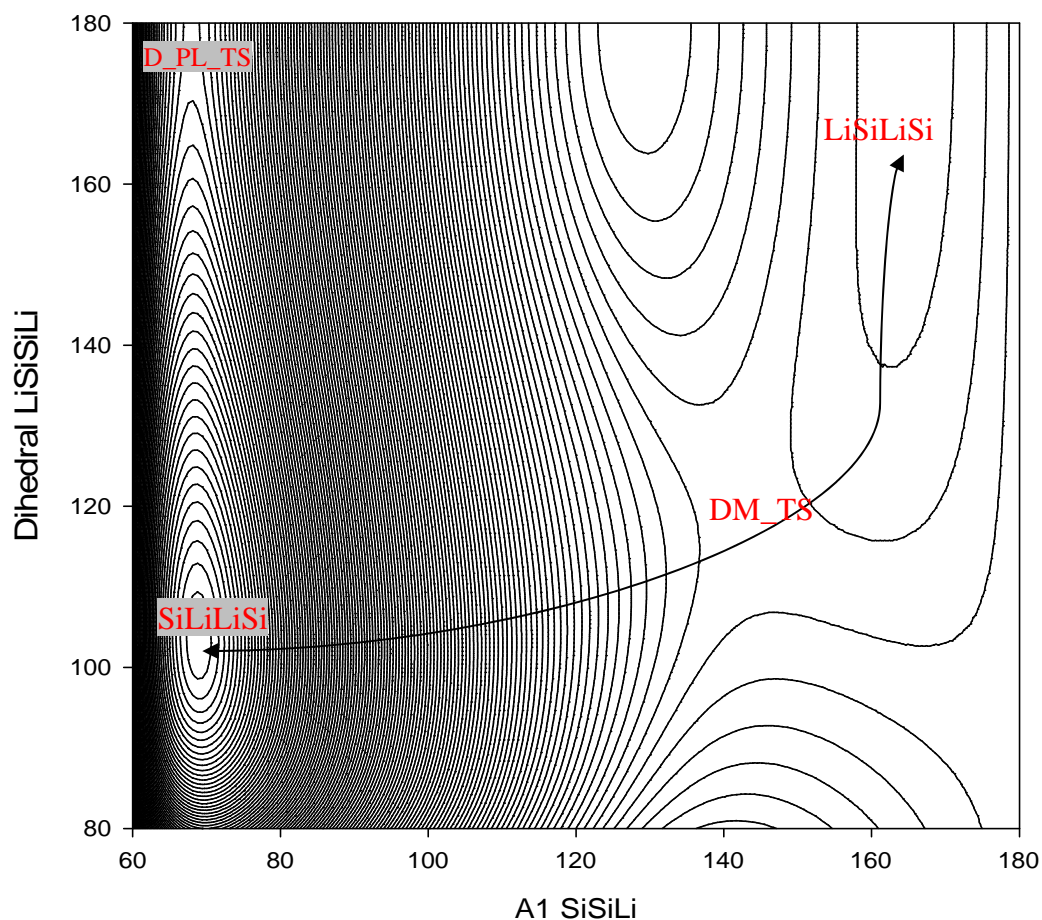
The fit reproduced the calculated geometric properties well as seen in Table 7.2-5. The differences in bond distances obtained by the fit with comparison to those calculated at the F12 level are in the range of 0.0005 Å (for the LiSiLiSi isomer) to 0.0024 Å (for the D_PL_TS structure). The angles are reproduced in the range of 0.01° to 0.7° (both in the LiSiLiSi isomer).

Table 7.2-5. Geometric properties of the Si₂Li₂ isomers on the fitted potential and optimized at the CCSD(T)-F12a/VTZ-F12 level of theory.

	Si ₂ Li ₂	
	Fit	CCSD(T)-F12a/ VTZ-F12
SiLiLiSi		
SiLi ^a	2.5538	2.5524
SiSi ^a	2.1680	2.1660
α SiSiLi ^b	64.95	64.90
β LiSiSiLi ^b	102.60	102.58
LiSiLiSi		
Si1Li2 ^a	2.5136	2.5141
Li1Si2 ^a	2.4082	2.4098
SiSi ^a	2.1330	2.1335
α Si1Si2Li1 ^b	163.50	164.22
α Si2Si1Li2 ^b	66.08	65.58
β LiSiSiLi ^b	180.00	180.00
D_PL_TS		
SiLi ^a	2.5228	2.5217
SiSi ^a	2.1603	2.1627
α SiSiLi ^b	64.63	64.62
β LiSiSiLi ^b	180.00	180.00
DM_TS		
Si1Li2 ^a	2.5265	2.5249
Li1Si2 ^a	2.3998	2.4017
SiSi ^a	2.1354	2.1372
α Si1Si2Li1 ^b	141.88	142.49
α Si2Si1Li2 ^b	65.75	66.15
β LiSiSiLi ^b	122.75	123.38
^a ångström		
^b degrees		

The contour plot depicted in Figure 7.2-3 represents the final fitted PES. The arrowed line shows the reaction path between the SiLiLiSi and the LiSiLiSi isomers.

Figure 7.2-3. A two-dimensional cut through the six-dimensional potential energy surface using the bond-length, bond-angles coordinate system.



Discussion and Conclusions

The DMC calculations for the critical points did not show any holes in the PES. However, with the addition of a correction term to avoid unphysically low energies at ϕ angles below 60° , the calculated full-dimensional potential energy surface was of sufficient quality to perform variational-vibrational calculations using the WAVR4 program. This issue will be discussed in more detail in the next chapter.

8 Vibrational properties of the Si₂Li₂ isomers.

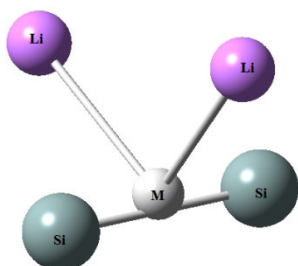
8.1 Vibrational calculations.

The perturbation theory discussed in section 2.1 (theoretical introduction to molecular vibrations) is used to approximate diagonalization of the Hamiltonian matrix, and solve the Schrödinger equation in a fast and efficient way. However, if more accurate results are required, other methods should be employed. Thus, the variational method of diagonalization of the Hamiltonian matrix, which allows solving the Schrödinger equation “exactly”, can be used instead of perturbation theory. The WAVR4 program [215], which is based on the variational method, will be used here to calculate vibrational spectra for the Si₂Li₂ potential energy surface.

The WAVR4 program employs primitive basis set functions which are composed of the following: a bending basis set defined by j_{\max} , l_{\max} and k_{\max} and a radial basis set defined by n_1 , n_2 and n_3 for the M–Li stretches and Si–Si stretch where M is the orthogonal canonical point, see Figure 8.1-1. M is close to the centre-of-mass of the molecule. The radial functions employ the discrete variables representation (DVR) [117, 215] approach. A product of either Morse-oscillator or spherical oscillator functions is used for the radial coordinates. Morse-oscillator functions will be used here for all the radial coordinates. The angular basis for the bending-rotation functions is a non-direct-product finite basis representation (FBR) [117, 215]. An explicit sequential-diagonalisation and truncation approach and the mixed FBR–DVR basis representation are used in the WAVR4 program. The sequential-diagonalisation and truncation method is employed to avoid problems caused by large Hamiltonian matrices, which can arise during the calculations. If the primitive basis set is large enough for convergence then it is possible to calculate accurate wavefunctions and eigenvalues for the Schrödinger equation [117, 215].

To avoid large changes in the radial coordinates, including those involving the Li atoms, orthogonal satellite coordinates were employed here. Orthogonal satellite coordinates were developed by Mladenovic [216] and are shown in Figure 8.1-1. These coordinates are very useful to study isomerising systems.

Figure 8.1-1. Graphical representation of the orthogonal satellite coordinates for Si_2Li_2 , where M is the orthogonal canonical point.

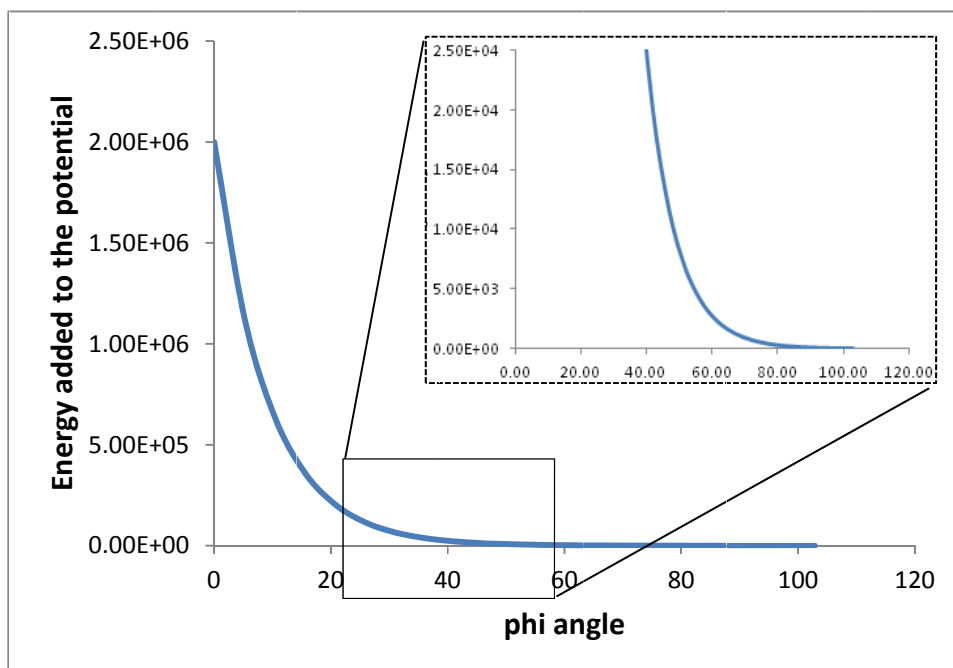


All calculations were performed using the 12000 cm^{-1} potential energy surface calculated previously at the CCSD(T)-F12a/cc-pVTZ-F12 level of the theory. All calculations were carried out on the new EastChem Research Computing Facility, which provides access to a 2376-core Intel Xeon cluster hosted by the School of Mathematics and Statistics at the University of St Andrews.

It was shown in the previous chapter that the 12000 cm^{-1} potential energy surface (PES) contains a region of unphysical low (negative) potential energy. This issue was also noticed during the ro-vibrational calculations as the ZPE of the global minimum was found to be negative, because the wavefunction is localized at the negative region. This can be explained by the sparse sampling for Si_2Li_2 geometries with ϕ (dihedral) angles below 60° . Thus, a correction term was implemented to the program code to avoid the appearance of the negative potential energy region on the surface during vibrational calculations.

The term $2 \cdot 10^6 \cdot e^{-0.11x}$ where x is the ϕ angle value was added to the potential energy as a function of the ϕ angle as seen in Figure 8.1-2.

Figure 8.1-2. The energy value added as a function of phi angles of the Si₂Li₂ structures.



A test was performed to check the improvement achieved by this approach. We calculated the energy in the phi angle range 72° to 32°, at the CCSD(T)-F12a/VTZ-F12 level of theory using the MOLPRO package. Table 8.1-1 compares the differences between the energies calculated by MOLPRO and the energies calculated by the original fitted surface as well as the surface with the additional term added.

Table 8.1-1. Difference between values calculated with CCSD(T)-F12/VTZ-F12 and the surface with the correction term added as well as the original fitted surface.

phi angle ^a	Differences between CCSD(T)-F12/VTZ-F12 energy and the potential augmented with the correction term ^b	Differences between CCSD(T)- F12/VTZ-F12 energy and the original fitted potential ^b
36.00	-4414.7	33711.7
41.14	2343.4	23997.4
46.29	4062.4	16360.8
51.43	3547.0	10531.9
56.57	2326.5	6293.7
61.71	1157.0	3410.2
66.86	337.7	1617.4
72.00	-85.0	641.8
^a degrees		
^b cm ⁻¹		

It can be seen that after introduction of the correction term to the potential the appearance of the negative well is avoided. However, the potential energy rises too steeply, so the vibrational energies calculated here will be too high.

The primitive vibrational basis sets were modified to achieve approximate convergence, in particular so that the calculated ZPE value was close to the value obtained by a second-order perturbation theory anharmonicity calculation done at the MP2/aug-cc-pVTZ level of theory which is 943.02 cm⁻¹. Table 8.1-2 shows the ZPE calculated with different sizes of the radial and angular basis sets. It can be seen the large changes in the ZPE occurred when the angular basis was increased. The same pattern was observed when higher energy levels were analysed. For instance, when the radial basis n_1 , n_2 and n_3 (5, 5, 5) and angular basis j_{\max} , l_{\max} and k_{\max} (10, 10, 8) were employed the first calculated energy level above the ground state was 306.1 cm⁻¹ and the eighth one was 964.9 cm⁻¹, whereas with the radial basis n_1 , n_2 and n_3 (5, 5, 5) and angular basis j_{\max} , l_{\max} and k_{\max} (20, 20, 14), the first calculated energy level above the ground state dropped to 130.6 cm⁻¹ and the eighth one went to 626.5 cm⁻¹.

Table 8.1-2. ZPE calculated with different sizes of the radial and angular basis sets.

ZPE ^a	radial basis ^b	angular basis ^c	cpu time [s]
1781.8	4, 4, 4	8 , 8, 7	3
1710.4	5, 5, 5	8, 8, 7	6
1411.9	5, 5, 5	10, 10, 8	54
1131.2	5, 5, 5	14, 14, 10	888
1022	5, 5, 5	18, 18, 12	12030
992	5, 5, 5	20, 20, 14	43323
972.7	6, 6, 5	21, 21, 15	141017
966.2	6, 6, 6	22, 22, 15	396958

^a cm⁻¹

^b basis defined by n_1 , n_2 and n_3 the first two correspond to the M–Li stretches and the last one to the Si–Si stretch

^c basis defined by j_{\max} , l_{\max} and k_{\max}

Approximate convergence was achieved when 6 radial basis functions each for all three stretches were used and angular basis j_{\max} , l_{\max} and k_{\max} (22, 22, 15) values for the bending basis were employed. The zero point energy calculated at this level was 966 cm⁻¹, 23 cm⁻¹ higher than that calculated by the MP2/aug-cc-pVTZ second-order perturbation theory calculations. It was not possible to achieve more accurate zero-point energies, as the variational vibrational calculations are very CPU-time demanding and the final calculation already took several days.

We investigated the changes in the calculated energy levels above the ground state with respect to increasing size of the radial and angular basis sets. The comparison can be seen in Table 8.1-3. Only the lowest 2400 totally symmetric energy levels (vibrational states of A₁ symmetry) were calculated.

The first six and 8th-9th energy levels show small differences with respect to the increasing size of the radial and angular basis sets, however, for the 7th and 10th-12th energy levels the differences are significantly larger. A similar picture can be seen for the higher (above 12th) energy levels as well. The average difference for the first 35 totally symmetric energy levels is 14.5 cm⁻¹. Thus, we decided to assign only the lower reasonably converged energy levels. Additionally the 1000th energy level has energy 3143.9 cm⁻¹, and the 2400th energy level has energy 4121.9 cm⁻¹. The differences with

respect to the increasing size of the radial and angular basis sets for these levels are: 76.7 cm^{-1} and 152.9 cm^{-1} , respectively.

The identification of the energy levels was difficult as the vibrational levels were very close to each other as seen in Table 8.1-3. To solve this issue, a program developed by Kozin et al. [217] was used. The program analyses the wave functions calculated by WAVR4 and produces probability densities with respect to the phi or theta angles which are very helpful to assign an energy level. The information provided by the MP2 anharmonicity calculations were also used as additional references and can be seen in Table 8.1-4.

Table 8.1-3. Energy levels calculated using two different combinations of the radial and angular basis sets

ZPE	angular basis	radial basis	ZPE	angular basis	radial basis	difference [cm ⁻¹]
966.2	6, 6, 6	22, 22, 15	972.7	6, 6, 5	21, 21, 15	
energy lvl.	energy [cm ⁻¹]		energy lvl.	energy [cm ⁻¹]		
1	0.00		1	0.00		
2	102.96		2	106.40		-3.44
3	249.71		3	252.59		-2.88
4	289.18		4	290.98		-1.80
5	412.10		5	413.43		-1.32
6	457.66		6	462.77		-5.11
7	491.79		7	518.13		-26.34
8	523.67		8	528.33		-4.66
9	554.14		9	554.85		-0.70
10	571.64		10	609.62		-37.97
11	631.45		11	646.63		-15.18
12	641.85		12	659.95		-18.10
13	657.25		13	663.60		-6.35
14	661.77		14	668.74		-6.97
15	708.38		15	718.49		-10.12
16	716.66		16	760.97		-44.31
17	768.51		17	771.61		-3.10
18	777.37		18	774.32		3.06
19	782.10		19	811.37		-29.27
20	810.62		20	824.76		-14.14
21	836.07		21	839.35		-3.28
22	838.26		22	847.42		-9.16
23	846.37		23	861.11		-14.74
24	853.90		24	894.55		-40.65
25	882.62		25	899.93		-17.32
26	898.40		26	918.82		-20.42
27	912.81		27	925.41		-12.61
28	918.93		28	947.32		-28.39
29	926.29		29	956.91		-30.62
30	958.02		30	962.13		-4.11
31	967.88		31	969.43		-1.55
32	970.55		32	1020.17		-49.62
33	999.41		33	1021.60		-22.19
34	1017.55		34	1027.23		-9.68
35	1021.64		35	1038.07		-16.43

Table 8.1-4. Vibrational information on the dibridged Si_2Li_2 isomer provided by anharmonicity calculations at the MP2/aug-cc-pVTZ level of theory and second order perturbation theory.

MP2/AVTZ				
mode	Symmetry	anharmonic vibration wavenumber [cm^{-1}]	harmonic vibration wavenumber [cm^{-1}]	vibrational motion descriptions
ν_1	A_1	543	548	SiSi str.
ν_6	B_2	433	422	SiLi antisym. str.
ν_2	A_1	442	408	SiLi sym. str.
ν_4	A_2	208	196	SiLi antisym. str.
ν_5	B_1	199	193	SiLi antisym. str.
ν_3	A_1	97	104	Butterfly

Note, that the anharmonic vibration levels for the ν_2 , ν_4 , ν_5 and ν_6 vibration modes have higher energies than their corresponding harmonic vibration levels. This effect could be caused by Fermi resonances (for the $\nu_2/2\nu_4$, $\nu_2/2\nu_5$ and $\nu_6/\nu_4+\nu_5$ vibration modes) which can be responsible for the breakdown of the second order perturbation theory (which assumes weak interactions between vibrations) in the calculation of the anharmonic corrections (for the ν_2 , ν_4 , ν_5 and ν_6 vibration modes). Fermi resonances could also explain the presence of large positive values for anharmonic constants: χ_{23} and χ_{26} shown in Table 4.5-6 (Chapter 4.5).

Table 8.1-5. The assigned energy levels of the Si₂Li₂ dibridged structure calculated using the WAVR4 program.

energy levels	energy cm ⁻¹	mode ^a	mode ^b
1	0.00	Ground state	
2	102.96	v ₃	
3	249.71	2v ₃	
4	289.18	3v ₃	
5	412.10	v ₂	
6	457.66	4v ₃	
7	491.79		2v ₄ /2v ₅
8	523.67	v ₃ +v ₂	
9	554.14	v ₁	
10	571.64		2v ₄ /2v ₅
11	631.45		v ₃ +2v ₄ /2v ₅

^a conclusive assignment of modes
^b not easy to define mixture of modes

The wave function analysis allowed us to assign the first 11 energy levels which are all vibrational levels of the dibridged structure. The results are shown in Table 8.1-5. Note that all of the states can be only approximately assigned. Thus, the higher vibrations are a mixture of the states shown in last column of the table. Nevertheless, the wavefunction analysis allows us to identify with reasonable accuracy these low-lying energy levels of the dibridged structure.

We had to limit our analysis to the vibration levels of the dibridged isomer only, as the PES contains holes even after the correction term and this prohibited us doing vibrational calculations that cover the monobridged vibrational states (higher than 4200 cm⁻¹). However, it gave us an opportunity to locate the regions with sparse sampling on the PES which could be fixed by introducing a wider grid sampling procedure.

The program developed by Kozin et al. [217] used in the above assignment process gives us an opportunity to create probability-density plots for the phi, MSiLi1 and MSiLi2 angles. The MSiLi1 and MSiLi2 angles will be abbreviated as theta1 and theta2, respectively. The probability-density plots were created for the 3rd, 7th, 8th and 10th energy levels and can be seen in Figure 8.1-3 to Figure 8.1-6. We have a conclusive assignment of the modes for the 3rd and 8th energy levels. However, the 7th and 10th

energy levels are composed from a mixture of states, and thus, the assignment of the modes is not straightforward. The plots below can help a reader to understand the issues we were struggling with during the process of assignment of the modes.

Figure 8.1-3 shows no quantum excitation for the theta1 and theta2 angles however, a two-quantum excitation can be found for the phi angle. These give conclusive assignment of mode as $2\nu_3$. A similar picture can be found for the 8th energy level (Figure 8.1-5). There is no quantum excitation for the theta1 and theta2 angles however, a one-quantum excitation is observed for the phi angle including one quantum of excitation in ν_3 . These is consistent with the $\nu_3+\nu_2$.

Figure 8.1-3. Probability densities for the phi, theta1 and theta2 angles of the 3rd energy level.

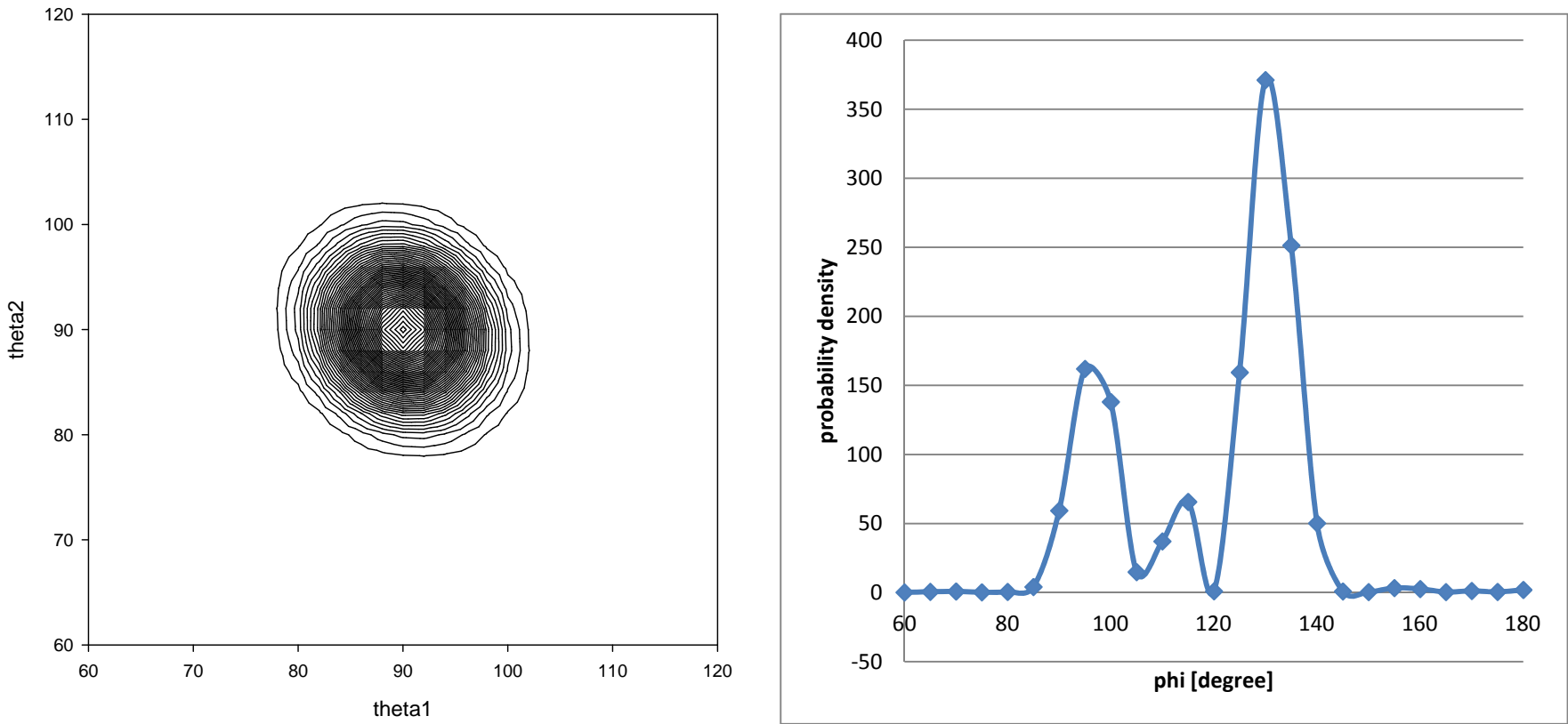


Figure 8.1-4. Probability densities for the phi, theta1 and theta2 angles of the 7th energy level.

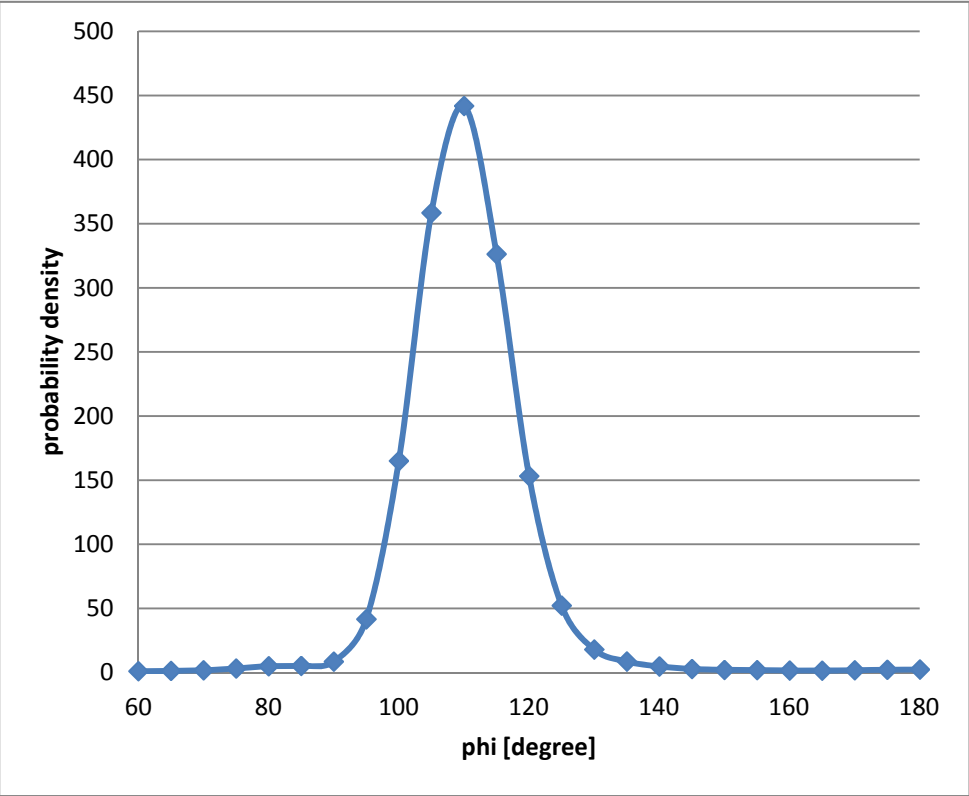
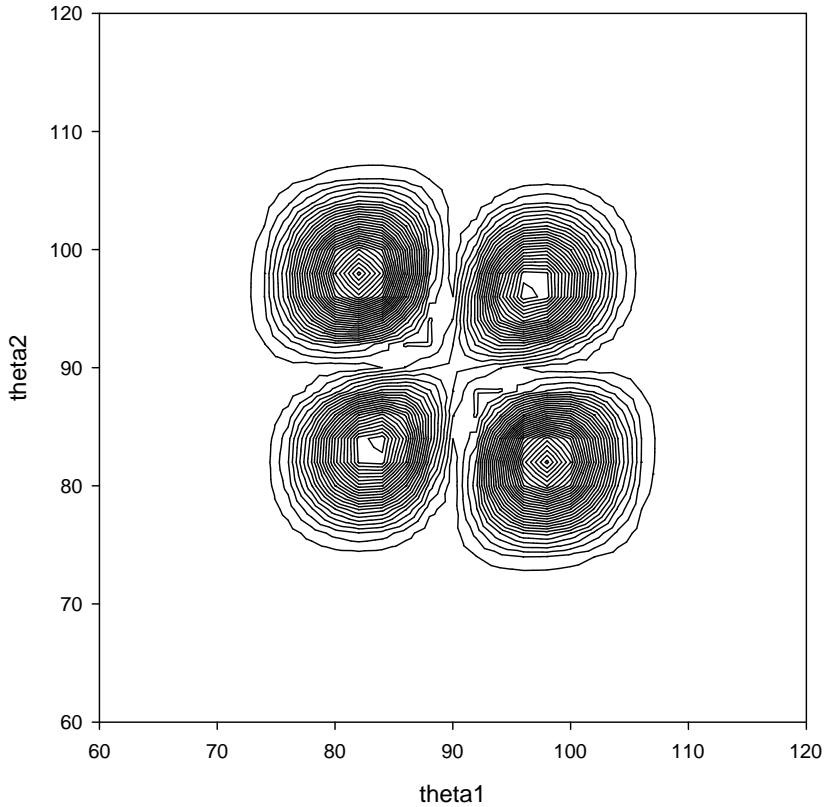


Figure 8.1-5. Probability densities for the phi, theta1 and theta2 angles of the 8th energy level.

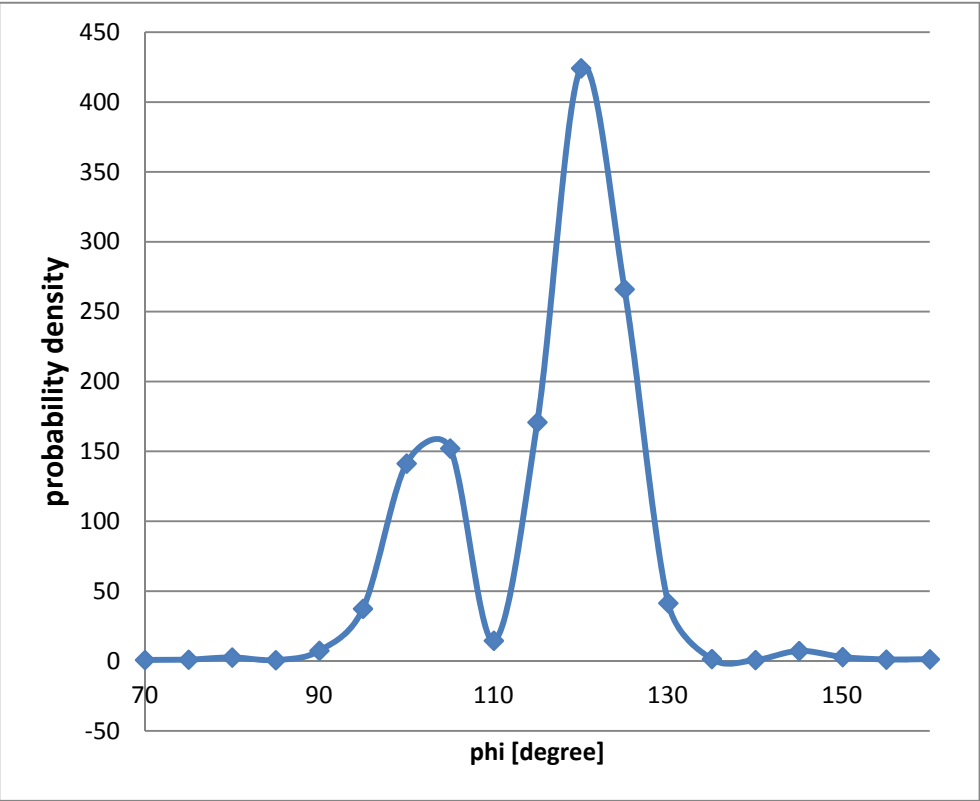
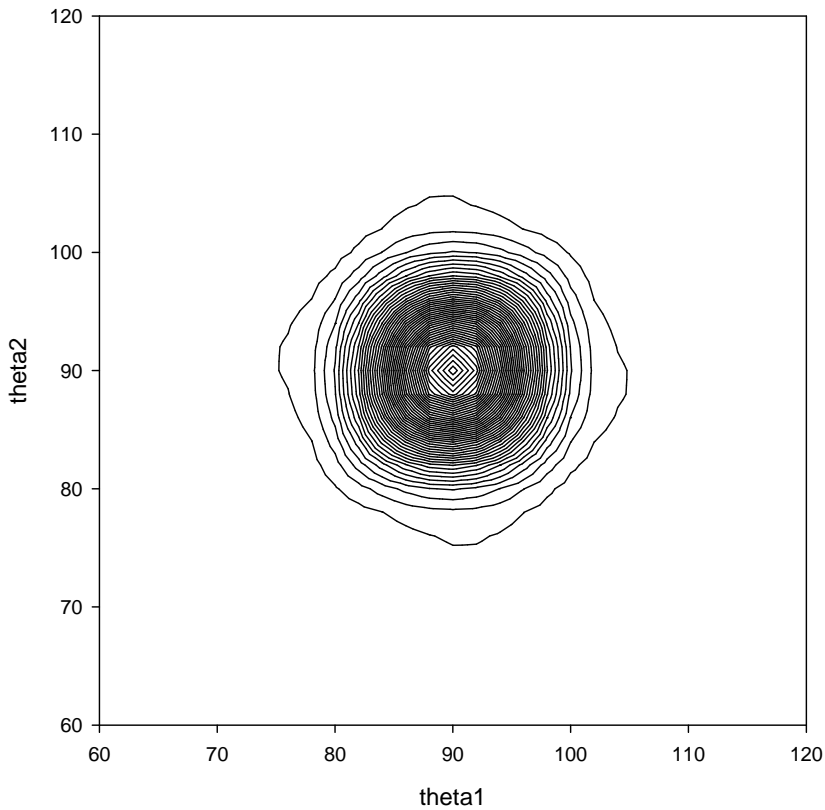


Figure 8.1-6. Probability densities for the phi, theta1 and theta2 angles of the 10th energy level.

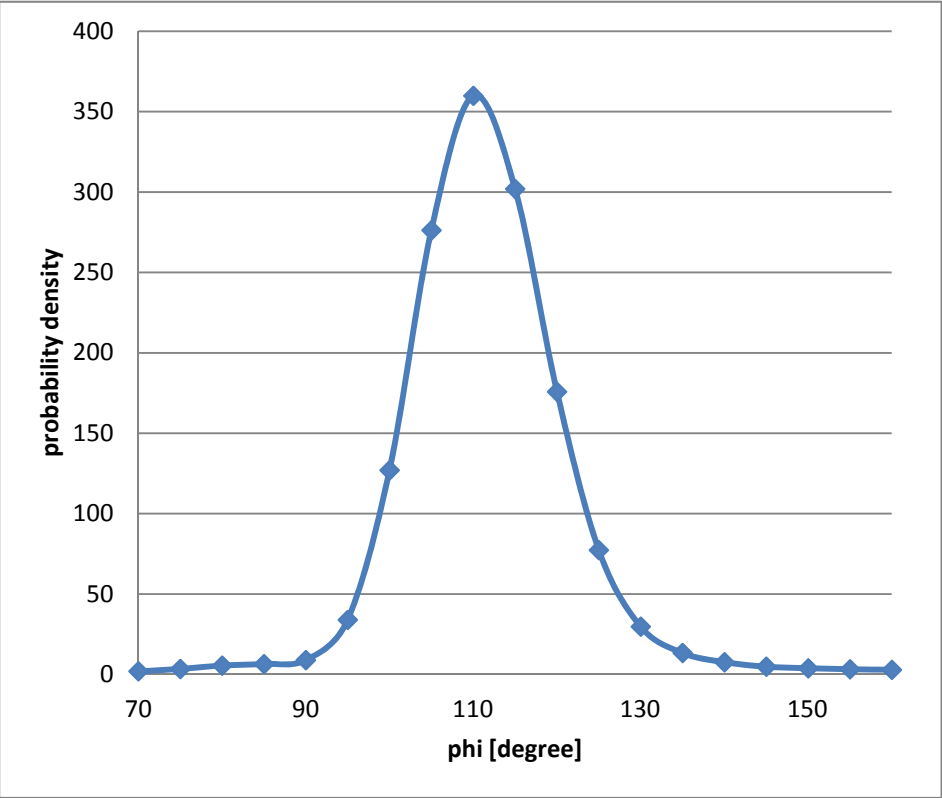
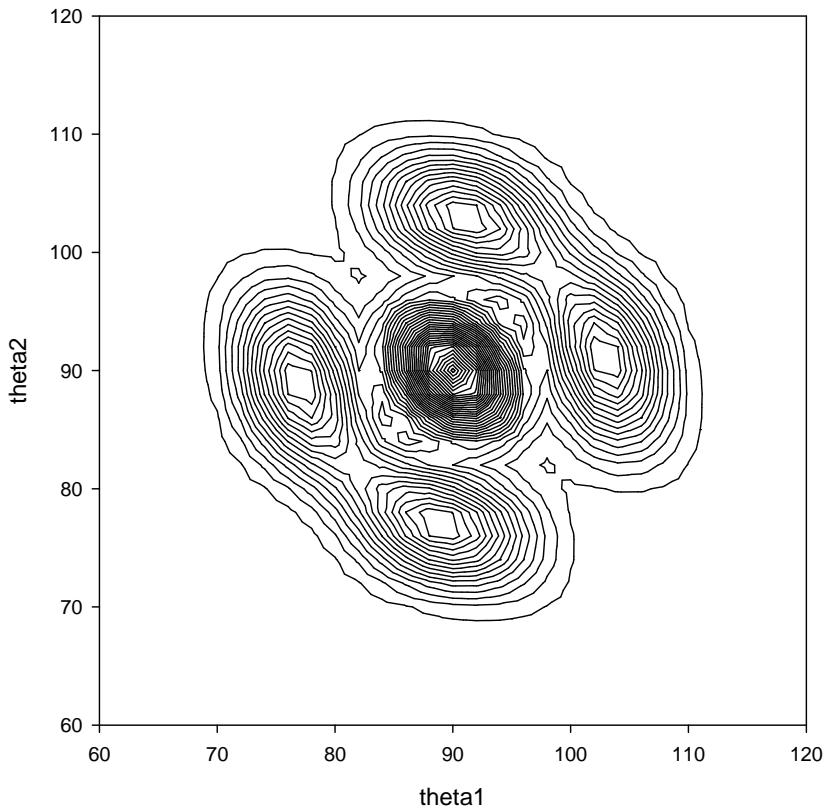


Figure 8.1-4 shows a one-quantum excitation for the theta1 angle and a one-quantum excitation for the theta2 angle, whereas no quantum excitation was observed for the phi angle. Thus, these can be assigned as a mixture of two states $2\nu_4$ and $2\nu_5$ (which involve respectively antisymmetric and symmetric distortions of the theta1 and theta2 angles). A similar picture is observed for the 10th energy level (Figure 8.1-6): a one-quantum excitation for the theta1 angle, a one-quantum excitation for the theta2 angle, and no quantum excitation for the phi angle. Thus, these can be also assigned as a mixture of the states $2\nu_4$ and $2\nu_5$.

Discussion and conclusions:

The calculated full-dimensional potential energy surface was used to perform variational-vibrational calculations using the WAVR4 program. We are aware of a hole in the PES for phi values below 60°, however, the implementation of the additional term of $2 \cdot 10^6 \cdot e^{-0.11x}$ to the potential allowed us to calculate successfully the lowest 2400 energy levels of the Si₂Li₂ structure. The low-lying energy levels are qualitatively corrected.

The hole in the potential energy surface prevented us from performing successful variational-vibrational calculations for energy levels above 4200 cm⁻¹ which would cover the monobridged isomer. A potential energy surface accurate over a wider range is required to do so.

9 Conclusions

Calculations of the Si_2HX and Si_2Li_2 systems (where $\text{X} = \text{H}, \text{Li}, \text{F}$ and Cl) showed that bridged minima occur in all cases while trans and vinyl minima can be found only in the $\text{X} = \text{H}, \text{F}$ and Cl systems. The bridged structures (monobridged or dibridged) are global minima in all cases. The disilynes have significantly different isomerisation properties compared with the C_2H_2 species. The CCSD(T)-F12a/cc-pVTZ-F12 level of theory showed accuracy comparable to the CCSD(T)/cc-pV(6+d)Z level for geometric properties and to the CCSD(T)/cc-pV(Q+d)Z level for harmonic vibrational frequencies. Thus, I recommend the CCSD(T)-F12a/cc-pVTZ-F12 level of theory as the most accurate for calculation on small silicon systems including full dimensional potential energy surface calculations. It was concluded that core-valence contributions are more important than relativistic corrections for Si_2XLi structures (where $\text{X} = \text{H}$ or Li). The B3LYP/6-311+G(d) method gives the most accurate electron affinity results. However, the B3LYP/6-311+G(d) method is not reliable for calculating the H^+ and Li^+ binding energies.

The Neural Network approach proved to be an effective and fast potential energy surface fitting tool. The DMC sampling procedure employed here was successful. However, the coordinate sampling ranges used in the wider grid sampling procedure were too ambitious and many calculated points were found in regions with energies above 50000 cm^{-1} . Thus, not enough points were available to fit the potential energy surface above 12000 cm^{-1} . Additional calculations using smaller coordinate sampling ranges will be required to obtain more accurate results. The calculated full-dimensional potential energy surface was of sufficient quality to perform variational-vibrational calculations using the WAVR4 program. The Si_2Li_2 system possesses a high density of vibrational energy levels, which makes identification of the vibrational modes difficult. Nevertheless, conclusive assignments of the vibrational modes of Si_2Li_2 were made for the eleven lowest-lying energy levels.

10 Publication and presentations resulting from this thesis

10.1 Publication

"Theoretical studies of bridging structures and isomerism in substituted disilynes"

Lukasz M. Serafin, Tanja van Mourik and Mark M. Law

Manuscript in preparation (for submission to *Organometallics*)

10.2 Presentations and posters

13th May 2009, ScotCHEM Computational Chemistry Symposium, Heriot-Watt University Edinburgh – POSTER

8th April 2010, ScotCHEM Computational Chemistry Symposium, University of Strathclyde – POSTER

6th July 2010, RSC Theoretical Chemistry Group Conference, University of Nottingham – POSTER

14th-18th February 2011, Workshop on Theoretical Chemistry – Explicitly correlated methods, Mariapfarr, Austria – TALK

7th June 2011, ScotCHEM Computational Chemistry Symposium, University of Edinburgh – TALK

27th-29th June 2011, RSC Theoretical Chemistry Group Conference, University of Nottingham – TALK

26th January 2012, University of St Andrews – TALK

11 Bibliography

- [1] S. Sriraman, P. Mahalingam, E.S. Aydil, D. Maroudas, *Surf. Sci.*, 540 (2003) 623.
- [2] C. Exley, A. Tollervey, G. Gray, S. Roberts, J.D. Birchall, 253 (1993) 93.
- [3] C.H. Jr., L. Roberts, A. Larson, *Animal Diversity*, New York: McGraw-Hill, 2003.
- [4] Y. Osamura, R.I. Kaiser, *Astron. Astrophys.*, 432 (2005) 559.
- [5] D. Sillars, *Chem. Phys. Lett.*, 305 (2004) 141.
- [6] D. Sillars, C.J. Bennett, Y. Osamura, R.I. Kaiser, *Chem. Phys. Lett.*, 392 (2004) 541.
- [7] A.V. Shavrina, Y.V. Glagolevskij, J. Silvester, G.A. Chuntanov, V.R. Khalack, Y.V. Pavlenko, *Mon. Not. R. Astron. Soc.*, 401 (2010) 1882.
- [8] E. Wiberg, *Lehrbuch der Anorganischen Chemie*, 22-23 (1943).
- [9] J. Gaubeau, *Angew. Chem.*, 69 (1957) 77.
- [10] R.S. Mulliken, *J. Am. Chem. Soc.*, 77 (1955) 884.
- [11] J.S. Binkley, *J. Am. Chem. Soc.*, 106 (1984) 603.
- [12] H. Lishka, H.J. Kohler, *J. Am. Chem. Soc.*, 105 (1983) 6646.
- [13] S. Koseki, M.S. Gordon, *J. Phys. Chem.*, 92 (1988) 364.
- [14] M. Lein, A. Krapp, G. Frenking, *J. Am. Chem. Soc.*, 127 (2005) 6290.
- [15] P.P. Power, *Organometallics*, 26 (2007) 4362.
- [16] V.Y. Lee, A. Sekiguchi, *Acc. Chem. Res.*, 40 (2007) 410.
- [17] K. Tarcsay-Petrov, T. Veszpremi, *Int. J. Quantum Chem.*, 109 (2009) 2526.
- [18] S. Zou, J.M. Bowman, *Chem. Phys. Lett.*, 368 (2003) 421.
- [19] W.C. Lineberger, K.M. Ervin, *J. Chem. Phys.*, 91 (1989) 5974.
- [20] G.A. Petersson, *J. Am. Chem. Soc.*, 114 (1992) 6133.
- [21] N. Chang, M. Shen, C. Yu, *J. Chem. Phys.*, 106 (1997) 3237.
- [22] B. Wirsam, *Theor. Chim. Acta* 25 (1972) 169.
- [23] S. Obara, K. Kitaura, K. Morokuma, *Theor. Chim. Acta* 25, 60 (1981) 227.
- [24] R.S. Grev, H.F. Schaefer, *J. Chem. Phys.*, 97 (1992) 7990.
- [25] M. Bogey, H. Bolvin, C. Demuynck, J.L. Destombes, *Phys. Rev. Lett.*, 66 (1991) 413.
- [26] M. Cordornier, M. Bogey, C. Demuynck, J. L. Destombes, *J. Chem. Phys.*, 97 (1992) 7984.
- [27] A. Sekiguchi, R. Kinjo, M. Ichinohe, *Science*, 305 (2004) 1755.
- [28] N. Wiberg, W. Niedermayer, G. Fischer, H. Nöth, M. Suter, *Eur. J. Inorg. Chem.*, 2002 (2002) 1066.
- [29] R. Stegmann, G. Frenking, *Organometallics*, 14 (1995) 5308.
- [30] Y.L. Bei, S.Y. Feng, *Acta Chimica Sinica*, 57 (1999) 1306.
- [31] S.C. Park, R.A. Stansfield, D.C. Clary, *J. Phys. D: Appl. Phys.*, 20 (1987) 880.
- [32] J. Pelletier, *J. Phys. D: Appl. Phys.*, 20 (1987) 858.
- [33] W.D. Allen, H.F. Schaefer, *Chem. Phys.*, 108 (1986) 243.
- [34] B.P. Prascher, R.M. Lucente-Schultz, A.K. Wilson, *Chem. Phys.*, 359 (2009) 1.
- [35] R. Walsh, *J. Chem. Soc.*, 79 (1983) 2233.
- [36] E.W. Ignacio, H.B. Schlegel, *J. Chem. Phys.*, (1990) 5404.
- [37] E.W. Ignacio, H.B. Schlegel, *J. Chem. Phys.*, 96 (1992) 5830.
- [38] K. Koyasu, M. Akutsu, M. Mitsui, A. Nikajima, *J. Am. Chem. Soc.*, 127 (2005) 4998.
- [39] J.B. Jaeger, T.D. Jaeger, M.A. Duncan, *J. Phys. Chem. A*, 110 (2006) 9310.
- [40] P.C. Gomez, M.A. Palafox, L.F. Pacios, *J. Phys. Chem. A* 103 (1999) 8537.
- [41] J.A. Morrison, M.A. Ring, *Inorg. Chem.*, 6 (1967) 100.

- [42] C. Sporea, F. Rabilloud, M. Aubert-Frecon, *J. Mol. Struc. (Theochem)*, 802 (2007) 85.
- [43] C. Sporea, F. Rabilloud, X. Cosson, A.R. Allouche, M. Aubert-Frécon, *J. Phys. Chem. A*, 110 (2006) 6032.
- [44] J.-C. Yang, L. Lin, Y. Zhang, A.F. Jalbout, *Theor. Chem. Account*, 121 (2008) 83.
- [45] D. Hao, J. Liu, J. Yang, *J. Phys. Chem. A*, 112 (2008) 10113.
- [46] H.R. Ihle, C. Wu, M. Miletic, K.F. Zmbov, *Adv. Mass Spectrom.*, 7 (1978) 670.
- [47] B.S. Jursic, *J. Mol. Struc. (Theochem)*, 459 (1999) 221.
- [48] B.S. Jursic, *J. Mol. Struc. (Theochem)*, 491 (1999) 1.
- [49] N. Matsunaga, S. Koseki, M.S. Gordon, *J. Chem. Phys.*, 104 (1996) 7988.
- [50] S.-G. He, H. Lin, H. Burger, W. Thiel, Y. Ding, Q.-S. Zhu, *J. Chem. Phys.*, 116 (2002) 105.
- [51] K.G. Nakamura, *Chem. Phys. Lett.*, 285 (1998) 21.
- [52] M.M. Law, J. T.Fraser-Smith, C.U. Perotto, *Phys. Chem. Chem. Phys.*, 14 (2012) 6922.
- [53] P.J. Mohr, B.N. Taylor, D.B. Newell, *J. Phys. Chem. Ref. Data*, 37 (2008) 1187.
- [54] M. Born, R. Oppenheimer, *Annalen der Physik*, 84 (1927) 457.
- [55] F. Jensen, *Introduction to Computational Chemistry*, Wiley, 2001.
- [56] J.B. Foresman, Æ. Frisch, *Exploring Chemistry with Electronic Structure Methods, Second (Ed.)*, Gaussian, Inc, 1996.
- [57] W.J. Hehre, R.F. Stewart, J.A. Pople, *J. Chem. Phys.*, 51 (1969) 2657.
- [58] T.H. Dunning, *J. Chem. Phys.*, 90 (1989) 1007.
- [59] E. Schrödinger, *Annalen der Physik*, 80 (1926) 734.
- [60] P.A.M. Dirac, *Math. Proc. Camb. Phil. Soc.*, 35 (1939) 416.
- [61] J. Cížek, *J. Chem. Phys.*, 45 (1966) 4256.
- [62] T.D. Crawford, H.F. Schaefer, *Reviews in Computational Chemistry*, 14 (1998) 33.
- [63] T.J.L.a.P.R. Taylor, *Int. J. Quantum Chem.*, 23 (1989) 199.
- [64] J.M.L. Martin, T.J. Lee, G.E. Scuseria, *J. Chem. Phys.*, 97 (1992) 6549.
- [65] Z.L. Cai, J.M.L. Martin, J.P. Francois, R. Gijbels, *Chem. Phys. Lett.*, 252 (1996) 398.
- [66] T.B. Adler, G. Knizia, H.J. Werner, *J. Chem. Phys.*, 127 (2007) 221106.
- [67] B.T. Colegrove, H.F. Schaefer, *J. Chem. Phys.*, 94 (1990) 5593.
- [68] G. Knizia, T.B. Adler, H.J. Werner, *J. Chem. Phys.*, 130 (2009) 054104.
- [69] E.A. Hylleraas, *Z. Phys.*, 54 (1929) 347.
- [70] W. Kutzelnigg, W. Klopper, *J. Chem. Phys.*, 94 (1991) 1985.
- [71] J. Noga, W. Kutzelnigg, *J. Chem. Phys.*, 101 (1994) 7738.
- [72] J. Noga, W. Kutzelnigg, W. Klopper, *Chem. Phys. Lett.*, 199 (1992) 497.
- [73] R.J. Gdanitz, *J. Chem. Phys.*, 109 (1998) 9795.
- [74] W. Kutzelnigg, *Theor. Chim. Acta*, 68 (1985) 445.
- [75] M. Reed, B. Simon, *Methods of Modern Mathematical Physics*, in, 1981.
- [76] D.P. Tew, W. Klopper, *J. Chem. Phys.*, 125 (2006) 094302.
- [77] K. Szalewicz, B. Jeziorski, H.J. Monkhorst, J.G. Zabolitzky, *Chem. Phys. Lett.*, 91 (1982) 169.
- [78] S. Ten-no, F.R. Manby, *J. Chem. Phys.*, 119 (2003) 5358.
- [79] E.F. Valeev, *Chem. Phys. Lett.*, 395 (2004) 190.
- [80] P. Cársky, J. Paldus, J. Pittner, *Recent Progress in Coupled Cluster Methods*, in, 2010, pp. 573.
- [81] S. Ten-no, *Chem. Phys. Lett.*, 398 (2004) 56.

- [82] A.J. May, F.R. Manby, *J. Chem. Phys.*, 121 (2004) 4479.
- [83] D.P. Tew, W. Klopper, C. Hättig, *Chem. Phys. Lett.*, 452 (2008) 326.
- [84] D.P. Tew, W. Klopper, C. Neiss, C. Hättig, *Phys. Chem. Chem. Phys.*, 9 (2007) 1921.
- [85] H.J. Werner, P.J. Knowles, G. Knizia, F.R. Manby, M. Schütz, and others, *MOLPRO*, version 2010.1, a package of *ab initio* programs.
- [86] L. Fox, H.D. Huskey, J.H. Wilkinson, *Quarterly Journal of Mechanics and Applied Mathematics* 1(1948) 149.
- [87] M.R. Hestenes, *Journal of Optimization Theory and Applications* 11 (1973) 323.
- [88] C. Hampel, K.A. Peterson, H.J. Werner, *Chem. Phys. Lett.*, 190 (1992) 1.
- [89] *Molpro manual*, 2010.1
- [90] P. Atkins, R. Friedman, *Molecular Quantum Mechanics*, Oxford University Press, 2005.
- [91] L.H. Thomas, *Proc. Camb. Phil. Soc.*, 23 (1927) 542.
- [92] P.A.M. Dirac, *Proc. Camb. Phil. Soc.*, 26 (1930) 376.
- [93] W. Kohn, L.J. Sham, *Phys. Rev. A*, 140 (1965) 1133.
- [94] D.M. Ceperley, B.J. Alder, *Phys. Rev. Lett.*, 45 (1980) 566.
- [95] S.J. Vosko, L. Wilk, M. Nusair, *Can. J. Phys.*, 58 (1980) 1200.
- [96] A. St-Amant, W.D. Cornell, P.A. Kollman, T.A. Halgren, *J. Comput. Chem.*, 16 (1995) 1483.
- [97] J.P. Perdew, Y. Wang, *Phys. Rev. B* 45 (1992) 13244.
- [98] A.D. Becke, *J. Chem. Phys.*, 98 (1993) 1372.
- [99] K. Kim, K.D. Jordan, *J. Phys. Chem.*, 98 (1994) 10089.
- [100] A.D. Becke, *J. Chem. Phys.*, 98 (1993) 5648.
- [101] P.O. Löwdin, *Phys. Rev.*, 97 (1955) 1474.
- [102] F. Weinhold, C.R. Landis, *Chemistry Education: Research and Practice in Europe*, 2 (2001) 91.
- [103] A.E. Reed, L.A. Curtiss, F. Weinhold, C.R. Landis, *Chem. Rev.*, 88 (1988) 899.
- [104] A.G. Császár, *Computational Molecular Spectroscopy*, P. Jensen, P.R. Bunker (Eds.), Wiley, 2000, pp. 55.
- [105] P.A.M. Dirac, *Proc. R. Soc.*, 117 (1928) 610.
- [106] G. Tarczay, A.G. Császár, W. Klopper, H.M. Quiney, *Mol. Phys.*, 99 (2001) 1769.
- [107] R.D. Cowan, D.C. Griffin, *J. Opt. Soc. Am.*, 66 (1976) 1010.
- [108] E.B. Wilson, J.C. Decius, P.C. Cross, *Molecular Vibrations*, McGraw-Hill, London, 1955.
- [109] S. Califano, *Vibrational States*, Wiley, 1976.
- [110] E.G. Lewars, *Computational Chemistry*, Springer Science, 2011.
- [111] G. Herzberg, *Infrared and Raman Spectra of Polyatomic Molecules*, Van Nostrand, New Jersey, 1945.
- [112] J. Tennyson, *Computational Molecular Spectroscopy*, P. Jensen, P.R. Bunker (Eds.), Wiley, 2000, pp. 305.
- [113] J.C. Light, I.P. Hamilton, J.V. Lill, *Chem. Phys.*, 82 (1985) 1400.
- [114] J. Tennyson, J.R. Henderson, N.G. Fulton, *Comp. Phys. Comm.*, 86 (1995) 175.
- [115] P.N. Roy, T. Carrington, *Chem. Phys. Lett.*, 257 (1996) 98.
- [116] I.N. Kozin, M.M. Law, J. Tennyson, J.M. Hutson, *Comp. Phys. Comm.*, 163 (2004) 117.
- [117] I.N. Kozin, M.M. Law, J. Tennyson, J.M. Hutson, *J. Chem. Phys.*, 118 (2003) 4896.

- [118] S. Zou, J.M. Bowman, *Chem. Phys. Lett.*, 368 (2003) 421.
- [119] R.A. Kendall, T.H. Dunning, R. J. Harrison, *J. Chem. Phys.*, 96 (1992) 6796.
- [120] H.J. Werner, P.J. Knowles, G. Knizia, F.R. Manby, M. Schütz, and others, *MOLPRO*, version 2006.1, a package of *ab initio* programs.
- [121] C. Moller, M.S. Plesset, *Phys. Rev. Lett.*, 46 (1934) 618.
- [122] C.C.J. Roothan, *Rev. Mod. Phys.*, 23 (1951).
- [123] D.B. Chesnut, *Heteroatom Chemistry*, 13 (2002).
- [124] M. Bittner, H. Köppel, *Phys. Chem. Chem. Phys.*, 5 (2003) 4604.
- [125] J. Palaudoux, M. Hochlaf, *J. Phys. Chem.*, 126 (2007) 044302.
- [126] J.Q. Sun, K. Ruedenberg, *J. Chem. Phys.*, 99 (1993) 5257.
- [127] B.D. Saksena, *J. Chem. Phys.*, 20 (1952) 95.
- [128] S. Joseph, A.J.C. Varandas, *J. Phys. Chem. A*, 114 (2010) 13277.
- [129] S. Boyé-Péronne, D. Gauyacq, J. Liévin, *J. Chem. Phys.*, 124 (2006) 214305.
- [130] M. J. Frisch, G. W. Trucks, H. B. Schlegel, G. E. Scuseria, J.R.C. M. A. Robb, V. G. Zakrzewski, J. A. Montgomery Jr., R. E. Stratmann, J. C. Burant, S. Dapprich, J. M. Millam, A. D. Daniels, K. N. Kudin, M. C. Strain, O. Farkas, J. Tomasi, V. Barone, M. Cossi, R. Cammi, B. Mennucci, C. Pomelli, C. Adamo, S. Clifford, J. Ochterski, G. A. Petersson, P. Y. Ayala, Q. Cui, K. Morokuma, P. Salvador, J. J. Dannenberg, D. K. Malick, A. D. Rabuck, K. Raghavachari, J. B. Foresman, J. Cioslowski, J. V. Ortiz, A. G. Baboul, B. B. Stefanov, G. Liu, A. Liashenko, P. Piskorz, I. Komaromi, R. Gomperts, R. L. Martin, D. J. Fox, T. Keith, M. A. Al-Laham, C. Y. Peng, A. Nanayakkara, M. Challacombe, P. M. W. Gill, B. Johnson, W. Chen, M. W. Wong, J. L. Andres, C. Gonzalez, M. Head-Gordon, E. S. Replogle, and J. A. Pople, *Gaussian 98*, Gaussian, Inc., Pittsburgh, PA, 1998.
- [131] NBO: Tutorial, in: <http://www.chem.wisc.edu/~nbo5/tutorial.html>
- [132] H.J. Werner, T. Adler, F.R. Manby, *J. Chem. Phys.*, 126 (2007) 164102.
- [133] K.A. Peterson, T.B. Adler, H.J. Werner, *J. Chem. Phys.*, 128 (2008) 084102.
- [134] K.E. Yousaf, K.A. Peterson, *J. Chem. Phys.*, 129 (2008) 184108.
- [135] F. Weigend, *Phys. Chem. Chem. Phys.*, 4 (2002) 4285.
- [136] F. Weigend, A. Köhn, C. Hättig, *J. Chem. Phys.*, 116 (2002) 3175.
- [137] M. Bogey, H. Bolvin, M. Cordonnier, C. Demuynck, J.L. Destombes, A.G. Császár, *J. Chem. Phys.*, 100 (1994) 8614.
- [138] M. J. Frisch, G. W. Trucks, H. B. Schlegel, G. E. Scuseria, J.R.C. M. A. Rob, J. A. Montgomery Jr., T. Vreven, K. N. Kudin, J. C. Burant, J. M. Millam, S. S. Iyengar, J. Tomasi, V. Barone, B. Mennucci, M. Cossi, G. Scalmani, N. Rega, G. A. Petersson, H. Nakatsuji, M. Hada, M. Ehara, K. Toyota, R. Fukuda, J. Hasegawa, M. Ishida, T. Nakajima, Y. Honda, O. Kitao, H. Nakai, M. Klene, X. Li, J. E. Knox, H. P. Hratchian, J. B. Cross, V. Bakken, C. Adamo, J. Jaramillo, R. Gomperts, R. E. Stratmann, O. Yazyev, A. J. Austin, R. Cammi, C. Pomelli, J. W. Ochterski, P. Y. Ayala, K. Morokuma, G. A. Voth, P. Salvador, J. J. Dannenberg, V. G. Zakrzewski, S. Dapprich, A. D. Daniels, M. C. Strain, O. Farkas, D. K. Malick, A. D. Rabuck, K. Raghavachari, J. B. Foresman, J. V. Ortiz, Q. Cui, A. G. Baboul, S. Clifford, J. Cioslowski, B. B. Stefanov, G. Liu, A. Liashenko, P. Piskorz, I. Komaromi, R. L. Martin, D. J. Fox, T. Keith, M. A. Al-Laham, C. Y. Peng, A. Nanayakkara, M. Challacombe, P. M. W. Gill, B. Johnson, W. Chen, M. W. Wong, C. Gonzalez, and J. A. Pople, *Gaussian 03*, Gaussian, Inc., Wallingford, CT, 2003.
- [139] M. J. Frisch, G. W. Trucks, H. B. Schlegel, G. E. Scuseria, M. A. Robb, J. R. Cheeseman, G. Scalmani, V. Barone, B. Mennucci, G. A. Petersson, H. Nakatsuji, M.

- Caricato, X. Li, H. P. Hratchian, A. F. Izmaylov, J. Bloino, G. Zheng, J. L. Sonnenberg, M. Hada, K.T. M. Ehara, R. Fukuda, J. Hasegawa, M. Ishida, T. Nakajima, Y. Honda, O. Kitao, H. Nakai, T. Vreven, J. A. Montgomery, Jr., J. E. Peralta, F. Ogliaro, M. Bearpark, J. J. Heyd, E. Brothers, K. N. Kudin, V. N. Staroverov, R. Kobayashi, J. Normand, K. Raghavachari, A. Rendell, J. C. Burant, S. S. Iyengar, J. Tomasi, M. Cossi, N. Rega, J. M. Millam, M. Klene, J. E. Knox, J. B. Cross, V. Bakken, C. Adamo, J. Jaramillo, R. Gomperts, R. E. Stratmann, O. Yazyev, A. J. Austin, R. Cammi, C. Pomelli, J. W. Ochterski, R. L. Martin, K. Morokuma, V. G. Zakrzewski, G. A. Voth, P. Salvador, J. J. Dannenberg, S. Dapprich, A. D. Daniels, Ö. Farkas, J. B. Foresman, J. V. Ortiz, J. Cioslowski, and D. J. Fox, *Gaussian 09, Revision B.01*, Gaussian, Inc., Wallingford CT, 2009.
- [140] V.W. Laurie, *J. Chem. Phys.*, 26 (1957) 1359.
- [141] J.H. Richardson, L.M. Stephenson, J. Brauman, *Chem. Phys. Lett.*, 30 (1975) 18.
- [142] C. Newman, J.K. O'Loane, S.R. Polo, M.K. Wilson, *J. Chem. Phys.*, 25 (1956) 855.
- [143] J. Moc, Z. Latajka, H. Ratajczak, *Chem. Phys. Lett.*, 136 (1987) 122.
- [144] N. Dimov, *Electrochimica Acta*, 48 (2003) 1579.
- [145] R.A. Huggins, Y. Cui, *Nature Nanotech.*, 3 (2008) 31.
- [146] R. Ruffo, *J. Phys. Chem. C*, 113 (2009) 11391.
- [147] Y. Kubota, *J. of Alloys and Compounds* 458 (2008) 151.
- [148] J.G. Hill, K.A. Peterson, *Phys. Chem. Chem. Phys.*, 12 (2010) 10460.
- [149] D.E. Woon, T.H. Dunning, *J. Chem. Phys.*, 98 (1993) 1358.
- [150] T.H. Dunning, K.A. Peterson, A.K. Wilson, *J. Chem. Phys.*, 114 (2001) 9244.
- [151] A. Halkier, W. Klopper, T. Helgaker, P. Jorgensen, P.R. Taylor, *J. Chem. Phys.*, 111 (1999) 9157.
- [152] J.M.L. Martin, in: M.E.M.d. Piedade (Ed.), *NATO ASI series C*, 1999, pp. 373.
- [153] G.E. Scuseria, T.J. Lee, *Chem. Phys.*, 93 (1990) 5851.
- [154] D.E. Woon, T.H. Dunning, *J. Chem. Phys.*, 103 (1995) 4572.
- [155] K.A. Peterson, T.H. Dunning, *J. Chem. Phys.*, 117 (2002) 10548.
- [156] W. Cencek, J. Rychlewski, R. Jaquet, W. Kutzelnigg, *J. Chem. Phys.*, 108 (1998) 2831.
- [157] S.N. Yurchenko, J. Zheng, H. Lin, P. Jensen, W. Thiel, *J. Chem. Phys.*, 123 (2005) 134308.
- [158] B. Prascher, D.E. Woon, K.A. Peterson, T.H. Dunning, A.K. Wilson, *Theor. Chem. Acc.*, 128 (2011) 69.
- [159] B.A. Hess, *Phys. Rev. A*, 33 (1986) 3742.
- [160] A. Sekiguchi, M. Nanjo, C. Kabuto, H. Sakurai, *Angew. Chem. Int.Ed.*, 36 (1997) 113.
- [161] S. Inoue, M. Ichinohe, A. Sekiguchi, *Angew. Chem. Int.Ed.*, 46 (2007) 3346.
- [162] T. Matsuno, M. Ichinohe, A. Sekiguchi, *Angew. Chem. Int.Ed.*, (2002) 1575.
- [163] T. Iwamoto, J. Okita, C. Kabuto, M. Kira, *J. Am. Chem. Soc.*, 124 (2002) 11604.
- [164] K. Abersfelder, D. Scheschke, *J. Am. Chem. Soc.*, 130 (2008) 4114.
- [165] M. Nakamoto, T. Fukawa, V. Ya. Lee, A. Sekiguchi, *J. Am. Chem. Soc.*, 124 (2002) 15160.
- [166] J.G. Hill, S. Mazumder, K.A. Peterson, *J. Chem. Phys.*, 132 (2010) 054108.
- [167] P.v.R. Schleyer, A.E. Reed, *J. Am. Chem. Soc.*, 110 (1988) 4453.
- [168] Y. Yamaguchi, B.J. DeLeeuw, C.A. Richards, H.F. Schaefer, G. Frenking, *J. Am. Chem. Soc.*, 116 (1994) 11922.

- [169] R. Cohen, N. Zenou, D. Cahen, S. Yitzchaik, *Chem. Phys. Lett.*, 279 (1997) 270.
- [170] K.R. Asmis, T.R. Taylor, D.M. Neumark, *Chem. Phys. Lett.*, 308 (1999) 347.
- [171] I. Musa, D.A.I. Munindrasdasa, G.A.J. Amaratunga, W. Eccleston, *Nature*, 395 (1998) 362.
- [172] J.C. Rienstra-Kiracofe, G.S. Tschumper, S. Nandi, G.B. Ellison, H.F. Schaefer, *Chem. Rev.*, 102 (2002) 231.
- [173] H. Hotop, W.C. Lineberger, *J. Phys. Chem. Ref. Data*, 4 (1975) 539.
- [174] H. Hotop, W.C. Lineberger, *J. Phys. Chem. Ref. Data*, 14 (1985) 731.
- [175] J.L. Davidson, W.P. Kang, K. Subramanian, Y.M. Wong, *Phil. Trans. R. Soc.*, 366 (2008) 1863.
- [176] W.P. Kang, J.L. Davidson, A. Wisitsor, Y.M. Wong, R. Takalkar, K. Holmes, D.V. Kernsb, *Diamond & Related Materials* 13 (2004) 1944.
- [177] L.A. Curtiss, P.C. Redfern, K. Raghavachari, J.A. Pople, *J. Chem. Phys.*, 109 (1998) 7764.
- [178] L.A. Curtiss, K. Raghavachari, G.W. Trucks, J.A. Pople, *J. Chem. Phys.*, 94 (1991) 7221.
- [179] T.H. Dunning, K.A. Peterson, T. van Mourik, Guberman, S. L., Ed.; Kluwer Academic, (2003) 415.
- [180] F. Jensen, *J. Chem. Theory Comput.*, 6 (2010) 2726.
- [181] M.R. Nimlos, L.B. Harding, G.B. Ellison, *J. Chem. Phys.*, 87 (1987) 5116.
- [182] T.N. Kitsoupoulos, C.J. Chick, A. Weaver, D.M. Neumark, *J. Chem. Phys.*, 95 (1991) 1441.
- [183] C. Pak, L. Sari, J.C. Rienstra-Kiracofe, S.S. Wesolowski, L. Horný, Y. Yamaguchi, H.F. Schaefer, *J. Chem. Phys.*, 118 (2003) 7256.
- [184] A.K. Wilson, T. van Mourik, T.H. Dunning, *J. Mol. Struc. (Theochem)*, 388 (1996) 339.
- [185] O.M. Manuel Alcamí, José Juis G. de Paz and Manuel Yáñez, *Theor. Chim. Acta*, 77 (1990) 1.
- [186] J.S. Lee, S.A. Krasnokutski, D.-S. Yang, *J. Chem. Phys.*, 134 (2011) 024301.
- [187] O. Mo, M. Yanez, J.-F. Gal, P.-C. Maria, M. Decouzon, *Chem. Eur. J.*, 9 (2003) 4330.
- [188] G.J. Kramer, R.A.v. Santen, *J. Am. Chem. Soc.*, 115 (1993) 2887.
- [189] L.A. Curtiss, H. Brand, J.B. Nicholas, L.E. Iton, *Chem. Phys. Lett.*, 184 (1991) 215.
- [190] J. Leszczynski, J.Q. Huang, P.R. Schreiner, G. Vacek, J. Kapp, P.v.R. Schleyer, H.F. Schaefer, *Chem. Phys. Lett.*, 244 (1995) 252.
- [191] Z. Palagyi, H.F. Schaefer, E. Kapuy, *J. Am. Chem. Soc.*, 115 (1993) 6901.
- [192] S.Gironcoli, *Phys. Rev. B*, 46 (1992) 2412.
- [193] Wolfram Research, *Mathematica* 8, 2012.
- [194] R. Marcellin, *Annalen der Physik*, 3 (1915) 158.
- [195] H. Eyring, *J. Chem. Phys.*, 3 (1935) 107.
- [196] H. Eyring, M. Polanyi, *Z. Phys. Chem.*, B12 (1931) 279.
- [197] P.M. Morse, *Phys. Rev.*, 34 (1929) 57.
- [198] K.C. Thompson, M.J.T. Jordan, M.A. Collins, *J. Chem. Phys.*, 108 (1998) 8302.
- [199] M.A. Collins, *J. Chem. Phys.*, 127 (2007) 024104.
- [200] J.M. Bowman, T. Carrington, H.D. Meyer, *Molec. Phys.*, 106 (2008) 2145.
- [201] O. Vendrell, F. Gatti, H.D. Meyer, *Angew Chem. – Int. Ed.*, 48 (2009) 352.
- [202] H. Koizumi, G.C. Schatz, S.P. Walch, *J. Chem. Phys.*, 95 (1991) 4130.

- [203] R.P.A. Bettens, M.A. Collins, *J. Chem. Phys.*, 111 (1999) 816.
- [204] A. Jackle, H.-D. Meyer, *J. Chem. Phys.*, 109 (1998) 3772.
- [205] T. Ishida, G.C. Schatz, *Chem. Phys. Lett.*, 314 (1999) 369.
- [206] S. Manzhos, X. Wang, R. Dawes, T. Carrington, *J. Chem. Phys. A*, 110 (2006) 5295.
- [207] C.M. Bishop, *Neural Networks for Pattern Recognition*, in, Oxford University Press, 1995.
- [208] M. Smith, *Neural Networks for Statistical Modeling*, Van Nostrand Reinhold, 1993.
- [209] S. Nissen, *Implementation of a Fast Artificial Neural Network library (FANN)*, DIKU, 2003.
- [210] K. Levenberg, *The Quarterly of Applied Mathematics*, 2 (1944) 164.
- [211] J.B. Anderson, *J. Chem. Phys.*, 63 (1975) 1499.
- [212] P.D. Duncan, M.M. Law, *DMCP program*, University of Aberdeen, 2001-2009.
- [213] B.J. Braams, J.M. Bowman, *Int. Rev in Phys. Chem.*, 28 (2009) 577.
- [214] MATLAB Software, Version 7.9, R2009b (Ed.), 2009.
- [215] I.N. Kozin, M.M. Law, J. Tennyson, J.M. Hutson, *Computer Physics Communications*, 163 (2004) 117.
- [216] M. Mladenovic, *J. Chem. Phys.*, 112 (2000) 1070.
- [217] I.N. Kozin, M.M. Law, *WFN2 program package*, University of Aberdeen, 2003-2011.

12 Appendix

Fortran subroutine programs and MATLAB script written by Lukasz M. Serafin for the work described in this thesis:

12.1 The Neural Network MATLAB script.

```
function net = mine_new(PES,energy)
% CREATE_FIT_NET Creates and trains a fitting neural network.
%
% NET = CREATE_FIT_NET(PES(inputs),energy(targets)) takes these arguments:
% PES - RxQ matrix of Q R-element input samples
% energy - SxQ matrix of Q S-element associated target samples
% arranged as columns, and returns these results:
% NET - The trained neural network
%
% net = mine(PES,energy);

net.numInputs=7;          % input of each NN is a combination of i variables
net.input{1}.size=7;
net.numLayers=2;
net.layers{1}.size=7;
net.layers{2}.size=10;
net.inputConnect(1)=1;    % connect the input to the input layer
net.layerConnect(2,1)=1;
net.outputConnect(2)=1;

% Transfer Functions
net.layers{1}.transferFcn='tansig'; % Transfer function of 1st layer
net.layers{2}.transferFcn='purelin'; % Transfer function of 2nd layer

% weights biases
net.biasConnect=[1;1];

net.initFcn='initlay';
net.layers{1}.initFcn='initnw';
net.layers{2}.initFcn='initnw';

% Create Network
numHiddenNeurons = 96; % Adjust number of neurons as desired
net = newfit(PES,energy,numHiddenNeurons);
net.divideParam.trainRatio = 80/100; % Adjust a training ratio as desired
net.divideParam.valRatio = 10/100; % Adjust a validation ratio as desired
net.divideParam.testRatio = 10/100; % Adjust a test ratio as desired
```

```

net.trainFcn = 'trainlm'; % Training function Levenberg-Marquardt

% For a list of all training functions type: help nntrain
% Choose a Performance Function
% For a list of all performance functions type: help nnperformance
net.performFcn = 'mae'; % Mean absolute error

% Train and Apply Network
[net,tr] = train(net,PES,energy);
outputs = sim(net,PES);

bias1=net.b{1}
bias2=net.b{2}
iweight=net.IW{1,1}
lweight=net.LW{2,1}

% write down out's into a *.dat file

dlmwrite('outbw.dat', bias1,'-append','delimiter', '\t', 'precision', '%.6f');
dlmwrite('outbw.dat', bias2,'-append','delimiter', '\t', 'precision', '%.6f');
dlmwrite('outbw.dat', iweight,'-append','delimiter', '\t', 'precision', '%.6f');
dlmwrite('outbw.dat', lweight,'-append','delimiter', '\n', 'precision', '%.6f');

% max and min for all input data
dlmwrite('outbw.dat',min(PES,[],2),'-append','delimiter', '\t', 'precision', '%.6f');
dlmwrite('outbw.dat',max(PES,[],2),'-append','delimiter', '\t', 'precision', '%.6f');
dlmwrite('outbw.dat',min(energy,[],2),'-append','delimiter', '\t', 'precision', '%.6f');
dlmwrite('outbw.dat',max(energy,[],2),'-append','delimiter', '\t', 'precision', '%.6f');

% output energy after fitting
dlmwrite('out_ene.dat', outputs,'-append','delimiter', '\t', 'precision', '%.6f');

% Plot
plotperf(tr)
plotregression(energy,outputs)

```


12.2 Fortran programs.

Program to transform the Cartesians to the polynomials coordinates and create inputs files, which will be used in MATLAB NEURAL NETWORK tool box.

```
PROGRAM READER
!
IMPLICIT NONE
DOUBLE PRECISION
::T1,AX1,AY1,AZ1,AX2,AY2,AZ2,AX3,AY3,AZ3,AX4,AY4,AZ4,SCF,ENERGY,BOHR,C
M,MINIMUM_F12,MINIMUM_SCF
CHARACTER(LEN=*), PARAMETER :: FMT1 =
"(T1,F10.8,1X,F7.4,1X,F7.4,1X,F6.2,1X,F6.2,1X,F7.2,1X,F13.6,1X,F13.6)"
CHARACTER(LEN=*), PARAMETER :: FMT2 = "(/)"
PARAMETER (MINIMUM_F12= -593.0647637D0)
PARAMETER (MINIMUM_SCF= -592.7489725D0)
PARAMETER (BOHR=0.0174532925D0)
PARAMETER (CM = 219474.63D0)
!
INTEGER :: nDATA,i
!
OPEN (unit=5,FILE='print.temp2')
OPEN (unit=9,FILE='in_atom.dat')
OPEN (unit=10,FILE='poly.dat')
OPEN (unit=11,FILE='target.dat')
!
WRITE (6,*) MINIMUM_F12,CM
!
READ (5,*) nDATA
!
DO i=1,nDATA
READ(5,*) T1,AX1,AY1,AZ1,AX2,AY2,AZ2,AX3,AY3,AZ3,AX4,AY4,AZ4,SCF,ENERGY

IF (T1.GT.0.0500) THEN
WRITE (6,*) 'WARNING !!!! T1 DIAGNOSTIC TO HIGH!!!!'
END IF
```

```

IF (T1.GT.1.0D-6) THEN
  CALL IN_ATOMICS
  CALL TARGET_CM
END IF
END DO
!
CLOSE (5)
CLOSE (9)
CLOSE (10)
CLOSE (11)
!
CONTAINS
!
! Subroutine to calculate inter atomics and transfer them to polynomials
!
SUBROUTINE IN_ATOMICS
!
IMPLICIT NONE
DOUBLE PRECISION R1,R2,R3,R4,R5,R6,BOHR
DOUBLE PRECISION P1,P2,P3,P4,P5,P6,P7,e0,e1,f0,f1
PARAMETER (BOHR=0.0174532925)
!
602 FORMAT (1X,F15.12,1X,F15.12,1X,F15.12,1X,F15.12,1X,F15.12,1X,F15.12)
!
R1=sqrt((AX1-AX2)**2 +(AY1-AY2)**2+(AZ1-AZ2)**2)
R2=sqrt((AX1-AX3)**2 +(AY1-AY3)**2+(AZ1-AZ3)**2)
R3=sqrt((AX1-AX4)**2 +(AY1-AY4)**2+(AZ1-AZ4)**2)
R4=sqrt((AX2-AX3)**2 +(AY2-AY3)**2+(AZ2-AZ3)**2)
R5=sqrt((AX2-AX4)**2 +(AY2-AY4)**2+(AZ2-AZ4)**2)
R6=sqrt((AX3-AX4)**2 +(AY3-AY4)**2+(AZ3-AZ4)**2)
!
e0=(R2+R5)/2
e1=(R3+R4)/2
f0=(R2+R4)/2
f1=(R3+R5)/2

```

```

P1=(R5+R2+R3+R4)/4
P2=(e0**2+e1**2)/2
P3=R1
P4=(f0**2+f1**2)/2
P5=(R3**2+R2**2+R4**2+R5**2)/4
P6=R6
P7=(R3**3+R2**3+R4**3+R5**3)/4
!
WRITE (10,602) P1,P2,P3,P4,P5,P6,P7
END SUBROUTINE IN_ATOMICS
!
! Subroutine to get cm-1
!
SUBROUTINE TARGET_CM
IMPLICIT NONE
602 FORMAT (1X,F14.7)
DOUBLE PRECISION F12
!
F12=(ENERGY-MINIMUM_F12)*CM
WRITE (11,602) F12
END SUBROUTINE TARGET_CM
END PROGRAM

```

Program to transform the satellite coordinates to the polynomials coordinates and create inputs files, which will be used in MATLAB NEURAL NETWORK tool box.

```
PROGRAM READER2
!
IMPLICIT NONE
DOUBLE PRECISION ::Rr2,Rr3,Rr1,A1,A2,D1
CHARACTER(LEN=*), PARAMETER :: FMT1 =
"(T1,F10.8,1X,F7.4,1X,F7.4,1X,F7.4,1X,F6.2,1X,F6.2,1X,F7.2,1X,F13.6,1X,F13.6)"
CHARACTER(LEN=*), PARAMETER :: FMT2 = "(/)"
!PARAMETER (MINIMUM_F12= -593.0647637D0)
!PARAMETER (MINIMUM_SCF= -592.7489725D0)
!PARAMETER (MAX_E= -592.8369477D0) !50k
!PARAMETER (MAX_E= -592.9280736D0) !30k
!PARAMETER (MAX_E= -592.9052920D0) !35k
!PARAMETER (MAX_E= -593.0374257D0) !6k
!PARAMETER (MAX_E= -593.0192003D0) !10k
PARAMETER (MAX_E= -593.0100877D0) !12k
!PARAMETER (MAX_E= -592.9736370D0) !20k
!
INTEGER :: nDATA,i
!
OPEN (unit=5,FILE='satelite.dat')
OPEN (unit=9,FILE='R1-R6.dat')
!
READ (5,*) nDATA
!
DO i=1,nDATA
READ(5,*) Rr1,Rr2,Rr3,A1,A2,D1
!
CALL IN_ATOMICS
! CALL TARGET_CM
END DO
!
CLOSE (5)
```

```

CLOSE (9)
!
CONTAINS
!
! Subroutine to calculate inter atomics and transfor them to polynomials
!
SUBROUTINE IN_ATOMICS
!
IMPLICIT NONE
DOUBLE PRECISION R1,R2,R3,R4,R5,R6,X1,Y1,Z1,Rxy,X2,Y2,Z2,BOHR,PI
DOUBLE PRECISION P1,P2,P3,P4,P5,P6,P7,e0,e1,f0,f1
PARAMETER (BOHR=0.0174532925)
PARAMETER (PI=3.141592654D0)
!
602 FORMAT (1X,F15.12,1X,F15.12,1X,F15.12,1X,F15.12,1X,F15.12,1X,F15.12,1X,F16.12)
!
R3=Rr3
R1=SQRT((Rr3/2.0D0)**2+Rr1**2-(2*(Rr3/2.0D0)*Rr1*COS(BOHR*A1)))
R2=SQRT((Rr3/2.0D0)**2+Rr2**2-(2*(Rr3/2.0D0)*Rr2*COS(BOHR*(180.0D0-A2))))
R4=SQRT((Rr3/2.0D0)**2+Rr1**2-(2*(Rr3/2.0D0)*Rr1*COS(BOHR*(180.0D0-A1))))
R5=SQRT((Rr3/2.0D0)**2+Rr2**2-(2*(Rr3/2.0D0)*Rr2*COS(BOHR*A2)))
X1=Rr1*SIN((A1)*PI/180.0D0)
Y1=0.0D0
Z1=Rr1*COS((A1)*PI/180.0D0)
X2=Rr2*SIN(A2*PI/180.0D0)*COS(D1*PI/180.0D0)
Y2=Rr2*SIN(A2*PI/180.0D0)*SIN(D1*PI/180.0D0)
Z2=Rr2*COS(A2*PI/180.0D0)
!
R6=DSQRT((X1-X2)**2+(Y1-Y2)**2+(Z1-Z2)**2)
!
WRITE (9,602) R1,R2,R3,R4,R5,R6
!
END SUBROUTINE IN_ATOMICS
! Subroutine to get cm-1 same like in the program above
END PROGRAM

```

Example of a print.temp2 input file which is needed for the above Fortran subroutine programs:

T1	D1	Cartesians											SCF	F12
0.023	0.319	0.0650	-1.1958	0.3647	-0.0455	1.0625	-1.2064	1.9903	-0.1639	-1.2641	-1.8029	-0.0584	-592.7429	-593.0586
0.023	0.339	-0.0185	-1.1264	0.2567	0.0305	1.1338	-1.4013	1.8652	0.1234	-1.1342	-1.8508	0.0911	-592.7429	-593.0592
0.023	0.335	0.0866	-1.1155	0.4139	0.1245	1.1036	-1.4551	1.8298	0.0279	-1.3543	-1.8043	-0.0769	-592.7435	-593.0569
0.023	0.306	-0.0072	-1.0997	0.2928	-0.1194	1.1254	-1.4763	1.7567	-0.0160	-1.4811	-1.8854	-0.0786	-592.7432	-593.0568
0.023	0.198	0.0409	-1.1583	0.2013	-0.0356	1.1193	-1.3495	1.9121	-0.2775	-1.2799	-1.8425	-0.1190	-592.7419	-593.0590
0.022	0.338	0.0792	-1.0185	0.2830	-0.0470	1.2179	-1.3211	1.8268	0.1108	-1.2586	-1.9216	-0.0843	-592.7447	-593.0598
0.023	0.290	-0.0382	-1.2200	0.2820	0.1176	1.0340	-1.2287	1.6580	0.0978	-1.4548	-1.9289	-0.1446	-592.7376	-593.0545
0.023	0.457	0.0212	-1.1128	0.2261	0.0375	1.0915	-1.3519	1.8937	0.0797	-1.5657	-1.6342	-0.0137	-592.7440	-593.0577
.														
.														
.														

The table can be easily created using the table command in molpro:

```
table qlabel, ii, ti, di, ax1, ay1, az1, ax2, ay2, az2, ax3, ay3, az3,  
ax4, ay4, az4, escf, e  
head qlabel, ii, t1, d1, ax1, ay1, az1, ax2, ay2, az2, ax3, ay3, az3,  
ax4, ay4, az4, scf, energy
```

Then by using the "grep" and "cat" UNIX commands:

- `grep QQ *.out | grep -v QLABEL > print.temp (>> append)`
- `cat print.temp | sed 's/[\t]*^t/g' | cut -f4,6-19 > print.temp2`